The treatment of carwash wastewater using an integrated chemical coagulation and adsorption process

by

Fabian Roman

A thesis submitted in fulfilment of the requirements for the degree

Master of Engineering: Chemical Engineering

in the

Faculty of Engineering and the Built Environment

at the

Cape Peninsula University of Technology

Supervisor**: Dr Mujahid Aziz**

July 2021

I, Fabian Roman, hereby declare that the contents of this dissertation/thesis represent my own unaided work, and that the dissertation/thesis has not previously been submitted for academic examination towards any qualification. Furthermore, it represents my own opinions and not necessarily those of the Cape Peninsula University of Technology.

Signed: *Fabian Roman* Date: *July 2021*

Abstract

Clean water is a valuable and scarce resource in any society today. The water scarcity being faced globally will deteriorate unless water consumption is reduced, and water reuse is implemented globally. Affordable wastewater treatment technologies have the potential to alleviate this crisis being faced today.

Greywater is an excellent source for water reuse and includes domestic, carwash, laundry and hospital water. Greywater contains different pollutants such as organic and inorganic components making it challenging to treat and potentially harm the environment. Chemical coagulation is an excellent treatment process for removing turbidity, grease and COD but struggles to remove specific compounds such as cleaning agents. Therefore, introducing a secondary treatment process like adsorption offers a viable solution for removing harmful pollutants from greywater.

In this study a lab scale integrated treatment process was used to investigate carwash wastewater's successful treatment. Chemical coagulation and adsorption were the treatment steps used to remove COD, FOG and anionic surfactants from the carwash wastewater for reuse application.

The chemical coagulation process with polyferric sulphate (PFS) was applied to treat industrial carwash wastewater collected from a service station in Cape Town, South Africa. Polyferric sulphate concentration was tested to determine the optimum dosage concentration for the removal of pollutants. After that, adsorption using a commercial powdered activated carbon was used as a secondary treatment step. Operating conditions such as temperature, adsorbent dosage and pH were investigated to determine the effect on removing COD, FOG, and anionic surfactants (AS). The commercial activated carbon was characterized using Scanning Electron Microscopy (SEM) and Fourier Transform Infrared Spectroscopy (FTIR). Design Expert 10 was used to generate a predictive model using the Box-Behnken Design (BBD) approach to describe the effect of operating conditions on COD and Anionic Surfactant (AS) removal. Origin 2021 professional software package was used to fit adsorption (Langmuir, Freundlich, Temkin and Dubinin-Radushkevich) and kinetic models (Pseudo-First Order (PFO), Pseudo-Second Order (PSO), Intra-Particle Diffusion (IPD) and Elovich) to the experimental data collected for Anionic Surfactants (AS).

The removal percentage of COD, FOG and AS were found to be 79.5%, 96.25 and 44.82 respectively after chemical coagulation at a PFS concentration of 120mg/l. This was deemed a sufficient coagulant dosage. The best percentage removal after adsorption for FOG, COD and AS was found to be 100, 94 and 98% respectively at operating conditions of pH: 6, Temperature: 50^0C and dosage: 300mg/l powdered activated carbon (PAC). The best overall removal for COD, FOG and AS was found to be 98.5, 100 and 98% respectively. This shows that the treated effluent is in line with national standards for safe disposal or reuse.

The SEM images revealed a porous structure suitable for the adsorption of COD, FOG and AS. The FTIR revealed the PAC contained bonds that are advantageous for the adsorption of AS. The adsorption kinetic data for AS was shown to follow pseudo-second order (PSO) reaction kinetics the best and follow the Freundlich and Temkin adsorption isotherms the closest. The adsorption thermodynamics showed the adsorption of AS onto commercial PAC being an endothermic process. It was observed that the predictive model successfully described the optimal operating conditions for the removal of COD and AS within the design space of the model.

Research Outputs

Myburgh D; Aziz M; **Roman F**; Jardim J; Chakawa S; 2019; Removal of COD from industrial biodiesel wastewater using an integrated process: Electrochemical-oxidation with IrO_2-Ta_2O_5/Ti anodes and chitosan powder as an adsorbent, *Environmental Processes an International Journal*, 6, 818-840 [ISSN 2198-7505 / DOI:1007/540710-019-00401-x]

Roman F & Aziz M; 2021; Removal of Anionic Surfactants (AS) and Chemical Oxygen Demand (COD) from industrial carwash wastewater using an integrated process: Chemical coagulation and Adsorption, *IWA: Water Science and Technology.* Submitted XX April 2021 [Paper ID.: XX-XX-XX]

Acknowledgements

I thank God for giving me the strength to succeed with this project, for protecting me, and for blessing me with my family and friends.

This research project was undertaken within the Chemical Engineering Department at the Cape Peninsula University of Technology between January 2018 and November 2020.

I want to express my gratitude to the following people for their contributions towards the completion of this thesis:

My Supervisor, Dr Mujahid Aziz, for his incomparable supervision, persistent guidance, motivation, encouragement and technical expertise in the field of this research. I am thankful for his sustained academic, moral and fatherly assistance throughout my academic journey.

The technical and administrative staff in the Chemical Engineering Department Mrs Hannelene Small, Mrs Elizma Alberts and Mr Alwyn Bester, always willing to assist.

The Environmental Engineering Research Group (*EnvERG*) in the Department of Chemical Engineering.

My deep and sincere gratitude goes to my family for their continuous and exceptional love, help and support. I am grateful to my brothers for always being there for me. I am forever indebted to my parents for their continued moral and financial support.

The National Research Foundation (NRF-SA) financial assistance for the scholarship and the CPUT bursary towards the success of this research is acknowledged.

Dedication

Warrick and Anthea Roman, for their endless love, support, encouragement and inspiration.

To my parents and role models,

This achievement would not be possible without you. I am forever grateful for your presence in my life.

Table of Contents

List of Tables

List of Figures

List of Abbreviations

COD	Chemical Oxygen demand
BOD	Biological Oxygen Demand
FOG	Fats, Oils and Grease
TDS	Total Dissolved Solids
EC	Electrical Conductivity
PFS	Polyferric Sulphate
PAC	Powdered Activated Carbon
MBAS	Methylene Blue Active Substance
DI	De-ionised
D-R	Dubinin-Raduschkevich
FTIR	Fourier Transform Infrared Spectrometer
SEM	Scanning Electron Microscopy
GAC	Granular Activated Carbon
CWW	Carwash Wastewater
CC	Chemical Coagulation
RSM	Response Surface Methodology
PFO	Pseudo-First Order
PSO	Pseudo Second Order
IPD	Intraparticle diffusion
RPM	Revolutions Per Minute
MBR	Membrane Bioreactor
AS	Anionic Surfactant

List of Photographs

List of Symbols

List of symbols		
Symbol	**Definition**	**Unit**
q_e	amount of Surfactant adsorbed at equilibrium	mg/g
q_t	amount of Surfactant adsorbed at a time t	mg/g
C_0	initial concentration of surfactant in solution	mg/l
C_e	concentration of surfactant in solution at equilibrium	mg/l
V	volume of solution	litre
m	mass of adsorbent used	g
q_m	practical limiting adsorption capacity	mg/g
K_L	Langmuir constant	L/mg
R_L	dimensionless constant separation factor	
K_F	Freundlich constant	$(mg/g)(L/mg)^{1/n}$
n	heterogeneity factor	
K	constant related to adsorption energy	mol^2/kJ^2
Ɛ	Polanyi potential	J/mol
R	universal gas constant	J/mol. K
T	temperature	Kelvin/ Celsius
K_{id}	Intraparticle diffusion constant	$mg/g.min^{0.5}$
K_T	Temkin Constant	l/mg
B_1	Heat of adsorption	
g	mass	gram
k_f	Pseudo-first order rate constant	min^{-1}
k_s	Pseudo-second order rate constant	g/mg.min
m^3	cubic meter	m^3
C	Related to boundary layer thickness	mg/g
∆H	Enthalpy	KJ/mol
ΔS	Entropy	KJ/mol
ΔG	Gibbs free energy	KJ/mol
R^2	Correlation Coefficient	

CHAPTER 1

Introduction

1 Chapter 1 Introduction

1.1 Background

Water is essential to all human activity and wildlife ecosystem health. All productive sectors within society require the use of water in one form or another. How these water resources are managed and allocated are fundamental to sustainable development and human wellbeing (Bertule et al., 2018). The water supply pressure is driven by population growth, climate change, and environmental degradation. The current climate of water scarcity will only worsen unless steps are taken to reduce water consumption and increase reuse water applications (Akhmouch et al., 2018). Measures to recycle greywater needs to be put in place to cope with the current water scarcity problems world-wide. Greywater recycling offers affordable solutions to the current water supply problems being faced globally. Greywater includes industrial, household and hospital water to name a few sources (Oh et al., 2018). Industrial greywater sources include dairy, carwashes, textiles, paper which are considered the most important sources of water pollution even in low quantities (Sarmadi et al., 2020).

The carwash industry is ever-expanding because of the constant increase of automobiles on the roads. A rapid increase of these automobiles on the roads, results in more freshwater required to keep vehicles clean. It is no secret that today's population is facing a global water crisis and with an increase in water required for the carwash industry, radical changes needs to be made in order for the industry to be sustainable. Kumar & Chauhan (2018) state that by the year 2025 the world population would have eclipsed 2 billion people worldwide without enough access to fresh water, resulting to insufficient access to fresh water. Therefore, it is fundamentally vital to treat all waste water for reuse application. Lau (2013) states that carwash stations generally use between 150 to 600 litres of water per car producing an astronomical amount of wastewater. Another aspect of the carwash industry that cannot be overlooked is the copious amounts of waste it produces. Carwash wastewater (CWW) can harm the environment if not managed correctly or appropriately discharged. The pollutants in carwash wastewater are accumulated from traffic pollutants (which include road surfacing and atmospheric pollutants), chemical pollutants and car exploitation pollutants.

Carwash wastewater is characterized by having high surfactants, low levels of COD and FOG and low concentrations of metals which are harmful to the environment. CWW also contains phosphates, which cause excessive growth of plants in aquatic environments, biodegradable soaps, and detergents harmful to fish mucus membranes and gills disrupting oxygen supply

leaving fish susceptible to bacteria and parasites. Detergents can also kill fish in concentrations of 15ppm and fish eggs at 5ppm ((Tony & Bedri, 2014))

Most carwash stations in South Africa do not have any kind of recycling systems in place and are discharging the wastewater directly into the environment and or municipal stormwater drains. Due to the nature of carwash wastewater and the expanding industry, it is essential to develop economically viable and sustainable methods for treating these wastewaters. Many reclamation processes have been tried as remedial application, such as Membrane Technology, Adsorption, Chemical coagulation (CC), oxidation processes and Membrane bioreactor (MBR) (Moazzem et al., 2018) however the performance has not been compared or ensured. CWW treatment systems generally comprise of a primary and secondary treatment step. In the primary treatment systems, a significant portion of total solids and suspended organic material including oil and grease, COD and BOD are removed from CWW. These primary treatment processes generally include processes like coagulation, dissolved air flotation and sedimentation chambers. Secondary treatment processes are classified as adsorption, electrochemical and biological processes. The recognition and methods of CWW treatment with consideration to the pollutants and compounds are among the most important considerations in recycling potential resources (Sarmadi et al., 2020).

Coagulation based processes are found in over 70% of global water treatment plants making it a critical water treatment process. Coagulation is highly effective in removing TSS and turbidity however less effective for the removal of organic matter such as COD and BOD from greywater such as CWW (Foroughi et al., 2018). Therefore, it is preferred to be applied in combination with other methods especially adsorption or membrane processes. Adsorption is a common technique applied in wastewater treatment; however, it has not been widely applied in CWW treatment processes. The main reason for this could be the complex nature of CWW and cannot be treated by one unique process. However, in the limited studies available adsorption has shown to be an efficient process for removing organic and inorganic pollutants such as surface-active substance, oil and grease, TDS and heavy metals (Enoh & Christopher, 2015). Membrane treatment systems such as microfiltration, ultrafiltration, nanofiltration and reverse osmosis are the most immediate membrane processes when CWW treatment is concerned. These systems have high removal efficiency when removing solids, organic matter, TOC, turbidity and surfactants. However, membrane fouling is the main restriction regarding these processes and thus is generally used in combination with other process such biological treatment or coagulation. Considering individual treatment options may not remove all pollutants effectively and the use of one process may not be feasible in full-scale systems,

the use of integrated systems seems to be more effective and economically viable than a unique system (Sarmadi et al., 2020).

Due to the multitude of contaminants in carwash wastewater it is important to provide a solution that effective and simple to implement and affordable. Membrane technologies have been shown to provide the most outstanding efficiency at pollutant removal however the membrane fouling and high energy cost should be considered and thus at a disadvantage to other processes like adsorption (Leiknes & Ødegaard, 2007).

Several studies have been investigated to remove COD and anionic surfactants from industrial wastewater using chemical coagulation (CC) and adsorption process in recent years. Baddor et al. (2014) performed a study where bentonite was also used as an adsorbent found a COD removal of 80%, anionic surfactant removal of 83% and a FOG removal of 86%. Asha et al. (2016) performed an integrated treatment process for CWW treatment where adsorption, sugarcane bagasse, and chemical coagulation, alum, was used. The results of the study showed a max COD removal of 86% and FOG of 93%. The integrated method for CCW treatment shows excellent potential to mitigate this problem. Therefore, this study sought to explore the possibility of using combined CC and adsorption to treat CCW.

1.2 Research Problem

Carwash wastewater (CWW) is classified as industrial wastewater. The "City of Cape Town: Wastewater and Industrial Effluent By-law, 2013" governs industrial wastewater disposal in the City of Cape Town. Currently, CWW is discharged into the sewer that does not comply with the industrial discharge standards. Therefore, research studies are being conducted to effectively treat CWW to reduce the adverse effects on the environment and biological processes in wastewater treatment facilities, abide by more stringent effluent requirements and avoid fines. Effective treatment of the wastewater may result in the recycling of the water during the production process.

1.3 Research Questions

1.3.1 Can chemical coagulation (CC) followed with adsorption treat carwash wastewater (CWW) to meet the required industrial wastewater discharge standards?

1.3.2 How will the pH, adsorbent dosage and temperature affect pollutant removal rate during the adsorption process of CWW?

1.4 Aims and Objectives

This research aims to improve the quality of carwash wastewater (CWW) in an integrated chemical coagulation (CC) and adsorption process to meet safe discharge and reuse standards.

The specific objectives were

1.4.1 Investigate the different poly-ferric sulphate (PFS) concentrations as a pre-treatment on the removal of pollutants such as chemical oxygen demand (COD); fats, oils & greases (FOG) and anionic surfactants (AS); during a batch chemical coagulation process.

1.4.2 Study the effect of powder activated carbon (PAC) concentration, pH and temperature on COD, FOG and anionic surfactants removal efficiencies during a batch adsorption process.

1.4.3 Investigate Kinetic, Isotherm and thermodynamic studies on the removal of anionic surfactants (AS).

1.5 Significance of this research

The effective treatment of carwash wastewater may result in compliance with wastewater discharge standards, cost savings and protect the environment while reducing freshwater usage by recycling in the production process.

.

1.6 Delineation of study

During this study, the removal of COD, FOG and anionic surfactants from carwash wastewater was observed through an integrated treatment process, which consists of two steps

1. Chemical coagulation (CC) using polyferric sulphate (PFS)
2. Adsorption using powdered activated carbon (PAC)

Chemical coagulation occurred using PFS, while adsorption occurred using PAC

All other variables are delineated.

1.7 Structure of Thesis

This thesis contains six chapters, with a brief introduction as follows:

Chapter 1: Introduction

This chapter presents an introduction and background information about the evaluating the performance of the adsorption and chemical coagulation process in the removal of surfactants, COD and FOG from Carwash wastewater effluents. After that follows the problem statement, aim, objectives and delineation.

Chapter 2: Literature Review

This chapter presents a comprehensive literature review in which adsorption and chemical coagulation are discussed compared to other industrial effluents treatment technologies. The characteristics of wastewater determine the choice of treatment technology. Water and wastewater effluent quality discharge and reuse standards were reviewed and were found to be different globally

Chapter 3: Methodology

This chapter describes procedures; equipment and chemicals that were used in this study. It also shows the chemical analysis techniques used and the design of experiments using the Design-Expert software package.

Chapter 4: Results and Discussion

This chapter displays all the results from the experimental runs completed. The graphs are discussed to optimise the adsorption and chemical coagulation processes.

Chapter 5: Optimization using Response Surface Methodology (RSM)

This chapter shows the optimisation of the adsorption process using RSM. This includes developing the multilevel factorial design, central composite design and Box Behnken design predictive models. The best-fitted models were optimised to identify the optimum pH, temperature and dosage conditions for surfactants and COD removal in carwash wastewater effluent by evaluation and verification using Design-Expert Software.

Chapter 6: Conclusion and Recommendation

This chapter follow the results significances and concludes the thesis based on the findings and outputs. Recommendations are presented based on the understanding of the research and its findings.

CHAPTER 2

Literature Review

2 Literature Review and Theory

2.1 Introduction

This chapter presents a general overview of the carwash wastewater industry in South Africa and globally, characteristics of carwash wastewater, its effect on the environment, local effluent standards and the state of fresh water supply in South Africa. This chapter includes a review of the conventional methods used to treat carwash wastewater; however, the focus will be on chemical coagulation using PFS and adsorption using granular and powdered activated carbon.

2.2 Global state of fresh water supply

It is important to have background knowledge on the global water supply to understand the importance of water reuse and recycling. It is stated that approximately 70% of the earth is covered in water; however, only 3% is freshwater. Furthermore, of that 3%, only two-thirds of that 3% is usable; the rest is either stuck in glaciers, frozen in the Arctic's or not fit for human consumption (Colvin et al., 2016). Figure 2.1 represents the current global fresh water supply.

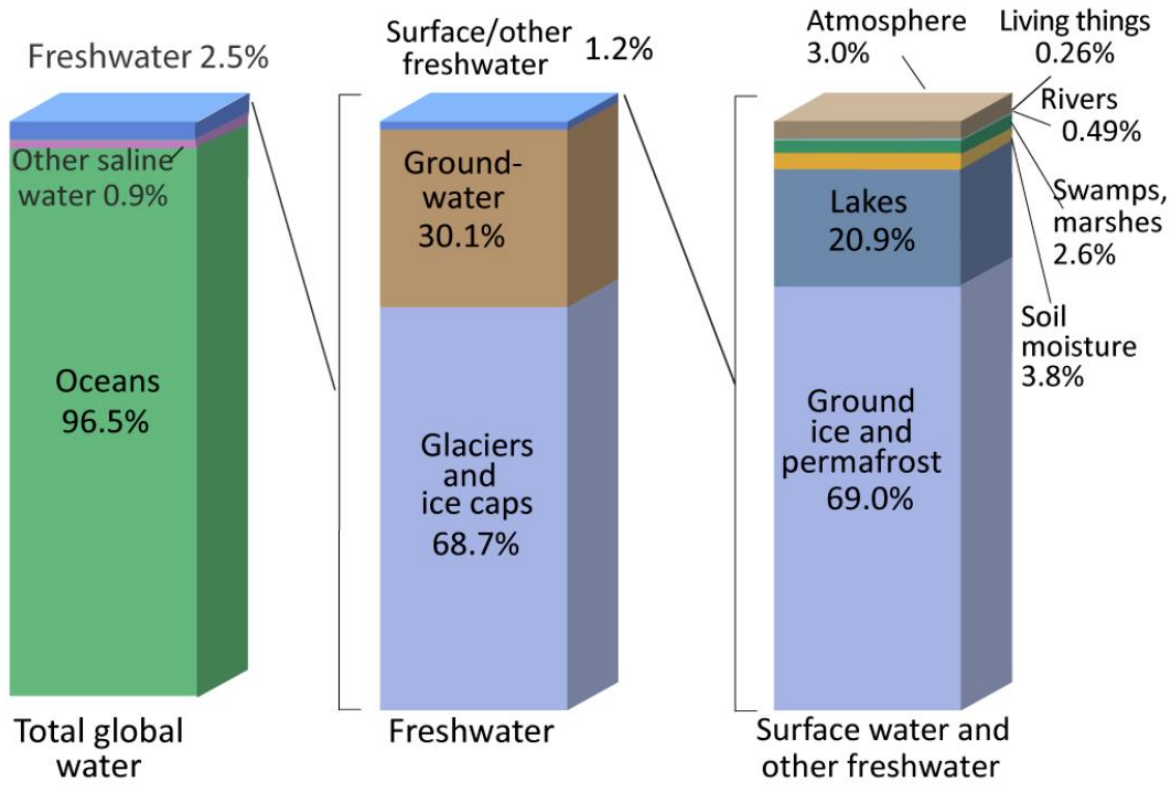

Figure 2-1: Global Water Supply *(Colvin et al., 2016)*

2.3 Fresh water supply in South Africa

Water availability in South Africa and Africa has become an increasingly prominent issue over the number of years. It is said that South Africa is considered a nation that is approaching water scarcity, and it is predicted by the year 2040, the country's water resources will be under considerable stress (Harding et al., 2017).

The water in South Africa is governed by the National Water Act (Act 36 of 1998). With the adoption of this act, the South African government recognised the need to properly manage and protect the already scarce water supplies available (RSA, 1998: 3). With the development of the NWA, water resources will be shifted from a centralised management position to a decentralised position allowing for the establishment of catchment management agencies (CMA). The catchment management agencies divided into 9 areas, previously 19, are responsible for the following:

- Develop a catchment management strategy
- Investigate and advise on the protection, use, development and control over the particular catchment water.
- Promote community participation
- Promote, coordinate and implement the catchment management strategy and plans from the water services act (RSA, 1998: 88).

The primary source of water in South Africa is rainfall. South Africa receives approximately 490mm of rainfall annually, approximately half of the world's average. In 2000 south experienced water stresses in the Oliphants, Nkomati, Thukela, Mvoti and Gouritz Water Management Areas. The national demands are expected to increase by 32% by 2030 (Bourblanc & Blanchon, 2014).

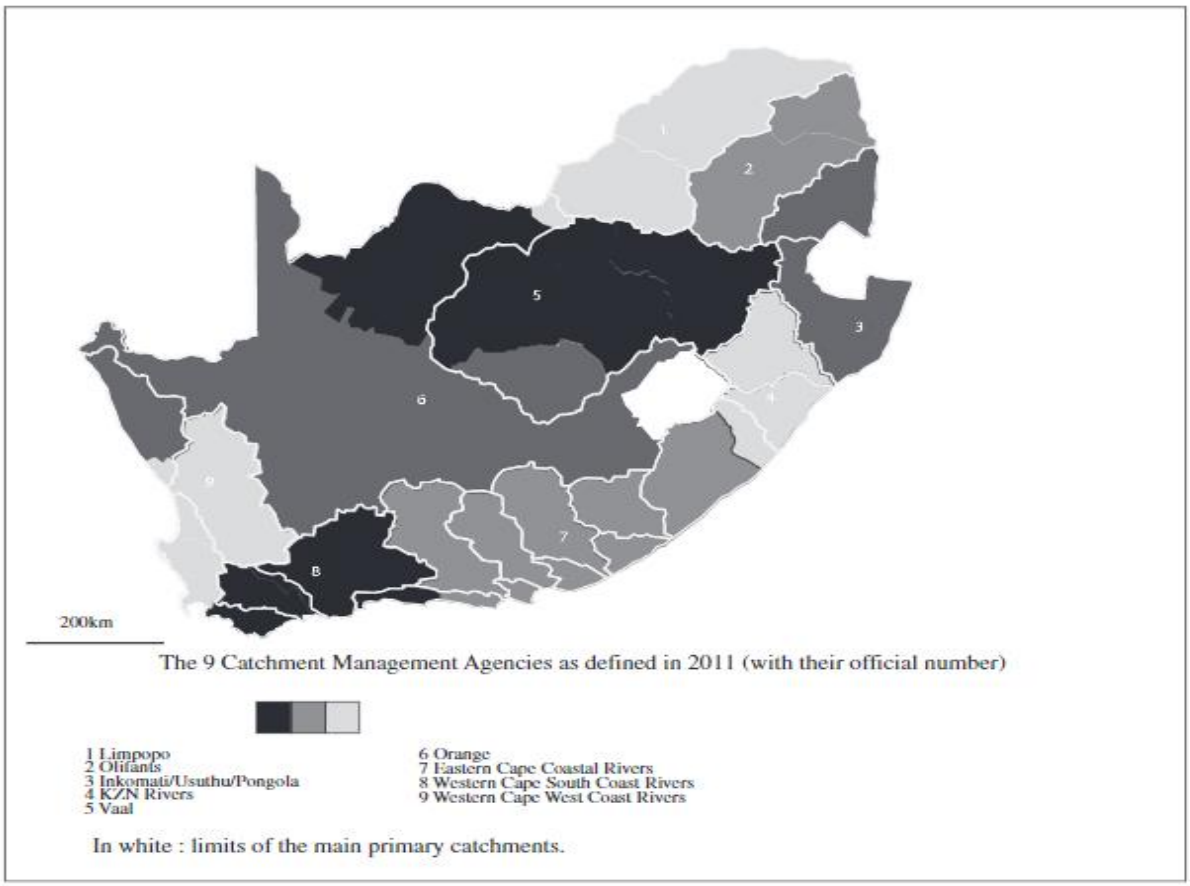

Figure 2-2: Catchment Management Areas in South Africa *(Bourblanc & Blanchon, 2014)*

The current national water resource strategy was last updated in 2013. The NWRS aims to ensure national water resources are managed towards achieving growth for 5 to 10 years. The NWRS is the legal implementation or operation for the National Water Act. According to the NWRS South Africa is considered a water stressed country and are faces various challenges and concerns including the security of water supply, environmental degradation and resource pollution (Department of Water Affairs and Forsetry, 2013). Figure 2.2 represents the catchment management areas in South Africa.

South Africa faces various types of water issues such as:

- Water scarcity: South Africa has low rainfall levels compared to the world average coupled with high evaporation rates due to the hot climate. South Africa also experiences growing challenges from increasing water pollution.
- Water Demand: South Africa currently can meet water demand however there is less water per person than other drier countries like Namibia and Botswana.

- Water Quality: South Africa faces serious water quality challenges with the main contributors to poor water quality being the mining sector, urban development, industries and agriculture.
- Inefficient water resources use: South Africa faces high wastage and inefficient use, with various municipalities reporting non-revenue water sits at 37% on average (Department of Water Affairs and Forsetry, 2013). The WRC reports that a further 25% of the 37% are losses due to physical leakage. They further state that this approximately adds up to 7 billion rand annually in non-revenue water (McKenzie et al., 2012). Figure 2.3 represents the water reconciliation in South Africa.

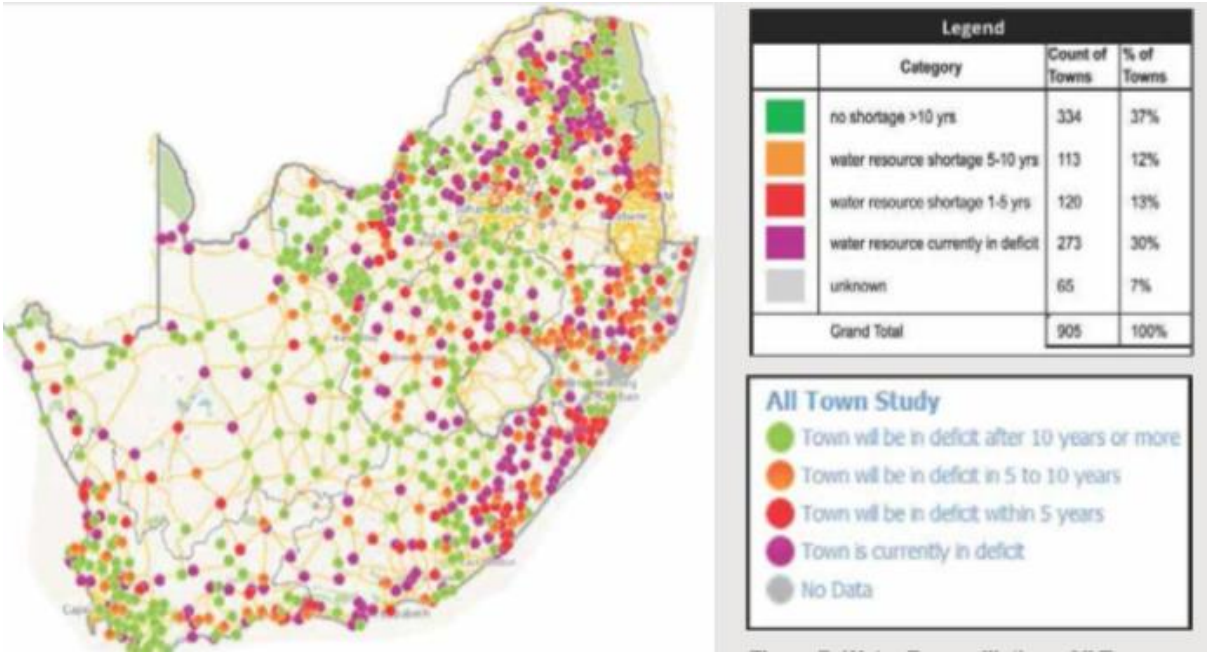

Figure 2-3: Water Reconciliation in South Africa (Department of Water Affairs and Forsetry, 2013)

2.4 Water usage in South Africa

The estimated urban and rural water demand in 2000 in South Africa was estimated at approximately 3471 million m^3/year. The WRC also states that South Africa has a high consumption of litres per capita per day, which is currently above the world average, highlighting the inefficient water use and becoming a growing concern for the government. Figure 2.4 represents the water usage from different sectors in South Africa.

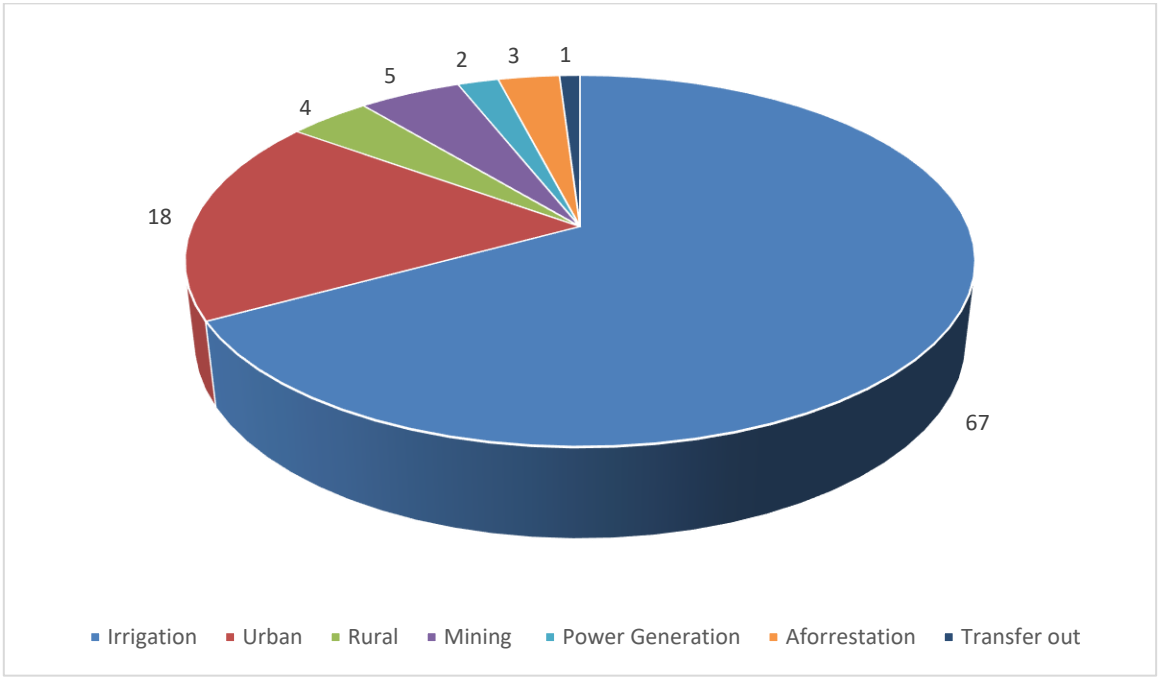

Figure 2-4: Water Usage from Different Sectors in South Africa (Department of Water Affairs and Forsetry, 2013)

The WRC report done in 2012 has highlighted the vast amount of water wastage in South Africa. The most glaring issue highlighted is the current non-revenue water percentage for South Africa which is in line with the world average. South Africa, however, cannot afford water losses of this magnitude being the 30th driest country in the world. The report also highlights poor infrastructure with many municipalities, poor revenue recovery and severe delivery backlogs. The high estimated per capita consumption highlights large volumes of water wastage within households around the country showing a lack of education and knowledge amongst the people of South Africa and presents an opportunity for government to educate the people on the importance of water and saving it (McKenzie et al., 2012).

The reuse of wastewater could provide an alternative or form part of the solution to water crisis currently happening in South Africa. Water reuse will drastically reduce the number of contaminants released into the environment or surface waters, and it is imperative to consider

water reuse as a tool to overcome current and future water shortage challenges in South Africa.

2.5 National Water Act Effluent Standards (Act 36 of 1998)

The national water act was established in 1998. The national water act states that wastewater is any liquid waste whether or not containing matter in solution or suspension and includes domestic wastewater and industrial effluent but excludes stormwater (South Africa, 2000).
Carwash services are considered commercial activities according to the classification of all economic activities published by the central services in 1993. Carwash services would thus fall under the sub-category of business services and transport. Thus, carwash wastewater discharge should follow the acts guidelines (South Africa, 1998).
The maximum limits of permitted discharges, relevant to this research project, are given in Table 2.1. The whole table with all the parameters, as per the By-law, can be found in Appendix A.

Table 2-1: Maximum limits of permitted discharges (South Africa, 1998)

Parameter	**Unit**	**Not less than**	**Not to exceed**
Temperature at point of entry	°C	0	40
Electrical conductivity at 25°C	mS/m		500
pH Value at 25°C		5.5	9.5
Chemical Oxygen Demand	mg/l		75
Soaps	mg/l		2.5
Oils, greases, waxes and fat	mg/l		2.5

2.6 Car wash wastewater characteristics

There are many different carwash stations cleaning vehicles of different makes and models and vehicles travelling through different geographical regions throughout the world; therefore, it is impossible to provide a distinguished composition of carwash wastewater. Generally, there is a wide variety of pollutants within carwash wastewater due to different chemicals being used to clean the cars, the type of dirt found on the car depending on the geographical region of the vehicle, the type of water used for cleaning and the make and model of the vehicle. The contaminants in carwash wastewater vary from organic and inorganic substances, heavy metals and microorganisms (Kumar & Chauhan, 2018.). (Rubí-Juárez et al., 2015) also states that in addition to detergents and dirt there are varying quantities of grease, oil, emulsified oil, heavy metals and organic pollutants which has the potential to foul or pass through traditional municipal wastewater treatment processes causing harm to the environment The types of pollutants commonly found in carwash wastewater can originate from various sources such as traffic, road surfacing, atmospheric pollutants, parts of the car such as brakes and rust, different carwash chemicals as exhaust particles (Hashim & Zayadi, 2016).

2.7 Why treat carwash wastewater?

The main reason for recycling carwash wastewater is environmental concerns and water conservation; as mentioned before, carwash wastewater contains high volumes of contaminants not suitable for disposable into the environment. Carwash wastewater contains high COD levels, BOD and high levels of heavy metals such as zinc and leads, making it unsuitable for disposable into the environment with treatment. Another concern with carwash wastewater is the sheer volume of wastewater produced. An estimated that 35 billion litres of wastewater are produced annually by carwash stations. This high volume of waste can thus be recycled, thus reducing the strain on the supply of freshwater worldwide.

2.8 Carwash wastewater treatment technologies

2.8.1 Membrane Technology

Membrane technology is one of the most common and effective ways of producing high-quality water for reuse. The most common membrane treatment technologies are, but not limited to, microfiltration, ultrafiltration, nanofiltration, and reverse osmosis. Membranes are classified concerning the material it is made out of, the driving force, the separation mechanism and the nominal size of separation achieved(Jiang et al., 2017). Previous studies performed using car wash wastewater with membrane technology have been used in conjunction with other treatment processes where membrane technology would be considered the primary treatment. The main reason for a pre-treatment is membrane fouling which severely affects membranes (Boussu et al., 2007).

2.8.2 Screening

A screen is a device with uniform size openings used to retain coarse materials in the wastewater. This process is beneficial for removing particles that can cause damage to process equipment. Screening is a preliminary treatment to remove heavy particles from wastewater (Moazzem et al., 2018).

2.8.3 Flotation

Flotation is a unit operation used to separate solid or liquid particles by introducing fine gas bubbles into the liquid phase. The primary advantage flotation has over sedimentation is the

time it takes to remove small or light particles, where flotation does this in a relatively short time. The process of flotation is generally used in oily wastewater applications. The disadvantage of this is that it produces scum which needs to be removed manually(Zaneti et al., 2013).

2.8.4 Ozonation

Ozone is regarded as an effective oxidizing agent widely used to treat wastewater processes to decompose dissolved compounds. In the process, reactive oxygen species are produced, which reacts with organic compounds and microorganisms. Ozonation can be used anywhere in water treatment, depending on the process's requirements or the desired product. It is an efficient process for disinfection and removing odour and colour, causing compounds as it can degrade the organic and inorganic pollutants(Rodriguez Boluarte et al., 2016).

2.9 A summary of various research based on different technologies carried out for carwash wastewater.

Table 2-2: Different carwash wastewater treatment processes

Technology	Material	Water	Parameters mg/l	Results %	Reference
Nanofiltration	NF 270	CWW	COD,TDS, Conductivity, Turbidity	70-91, 60, 60, 92	(Lau et al., 2013)
Ultrafiltration	UF PVD100	CWW	COD,TDS, Conductivity, Turbidity	56-82, 13.6-35.4, 13.6-35.4, 92	(Lau et al., 2013)
Ultrafiltration	UF PES30	CWW	COD,TDS, Conductivity, Turbidity	55-83, 13.6-35.4, 13.6-35.4, 92	(Lau et al., 2013)
Ultrafiltration	PVDF	CWW	TSS, FOG, TOC, COD, TDS	100, 98, 60, 62, 98	(Karakulski, 2003)
Ultrafiltration	PVC	CWW	TSS, FOG	100, 98	(Karakulski, 2003)
Ultrafiltration	PAN	CWW	TSS, FOG	100, 98	(Karakulski, 2003)
Ultrafiltration	Zirconium oxide ceramic membrane	CWW	Turbidity, COD,TDS	40, 20, 100	(Moazzem et al., 2018)
Reverse Osmosis	Spiral Wound	CWW	Turbidity, COD, TDS	70, 90, 0	(Moazzem et al., 2018)

Chemical Coagulation	Ferrous Chloride	CWW	Turbidity, COD	34, 65, 93	(Moazzem et al., 2018)
Coagulation and ozonation	PAC	CWW	COD, Turbidity	99%, 67%	(Rodriguez Boluarte et al., 2016)
MBR	AMBR	CWW	TSS, COD, Ammonia, COD	100%, 99.7%, 97.3%, 41%	(Rodriguez Boluarte et al., 2016)
Electrocoagulation and Electrochemical oxidation	Boron Doped Diamond and lead dioxide	CWW	COD	97%	(Panizza & Cerisola, 2010)
Chemical and electrical coagulation	PAC, Aluminium Electrodes	CWW	COD, BOD, TSS, MBAS	96%, 94%, 98%, 98%	(Bazrafshan et al., 2012)
Ultrafiltration, flocculation and activated carbon	CA hollow fibre membrane, blended flocculent with bentonite and $(Al_2SO_4)_3$	CWW	COD, BOD, Turbidity, TSS, Hardness, Na ions, Cl ions	50%, 46%, 99.9%, 99%, 0%, 0%, 0%	(Mazumber & Mukherjee, 2011)
Coagulation	Alum,	CWW	Oil and grease	100%	(Mazumber & Mukherjee, 2011)
Activated sludge	Suspended biomass	CWW	Oil and grease	70%	(Mazumber & Mukherjee, 2011)
Chemical Coagulation	Strychnos Potatorum	CWW	Turbidity	93%	(Al-Gheethi et al., 2016)

2.10 Treatment technologies used in this study

This research will focus on the following treatment processes

- Chemical Coagulation using PFS

Chemical coagulation is a widely used process in wastewater treatment. The main objective of this process is to reduce suspended solids and to remove organic matter. Chemical coagulation is typically used a primary treatment method as is used in this study. The coagulant used within this process is polyferric sulphate (PFS). PFS is a polymer coagulant and is widely used within the field of wastewater treatment. In this study PFS was synthesized according to the process prescribed by (Jiang & Graham, 1998b). The coagulant was used to treat CWW for the removal of COD, FOG and anionic surfactants. The process parameter looked at is coagulant dosage.

- Adsorption using Activated Carbon

The process of adsorption is commonly used process in wastewater treatment and is considered one of the most effective treatment methods available. Adsorption in this study was used as a secondary treatment to chemical coagulation. The adsorbent used in this study was powdered activated carbon (PAC) provided by a company called Rotocarb. In this study PAC was used to treat CWW for the removal to remove FOG, COD and anionic surfactants. The process parameters looked at were temperature, adsorbent dosage and wastewater pH

2.11 Coagulation/Flocculation

Chemical Coagulation is a process by which a chemical, known as a coagulant, is added to the water through rapid mixing to destabilize particles in the water after which the particles can stick together forming larger particles (Moazzem et al., 2018). In wastewater treatment chemical coagulation is generally used as a pre-treatment step to other types of treatments such as membrane technology or electrochemical methods.

In the process of coagulation/flocculation, there are many choices of coagulants, which play a significant role in the contaminants removed from the wastewater. There are also various coagulants such as inorganic, organic coagulants and natural coagulants (Fagundes-klen & Dotto, 2019). The most used chemical coagulants are inorganic coagulants such as aluminium and iron salts. Inorganic coagulants are the most widely used due to their availability which is better than most other coagulants available.

However, there is a significant issue with the use of inorganic coagulants in that it produces copious amounts of toxic sludge, which is harmful to the environment and humans. In recent studies, natural coagulants have been compared to inorganic coagulants. The main upside of using natural or plant-based coagulants is that no harmful sludge is being produced. The main plant-based coagulants being looked at are Moringa Oleifera and Nirmali seeds (Vijayaraghavan, G.; Sivakumar, 2011). In a study performed by Maya et al. (2014), the results showed that the natural coagulants produced a turbidity removal of over 90% whereas the commercial coagulants produced a removal of 80% at lower dosages but produced a much lower COD removal than the commercial coagulants

2.12 Pre polymerized coagulants

Chemical coagulation represents a fundamental part of the water treatment process. When chemical coagulation is carried out, a chemical coagulant is required. The most common coagulants used are Fe (III) salts. Generally, the Fe (III) coagulant is added directly to the water to be treated in concentrated liquid without any pre-treatment, ferric ions then hydrolyse in the water, producing a range of Fe (III) species which play an essential role in coagulation. The chemistry of Fe (III) salts revealed many factors that play into the speciation and precipitation kinetics of Fe (III) solutions, such as the anions in solution, the ratio of the moles of base added and bound to the moles of ferric iron, OH/Fe ratio, the mixing mode of a base with the Fe (III) solution, the nature and the strength of the base, and the strength of the Fe (III) solution. Traditional applications of Fe (Ill) chemicals for coagulation do not consider these factors sufficiently enough; Fe (III) salts added to water may not form the favourable Fe (III) species that are effective in water treatment. Reformed poly ferric chemicals, formed by the controlled basification (hydrolysis) of the ferric salt solution before the addition to the water to be treated, represent an essential advancement in Fe coagulants' application. Polyferric chloride (PFC) is one example of preformed poly ferric coagulants(Jiang & Graham, 1998b). Zouboulis. (2008) states that inorganic polymeric flocculants like poly ferric sulphate are a relatively new kind of coagulant. Polyferric sulphate contains complexions like Fe2 (OH)24+ or Fe3 (OH)45+ formed by sodium hydroxide bridges and many inorganic macromolecular compounds. The presence of polymeric species allows the PFS species to carry a high cationic charge, which improves the charge neutralisation capacity and becomes more effective than other conventional coagulants at a comparatively lower dosage. The author also reports that PFS exhibits greater efficiency in removing COD, BOD and turbidity than other conventional iron-based coagulants.

2.13 Synthesis of PFS

The synthesis of polyferric sulphate explained by Zouboulis et al. (2008) begins with ferrous sulphate oxidation to ferric sulphate in highly acidic conditions. The acid of choice used for the oxidation process is 96% sulphuric acid. The ferrous sulphate along with the water and sulphuric acid is placed in a reactor with a controlled temperature and mixing rate to allow for the oxidation of ferrous sulphate to ferric sulphate. The oxidising agent can either be nitric acid or hydrogen peroxide. Equation 2.1 shows the oxidation of ferrous sulphate to ferric sulphate.

$$FeSO_4 + \frac{1}{2}SO_4^{2-} + oxidising\ Agent \rightarrow \frac{1}{2}Fe_2(SO_4)_3$$

Equation 2-1

Zouboulis et al. (2008) go on to explain that after oxidation hydrolysis must occur. When the acid is limited, a hydroxide ion will replace the sulphate ion during hydrolysis and thus polymerisation will occur. A base of concentration of 0.5-2.5M must be added to the ferric solutions in order to produce hydrolysis. The bases used for the process of hydrolysis are either sodium hydroxide or sodium bicarbonate. Equation 2.2 shows the hydrolysis of ferric sulphate.

$$Fe_2(SO_4)_3 + nOH^- \rightarrow Fe_2(OH)_n\ (SO_4)_{3-\frac{n}{2}} + \frac{n}{2}SO_4^{2-}$$

Equation 2-2

Equation 2.3 shows the polymerisation process to form polyferric sulphate

$$mFe_2(OH)_n\ (SO_4)_{3-\frac{n}{2}} \rightarrow (\ Fe_2(OH)_n\ (SO_4)_{3-\frac{n}{2}}\ )_m$$

Equation 2-3

2.14 Adsorption

According to McCabe et al. (1993), adsorption can be defined as a separation process in which specific components of a fluid phase are transferred to the surface of a solid adsorbent. The adsorbent is generally held on a fixed bed where the fluid is continuously passed until the solid is saturated.

Most adsorbents are porous materials, and adsorption primarily occurs on the pores' walls or specific sites inside the particle. Separation occurs because of differences in molecular weight, shape and size or polarity, which causes some molecules to be held more strongly than others do on the surface. The adsorbing components are held strongly enough such that complete removal of the component occurs with minimal removal of other components. The regeneration of adsorbent can obtain the adsorbate in a nearly pure form (McCabe et al., 1993).

Applications of liquid-phase adsorption include removing organic compounds from water or organic solutions, coloured impurities from organics and various fermentation products from fermenter effluents. Separation includes paraffin from aromatics and fructose from glucose using zeolites. The gas phase adsorption applications include the removal of water from hydrocarbons and sulphur from natural gas (Geankoplis, 2003).

2.15 Activated Carbon

Activated carbon can be described as an amorphous carbonaceous material that exhibits a high degree of porosity and extended particle surface area. Activated carbon can be obtained in granular and powder form. The granular activated carbon contains a large internal surface area and tiny pores, whereas powdered activated carbon has large pore diameters and small internal surface areas. Active carbons are versatile adsorbents being used for various purposes, such as removing undesired odour, colour and taste; various organic and inorganic pollutants from domestic and industrial wastewater in the food and chemical industries mention a few of its uses(Bansal & Goyal, 2005).

2.15.1 Physiochemical properties of activated carbon

Activated carbon is an excellent adsorbent because of its wide range of application and excellent adsorbent abilities. However, activated carbon needs to have good physical and chemical properties in order to perform adsorption effectively. The desired properties of

activated carbon are characterized by well-developed pore structure, high surface area, low ash content and greater adsorption capacity (Mutegoa et al., 2014).
Activated carbon is considered one of the most effective media for removing of a wide range of contaminants from industrial and municipal wastewaters, landfill leachate and contaminated groundwater. As one of the most potent adsorbents activated carbon can remove multiple pollutants in the same water flow or be used to remove a specific pollutant in a multistage process (Tchobanoglus et al., 2003). Activated carbon is produced from different raw materials which affect the properties of the activated carbon. Apart from the raw materials, the specific process employed to make the activated carbon also affect its properties (De Gisi et al., 2016).

2.15.2 Low-Cost Adsorbents

Low-cost adsorbents made from the by-products of agricultural, household and industrial sectors have been a sustainable solution for wastewater treatment. Using low-cost adsorbents from waste materials allows for the removal of pollutants from wastewater and contributes to waste minimization, recovery, and reuse (Lofrano, 2012).
A large variety of low-cost adsorbents have been used and tested for their ability to remove various types of pollutants from water and wastewater. The overall aim of this would be to replace activated carbon (De Gisi et al., 2016).

2.16 Surfactants

Surface-active substances more commonly known as surfactants are amphiphilic compounds having a lyophilic, in a particular hydrophilic, part and a lyophobic, in a particular hydrophobic part. Surfactants can be classified into non-ionic and ionic which can, either anionic, cationic, amphoteric and zwitterionic nature according to the polar group (Möbius et al., 2001). Surfactants are essential ingredients in a large number of processes and many human activities. In present-day detergent products, surfactants account for approximately 15-25% of the total production with a production of approximately 9 million tons. Figure 2.5 illustrates a surfactant.

Figure 2-5: Illustration of surfactant (Kronberg, 2014)

2.16.1 Non-ionic surfactants

Non-ionic surfactants are amphiphilic compounds where the lyophilic, particularly the hydrophilic, art does not dissociate into ions has no charge. However, there are exceptions to this, such as tertiary amine oxides, which can charge specific pH values. Other non-ionic surfactants, such as long-chain carboxylic acids, are non-ionic under neutral and acidic conditions and anionic under primary conditions. Even non-ionic surfactants such as various polyether's are protonated in acidic conditions and exist in cationic form. Therefore, it can be said that non-ionic surfactants are those that have no charge in the predominant pH working range(Möbius et al., 2001)..

The production of non-ionic surfactants is approximately 2 million tons per year and occupies a quarter of the world surfactant production. Non-ionic surfactants are also the most versatile surfactants produced concerning their properties, structure and fractional composition(Möbius et al., 2001). Steber. (2007) states non-ionic surfactants represent the second most relevant group of surfactants in cleaning products by volume, with the most important representative being alcohol ethoxylates.

2.16.2 Mechanisms of surfactant Adsorption

Adsorption can be interpreted as partitioning of the adsorbate species between the interface and the bulk solution, this occurs if the surfactant favours the interface instead of the bulk solution. The following equation can describe the Adsorption density in the stern plane:

$$\Gamma_{\delta} = lCexp\left(\frac{-\Delta G^{0}_{ads}}{RT}\right)$$

Equation 2-4

Where l is the effective chain length, C is the bulk surfactant concentration, R is the gas constant, T is the absolute temperature and $-\Delta G^{0}_{ads}$ the standard free energy of adsorption. The standard free energy of adsorption is described as the sum of all the contributing or driving forces (Zhang & Somasundaran, 2006).

2.16.3 Driving forces of surfactant adsorption

a) Electrostatic interactions

Electrostatic interactions appear in systems with ionic surfactants and solid charged particles and play a governing role in adsorption.

b) Chemical interactions

Chemical interactions are a vital driving force in the adsorption of surfactants on solid surfaces. This interaction is specific to systems where covalent boding occurs between the solid surface and the surfactant.

c) Hydrophobic lateral interactions

Surfactants tend to form two dimensional aggregates at the solid-liquid interface, causing increased adsorption density; these aggregates are known as hemi-micelles or colloids. These aggregates are formed at concentrations above a threshold value.

d) Hydrophobic interaction between the hydrocarbon chains and hydrophobic sites on the solid

Hydrophobic interactions occur between the alkyl chain of the surfactant and the hydrophobic sites on the solid. These interactions are significant when adsorption occurs on fully or partially hydrophobic surfaces. These types of adsorption results in two-step isotherms.

e) Hydrogen Bonding

Hydrogen bonding could occur in systems where the surfactant species contains hydroxyl, phenolic, carboxylic and amine groups. An example in which hydrogen bonding could occur is the adsorption of nonionic surfactants such as ethoxylated alcohol. However, for hydrogen bonding to occur, the bond formed between surfactant functional groups and mineral surfaces should be more robust than those bonds formed between the mineral surface and interfacial water molecules.

f) Desolvation Energy

In the case a hydrated head group of a surfactant species transfers from the bulk to mineral solution interfacial region, partial removal of water from the secondary solvation shell around the surfactant head groups can occur. However, desolvation energy due to such processes is unfavourable for adsorption in contrast to other driving forces.

2.16.4 Adsorption of non-ionic surfactants

The adsorption of nonionic surfactants usually is reversible. Most non-ionic surfactants contain polar surfactant concentration, molecular structure (EO number and hydrocarbon chain length), temperature and electrolyte. Sugar-based surfactants form a novel class of environmentally benign non-ionic species compared to EO surfactants. The adsorption of nonionic surfactants depends on the number of hydrophilic groups and the hydrocarbon chain length. The saturation adsorption density is lower for molecules with a high degree of ethoxylation because of the increase in each molecule's packing area on the solid surface with the degree of ethoxylation. Similarly, the sugar-based head group's polymerisation degree also determines its saturation adsorption density(Zhang & Somasundaran, 2006) .

2.17 Adsorption Equilibria

If the adsorbent and adsorbate are contacted long enough, equilibrium will be established between the amount of adsorbate adsorbed and the amount adsorbate in solution. The equilibrium relationship is described by adsorption isotherms (Hill, 1952).

During the process of adsorption two main mechanisms are involved, namely physical adsorption and chemical adsorption. Physical adsorption occurs due to weak van der Waals forces while chemisorption occurs due to the formation of strong bonds between the solute and the adsorbent involving the transfer of electrons (Kajjumba et al., 2018).

The amount of pollutant adsorbed at equilibrium can be calculated using the following equation:

$$Q_e = \frac{(C_o - C_e)V}{m}$$

Equation 2-5

Where, q_e is the amount of pollutant adsorbed on the adsorbent at equilibrium (mg/g), C_o is the initial concentration of the pollutant in solution (mg/l), C_e is the concentration of the

pollutant in solution at equilibrium (mg/l), m is the mass of adsorbent used (g) and V the volume of pollutant solution (Bedin et al., 2016).

2.18 Adsorption Isotherms

The best method to study the effectiveness of the process is through mathematical models known as adsorption isotherms. The data collected from an experiment can thus be tested against various isotherms to determine the given data's best fit model. The purpose of these isotherms is to predict and compare adsorption performance, which is essential when designing an adsorption system, e.g., choosing equipment. Adsorption isotherms describe equilibrium relationships that describe how the pollutants interact with the adsorbent materials and thus are essential for optimising mechanism pathways, expression of surface properties and the capacity of the adsorbent(Ayawei et al., 2017).

An adsorption isotherm is described as an invaluable curve describing the phenomenon governing the retention (or release) or mobility of a substance from the aqueous porous media or aquatic environments to a solid-phase at a constant temperature and pH (Limousin et al., 2007). Adsorption equilibrium (the ratio between the adsorbed amount with the remaining in the solution) is established when an adsorbate containing phase has been in contact with the adsorbent for a sufficient time, with its adsorbate concentration in the bulk solution is in a dynamic balance with the interface concentration (Allen et al., 2004). Typically, the mathematical correlation, which constitutes a vital role towards the modelling analysis, functional design and applicable practice of the adsorption systems, is usually depicted by graphically expressing the solid-phase against its residual concentration (Ncibi, 2008). Its physicochemical parameters and the underlying thermodynamic assumptions provide an insight into the adsorption mechanism, surface properties, and the degree of affinity of the adsorbents (Ghiaci et al., 2004). As the insight into adsorption increased, a wide variety of equilibrium isotherm models (Langmuir, Freundlich, Brunauer–Emmett–Teller, Redlich–Peterson, to mention a few.) have been formulated in terms of three fundamental approaches. Kinetic consideration is the first approach to be referred (Foo & Hameed, 2010). In the first approach, adsorption equilibrium is defined as a dynamic equilibrium state, where both adsorption and desorption rates are equal(Langmuir, 1916). In thermodynamics, being the second approach, the base can provide a framework for deriving numerous forms of adsorption isotherm models (Myers & Prausnitz, 1965). The Potential theory being the base for the third approach, conveys the main idea in the generating characteristic curves (Dubinin, 1960). However, an exciting trend in isotherm modelling is the derivation in more than one approach, thus directing the difference in the physical interpretation of the model parameters (Foo & Hameed, 2010).

2.18.1 Langmuir Isotherm

The Langmuir adsorption isotherm was first developed to describe gas–solid-phase adsorption onto activated carbon and has conventionally been used to quantify and differentiate different bio-sorbents (Langmuir, 1916). The Langmuir model assumes monolayer adsorption (the adsorbed layer is one molecule in thickness), where adsorption can only occur at a finite (fixed) number of definite localized sites, which are identical and equivalent, with no lateral interaction and steric hindrance between the adsorbed molecules, even on adjacent sites (Vijayaraghavan et al., 2006). In its derivation, Langmuir isotherm refers to homogeneous adsorption, which each molecule possesses constant enthalpies and sorption activation energy (all sites possess equal affinity for the adsorbate), with no transmigration of the adsorbate in the plane of the surface. Graphically, it is characterized by a plateau, an equilibrium saturation point where once a molecule occupies a site, no further adsorption can occur (Foo & Hameed, 2010). The mathematical expression of Langmuir isotherm model is represented in equation 2.6:

$$q_e = \frac{q_m K_L C_e}{1 + K_L C_e}$$

Equation 2-6

Where C_e is the equilibrium solution concentration (mg/g), K_L is the Langmuir constant related to the affinity of binding sites (L/mg), q_e is the amount of pollutant adsorbed at equilibrium (mg/g) and q_m represents the limiting adsorption capacity (mg/g) which allows for the comparison of adsorption performance (Chiou & Li, 2002). K_L and q_m can be determined from the linearized form of equation 2.6 as shown below in equation 2.7:

$$\frac{C_e}{q_e} = \frac{1}{q_m} C_e + \frac{1}{K_L q_m}$$

Equation 2-7

C_e/q_e versus C_e's linearized plot gives a straight where the slope is $1/q_m$ and the intercept is $1/K_L q_m$. The Langmuir isotherms essential characteristics can be expressed by a dimensionless constant called the separation factor R_L. The values of R_L indicates whether adsorption is favourable when $0 < R_L < 1$, unfavourable when $R_L > 1$ and linear when $R_L = 1$ (Ayawei et al., 2017).

$$R_L = \frac{1}{1 + K_L C_o}$$

Equation 2-8

2.18.2 Freundlich Isotherm

Freundlich isotherm is the earliest known relationship describing the non-ideal and reversible adsorption, not restricted to monolayer formation. This empirical model can be applied to multilayer adsorption, with non-uniform distribution of adsorption heat and affinities over the heterogeneous surface. Historically, carbon adsorption is developed, demonstrating that the adsorbate ratio onto a given mass of adsorbent to the solute was not a constant at different solution concentrations. In this perspective, the amount adsorbed is the summation of adsorption on all sites (each having bond energy), with the more critical binding sites are occupied first, until adsorption energy is exponentially decreased upon the completion of the adsorption process. Freundlich isotherm is widely applied in heterogeneous systems, especially for organic compounds or highly interactive species on activated carbon and molecular sieves. The slope ranges between 0 and 1 consist of adsorption intensity or surface heterogeneity, becoming more heterogeneous as its value gets closer to zero. Whereas a value below unity implies chemisorption's process where 1/n above one is indicative of Cooperative adsorption (Adamson & Gast, 1967)

$$q_e = K_f C^{\frac{1}{n}}$$

Equation 2-9

The linearized form of the Freundlich equation is as follows:

$$log q_e = log K_F + \frac{1}{n} log C_e$$

Equation 2-10

Where K_F is the adsorption capacity (L/mg) and 1/n is the adsorption intensity. It also indicates the relative distribution of energy and heterogeneity of adsorbate sites (Ayawei et al., 2017)

2.18.3 Temkin isotherm

The Temkin isotherm model considers the effects of the adsorbate/adsorbent interactions during the adsorption process while ignoring very low and very high concentration values (N'diaye & Kankou, 2020). The model also assumes that adsorption heat is a function of temperature, of all molecules in the layer declines linearly rather than logarithmically due to increased surface coverage (Foo & Hameed, 2010). The Temkin model can be expressed both linearly and non-linearly as seen in equations 2.11 and 2.11 respectively:

$$q_e = \frac{RT}{b} \ln (KC_e)$$

Equation 2-11

$$q_e = B_T lnK + B_T lnC_e$$

Equation 2-12

where q_e is the equilibrium adsorption capacity (mg/g), R is the universal gas constant (J/mol.K) and T is the absolute Temperature (K), b is the Temkin isotherm constant and C_e is the equilibrium concentration (mg/l).

2.18.4 Dubinin-Radushkevich isotherm

The Dubinin-Radushkevich (D-R) isotherm is an empirical model generally used to express the adsorption mechanism with a Gaussian energy distribution onto a heterogenous surface. This model is generally used to distinguish the physical and chemical adsorption of metal ions (Al-Ghouti & Da'ana, 2020). Unlike Langmuir and Freundlich models, this model is semiempirical and the adsorption mechanism follows pore fitting. The D-R isotherm has both linear and non-linear forms and can be seen in equations 2.13 and 2.14, respectively.

$$qe = qs - e^{K^2}$$

Equation 2-13

$$\ln (qe) = qs - K^{e^2}$$

Equation 2-14

Where q_e is the equilibrium adsorption capacity (mg/g), q_s is the adsorption capacity at time t (mg/g), K is the D-R isotherm constant (mol^2/J^2) and ε is the Polanyi potential (J/mol). The type of adsorption is predicated by the parameter E_D (mean free adsorption energy) and calculated using equation 2.16. Furthermore, ε can be calculated using equation 2.15 where C_e is the equilibrium concentration (mg/l), R is the universal gas constant (J/mol.K) and T is the absolute Temperature (K). Determining the adsorption potential (ε) is an essential step for utilizing the D-R isotherm model. It reflects the Gibbs free energy change of the adsorbent after adsorption for a unit of the used adsorbate's molar mass (Zhou, 2020).

$$\varepsilon = RTln(1 + \frac{1}{C_e})$$

Equation 2-15

$$E_D = \sqrt{\frac{1}{2K}}$$

Equation 2-16

2.19 Adsorption kinetics

Adsorption kinetics are amongst the main factors that must be understood before the applicability of any adsorbent. In all adsorption processes, linear or non-linear analysis of the kinetics are applied. Adsorption kinetics are important because they determine the rate at which adsorption occurs. Adsorption kinetics is a curve or line that describe the retention rate from an aqueous environment to the solid phase interface at a given pH, temperature, adsorbent dosage and flow rate. Adsorption kinetics are influenced by surface complexity of the adsorbent, solute concentration and flow. Pseudo first order, pseudo second order, Elovich and intra particle models are a few of the kinetics that describes the interaction between the adsorbent and adsorbate.

2.19.1 Pseudo first order model (PFO)

PFO models describes the adsorption of solute onto the adsorbent following first order mechanisms (Kajjumba et al., 2018):

$$\frac{dq_t}{dt} = k_f(q_e - q_t)$$

Equation 2-17

Where q_t is the adsorbate adsorbed onto the adsorbent at a time t (mg/g), q_e is the equilibrium adsorption capacity (mg/g), k_f is the rate constant (per min). The integral of the equation from t = 0 to t = t and q_t = 0 to qt = qt:

$$ln(q_e - q_t) = lnq_e - k_1 t$$

Equation 2-18

The rate constant k_f is found by plotting $\ln(q_e - q_t)$ vs t.

2.19.2 Pseudo second order model (PSO)

The PSO model makes the assumption that the rate of adsorption of solute is proportional to the available sites on the adsorbent and the reaction rate is dependent on the amount of solute on the surface of the adsorbent (Tan & Hameed, 2017). The driving force (q_e-q_t) is proportional to the number of available active sites, the equation for PSO is as follows (Tran et al., 2017):

$$\frac{dq_t}{dt} = k_s(q_e - q_t)^2$$

Equation 2-19

Applying the integral for t = 0 to t = t and q_t = 0 to q_t = q_t, the linearized form of the PSO is:

$$q_t = \frac{t}{\frac{1}{k_s q_e^2} + \frac{t}{q_t}}$$

Equation 2-20

The PSO constants can be determined by plotting t/q_t vs t. The PSO model assesses the impact of observable rate parameters however the model may be affected by pH, dosage, particle size and temperature. The PSO can also be used to determine the initial solute uptake and the adsorption capacity of an adsorbent. However, adsorption mechanisms cannot simply be based on the fitting of a PSO model (Qiu et al., 2009). When the solute concentration is low a PSO model best describes the adsorption mechanism however at high initial solute concentrations a PFO model is favoured. This occurs because at low C_0, the value of $\ln(q_e-q_t)$ increases exponentially increasing the error function but is the opposite for high C_0 values. Even though linear models' application has improved, they may be misleading in the development of kinetic systems. Therefore, it can be concluding that PSO and PFO models do not explain the diffusion of the solute onto the adsorbent; thus, diffusion models should first be investigated before any conclusions are drawn about the adsorption mechanism (Azizian, 2004).

2.19.3 Elovich Model

To further assess the nature of chemisorption of adsorption, the Elovich model is applied. This model helps predict the mass and surface diffusion, activation and deactivation energy of a system. Although initially applied to gaseous systems (Rudzinski & Panczyk, 2000), its applicability in wastewater treatment systems are deemed meaningful. The model assumes the rate of adsorption of the solute decreases exponentially as the amount of adsorbed solute increases (Cheung et al., 2000).

$$\frac{dq_t}{d_t} = \alpha\, exp^{-\beta q_t}$$

Equation 2-21

As $q_t \approx 0$, $\frac{dq_t}{d_t} \approx \alpha$ which is the initial adsorption rate, and β is the desorption constant. Integrating and applying the following limits t (0, t) and q_t (0; q_t) the equation becomes:

$$q_t = \frac{1}{\beta}\ln\left(t + \frac{1}{\alpha\beta}\right) - \frac{1}{\beta}\ln\left(\alpha\beta\right)$$

Equation 2-22

As the system approaches equilibrium where t >> $\frac{1}{\alpha\beta}$ the equation becomes:

$$q_t = \frac{1}{\beta}\ln(\alpha\beta) + \frac{1}{\beta}\ln\left(t\right)$$

Equation 2-23

The graph of q_t vs t helps determine the nature of the adsorption whether chemisorption or not

2.19.4 Intra particle diffusion model (IP)

The IP model has been widely used to determine the rate-limiting step during adsorption. The solute's adsorption in solution involves the mass transfer of the adsorbate (film diffusion), surface diffusion and pore diffusion. Film diffusion is an independent step, whereas surface and pore diffusion may co-occur. The IP is expressed as follows (Weber & Morris, 1963) :

$$q_t = K_d t^{1/2} + C$$

Equation 2-24

The k_d is the intra-particle diffusion rate constant (mg/g $min^{1/2}$), and C is the boundary layer thickness. The plot of qt vs $t^{1/2}$ gives a linear function. If the line passes through the origin, IPD controls the diffusion process; however, if it does not pass through the origin and gives multiple linear sections, these sections show that different mechanisms control the adsorption process. The first mechanism is the solute particles' mass transfer as soon as the adsorbate is placed in the water. However, this mechanism happens too fast and is not considered during the design process of kinetic systems. The second mechanism is called film diffusion and involves the slow movement of solutes from the boundary layer to the adsorbent's surface ((Kajjumba et al., 2018). When the solute reaches the adsorbent's surface, it enters the adsorbent's pores,

which is the third mechanism. Pore diffusion involves the rapid attachment of the solute to the active sites of the pores. Since the process is rapid, it is not considered during the engineering design of kinetics. If the adsorption system is characterised by small solute size, poor mixing and low concentration film diffusion becomes the controlling factor otherwise IP diffusion controls the process (Tran et al., 2017).

2.19.5 Liquid film diffusion

According to (Qiu et al., 2009) the liquid/solid adsorption system involves film diffusion, intraparticle diffusion and mass action. When physical adsorption occurs, mass action is negligible in kinetic studies due to the process's rapid nature. Therefore, the kinetic process of adsorption is always controlled by liquid film diffusion and intraparticle diffusion. According to Cooney. (1998), one of the processes should be the rate limiting step. Boyd et al. (1947) presents the film-diffusion mass transfer rate equation as follows
:

$$\ln\left(1 - \frac{q_t}{q_e}\right) = -R't$$

Equation 2-25

2.20 Adsorption Thermodynamics

When designing an adsorption system, the system's thermodynamic properties need to be extensively studied and understood. There are two types of thermodynamic properties required when designing adsorption systems, namely directly measurable properties like temperature, equilibrium constant, and properties that cannot be directly measured like Gibb's free energy, enthalpy, entropy isosteric heat of adsorption. The parameters, as mentioned earlier, are critical design variables in evaluating the performance and predicting the mechanism of an adsorption separation process and form part of the basic requirements for the characterization and optimization of an adsorption process (Saha & Chowdhury, 2011).

2.20.1 Activation Energy

Activation energy determines the temperature dependence of the reaction rate. in adsorption systems it can be defined as the energy required for the adsorbate to overcome to interact with the functional groups on the surface of the adsorbent (Saha & Chowdhury, 2011). Activation energy can be determined using the following Arrhenius equation:

$$\ln k = \ln A - \frac{E_a}{RT}$$

Equation 2-26

Where k is the adsorption rate constant, A is the frequency factor constant E_a is the activation energy (KJ/mol), R is the gas constant (8.314 J/mol.K) and T is the temperature (K). The ln(k)

versus 1/T plot gives values of E_a and A can be determined. The magnitude of the activation energy gives an idea of the type of adsorption taking place namely, chemisorption and physisorption.

2.20.2 Thermodynamic Parameters

Thermodynamic considerations of an adsorption system are important in determining whether the process is spontaneous or not. The Gibb's free energy change, ΔG^0, a chemical reaction's spontaneity, thus is an important factor. Reactions occur spontaneously at a given temperature if ΔG^0 is a negative value (Chowdhury et al., 2011). ΔG^0 is expressed as follows:

$$\Delta G° = \Delta H° - T\Delta S°$$

Equation 2-27

2.21 Error Function

Error functions are used to determine the kinetic model that best describes the interaction between the adsorbent and adsorbate (Kajjumba et al., 2018). The coefficient of correlations (R^2), sum of squared error (SSE) and the sum of absolute error (SAE) were the error functions considered for this study.

2.21.1 Coefficient of Corelation (R^2)

In most adsorption studies the coefficient of correlation is used, the R^2 value shows the degree of variability of the dependent variable which is explained by all independent variables (Al-Ghouti & Da'ana, 2020). The correlation coefficient can be found using equation 2.28:

$$\frac{\sum_{i=1}^{n}\left[q_{cal} - q_{exp}\right]^2}{\sum_{i=1}^{n}\left[q_{cal} - q_{exp}\right]^2 + \sum_{i=1}^{n}\left[q_{cal} - q_{exp}\right]^2}$$

Equation 2-28

2.21.2 Sum of Square Error (SSE)

This error function is widely used, and the magnitude of function indicates the goodness of the applied model. The only major flaw with this function is the error increases by increasing

concentration and so the model provides a better fit to the experimental data (Simsek & Beker, 2014). The SSE can be found using equation 2.29:

$$\sum_{i=1}^{n}\left[q_{cal}-q_{exp}\right]^2$$

Equation 2-29

2.21.3 Sum of Absolute Error (SAE)

This error function is similar to the SSE function and provides a better fit as the forward high concentration data (Ayawei et al., 2017). The SAE can be found using equation 2.30:

$$\sum_{i=1}^{n}\left|q_{cal}-q_{exp}\right|$$

Equation 2-30

2.22 Design of Experiments

2.22.1 Introduction

Response surface methodology (RSM) is a widely used mathematical and statistical tool used to evaluate the effects of different process variables on interest response. RSM measures optimal regional responses by using a sequence of designed experiments. The RSM implementation includes several steps, starting with selecting independent variables that affect the response. The following steps would then be to select an experimental design, conduct the experiments and finally analyze the obtained data and fit it to a polynomial function. RSM is a handy tool in reducing the required amount of experiments needed to find the optimum conditions (Isam et al., 2019). RSM with Design Expert 10 software was used to optimize COD and anionic surfactant removal via adsorption with PAC.

2.22.2 One Factor at a time

Several methods are used to optimize processed today; one such method is one factor at a time (OFAT). OFAT is a problem-solving technique to identify critical causes for an effect from a pool of potential causes. The approach is to change one variable while keeping the others constant and evaluating the process's effects(Czitrom, 1999). However, OFAT is at a disadvantage when it compares to the design of experiments (DOE). OFAT requires more resources (time, material) for information obtained. The effect of each factor is much less accurate than when using DOE. Another disadvantage of OFAT is the inability to assess factor interactions systematically. From this reasoning, it is logical to conclude that DOE is a much better solution for optimising the adsorption process

2.22.3 Factorial Design

Input variables are also known as factors and the experiments involving these factors are called factorial experiments. Each factor should have a minimum of two settings in order to explore the effect of change in each factor on the response surface. These settings are known as levels. A factorial design concerns the selection and arrangement of variable combinations in a factorial experiment (Mukerjee & Wu, 2007). There are different design approaches within the factorial design, such as full and fractional factorial designs. The fractional factorial method and the Taguchi orthogonal array exclude some of the factor-levels from the full-factorial design to achieve an optimized combination with minimum time and computational cost compared to the full-factorial method. While the full-factorial design requires a great number of expensive experiments or calculations, it offers exact results on the interaction between factors and avoids losing information on further erroneous conclusions (Cheng et al., 2012)

2.22.4 Response surface methodology

(a) Three-level factorial design

A three-level factorial design can be written as 3^K where k is represented by the factors considered at three levels each. The three-level factorial design is prohibited in terms of the total number of runs, cost and effort. However, they do provide greater accuracy in results (NIST/SEMATECH, 2012).

(b) Central composite Design

The central composite design is a rapid technique that extracts the relationship between the responses and process variables. Furthermore it may determine the optimum level of experimental factors required for a given response (Sun & Zhang, 2004). The central composite design (CCD) includes a 2^K factorial, 2^k axial and no center runs. For CCD design, two parameters must be specified (Bashiri & Farshbaf Geranmayeh, 2011).

(c) Box Behnken Design

The BBD approach is a three-level three factorial design approach. It is an independent quadratic design such that it does not contain an embedded factorial or fractional design. In this design approach, the variable combinations are at the midpoints of the process space's edges and the center. The BBD is useful when combined factor extremes should be avoided to prevent data loss (NIST/SEMATECH, 2012).

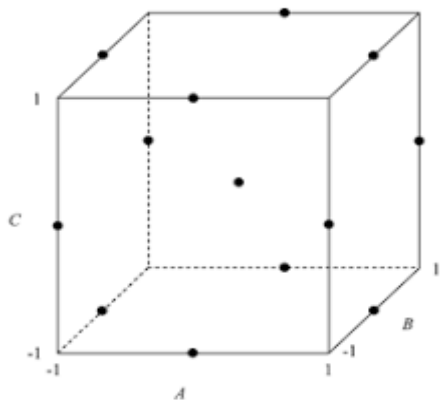

Figure 2-6: Box Behnken Cube

2.22.5 Evaluation of the design model

(a) Predicted vs actual value plot

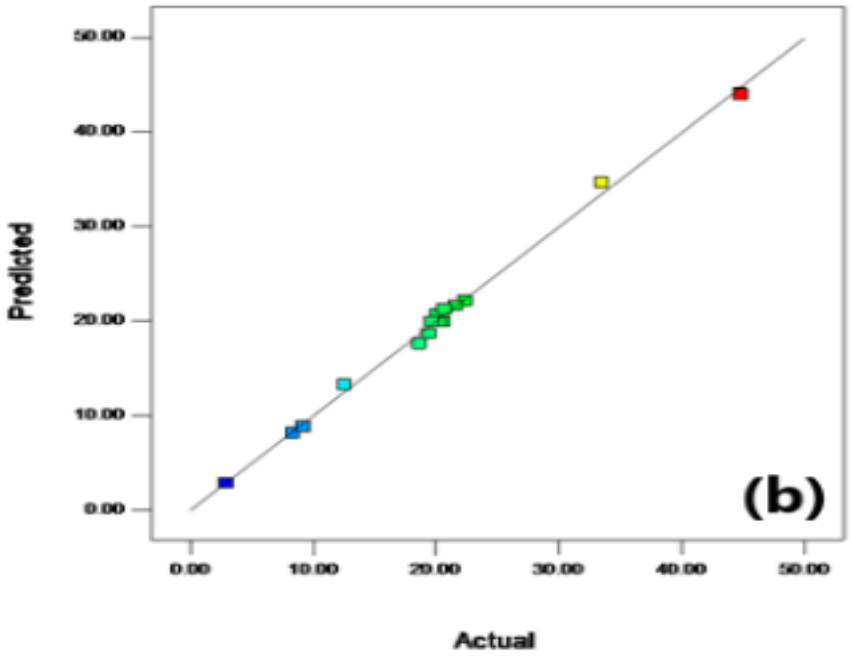

Figure 2-7: Predicted vs actual plot

The predicted vs actual plot allows for the evaluation of the model. This is done observing how close the data points are to the straight line the closer the points are the better the model. An example of such a plot is represented in Figure 2.7 (Isam et al., 2019)

(b) Residual vs predicted plot

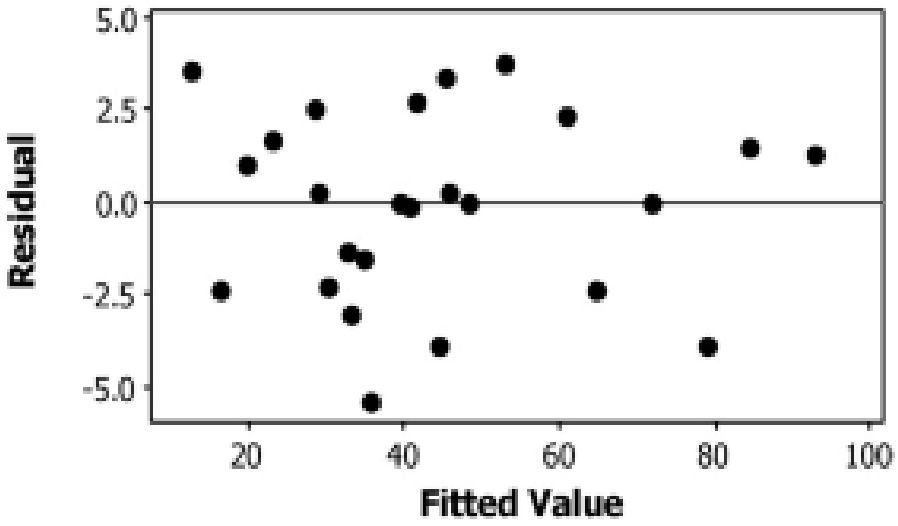

Figure 2-8: Residual vs predicted plot

Figure 2.8 describes a plot of the residuals vs the predicted response. If the residuals are scattered randomly about zero it means the errors have constant variance (Hasan et al., 2009).

(c) Normal probabilities vs residuals

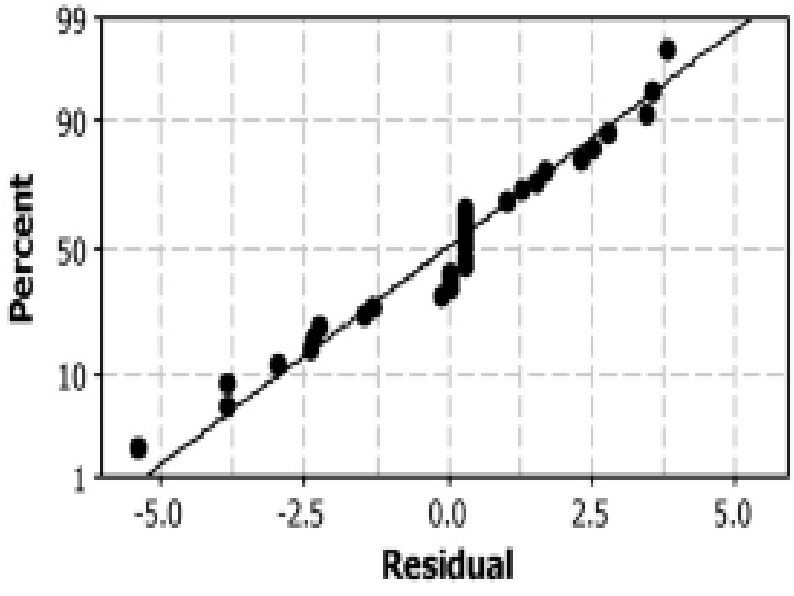

Figure 2-9: NPP plot

The normal probability plot of residuals is used to check whether a data set is usually distributed. Figure 2.9 shows a NPP plot if the points are close to the straight line it means the data is normally distributed (Hasan et al., 2009).

(d) Removal % vs reference point

The perturbation plot shows the effect of all factors at a particular point within the design space. The perturbation plot allows for comparisons of the effects of variables at specific points; however, it does not show the interaction of the design space variables. Figure 2.10 illustrates a perturbation plot (El Hassani et al., 2018).

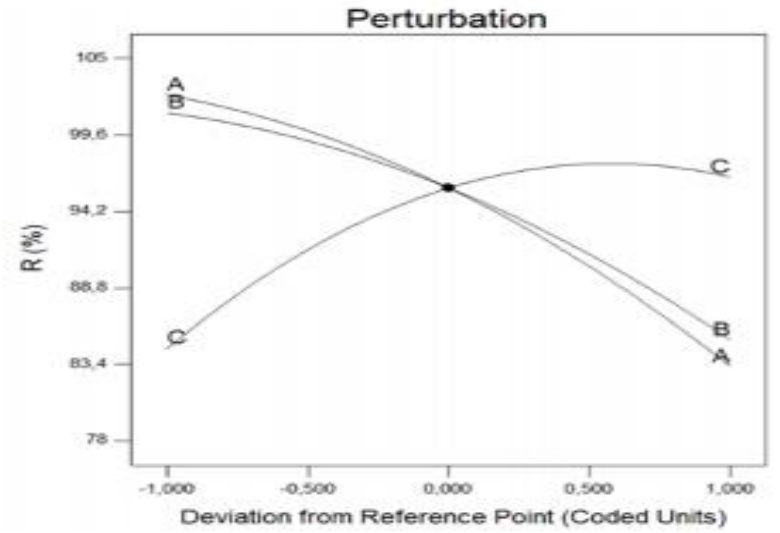

Figure 2-10: Perturbation plot

(e) 3D and contour plot

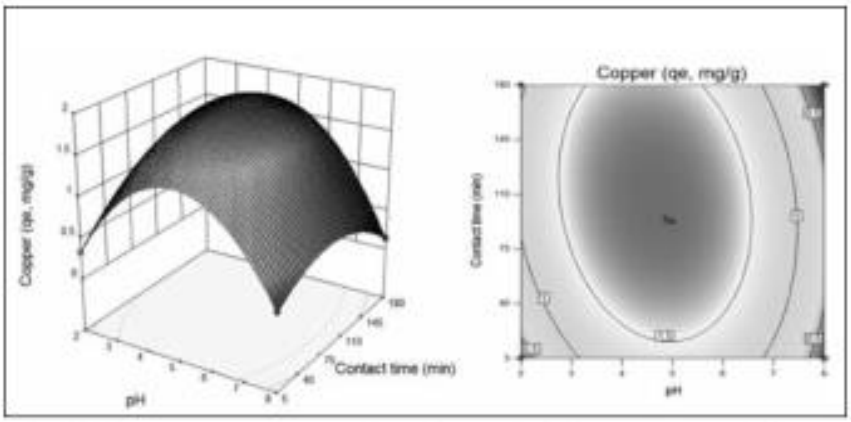

Figure 2-11: 2-D and 3-D contour plots

Two-dimensional and three-dimensional contour plots allow the user to observe variable interactions and their effects on responses. Figure 2.11 shows both plots and in general it is easier for the user to understand the 2-D contour plot (Ince & Ince, 2017).

CHAPTER 3

Experimental Procedure

3 Chapter 3 Research Methodology

3.1 Introduction

This chapter details the equipment, materials, and experimental procedures to be followed during experimental runs

3.2 Research design

A quantitative experimental approach was used during this research. This study consists of three parts. Firstly, the synthesis of the PFS coagulant. The second focuses on identifying the most suitable dosage of polyferric sulphate (PFS) for the coagulation process. The third part consists of using the identified PFS dosage as a pre-treatment for the adsorption process, where three variables were investigated.

3.3 Synthesis of PFS

The PFS coagulant synthesis process was followed according to the well-known method proposed by Jiang and Graham (1995). The batch process started by adding 100 g of ferrous sulphate, 8.2 ml sulphuric acid and 214.5 ml deionised water into a jacketed reactor. The solution was mixed vigorously using an overhead stirrer while being heated to a temperature of 50 ^{0}C. Once the solution reached 50 ^{0}C, 18 ml of nitric acid was added. After that, the solution was raised to a temperature of 90^{0}C and kept at that temperature for 2 hours. After 2 hours the solution temperature was reduced and kept at 50 ^{0}C. At this temperature 214 ml of 0.5N sodium bicarbonate solution was added to the bulk in the reactor at a rate of 1.6 ml per minute. Once the sodium bicarbonate solution was wholly added to the reaction, the solution was stirred gently for 2 hours at a constant temperature of 50^{0}C. After that, solution was cooled to room temperature and stored. Figure 3.1 represents the experimental set-up for the synthesis of PFS.

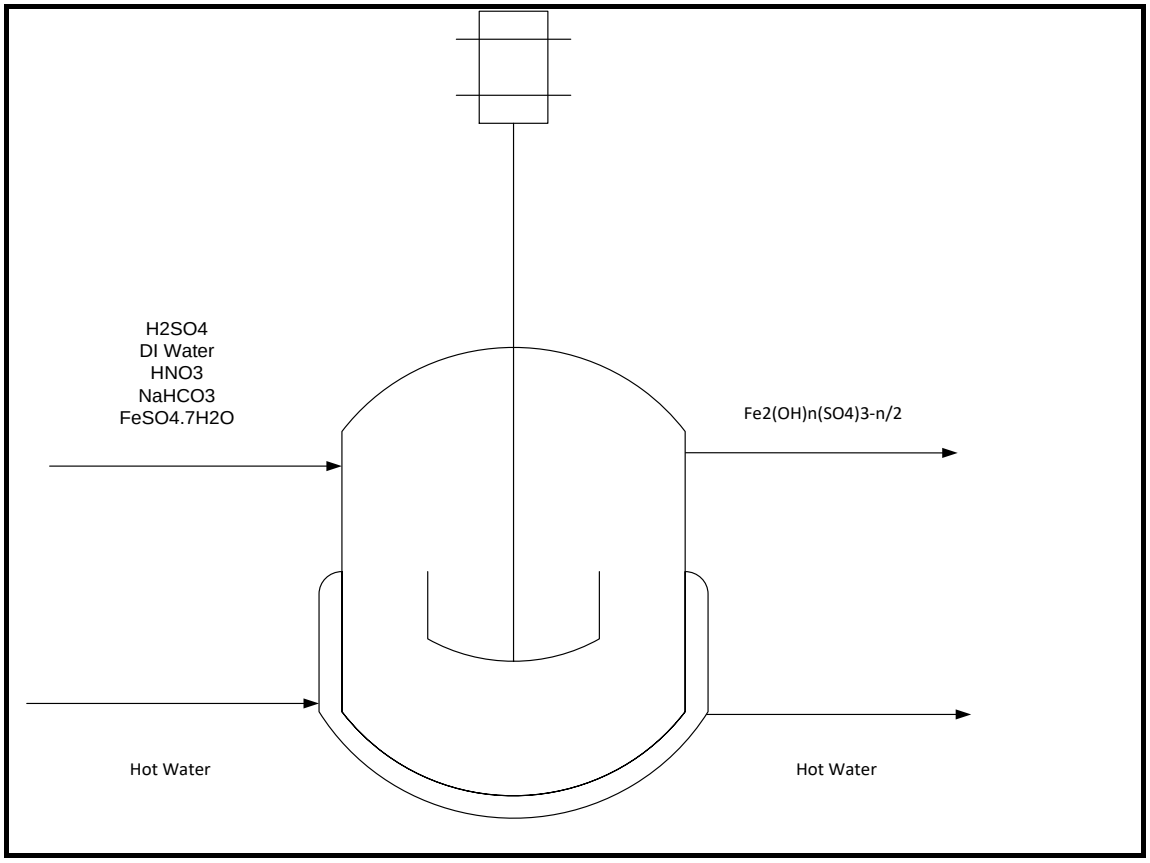

Figure 3-1: PFS Experimental Set-Up (Zouboulis et al., 2008)

3.4 Coagulation of CWW with PFS

The process of chemical coagulation was used as a pre-treatment to the adsorption process, where the synthesized PFS was used as the coagulant. The carwash wastewater underwent standard 500 ml volume jar tests with a magnetic stirrer at a constant speed. The mixing was divided into a rapid mixing phase of 300 rpm for 1 minute followed by a slow mixing phase of 25 minutes at 100 rpm. After coagulation, the particles were allowed to settle for 1 hour. During the coagulation process, the independent variables tested were the dosage of the coagulant ranging from 40mg/l - 120mg/l at an initial pH of 6. Table 3.1 represents the chemical coagulation design matrix.

After sedimentation, the sludge and supernatant were separated using a vacuum filtration unit through filter paper (Whatman grade 5). The treated water was analysed COD, FOG, surfactant, Fe concentration and turbidity. The experimental runs were done in duplication to validate the results statistically.

Table 3-1: Chemical Coagulation Experimental Design

Experimental Run	Dosage mg/l	pH
1	40	6
2	80	6
3	120	6

3.5 Adsorption of CWW using AC

Adsorption using powdered activated carbon (PAC) was a secondary treatment process after chemical coagulation. The water used for the adsorption process was a 25l stock solution of real coagulated CWW that was mixed to allow for a uniform concentration of COD, FOG and surfactants. The adsorption process was a batch process and took place using a shaker in a 1L conical flask at a volume of 500ml. The PAC had a particle size of 0-100 um. The factors tested during the adsorption process were temperature, dosage and pH while adsorption time, two hours, and shaking speed, 150rpm, were kept constant throughout. The temperature was tested through a range of 25-50 ^{0}C the dosage was tested through a range of 100g/l – 300mg/l and the pH were tested through a range of 2-10. After the treatment process, the following analysis was performed: EC, TDS, Salinity, Turbidity, COD, anionic surfactants and pH after which the samples were stored and sent away for the following further analysis: FOG.

3.6 Stock solution for real carwash wastewater (CWW)

To generate a uniform COD, FOG and surfactant concentration a stock solution of real CWW had to be made. To achieve this 25l of real carwash wastewater underwent chemical coagulation in 5L batches at the same conditions (pH: 6, Dosage: 120mg/l). Once the water was filtered it was stored in a 25l container and mixed with an overhead stirrer. The average COD, FOG and surfactant concentration of this solution were 300mg/l, 1.5mg/l and 15 mg/l respectively.

3.7 Adsorption Factorial Trial

The Box Behnken design (BBD) is a type of response surface methodology that does not contain an embedded factorial or fractional factorial design. Box Behnken designs treatment combinations at the midpoints of the experimental space's edges and requires at least three continuous factors.

Table 3-2: Factorial design of adsorption runs using design expert

	FACTORS		
Run	A: pH	B: Temp(^{0}C)	C: Dosage (mg/l)
1	2	37.5	100
2	10	37.5	300
3	6	25	300
4	10	50	200
5	10	37.5	100
6	6	25	100
7	2	25	200
8	10	25	200
9	6	37.5	200
10	6	50	300
11	6	50	100
12	2	37.5	300
13	2	50	200
14	2	37.5	100
15	10	37.5	300
16	6	25	300
17	10	50	200
18	10	37.5	100
19	6	25	100
20	2	25	200
21	10	25	200
22	6	37.5	200
23	6	50	300
24	6	50	100
25	2	37.5	300
26	2	50	200

3.8 Integrated treatment process

The integrated treatment of carwash wastewater consisted of the combination of chemical coagulation adsorption stages. Each process was investigated as a singular process and the best performing operating conditions of each process were used for the integrated treatment process. Once the best conditions of both processes were found the entire integrated process was performed.

3.9 Research apparatus

The following apparatus and equipment were used during the following experiments: production of PFS, chemical coagulation and adsorption processes.

3.9.1 Glassware

- 5L round bottom flask for the production and storage of carwash wastewater
- 500ml bottles to store the treated CWW after chemical coagulation and adsorption
- 500ml beakers to perform coagulation experiments
- 500ml Erlenmeyer flasks to perform adsorption experiments

3.9.2 Equipment

- Magnetic stirrer

A DragonLab MS-H-S magnetic heater/stirrer was used during chemical coagulation for stirring the solution at a constant rpm. During the coagulation and adsorption processes the magnetic stirrer/heater was only used for stirring purposes.

Photograph 3-1: magnetic stirrer, MS-H-S DragonLab, Beijing China

- Circulating Water bath

The water bath was used during the production of PFS. The purpose was to maintain the temperature of the reaction at desired temperatures.

Photograph 3-2 Circulating water bath, Precision CIR 19, Thermo Fisher scientific, Massachusetts USA

- Overhead stirrer

The overhead stirrer was used during the production of PFS to keep a constant rpm during the reaction.

Photograph 3-3 Overhead stirrer, OS20-S, DragonLab, Beijing China

- Jacketed glass reactor

The reactor was used for the production of PFS. The reactor was used for the various reactions and to maintain the reaction temperature.

Photograph 3-4: Jacketed glass reactor

- pH meter

Photograph 3-5 pH meter, HI8424, HANNA Instruments, Road Island USA

- Turbidity meter

Photograph 3-6: Turbidity meter, Turb 355 IR, Xylem analytics, Texas USA

- Multi-parameter photometer

The multi-parameter photometer was used to measure the cod concentrations

Photograph 3-7: Multi-parameter photometer, HI83399-02, HANNA instruments, Road Island USA

- Multimeter

The Multimeter was used to measure EC and TDS

Photograph 3-8: EC and TDS multimeter, CM 35+, Crison instruments, Alella Spain

- Thermo-reactor

The thermo-reactor was used during cod measurements

Photograph 3-9: COD test tube heater, HI839800-02, HANNA instruments, Road Island USA

- FMH shaking incubator

The shaking incubator was used for the experimental adsorption runs to control the shaking speed and temperature of the samples.

Photograph 3-10: Shaking incubator, ISKO 80, FMH instruments, Cape Town South Africa

- Anionic Surfactant Meter

The HI96769 Anionic Surfactant Portable Photometer (Hanna Instruments) is used to determine anionic surfactants concentrations as sodium dodecylbenzene sulfonate within a range of 0.0 to 3.5 mg/l.

Photograph 3-11: Anionic surfactant meter, HI96769, HANNA instruments, Road Island USA

- Peristaltic pump

The peristaltic pump was used in the application of making the chemical coagulant PFS and in the PSD experimental design

Photograph 3-12: Peristaltic pump, Sci-Q 323, Carl Roth, Karlsruhe Germany

3.9.3 Materials

The following consumables were used during experiments

- H_2SO_4
- NaOH
- $NaHCO_3$
- $FeSO_4$
- HNO_3
- Powdered Activated Carbon ‘

Chapter 4:

Results

&

Discussion

4 Results and Discussion

Results are presented in this chapter are presented into three sections

I. Chemical coagulation characterisation and performance
II. Characterisation and performance of activated carbon
III. Adsorption kinetics, isotherms and thermodynamics

4.1 Carwash wastewater characterization

Table 4-1: Carwash wastewater characteristics and requirements according to South Africa

Parameter	Unit	Tested value	NWA: Requirements
COD	mg/l	1200-1000	>75
FOG	mg/l	60-50	2.5
Surfactants	mg/l	35-25	2.5
Salinity	g/l	2.03	none
EC	mS/cm	3.5	70 - 150
TDS	g/l	2.3	4000
pH		7.5	5.5 - 9.5
Turbidity	NTU	100-40	none

The carwash wastewater used during this study was tested for specific parameters. The average values are shown in Table 4.1. The chemical oxygen demand (COD), anionic surfactants (AS) and fats, oil and greases (FOG) values were found to be much higher than what is required under the national water act. The COD, AS and FOG and surfactant concentrations were much higher than what is recommended. The pH, electrical conductivity and TDS were in line with South African wastewater discharge standards.

4.2 Chemical Coagulation characterization

Table 4-2 shows the polyferric sulphate (PFS) characteristics were used in the chemical coagulation (CC) of carwash wastewater.

Table 4-2: Important characteristics of PFS (Zouboulis et al., 2008)

pH	Fe (III) (g/l)	Conductivity (mS/cm)	r (OH/Fe)
1.15	40	44.5	0.3

4.3 Chemical coagulation of carwash wastewater

Chemical coagulation (CC) of carwash wastewater (CWW) was carried out using polyferric sulphate (PFS) at various concentrations for the removal of COD, FOG and surfactants. The jar tests performed at dosages of 40, 80 and 120 mg/l were conducted at an initial wastewater pH of 7.5 for all the experimental runs. The effects of pH and stirring speed were shown to have minimal impact on the removal of pollutant. (Zhai et al., 2017) concur with this observation and explained that the coagulant dosage was the most significant factor affecting the removal of COD, FOG, colour and TOC removal. When the pH increased from 2 -11 only a minimum amount of pollutants (<5%) were removed. Changing the stirring speed had a lesser effect. A similar study done by Aygun & Yilmaz. (2010) where detergent waters were treated using chemical coagulation found pH to have a smaller effect on the overall removal of COD than coagulant dosage. The study used ferric chloride as a coagulant and found that at a pH of 11 the removal efficiency was 20% better than at a pH of 4. (Jiang & Graham, 1998a) stated that PFS has a wide working pH range, and it is with this reasoning that only coagulant dosage was tested, as it would have the most significant impact on the removal of pollutants.

The addition of PFS to the CWW saw a drop in the initial pH of the water from 7.5 to 7-6.5. Figure 4.1 represents the effect of PFS dosages on the removal of COD, FOG and surfactants. It is observed from figure 4.1, 99% of oil was removed at concentrations of 40 and 80 mg/l while 96% was removed at concentration 120 mg/l. Higher coagulant concentrations place positive charges on particle surfaces, therefore re-dispersing solid particles that can cause higher FOG concentrations at higher coagulant dosages (Chatoui et al., 2017). Zhao et al. (2020) state that simple charge neutralization is the most significant factor affecting the coagulation/flocculation process. The authors continue stating that oil removal efficiency increases with the increase in coagulant concentration. However, when too much coagulant

is added, a reduction in efficiency is experienced, due to particle re-stabilization. This phenomenon can be seen in Figure 4.1 where a slight reduction in FOG removal efficiency was observed at a coagulant dosage of 120mg/l.

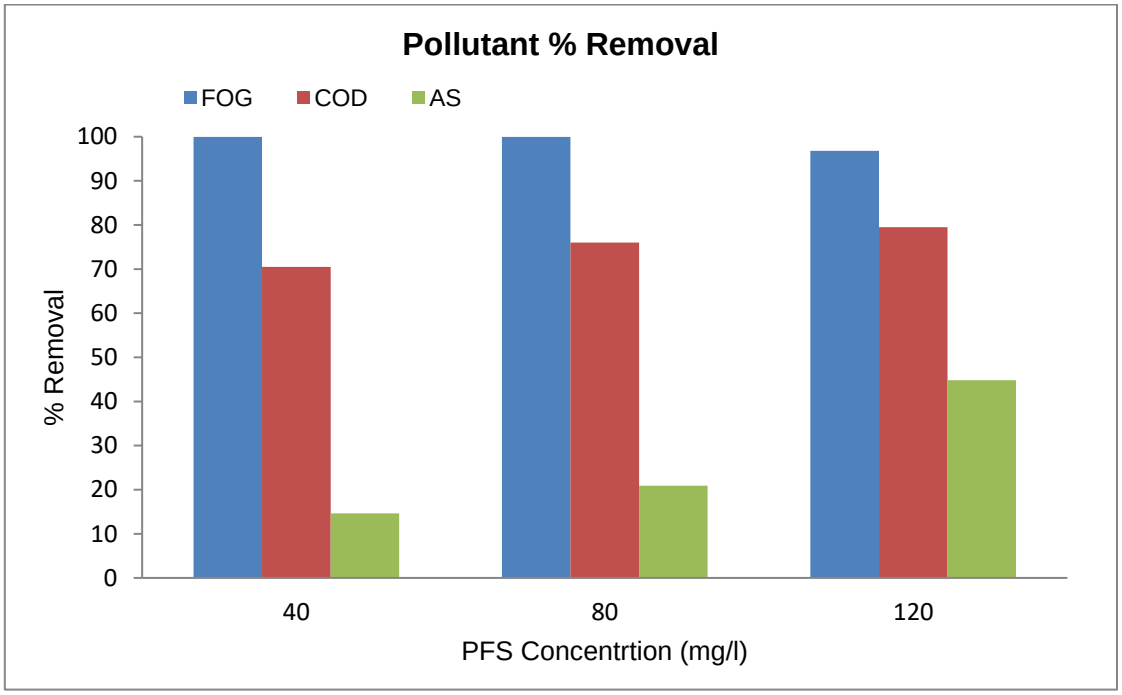

Figure 4-1: Effect of coagulant dosage on pollutant percentage removal

Figure 4.1 also shows the removal of anionic surfactants from CWW. It can be seen that as the adsorbent dose increased the removal percentage increased. The removal of AS is much lower when compared to COD and FOG removal. The AS removal achieved at 40 mg/l was 14% but showed a significant improvement to 44% at 120 mg/l. The primary mechanism for the removal of AS via chemical coagulation is adsorptive micellar flocculation (AMF). AMF involves cationic species attraction to the surface of anionic micelles and the flocculation as their mutual electrostatic repulsion is neutralised. This process creates an aggregate that can be easily filtered (Talens-Alesson et al., 2006). The Fe^{3+} ions bind to the micelles causing the following simultaneous effects: it supresses repulsive forces between micelles causing them to flocculate and effectively removing micellar surfactant from solution in the form of an aggregate, and it binds organic compounds to the flocs. In addition to the coagulation process, the AMF mechanism contributes to removing AS and organic matter (Aboulhassan et al., 2006). As seen in Figure 4.1, the COD removal was found to be between 70-79% and increased as the concentration of PFS increased. The difference between the lowest and highest dosage was less than 10%. The wastewater COD concentration decreased

significantly from 1000mg/l to 300mg/l, 240 mg/l and 205mg/l at PFS concentrations op 40, 80 and 120 mg/l respectively (Tables D-1, D-2, D-3 Appendix D).

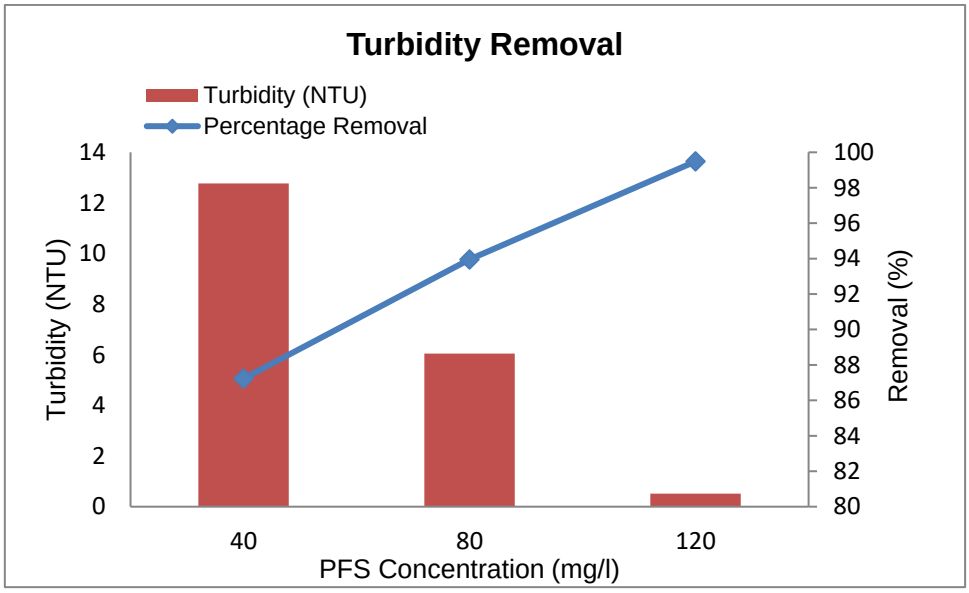

Figure 4-2: Turbidity removal at different PFS concentrations

.

Figure 4.2 shows the turbidity percentage removal at different PFS dosages. Figure 4.2 shows when the dosage of PFS is increased the less turbid the water becomes. At a PFS concentration, of 40 mg/l, 80mg/l and 120 mg/l the corresponding percentage removal achieved were 87% 93% and 99%, respectively. The higher turbidity removal at higher dosages can be explained by charge neutralization. The PFS adsorbs onto negatively charged species and thus neutralize their charge the particles thus get destabilized and aggregate. The greater the PFS concentration, the greater the degree of charge neutralization, thus leading to lower turbidity. However it should be noted that overdosing leads to reversal and particles start to destabilize (Malik, 2018).

Table 4-3: Coagulation PFS percentage removal

PFS Concentration	Removal %			
	Turbidity	COD	AS	FOG
40	87.73	70.50	14.64	99.50
80	93.95	76.00	20.89	99.50
120	99.49	79.50	44.82	96.79

In Table 4-3, the most favourable dosage was found to be 120 mg/l. This PFS coagulant dosage will be used as the chemical coagulation pre-treatment step before all adsorption

experimental runs. In Photograph 4-1 the colour change with a change of the three different PFS coagulant dozing can be seen. The far-right with the 120 mg/l PFS sample bottle shows the best clarity.

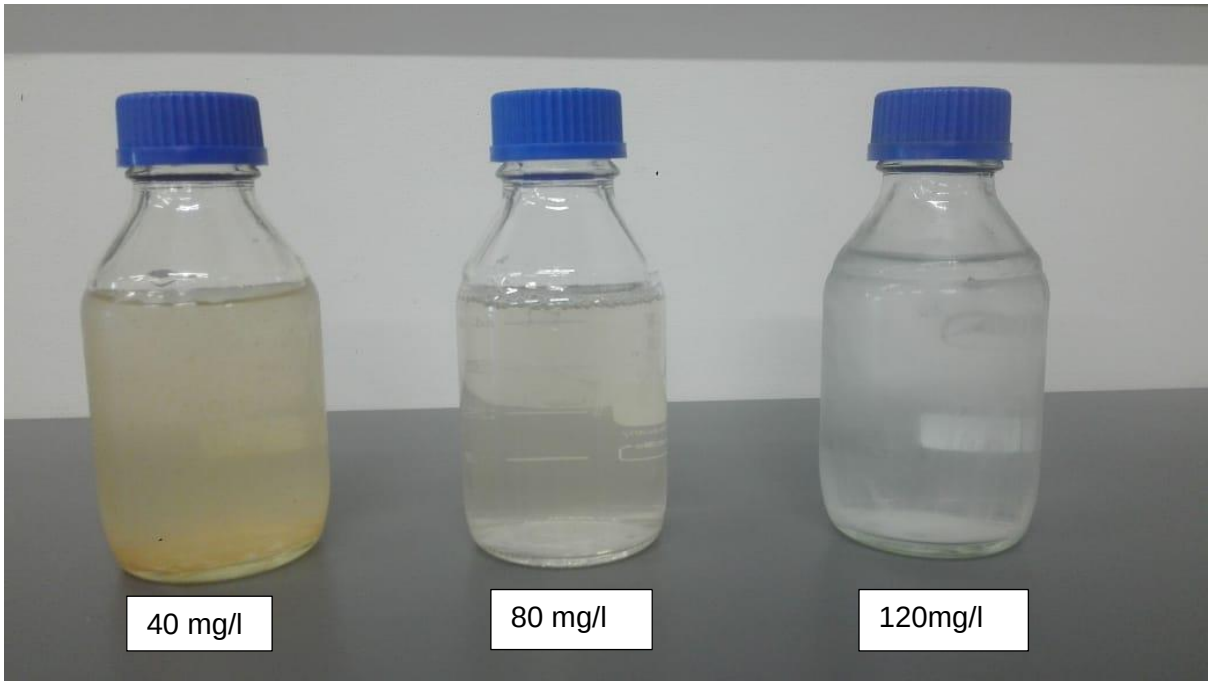

Photograph 4-1: CWW after chemical coagulation at different PFS concentrations

4.4 Activated Carbon characterisation

The activated carbon used in the research was obtained from a South African company called RotoCarb. The PAC is manufactured from macadamia nut shells through steam activation. The PAC had a mesh size of 0-100 micron. Size distribution was performed on the 1kg sample provided by the company was and found that 80% of particles had a size of <75 micron, 17.3% had a particle size between 75 and 55 micron, 1.78% had a size between 55 and 35 micron and only 0.88% had a size of 35 micron and below.

Table 4-4: PAC Specifications provided (RotoCarb, 2019)

PAC Specification	
Iodine number (mg/g)	950+
Ash content (wt%)	<3
Moisture content (wt%)	<3
Apparent density (g/cc)	0.38

4.4.1 Scanning electron microscope SEM Analysis of PAC

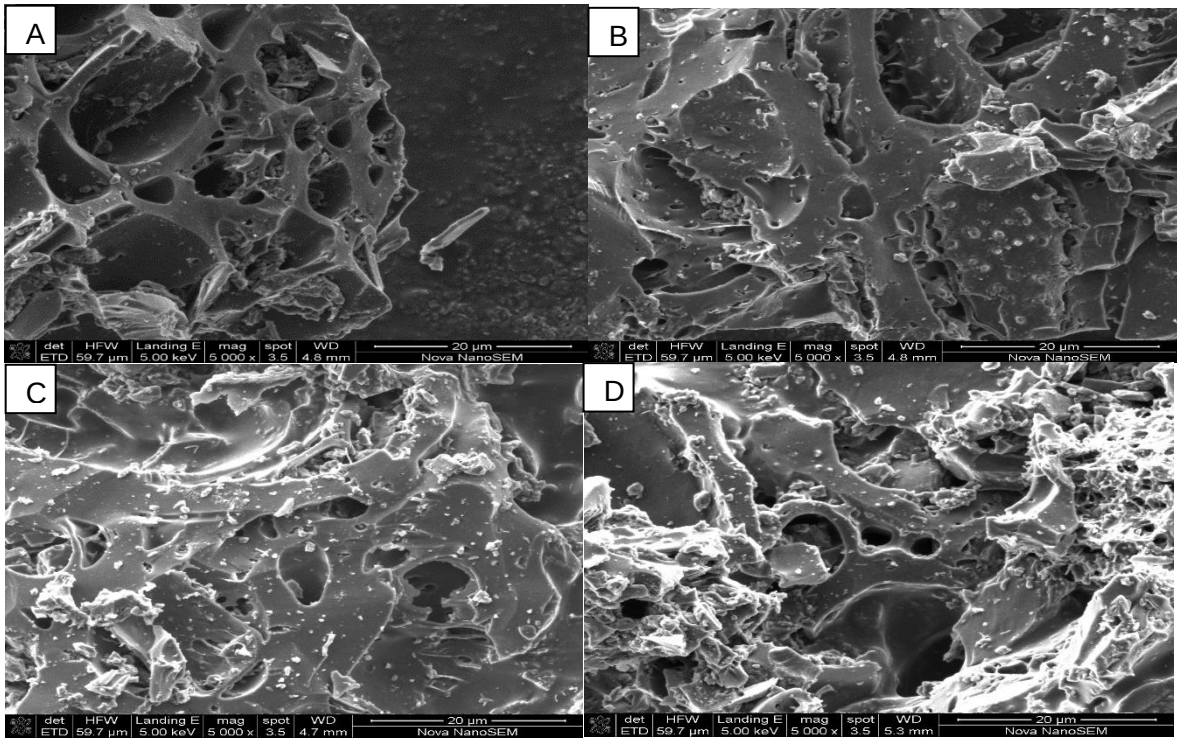

Figure 4-3: SEM analysis of PAC

,

SEM was used to observe the surface of the adsorbent. The morphology of the activated carbon received from RotoCarb is shown in Figures 4.3. The SEM analysis was conducted with a magnification of 20,000. Figure 4.3 shows the PAC's detailed surface characteristics with a large quantity of pores showing irregular granules (Dejang et al., 2015). It also shows the surface to have some debris present on it occupying the pores of the PAC (Kuang et al., 2020). The SEM images show the PAC to have a mesoporous structure that favours the adsorption of anionic pollutants.

4.4.2 FTIR Analysis

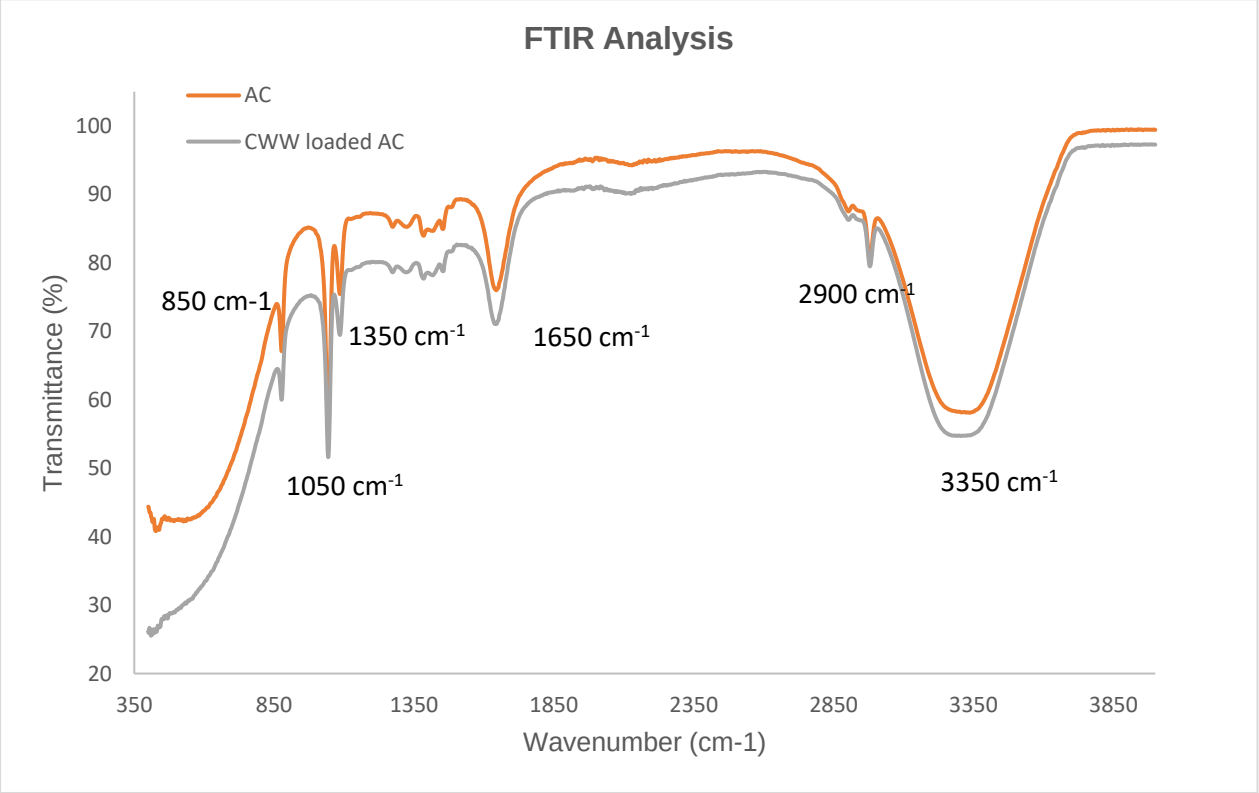

Figure 4-4: FTIR analysis of PAC

The chemical surface properties of the activated carbon were investigated using FTIR. Figure 4.4 shows a comparison between the unused activated carbon and the CWW loaded activated carbon. The broad band around 3350-3500 cm^{-1} is common in both spectra and can be attributed to O-H stretching vibration. The loaded CWW wastewater exhibits a peak at 2900 cm^{-1} unique to itself and can be ascribed to a C-H stretching vibration (Table 4.5) and is observed only in the loaded activated carbon. The bands at 1650 cm^{-1} are present in both adsorbents and can be attributed to a C=O stretching vibration in carboxyl and alkene groups and aromatic rings. The bands at 1350 can be assigned to C-C stretching additionally the bands at 1050 cm^{-1} can be attributed to C-O stretching in carboxyl acids, alcohols, phenols and esters (Martins et al., 2015). The band at 850 cm^{-1} found only in the loaded activated carbon represents the stretching oscillation of the C=C functional group which indicates that the carbon content increases in the activated carbon (Dao et al., 2020). The study performed by Gong et al. (2005) investigated the effect of chemical modification on anionic and cationic dye adsorption capacity of peanut hull found that carboxyl, amino and hydroxyl groups had an impact on anionic dye removal. The study found that carboxyl groups bearing a negative charge slightly reduced the adsorption capacity of anionic dyes. The study also showed that when amino and hydroxyl groups were removed, anionic dyes' adsorption capacity was highly

reduced, showing the importance of those groups in anionic dyes' adsorption. This shows that carboxyl and amine groups are essential for the adsorption of anionic species These groups are found in the commercial activated carbon provided, making it a good candidate for anionic surfactants' adsorption.

Table 4-5: Important groups for the adsorption of anionic surfactants onto PAC

Wavenumber (cm^{-1})	Band assignment	Reference
3350	O-Hs	(Gong et al., 2005)
2900	C-H	(Martins et al., 2015)
1050	C-O	(Dao et al., 2020)

4.5 Powder Activated Carbon (PAC) Adsorption for Carwash Wastewater (CWW)

During the experimental adsorption runs with PAC as adsorbent, the CWW feed was pre-treated with chemical coagulation (120 mg/l PFS as coagulant). Design Expert software was employed to develop the twenty-six (26) experimental runs to be performed in order to investigate the problem at hand. The factor range, levels and conditions for experimental runs are presented in Tables 3-2 (Chapter 3). In the experimental design one centre point was chosen therefore, 13 runs were produced. All experimental runs were duplicated; therefore 26 adsorption runs were performed.

A 3-level factor BBD was applied to develop the appropriate experimental conditions that influenced the COD and Anionic Surfactant (AS) removal efficiency from CWW. Initial pH (2, 6, 10); PAC concentration (100, 200, 300 mg/l); Temperature (25, 37.5, 50 ^{0}C) were taken as the process parameters. The design BBD indicated random order of experimental runs to be followed. The Adsorption experimental parameters kept constant throughout are the adsorption time of 2 hours and the shaking speed at 150rpm.

4.5.1 Chemical Oxygen Demand (COD) and Anionic Surfactant (AS) Removal

The elimination of organic matter in the carwash wastewater was assessed from the decay of the COD and AS, measured using HANNA COD and AS spectrophotometers. Figures 4-5 and 4-6 displays the COD and AS concentration and the average percentage removal at each experimental condition. The COD percentage removal ranges from a minimum of 30% for experimental run 2 (pH: 6, PAC: 100mg/l, Temperature: 25^{0}C) to a maximum of 94% for experimental run 9 (pH: 6, PAC: 300mg/l, Temperature: 50^{0}C). Whereas the AS percentage removal ranges from a minimum of 39.2% for experimental run 2 (pH: 6, PAC: 100mg/l, Temperature: 25^{0}C) to a maximum of 98% for experimental run 11 (pH: 2, PAC: 300mg/l, Temperature: 37.5^{0}C).

COD and AS percentage removal

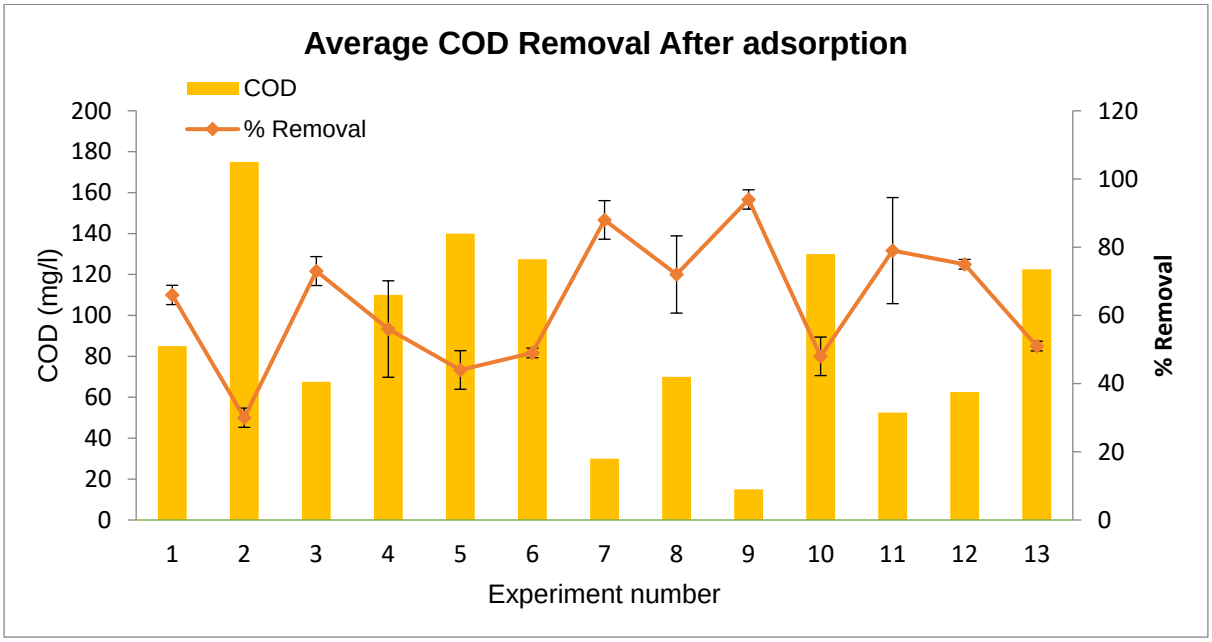

Figure 4-5: Adsorption average COD removal

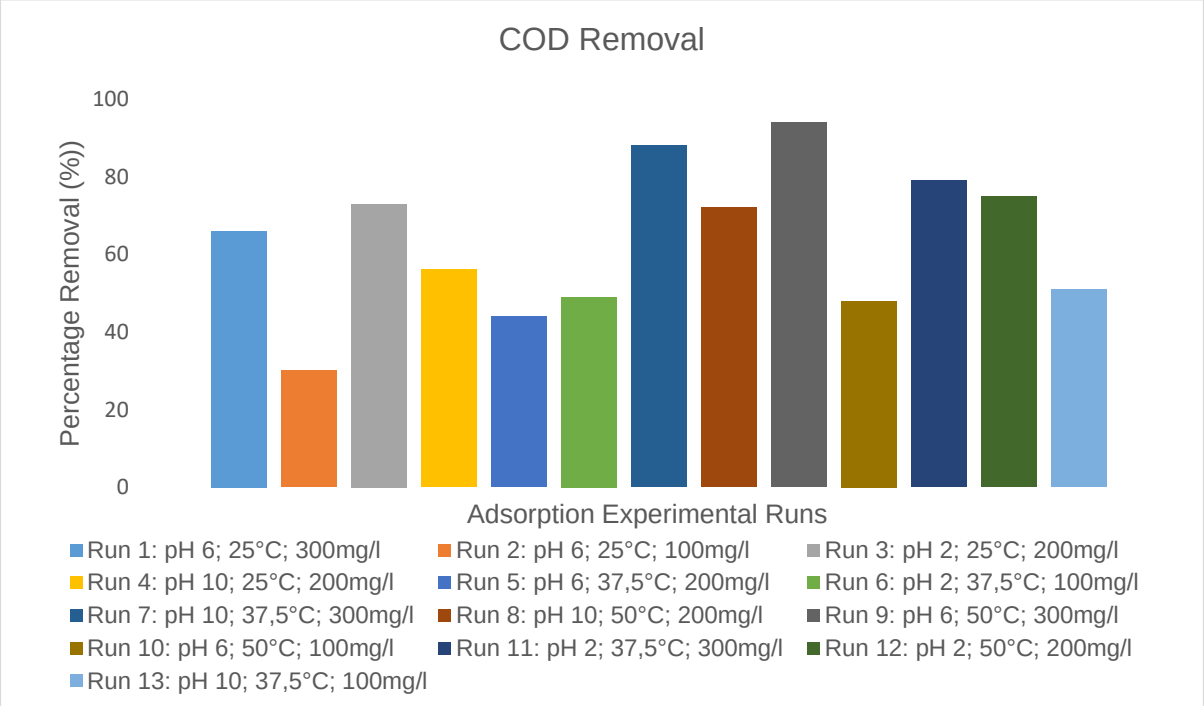

Figure 4-6: Average COD removal after adsorption

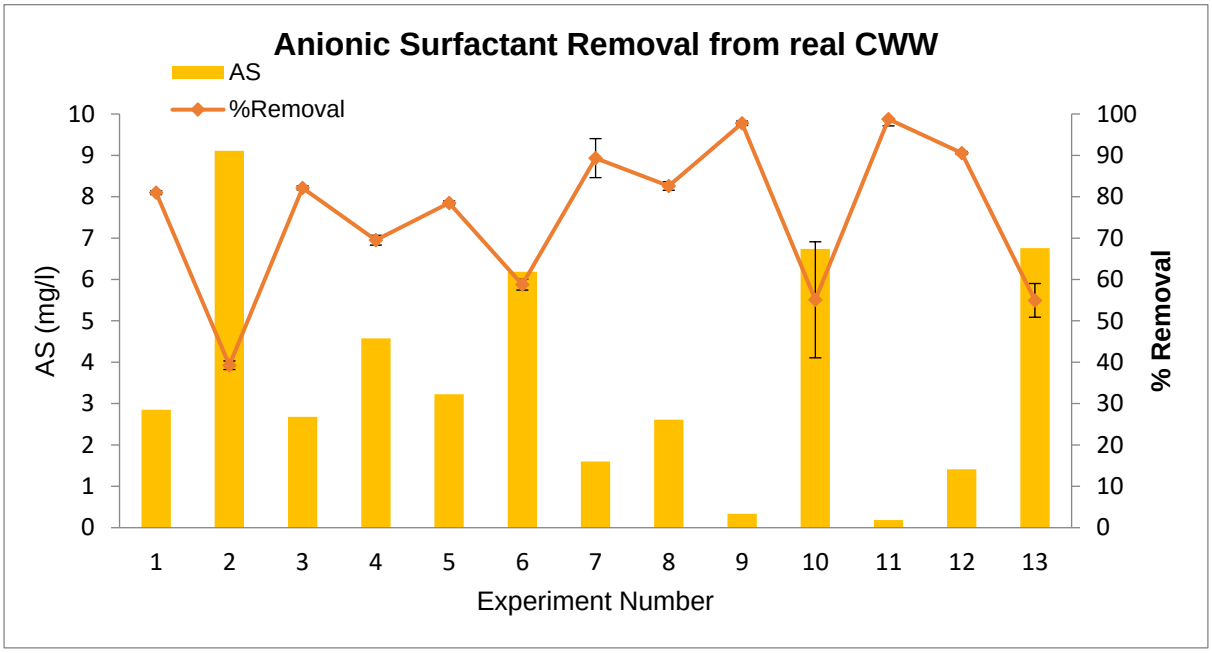

Figure 4-7: Adsorption average AS removal

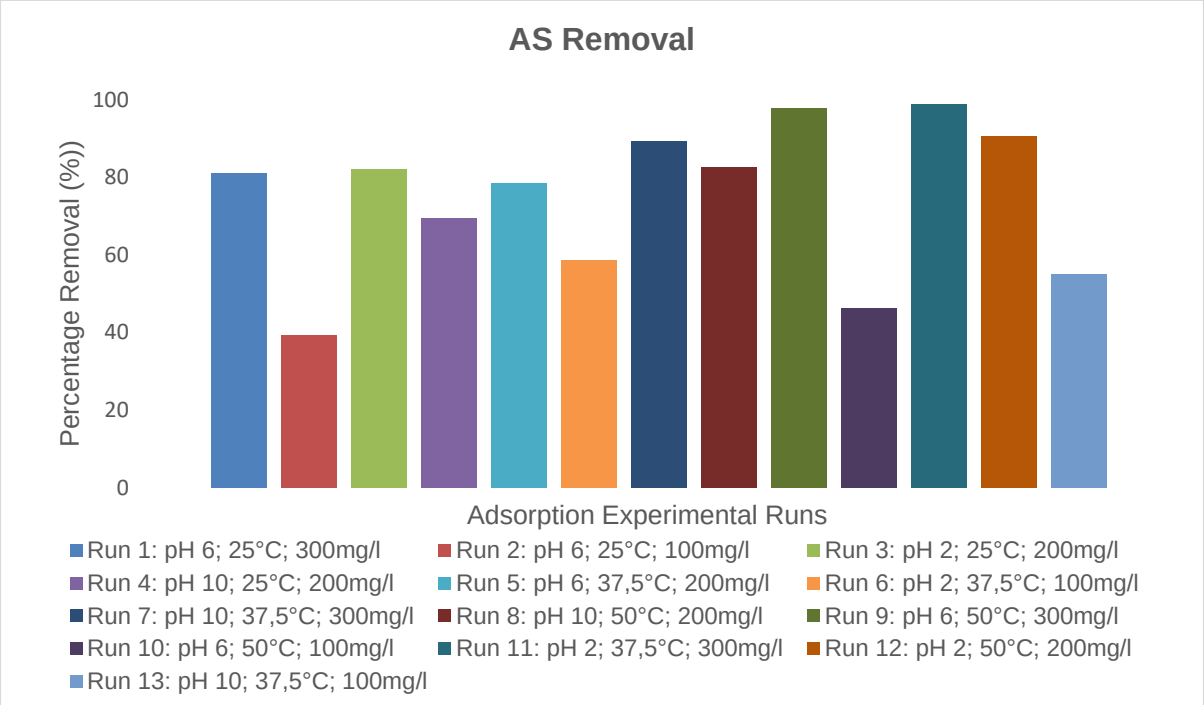

Figure 4-8: Average AS removal after adsorption

4.5.2 Effect of pH

The noticeable effect can be observed when looking at Figures 4.5 and 4.6. The pH has a negligible effect on the removal of COD and AS. When considering experimental runs 3 and 4; 7 and 11, 12 and 8, it can be noted there are higher COD and AS removals at the lower pH of 2 compared to the pH of 10. Pollutant removal is favoured in acidic media because as the pH increases, the pollutant removal decreases. This can be explained by the PAC's surface charge, which is a fundamental control variable. The variation in pH changes the electrostatic charge on the adsorbents. According to Siyal et al. (2020), the positive electrostatic charge is more suitable for anionic surfactants adsorption. Zor et al., (2004) states the OH^- ions decrease the adsorption of anionic surfactant ions to the surface, orienting the positive surface and making the solid surface more negative with increased concentrations of OH^- ions. This leads to more repulsion between the activated carbon and the anionic surfactant decreasing adsorption capacity with increased pH. The effect of pH shows the presence of electrostatic interactions. Surfactants are adsorbed through electrostatic interactions on adsorbents possessing an opposite charge and are thus dependent on the solution's pH (Siyal et al., 2020). However, the effect of pH was found to be marginal showing a maximum of 13% AS removal difference between experimental runs 3 (pH: 2) and 4 (pH: 10) and a 16% COD removal difference between the same experimental runs. Based on these findings electrostatic interactions do not play a significant role in the adsorption of AS onto PAC. A study performed by Bautista-Toledo et al. (2008) investigated the adsorption of sodium dodecylbenzene sulfonate (SDBS) on activated carbons found that pH had no significant effect on the adsorption of SDBS onto activated carbon and stated electrostatic interactions do not play a significant role in the adsorption process. These findings are in line this research's findings, showing that pH had no significant effect on the adsorption of AS onto PAC. Since pH had no significant effect on the adsorption of AS onto PAC, along with electrostatic interactions, there must be hydrophobic interactions between the adsorbate and adsorbent molecules (Pal et al., 2013).

4.5.3 Effect of Temperature

COD and Anionic Surfactants (AS) removal was evaluated over a range of 25, 37.5 and 50 ^{0}C, respectively. When considering Figures 4.6 and 4.8 it can be seen that an increase in temperature increases the AS and COD removal. From experimental runs 1 (pH:6, T: 25^{0}C, PAC: 300mg/l) and run 9 (pH:6, T: 50^{0}C, PAC: 300mg/l), run 1 achieved 81% and 66% removal while run 9 achieved 97% and 94% removal for AS and COD, respectively. This

shows an increase of 16% AS and a 28% increase for COD removal when the temperature is increased from 25^0C to 50^0C and all other variables remain constant. Similar findings can be seen when analysing runs 10 (pH:6, T: 50^0C, PAC: 100mg/l) and 2 (pH:6, T: 25^0C, PAC: 100mg/l) COD and AS removal were 18% and 7% higher in run 10 than run 2 respectively This shows that the system achieves higher rates of removal at temperatures of 50^0C than 25^0C. These results show that chemisorption is taking place. The adsorption capacity is largely dependent on chemical interactions between the PAC surface groups and the AS ions. The adsorption increase may result from increased chemical interactions between the AS ions and the functionalities of the PAC. The increase could also result from an increase in the rate of intraparticle diffusion of AS ions into the pores at higher temperatures as diffusion is an endothermic process These findings show that the system is endothermic (Karim et al., 2006).

4.5.4 Effect of PAC concentration

The effect of PAC concentration on COD and AS removal was evaluated over a concentration range of 100, 200 and 300 mg/l. The removal of COD and AS increased significantly when the concentration of PAC increased. This observation also shows that PAC concentration was the most significant contributing factor compared to pH and temperature. It can be seen from Figures 4.6 and 4.8 that pollutant removal increases sharply as the amount of adsorbent concentration does. This can be down to the fact that more adsorption sites or greater surface area are available and greater availability of specific surfaces of the adsorbent (Eletta et al., 2018). When comparing experimental runs 1 and 2 where pH and temperature are kept constant, and the adsorbent dosages are 100 and 300 mg/l, surfactant removal was 39% and 81%, respectively, showing an increase of 50% removal. The same can be observed in COD removal for the same runs showing a greater than 50% COD removal improvement. It can also be seen from Figure 4.9 that as the adsorbent dosage increases the adsorption capacity decreases. This is due to all active sites being utilized at lower PAC concentrations and only some of the active sites are exposed and occupied at higher PAC concentrations. Of the three variables looked at, its evident adsorbent concentration affects COD and surfactant removal the most significantly.

4.6 Adsorption Isotherms

The data obtained from the adsorption experiments where the anionic surfactant (AS) concentration was initially 15mg/l after the chemical coagulation process were fitted with the Langmuir, Freundlich, Dubinin-Radushkevich (D-R) and Temkin isotherms.

Chiou & Li. (2002) states that equilibrium adsorption isotherms describe the interactions between solutes and adsorbents. Isotherms form a central part of designing an adsorption system and understanding them could lower overall costs. The Langmuir and Freundlich models are widely accepted models for surface adsorption. However, since these models do not give information on the adsorption mechanism (Laus et al., 2010), the Dubinin-Raduschkevich (D-R) and Temkin isotherm models were applied.

According to Aksoyoglu. (1989), Dubinin-Raduschkevich isotherm (D-R) is an equivalent of the Langmuir isotherm but is more general since it does not assume a standardized surface or constant sorption potential. The D-R isotherm can be used to calculate the mean free energy of adsorption, which is used to identify chemical and physical adsorption. The Temkin model assumes that heat of adsorption of all molecules in the layer would decrease linearly rather than logarithmic with coverage. As implied in the equation, its derivation is characterized by a uniform distribution of binding energies (Balarak et al., 2017).

Previous studies using commercial activated carbon for the treatment of carwash wastewater found the best isotherm to be that of Langmuir (Veit et al., 2020) however it only covered Langmuir and Freundlich adsorption isotherm models.

The experimental runs were all performed at a pH of six, initial concentration of 15mg/l anionic surfactant concentration, temperature range (25, 37.5, 50 ^{O}C) and adsorbent PAC dosage range (100, 200, 300mg/l). Anionic Surfactant (AS) adsorption isotherm and kinetics design matrix can be followed in Table 4-5.

Factors affecting the adsorption process were optimized using response surface methodology (RSM). Four widely used isotherms, the Langmuir, Freundlich, Temkin, and Dubinin-Radushkevich, were used to assess the adsorption of AS onto PAC. The adsorption kinetics and intraparticle diffusion models were used to assess the adsorption mechanism.

Table 4-6: AS adsorption isotherm and kinetics design matrix

Experiment No	Run No	pH	Dosage (mg/l)	Temperature (°C)
1	3	6	300	25
2	6	6	100	25
3	11	6	200	37,5
4	9	6	300	50
5	10	6	100	50
6	27	6	200	25
7	28	6	200	50
8	29	6	100	37,5
9	30	6	300	37,5

Adsorption studies were carried out in order to determine the equilibrium isotherms. The equilibrium adsorption isotherms are known to provide information about the surface properties of adsorbent, the adsorption behaviour and the design of adsorption systems (Simsek & Beker, 2014). The data of equilibrium studies for adsorption of AS onto PAC was studied using the Langmuir, Freundlich; Dubinin-Raduschkevich (D-R) and Temkin isotherm models at three different PAC dosage and temperature levels (Table 4-5). The applicability of each isotherm models was judged using correlation coefficients, R^2. The parameters for each isotherm are presented in Table 4-6.

4.6.1 Effect of temperature on adsorption performance

Temperature influences the adsorption capacity of the various adsorbent dosages. The experimental runs were performed at different temperatures and adsorption dosages by maintaining the other parameters constant to investigate the influence of temperature on the adsorption process's efficiency. In Figure 4-9, PAC's adsorption capacity at three different temperature levels and three different adsorbent dosages are presented. The adsorption capacity decreases with PAC dosage increase from 100 to 300 mg/l with the opposite trend at all three temperature levels. The adsorption capacity of the 50 ^{o}C is higher than the 37,5 and 25 ^{o}C, indicating that an increase in temperature improves the adsorption of anionic surfactant by using PAC

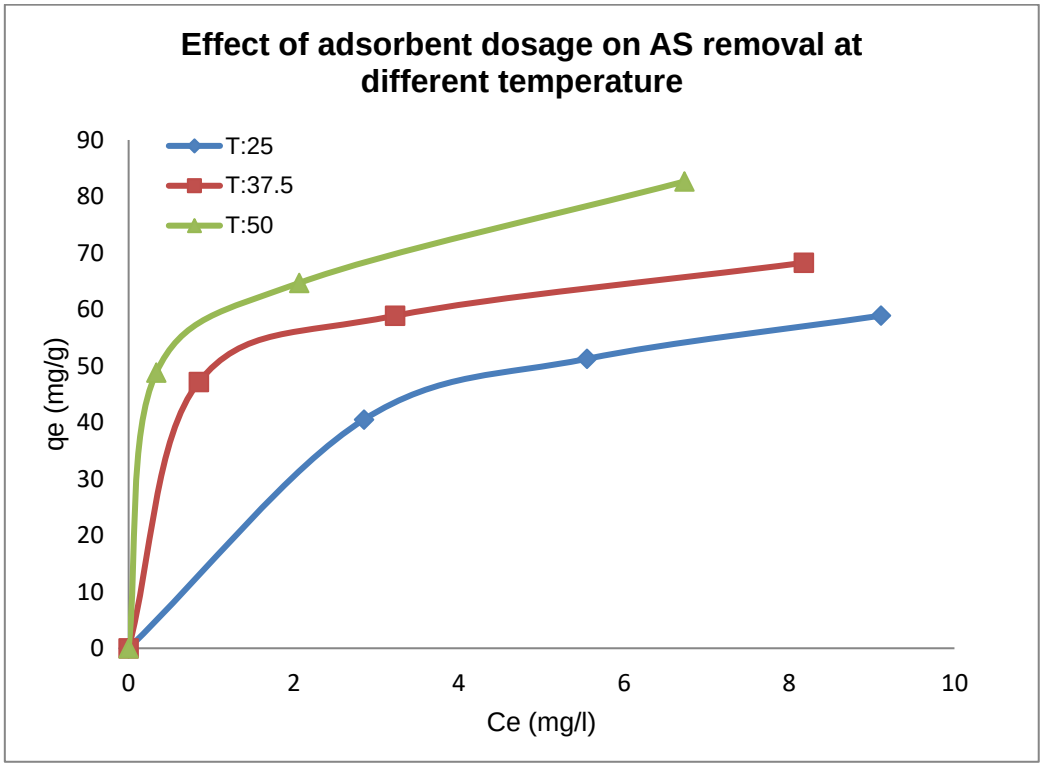

Figure 4-9: Effect of adsorbent dosage on anionic surfactant removal onto PAC (pH = 6: T = 25, 37.5, 50; dosage = 100mg/l, 200mg/l, 300mg/l)

Bazrafshan et al. (2012) say that increasing the temperature is known to increase the diffusion rate of the adsorbate molecules across the external boundary layer and in the adsorbents internal pores owing to the decrease in the viscosity of the solution. Furthermore, changing temperature will change the equilibrium capacity of the adsorbent for an adsorbate. A Similar finding was made in a study performed by Karim et al. (2006)) who found that an increase in temperature increased the adsorption capacity for the removal of anionic dyes. The author explains this can occur due to an increase in the rate of intraparticle diffusion since diffusion is an endothermic process. Rajamohan et al. (2014)concur and said that the uptake capacity increases with an increase in temperature and confirms sorption processes endothermic nature. The enhancement in uptake is attributed to better interaction between AS ions and PAC sorbent, creating new sorption sites and increased intraparticle diffusion at higher temperatures.

4.6.2 Langmuir Isotherm

The Langmuir isotherm model is valid for monolayer adsorption onto a surface containing a finite number of identical sites. The linear form of the model is described in equation 2.6. The adsorption parameters for all isotherms can be found in Table 4.7

$$q_e = \frac{q_m K_L C_e}{1 + K_L C_e}$$

The values of K_L and q_m were calculated from the linearized equation of 2.6. The intercept and slope from the plot Ce/qe vs Ce are shown in Table 4.7. The linearized plots of PAC dosages at different temperature are found in Figure 4.10

$$\frac{C_e}{q_e} = \frac{1}{q_m} C_e + \frac{1}{K_L q_m}$$

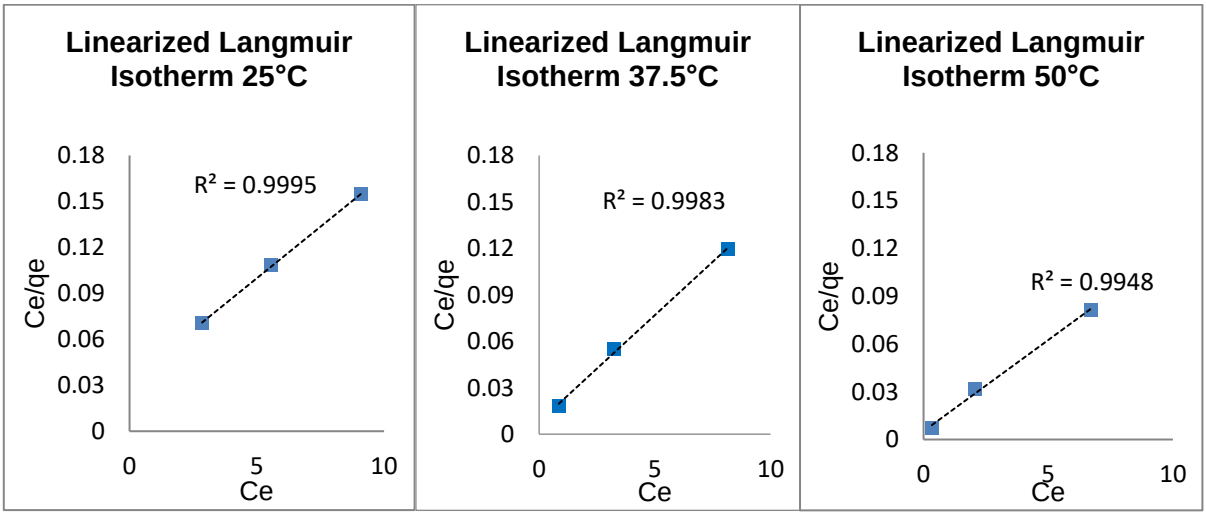

Figure 4-10: Linearized Langmuir isotherm at different temperature

The constant q_m is the monolayer sorption capacity and the constant K_L is related to the affinity of ions to the adsorption site. The values of q_m increase as the temperature increases thus indicating that the sorption process is endothermic.

The essential feature of the Langmuir isotherm is identifying the feasibility and favourability of the adsorption process and can be expressed by a dimensionless constant called separation factor (R_L) (Kaur et al., 2012). The separation factor can be calculated from equation 2.8:

$$R_L = \frac{1}{1 + K_L C_o}$$

It can be seen from Table 4.4 these values fall within the favourable range $0<R_L<1$ (Darwish et al., 2019). Since these results fall within this range it can be stated that AS adsorption onto PAC is favourable at these conditions

4.6.3 Freundlich Isotherm

The equilibrium data were fitted to the Freundlich isotherm given in equation 2.9:

$$q_e = K_f C^{\frac{1}{n}}$$

The linear form of the Freundlich isotherm, equation 2.10, was used to plot log q_e verse C_e and be seen in Figure 4.11. This plot allows for the calculation of K_f and n given in Table 4.7.

$$logq_e = logK_F + \frac{1}{n} logC_e$$

.

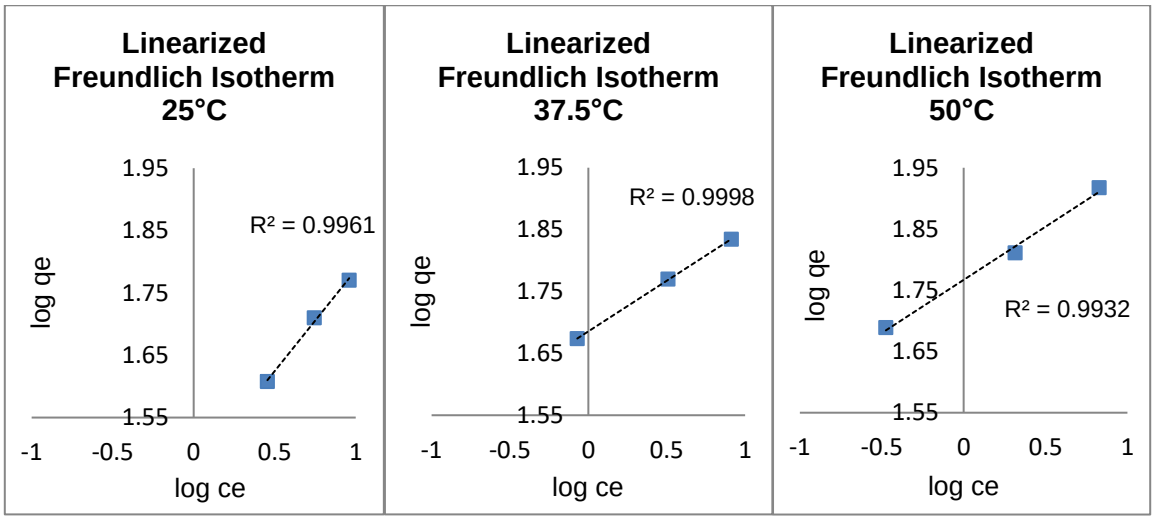

Figure 4-11: Linearized Freundlich isotherm at different temperature

The Freundlich isotherm constants gives an indication of the favourability of adsorption and the anionic surfactant adsorption capacity, respectively. The isotherm model applies to heterogeneous surfaces and the interaction between adsorbed molecules. The model's application also suggests that sorption energy exponentially decreases on completion of the sorption centre of an adsorbent. The n values indicate the degree of non-linearity between solution concentration and the adsorption as follows: if n = 1, adsorption is linear; n > 1, then adsorption is physical and if n < 1 adsorption is chemical. This shows that the adsorption of anionic surfactants on PAC is a physical process as shown by n values in Table 4.7 (Alasad, 2019). Kaur et al. (2012) also stated that values of n>1 show favourable adsorption. Table 4.7 shows the values of n are greater than one at all three temperatures showing favourable adsorption. The Freundlich isotherm adequately describes the adsorption of AS onto PAC.

4.6.4 Temkin Isotherm

The equilibrium data were fitted to the Temkin isotherm given in equation 2.11:

$$q_e = \frac{RT}{b} \ln (KC_e)$$

The Temkin isotherm's linear form, equation 2.11, was used to plot log q_e versus ln(C_e) and can be seen in Figure 4.11. This plot allows for the calculation of K and b given in Table 4.4

$$q_e = B_T lnK + B_T lnC_e$$

Where B_T represents:

$$B_T = \frac{RT}{b}$$

The Temkin isotherm equation suggests a linear decrease of sorption energy as the degree of an adsorbent's sorption centres decreases. This model accounts for indirect adsorbate and adsorbent interactions stating that the heat of adsorption of all molecules decreases linearly with coverage because of these interactions. The Temkin isotherm constants K_T and B can be calculated using linear plots q_e vs ln(C_e) as seen in Figure 4.12.

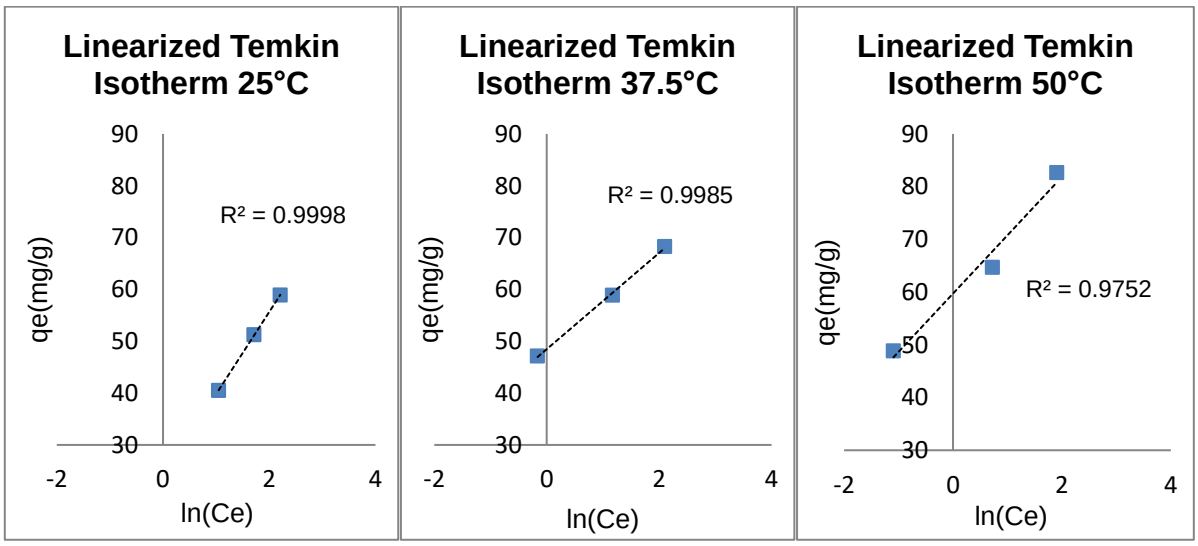

Figure 4-12: Linearized Temkin isotherm at different temperature

The Constant K_T is the equilibrium binding constant corresponding to the maximum binding energy and B relates to the heat of adsorption (Kaur et al., 2012). It can be seen from Table 4.7 the values of K_t increased with an increase in temperature while B decreased.

4.6.5 Dubinin-Radushkevich (D-R) Isotherm

The equilibrium data of each experiment was fitted to the D-R isotherm given in equation 2.14:

$$qe = qs - e^{K^2}$$

The Polanyi potential (Ɛ) (J/mol) was calculated with Equation 2.15.

$$\varepsilon = RTln(1 + \frac{1}{C_e})$$

The linear form of equation 2.14 allows for the values of q_m and K to be calculated plotting $\ln(q_e)$ versus $Ɛ^2$ as shown in figure 4.13.

$$\ln qe = lnqs - K^2$$

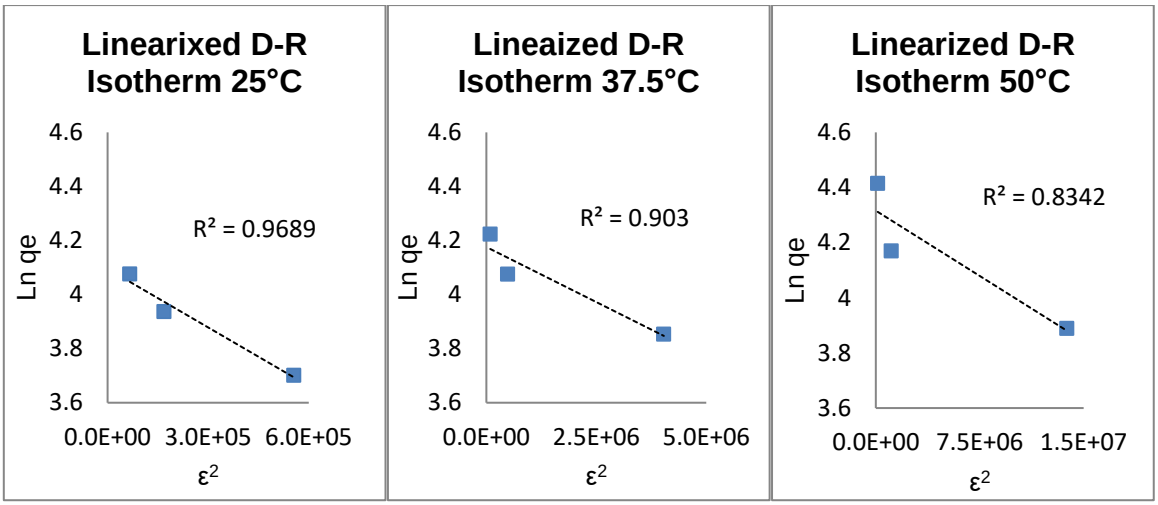

Figure 4-13': Linearized D-R adsorption isotherm

The D-R isotherm model is generally used for expressing the mechanism of adsorption with the distribution of Gaussian energy onto heterogeneous surfaces. The application of this model is generally used to distinguish between chemical and physical adsorption

A distinguishing feature of the D-R isotherm is the fact that it is temperature dependent; hence when adsorption data at different temperatures are plotted as a function of the logarithm of amount adsorbed versus the square of potential energy, all suitable data can be obtained (Ayawei et al., 2017)

This model's linear form allows the values of q_m and K to be calculated by plotting $\ln(q_e)$ versus ε^2 as shown in Figure 4.13. the parameters for the model are found in Table 4.7. the mean energy of adsorption can be calculated using the following equation:

$$E = -2K^{-1/2}$$

The values of E in Table 4.7 show the type of adsorption taking. Boubaker and Ridha. (2020) states that if the energy of adsorption is less than 8000 j/mol the adsorption is physical in nature. The values obtained in Table 4.7 shows that the adsorption process is a physical one.

Table 4-7: Adsorption isotherm parameters at different temperatures

Isotherms	**Parameters**	**Temperature**		
		25 ^{0}C	**37,5 ^{0}C**	**50 ^{0}C**
Langmuir	q_{max} (mg/g)	74,627	72,464	87,719
	K_L (L/g)	0,4110	1,7468	2,1509
	R_L	0,1395	0,0368	0,0301
	R^2	0,9995	0,9983	0,9948
Freundlich	K_F (mg/g)	4,1620	5,3951	5,8703
	n	3,0864	6,1124	5,7604
	R^2	0,9961	0,9998	0,9932
Temkin	K_T (L/g)	4,5310	184,96	221,72
	b (J/mol)	15,851	9,2846	11,056
	R^2	0,9998	0,9985	0,9752
D-R	q (mg/g)	60,039	65,085	74,888
	K (mol^2/J^2) $x10^{-6}$	0,7	0,08	0,03
	E (J/mol)	845,15	2500.0	4082,5
	R^2	0,9689	0,9030	0,8342

Figures 4-10, 4-11, 4-12 and 4-13 shows that the AS experimental measurements give an acceptable fit for all isotherm models with acceptable analogous and a linear average (3 Temperature levels) regression coefficient R2 of 0.9975, 0.9964, 0.9912 and 0.9020 (Table 4.7) for Langmuir, Freundlich, Temkin and Dubinin-Radushkevich, respectively. It can be noticed that the Dubinin-Radushkevich isotherm model simulation gives a less acceptable analogous for AS experimental measurements with regression coefficient R2 of 0.9020.

The constants in the isotherm equations were evaluated and reported in Table 4.7 and it was observed that Langmuir isotherm represented the equilibrium sorption best. This result suggests monolayer coverage of the surface of AS on PAC since the Langmuir isotherm assumes that the surface is homogeneous. A Similar isotherm fit for sorption has been reported (Rajamohan et al., 2014). As expected for an endothermic process, the values of qmax and K_L increased with an increase in temperature

4.7 Adsorption Kinetic modelling

The studies on the rate of removal are essential for the proper design of wastewater treatment projects. The rate of sorption is vital for designing batch adsorption experiments thus the effect of contact time on the removal of anionic surfactants was investigated. To further understand the adsorption rate mechanism of Anionic Surfactant onto powdered activated carbon, sorption kinetic studies were conducted. Kinetic studies are essential to understand the adsorption dynamics in terms of the order of the rate constant (Cazetta et al., 2011).

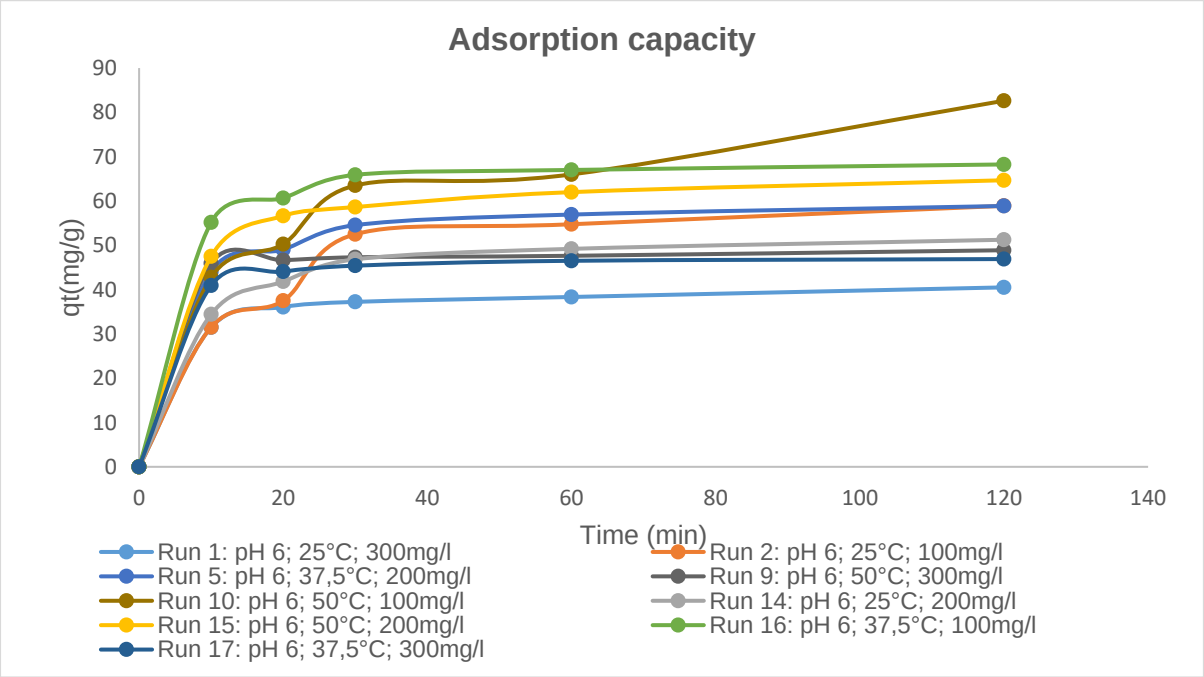

Figure 4-14: Adsorption capacity

The kinetic models used to evaluate the system were, pseudo-first-order, pseudo-second-order, intra-particle diffusion and Elovich. The regression coefficients and information are presented in Table 4.7. Figure 4.14 represent the removal of AS and the adsorption capacity over time, respectively where equilibrium is reached after 30 minutes for the experiments.

According to Sanda et al. (2017), the initial uptake can be attributed to the accumulation of anionic surfactants on the PAC surface. The mechanism of solute transfer to the solid includes diffusion through the fluid film surrounding the adsorbent particle and diffusion through pores to internal adsorption sites. The initial concentration gradient between the film layer and solid is large and thus the transfer of solute onto the solid surface is faster during the first 30 minutes. After 30 minutes intra-particle diffusion becomes the dominant mechanism and the solute takes increased time to transfer to the solid surface and internal adsorption sites through pores (Ragheb, 2013).

4.7.1 Pseudo-First Order (PFO) model

The kinetic data obtained from the experiments were fitted to the PFO model in equation 2.17

$$\frac{dq_t}{dt} = k_f(q_e - q_t)$$

The linear form of equation 2.11 was used to determine the values of K_f and q_e shown in equation 2.18

$$ln(q_e - q_t) = lnq_e - k_f t$$

The rate constant k_f and adsorption capacity q_e is found by plotting $ln(q_e\text{-}q_t)$ versus time.

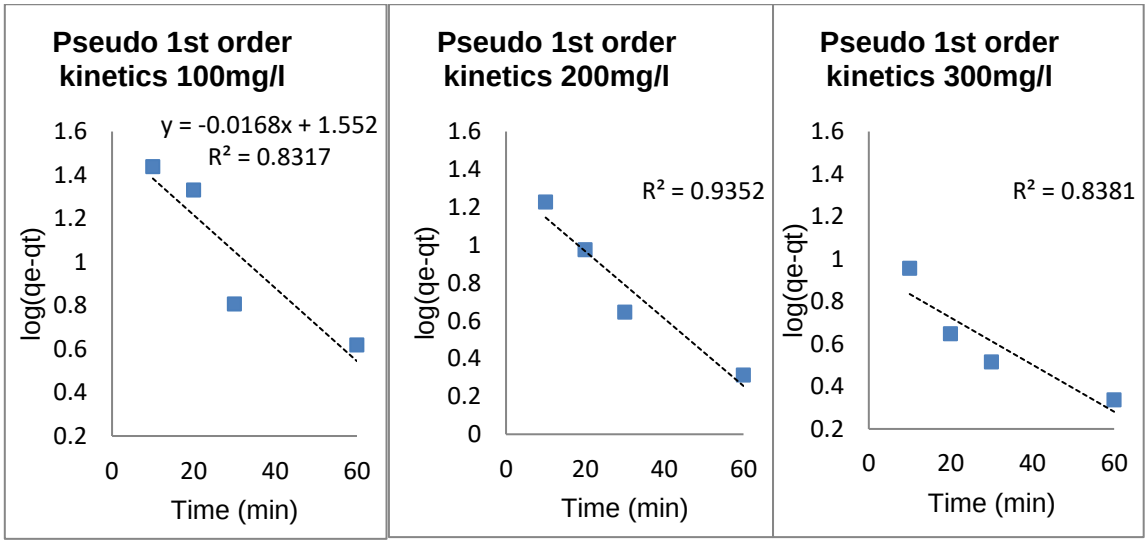

Figure 4-15: Linearized 1st order kinetics at 25^{0}C

The linearized pseudo-first-order rate equation was used to determine the value of K_f (rate constant of adsorption and q_e (calculated adsorption capacity). The values of these parameters can be found in Table 4.8. it can be observed that the calculated q_e values are not in agreement with the experimental q_e values of all runs performed. Moreover, the correlation coefficients (R^2) are significantly smaller than those found in the pseudo second-order kinetic model. This information indicates the adsorption kinetic data obtained cannot be explained by pseudo-first-order reaction kinetics.

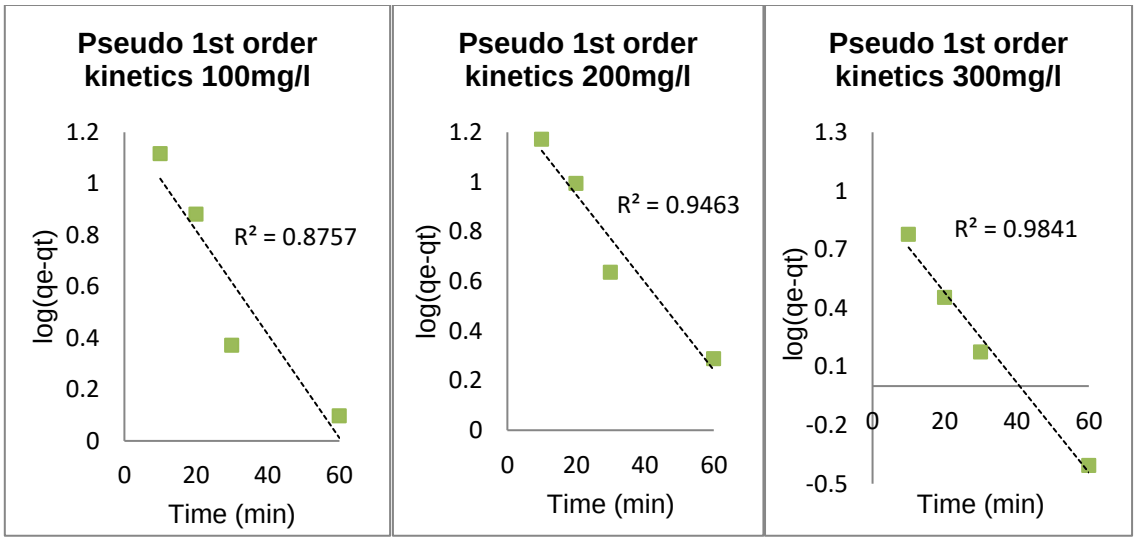

Figure 4-16: Linearized 1st order kinetics at 37.5^{0}C

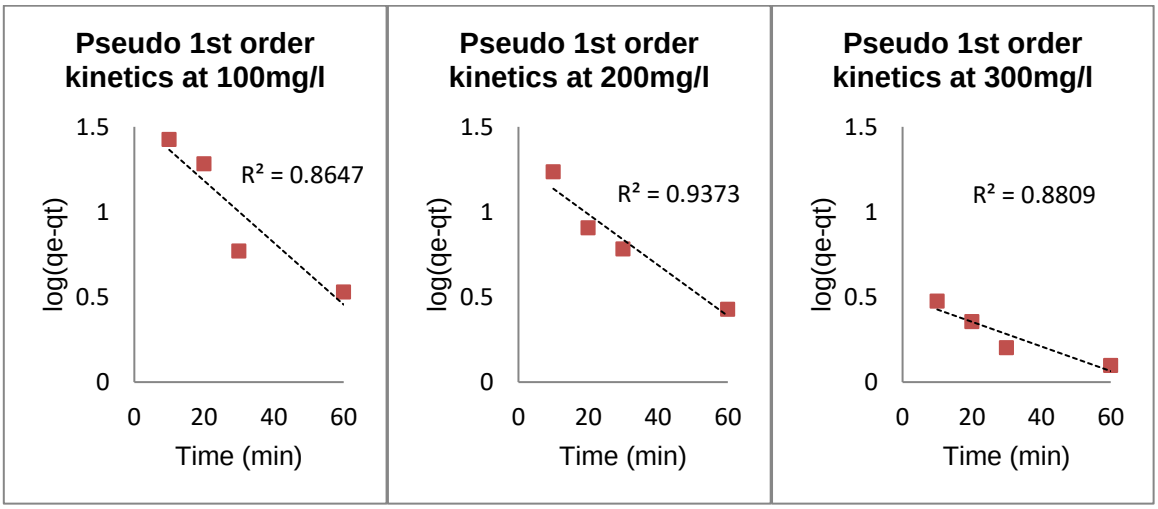

Figure 4-17: Linearized 1st order kinetics at 50^{0}C

4.7.2 Pseudo-Second Order (PSO) model

The kinetic data obtained from the experiments were fitted to the PSO model in equation 2.19

$$\frac{dq_t}{dt} = k_s(q_e - q_t)^2$$

The linear form of equation 2.20 was used to determine the values of k_s and q_e shown in equation 2.18

$$q_t = \frac{t}{\frac{1}{k_s q_e^2} + \frac{t}{q_t}}$$

The rate constant k_s and adsorption capacity q_e is found by plotting t/qt versus time.

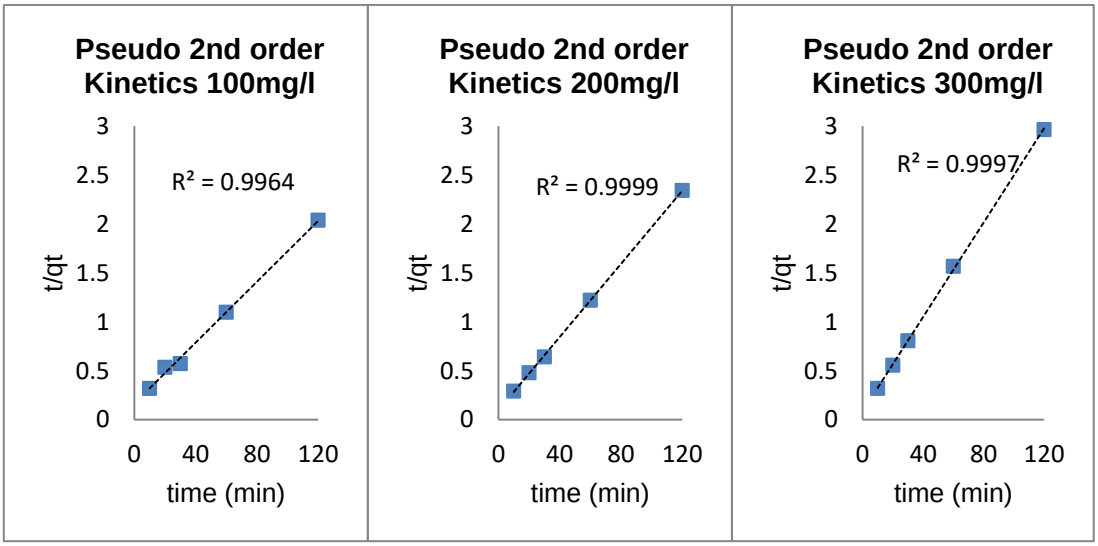

Figure 4-18: Linearized 2nd order kinetics at 25^{0}C

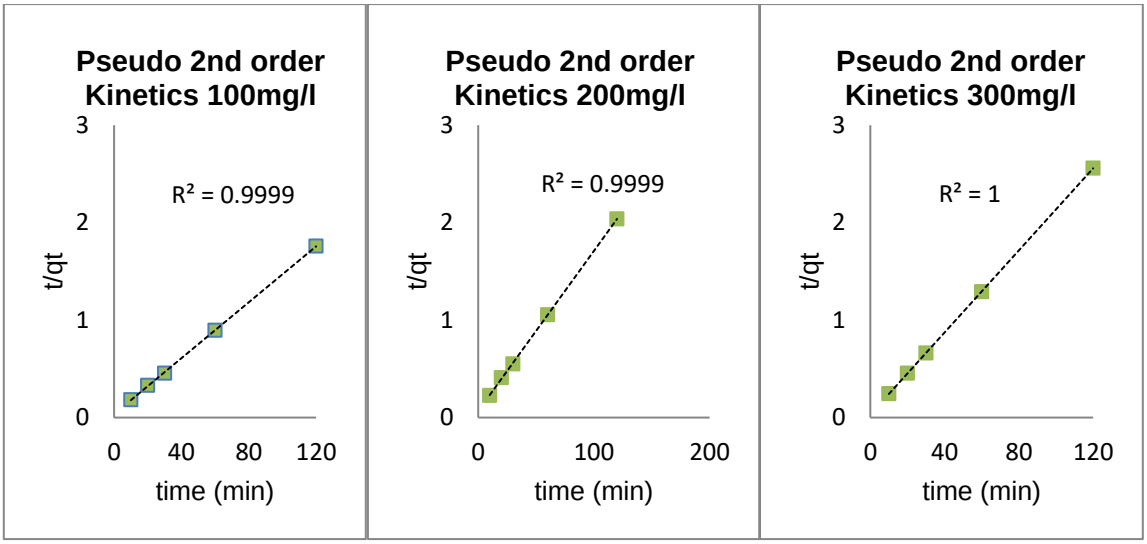

Figure 4-19: Linearized 2nd order kinetics at 37.5^{0}C

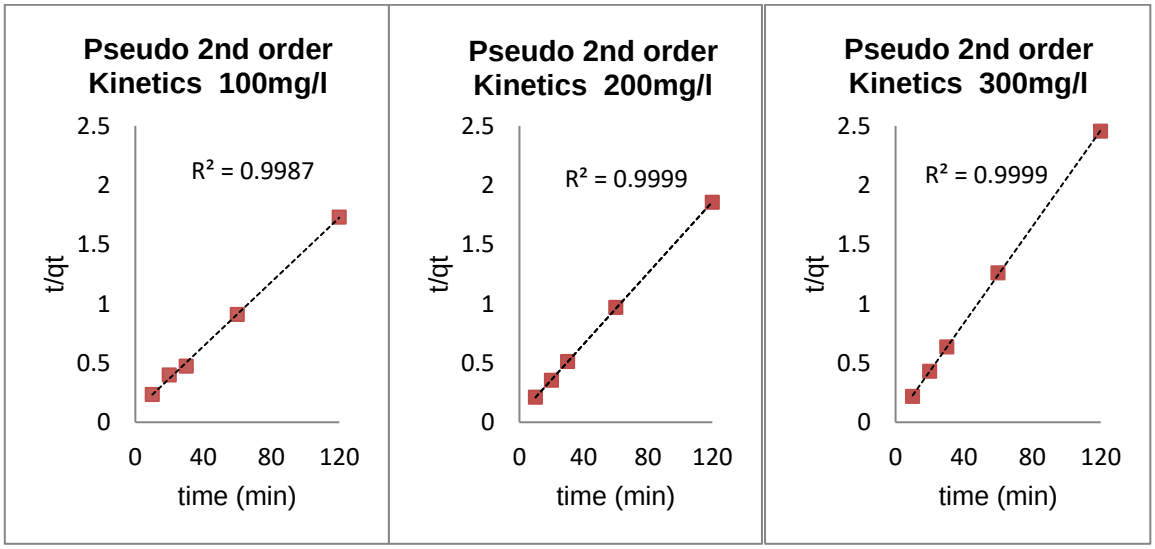

Figure 4-20: Linearized 2nd order kinetics at 50^{0}C

The linearized pseudo second-order rate equation was used to determine the value of k_s (rate constant of adsorption and q_e (calculated adsorption capacity). The values of these parameters can be found in table 4.5 and 4.6. The calculated and experimental q_e values are in agreement with each other in all the runs as well as the R^2 values for most of the runs being 0.99. This shows that the sorption can be approximated more appropriately by the pseudo second-order kinetic model than the first-order kinetic model for the adsorption of anionic surfactants onto PAC.

4.7.3 Intra-Particle Diffusion (IPD) Model

The kinetic data obtained from the experiments were fitted to the IPD model in equation 2.24

$$q_t = K_d t^{1/2} + C$$

The rate constant k_d and C is found by plotting qe versus $t^{0.5}$.

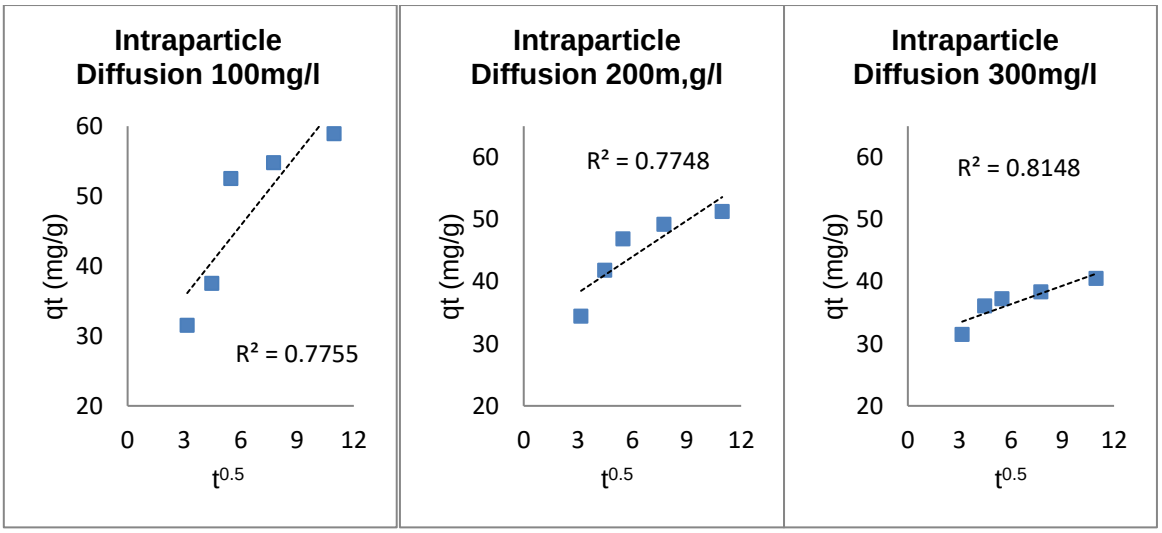

Figure 4-21: Linearized IPD at 25^{0}C

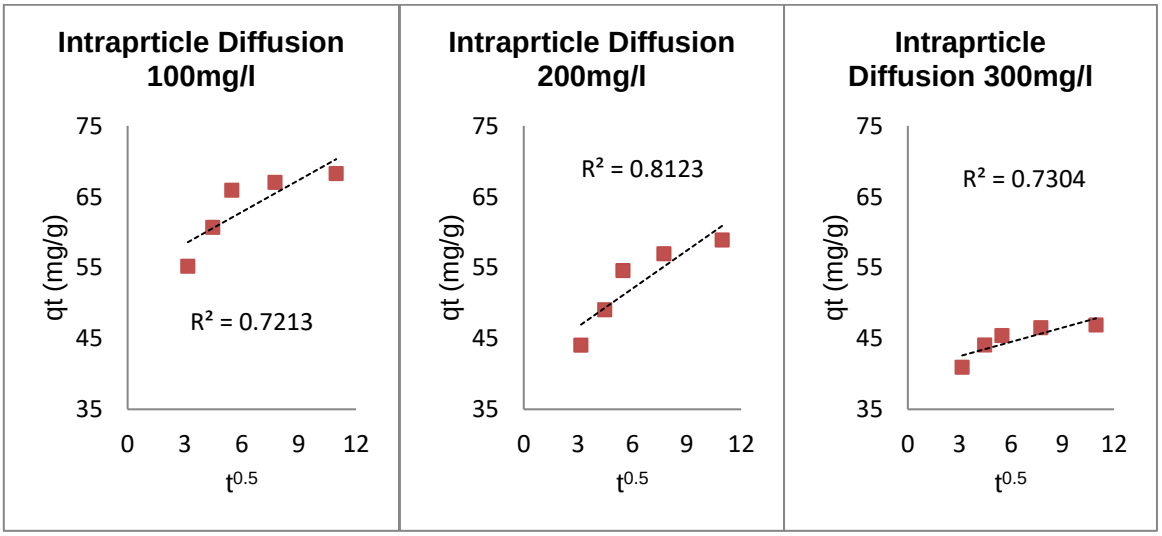

Figure 4-22: Linearized IPD at 37.5^{0}C

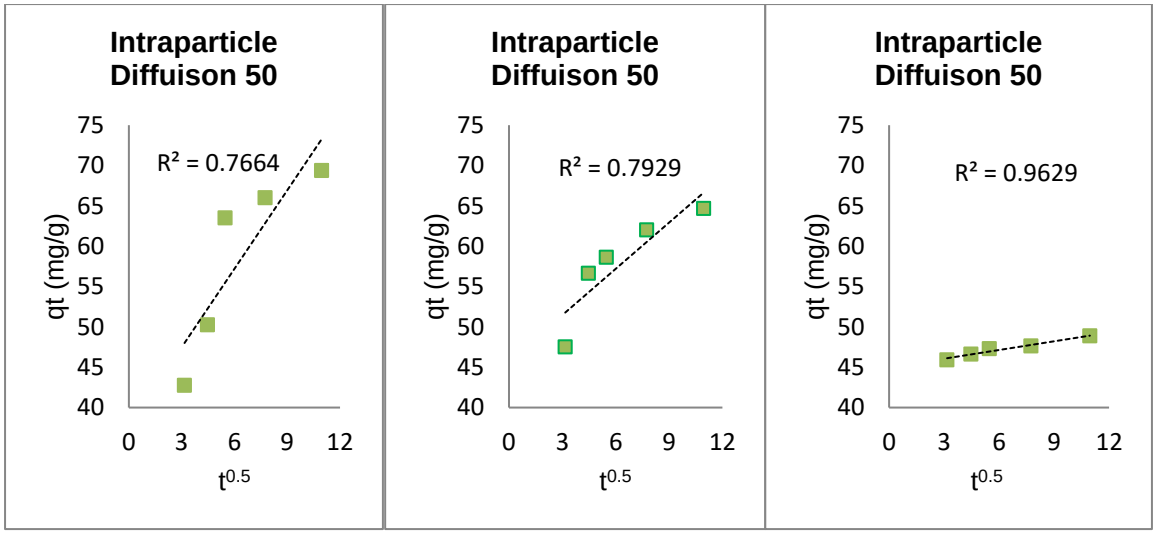

Figure 4-23: Linearized IPD at 50^0C

An empirical relationship common to most adsorption processes is that the uptake varies proportionally with $t^{0.5}$, the Weber-Morris plot (qt versus $t^{0.5}$) rather than contact time, t. The intraparticle diffusion models linearized form was used to determine the intraparticle diffusion rate constant (K_{id}) and the intercept C (mg/g). The values of C give an indication about the effect of the boundary layer, that is, a larger intercept indicates a larger boundary layer effect. this is attributed to the instantaneous utilization of the most readily available adsorbing sites on the adsorbent surface. The values of K_d and C are listed in Table 4.7. (Papegowda & Syed, 2017) states for intraparticle diffusion to be involved in the adsorption process and diffusion is a rate controlling step, the plot of qt versus $t^{0.15}$ has to be linear and pass through the origin. It can be observed from Figures 4.21, 4.22 and 4.23 this criterion is not met. Moreover, the R^2 values are much lower than those of pseudo-second-order kinetics. This indicates that intraparticle diffusion is not the only rate-limiting step.

4.7.4 Elovich Model

The kinetic data obtained from the experiments were fitted to the Elovich model in equation 2.23

$$q_t = \frac{1}{\beta}\ln(\alpha\beta) + \frac{1}{\beta}\ln(t)$$

The values of α and β are obtained from the intercept and slope of the plot of ln(t) versus qt(mg/g). The values of α and β are found in Table 4.8

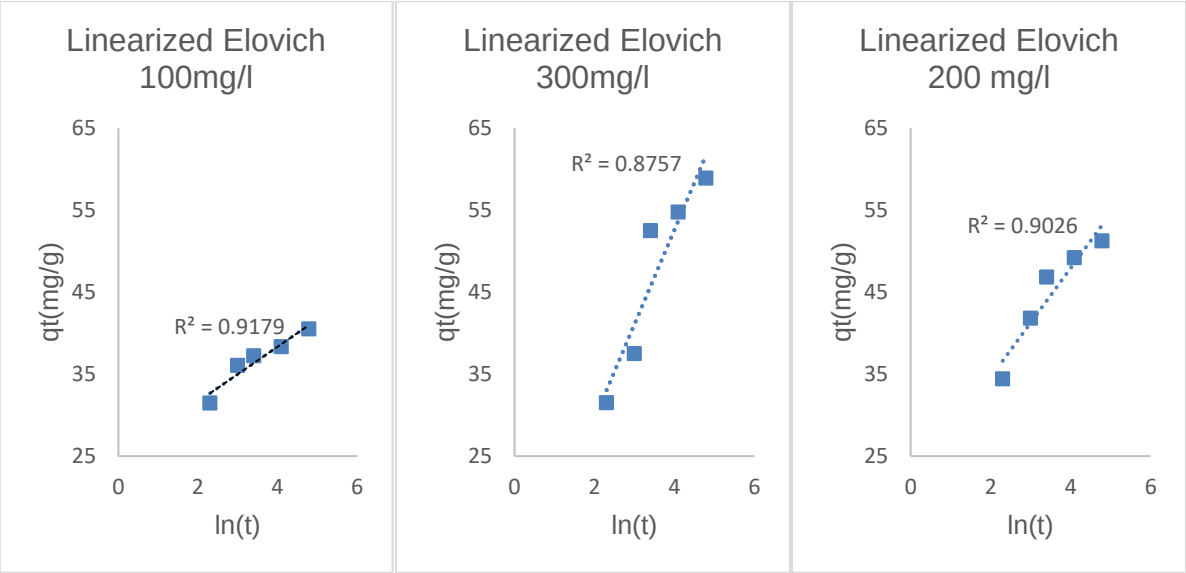

Figure 4-24: Elovich Model at 25^{0}C

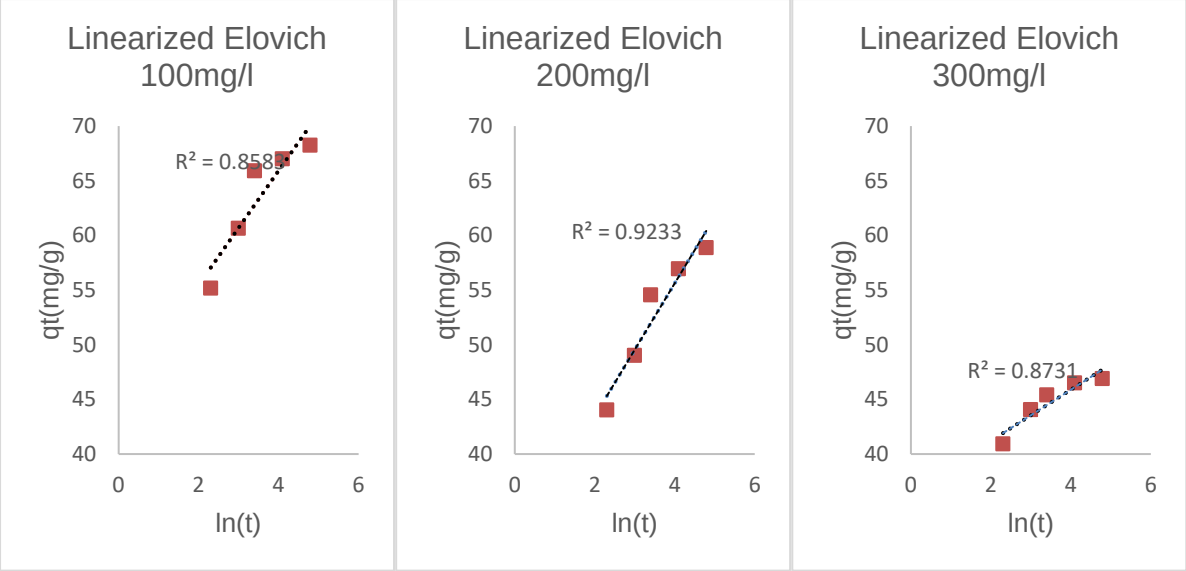

Figure 4-25: Elovich Model at 37.5^{0}C

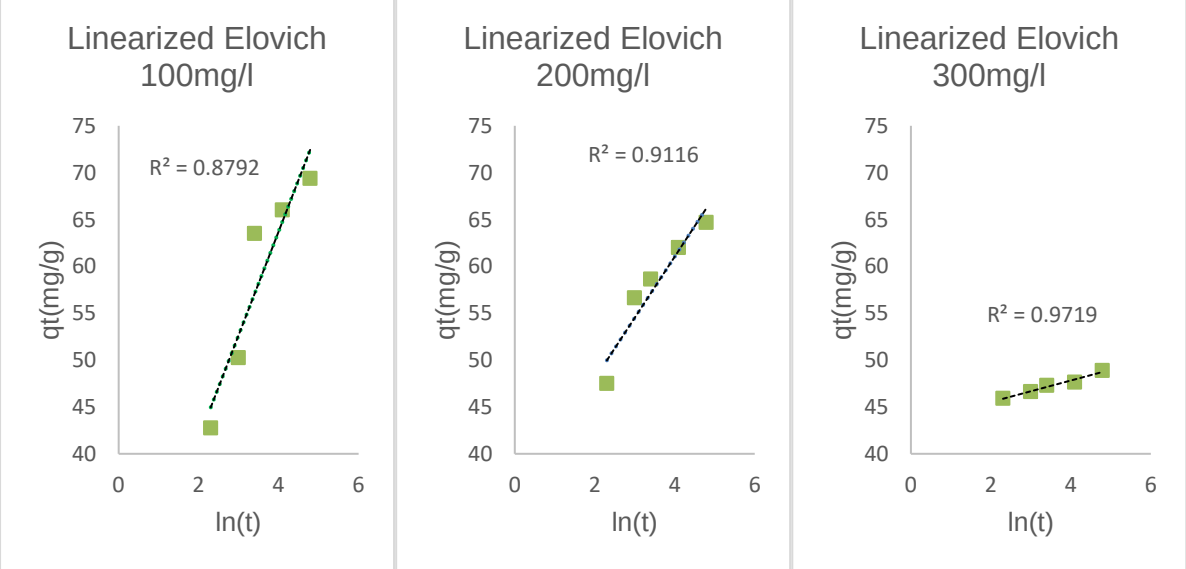

Figure 4-26: Elovich Model at 50^{0}C

The Elovich kinetic model considers the solid surface of the adsorbent is energetically heterogenous and the influence of the desorption process and interactions between adsorbed species on adsorption kinetics are not significant. The α parameter is related to the initial adsorption rate. As shown in Table 4.8 the values of α are high, which agrees with the kinetic data which showed equilibrium is reached after 30 minutes for all experiments. The β parameter is related to the desorption coefficient and has a range of 0.086 to 0.427. These values indicate a low desorption rate thus showing an effective interaction between AS and PAC (Pezoti et al., 2014).

Pseudo-first order (PFO), pseudo-second order (PSO), intra-particle diffusion (IPD) and Elovich model fitted to testing experimental data and are shown. These kinetic models were expressed in linear form as seen in Table 4-8. It can be seen from the kinetic parameters that the pseudo-second-order kinetic model best fitted the kinetic data.

The pseudo-first-order model displayed R^2 values of less than 0.9 in all but one experiment showing this model does not describe the kinetic data. The PFO model generally describes physical adsorption onto homogenous adsorbents (Belaid et al., 2013).

The best fit model that describes the kinetic data was the Pseudo second order model. From Table 4.8, the PSO model has the highest R^2 values across all the experimental run compared to the other kinetic models. The calculated q_e values are also very close to the experimental q_e values making it the best fit mode. Based on this evidence it can be stated that the adsorption of AS onto PAC is chemisorption. It can be seen from the R^2 The pseudo-second-order model assumes that two surface sites will be occupied by one sorbate ion (Aguayo-Villarreal et al., 2011).

The Elovich model fits the data adequately with an average R^2 value of 0.9 across all 9 experimental runs (R^2 values in Table 4.8). It can be said that the Elovich model can be accepted as one of the characteristics of the adsorption process based on the evidence in Table 4.8. Belaid et al. (2013) state an initial fast adsorption followed by a slow chemisorption is well expressed by the Elovich model when the adsorption process is described by PSO kinetics which is the case in this study.

The pseudo-second-order model could not identify the diffusion mechanism. Due to this, intra-particle diffusion was employed. If the plot passes through the origin, then intraparticle diffusion is the rate-controlling step. However a larger intercept was observed in this experiment which confirmed that the boundary layer effect is greater. (Rajamohan et al., 2014).

4.7.5 Adsorption kinetics parameters

Table 4-8: Linearized adsorption kinetic paramters

Equation	Parameter	1	2	3	4	5	6	7	8	9
PFO	q_e exp (mg/g)	40,5	58,90	48,83	82.65	58,87	51,25	64,68	68,25	46,89
	q_e cal (mg/g)	8,82	35,65	3,156	43,47	20,04	21,06	19,31	16,64	8,72
	k_f (min-1)	0,0255	0,0013	0,017	0,017	0,041	0,041	0,035	0,047	0,053
	R^2	0,830	0,830	0,880	0,780	0,940	0,935	0,937	0,876	0,984
PSO										
	q_e exp (mg/g)	40,5	58,89	48,83	69,75	58,87	51,25	64,68	68,25	46,89
	q_e cal (mg/g)	40	66,25	48,08	75,19	60,98	53,48	66,67	69,93	47,62
	k_s (g/mg min)	0,01	0,0013	0,040	0,001 6	0,004	0,0036	0,0037	0,0058	0,014
	R^2	0,99	0,97	0,99	0,990	0,99	0,990	0,990	0,990	0,990
IPD										
	k_{id} (mg/g min0.5)	1,37	5,33	0,38	5,23	2,82	1,94	0,359	1,504	0,672
	C (mg/g)	28,99	16,23	44,90	28,37	36,42	32,39	44,98	53,82	40,48
	R^2	0,78	0,83	0,89	0,840	0,89	0,775	0,721	0,730	0,963
Elovich										
	α (mg/g.min)	2025	5147.9	$2.4x10^{16}$	64.43	174.3	163.7	1385.7	28851	6050477
	β (g/mg)	0.086	0.29	0.87	0.090	0.164	0.150	0.153	0.191	0.427
	R^2	0.87	0.91	0.97	0.87	0.92	0.90	0.91	0.85	0.87

4.8 Adsorption thermodynamics

Thermodynamic considerations of an adsorption system are essential in determining whether the process is spontaneous or not and if its endothermic or exothermic. The Gibbs free energy is a measure of the systems spontaneity and is significant for values less than zero (Papegowda & Syed, 2017).

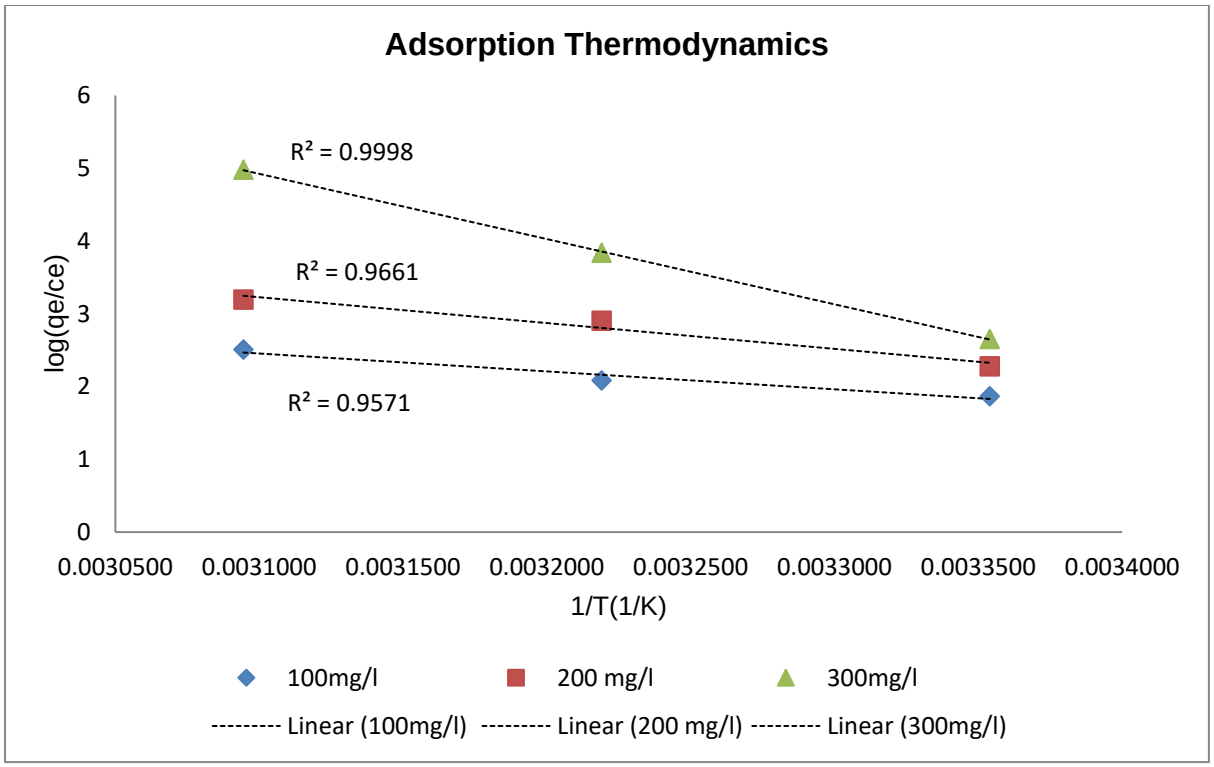

Figure 4-27: Adsorption thermodynamics

Table 4-9: Adsorption thermodynamic properties

concentration adsorbent (mg/l)	ΔH (Kj/mol)	ΔS (KJ/mol.K)	ΔG (KJ/mol)		
			298.15 K	310.65 K	323.15 K
100	20.456	0.084	-4.533	-5.581	-6.629
200	29.505	0.118	-5.744	-7.222	-8.700
300	74.549	0.272	-6.558	-9.958	-13.359

The thermodynamic adsorption parameters are summarized in Table 4.7. The entropy and enthalpy values were found from the intercept and slope of figure 4.27. The negative values of ΔG^0 indicate the adsorption process happens spontaneously and the positive ΔH^0 values show the process is endothermic. An increase in temperature increased the uptake capacity of anionic surfactant ions. Positive ΔS^0 values showed an affinity of the adsorbent towards the adsorbate and that there was also greater randomness at the adsorbent-adsorbate interface (Obayomi et al., 2020).

4.9 Nonlinear regression

From the linear regression data provided PSO best describes the kinetic data exhibiting the highest coefficient of determination (R^2) value, and the q_e calculated values agree with q_e experimental values. The R^2 values are for PFO and IPD were significantly lower than that of PSO and the qe calculated values for PFO were not in agreement with the qe experimental values. However, the use of R^2 values not alone good enough to determine which kinetic model is the best fit for the data. An error function assessment is required to properly evaluate a model equation's suitability to experimental results (Jasper et al., 2020). Error functions are used to measure the deviation of theoretically predicted data from actual experimental data values. The problem arises when error functions are used with linearized equations of nonlinear functions to determine a model's suitability. In some linear models to reduce the error factor, log or square root transforms are applied if the error increases with the dependent factor, and if the error variance decreases with increasing dependent factor then exponential or square alters are applied. However, the use of the R^2 or the Sum of the Squares of the Errors (SSE) does not detect the biasness of the parameters. Therefore making conclusions based on R^2 and linear models only can be somewhat misleading (Kajjumba et al., 2018). Based on these reasons nonlinear regression and error analysis are essential to determine the sorption kinetics and isotherms of the process

4.9.1 Nonlinear adsorption isotherm regression

The nonlinear regression performed on the experimental data was performed using Orginlab 2021 software. The results of the regression analysis are found in Figures 4.28, 4.29, 4.30 and Table 4.8. The data was fitted to Langmuir, Freundlich, Temkin and D-R isotherms to determine the best fit isotherm and compare the findings to that of linear regression.

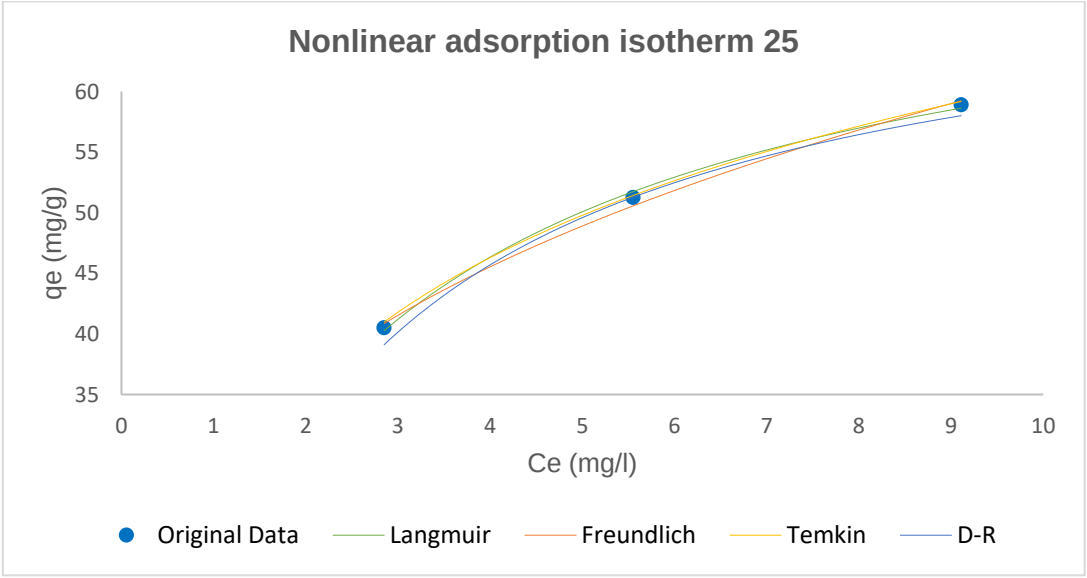

Figure 4-28 Nonlinear adsorption isotherm regression at 25^0C

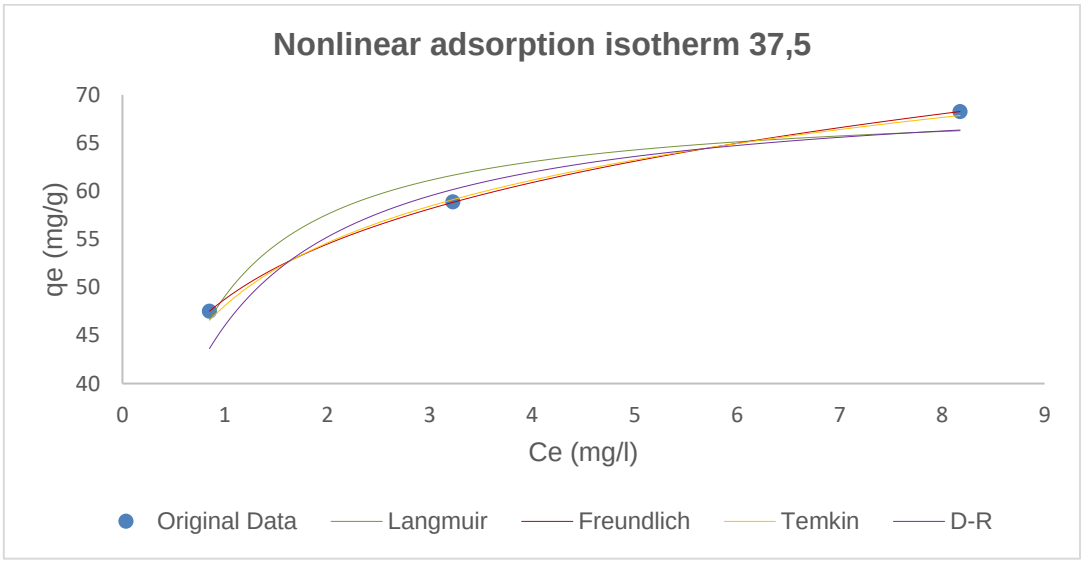

Figure 4-29 Nonlinear adsorption isotherm regression at 37.5^0C

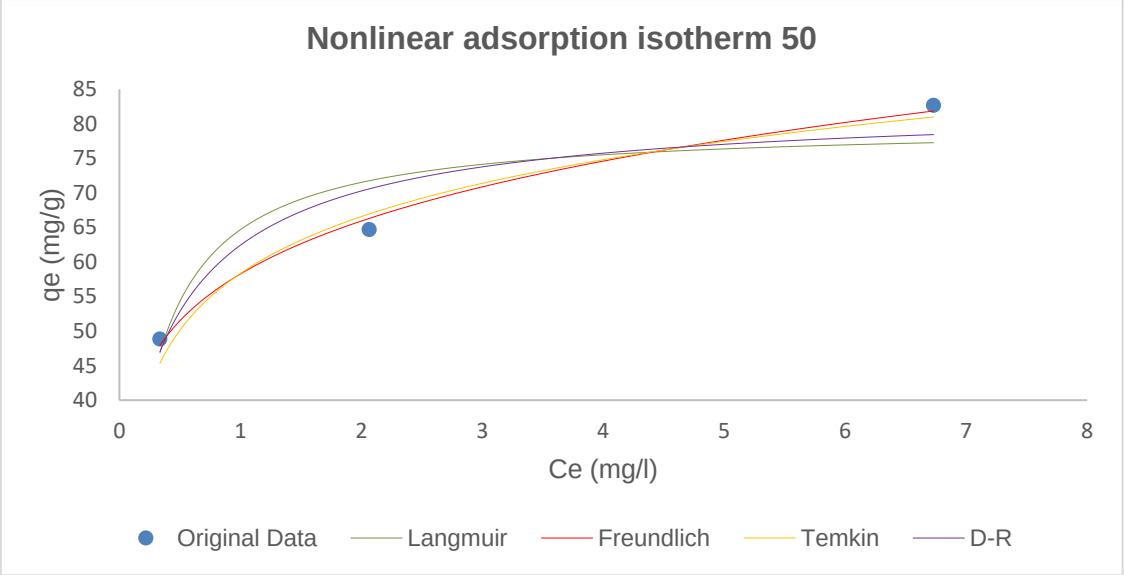

Figure 4-30 Nonlinear adsorption isotherm regression at 50^0C

The findings from Figures 4.28, 4.29 and 4.30 shows the data follows the Freundlich adsorption isotherm. The Temkin isotherm follows the Freundlich isotherm very closely while the Langmuir and D-R isotherms did not fit very well. This can be seen in Table 4.10 where Freundlich and Temkin show R^2 values of 0.99 across all temperatures but the Langmuir and D-R isotherms R^2 values drop as the temperature increases showing a lack of fit at higher temperatures. Another area tested to evaluate the best fit isotherm was error analysis. From Tables 4.12 and 4.13it can be seen Freundlich isotherm has the smallest SSE and the average relative error (SAE) values followed by Temkin, Langmuir and D-R isotherms, respectively. Based on the R^2 being the closest to unity and having the smallest SSE and SAE values it can be seen the adsorption data follows the Freundlich isotherm. In a study performed by (Ayranci & Duman, 2007) where the removal of anionic surfactants from aqueous solutions using activated carbon was studied found that the data fitted the Freundlich isotherm better than Langmuir. In a similar study performed by Gupta et al. (2003) where a low cost waste activated carbon was tested for the removal of sodium dodecyl sulfate (SDS) in aqueous solutions. The study found the data best fitted to the Freundlich isotherm which agrees with the findings of this study. However in the study performed by (Veit et al., 2020) who investigated the adsorption of anionic surfactants from CWW onto activated carbon found the data to best fit the Langmuir isotherm. From the nonlinear regression it is much easier to distinguish which model the data follows. The n values were found to show favourability to the Freundlich isotherm as the values of 1/n were between zero and one. The values of 1/n also indicate the degree of nonlinearity between solution concentration and the sorption process. If the value is below unity the process is chemical and if the value is above unity the process

is physical. The values of 1/n in Table 4.10 are below unity thus showing the process is a chemical one (Jasper et al., 2020).

4.9.2 Nonlinear adsorption isotherm constants

Table 4-10: Nonlinear adsorption isotherm constants

Isotherms	Parameters	Temperature		
		25	37,5	50
Langmuir	q_{max} (mg/g)	73,9	69,6	82,9
	K_L (L/mg)	0,41	2,38	4,225
	R_L	0,139	0,0272	0,0155
	R^2	0,997	0,94	0,85
Freundlich	K_F (mg/g) $(L/mg)^{1/n}$	29,4	48,7	58,26
	n	3,12	6,24	5,6
	R^2	0,99	0,99	0,99
Temkin	K_T (L/mg)	4,81	166,5	136,1
	b	158,3	263,5	208,7
	R^2	0,99	0,99	0,99
D-R	q (mg/g)	71,4	70,76	83,03
	K_{D-R} x 10^{-6} (mol^2/kj^2)	404	170	83
	E (KJ/mol)	35,16	54,23	77,61
	R^2	0,98	0,95	0,902

4.9.3 Nonlinear adsorption kinetics graphs

The nonlinear regression performed on the experimental data was performed using OrginLab 2021 software. The results of the regression analysis are found in Figures 4.27-4.36 and Table 4.11. The data was fitted to PFO, PSO and IPD kinetics to determine the best fit equation and compare the findings to that of linear regression

The data was shown to follow PSO kinetics making it the best model to describe the data. The PSO model was shown to have the highest R^2 values across all the runs and exhibit the lowest SSE and SAE across all the runs. The values of q_{exp} and q_{cal} were well within agreement with each other for the PSO kinetic model more than the PFO model. The PSO model also exhibits significantly lower rate constants than the PFO which further supports the agreement between the experimental and calculated qe values. in the studies performed by (Gupta et al., 2003) and (Ayranci & Duman, 2007) both found the adsorption of anionic surfactants (AS) onto activated carbon to best follow the PSO reaction kinetics. The following of PSO reaction kinetics further supports the adsorption of anionic surfactants onto activated carbon as chemisorption.

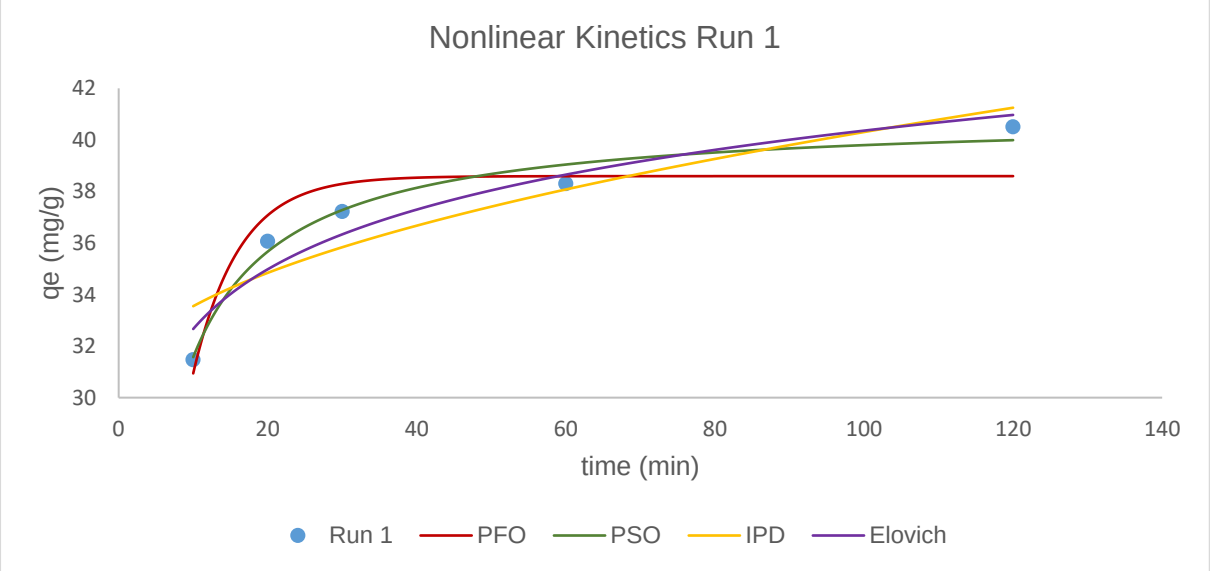

Figure 4-31: Nonlinear adsorption kinetics run 1

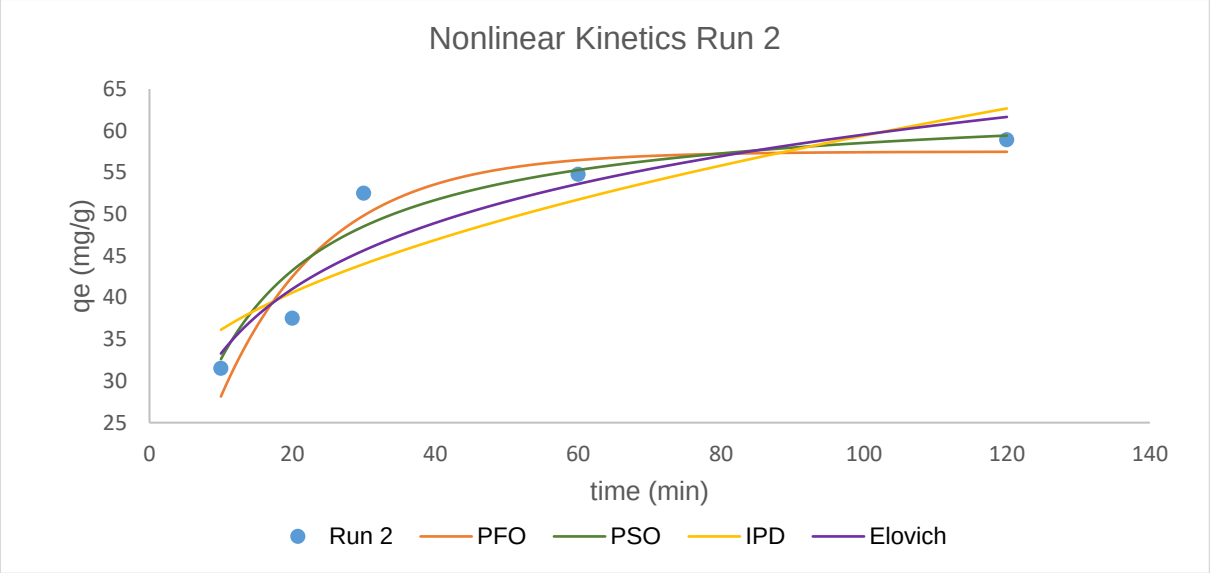

Figure 4-32: Nonlinear adsorption kinetics run 2

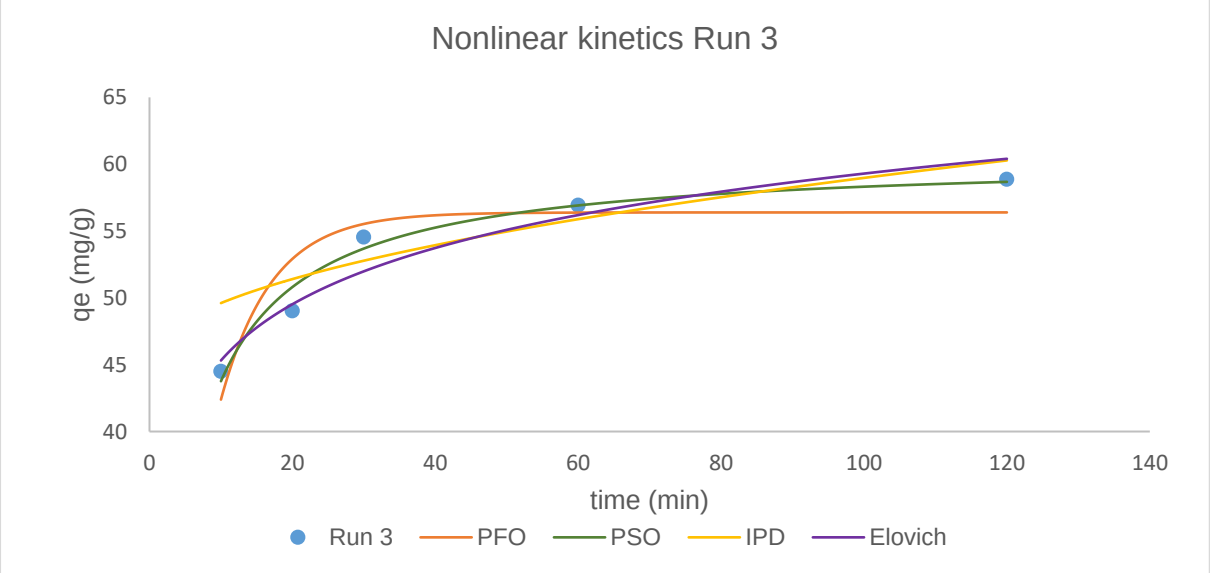

Figure 4-33: Nonlinear adsorption kinetics run 3

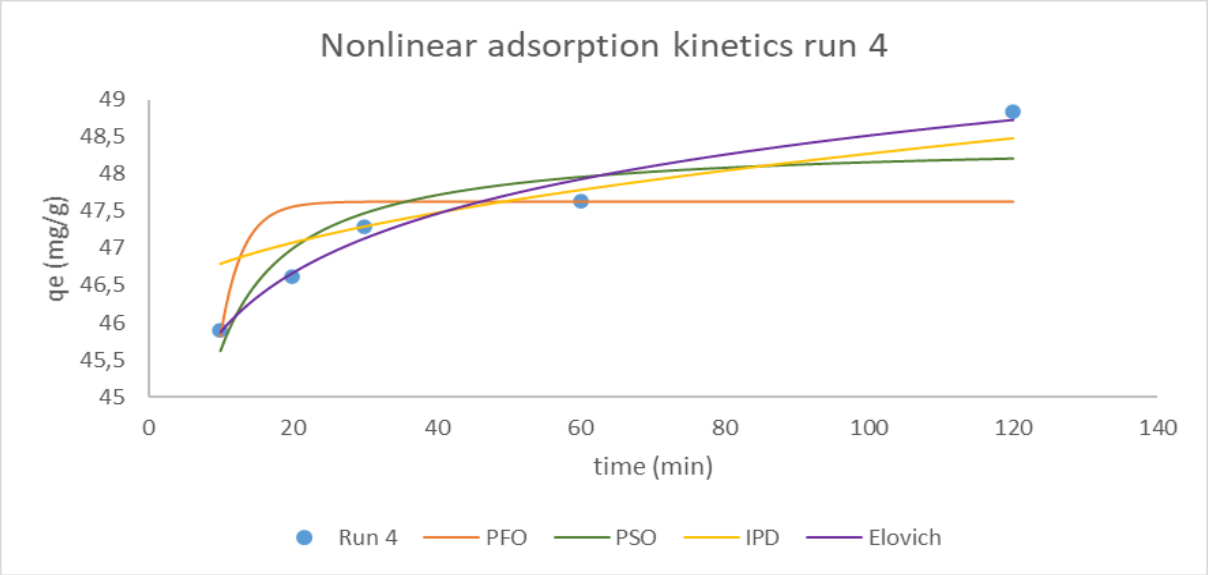

Figure 4-34: Nonlinear adsorption kinetics run 4

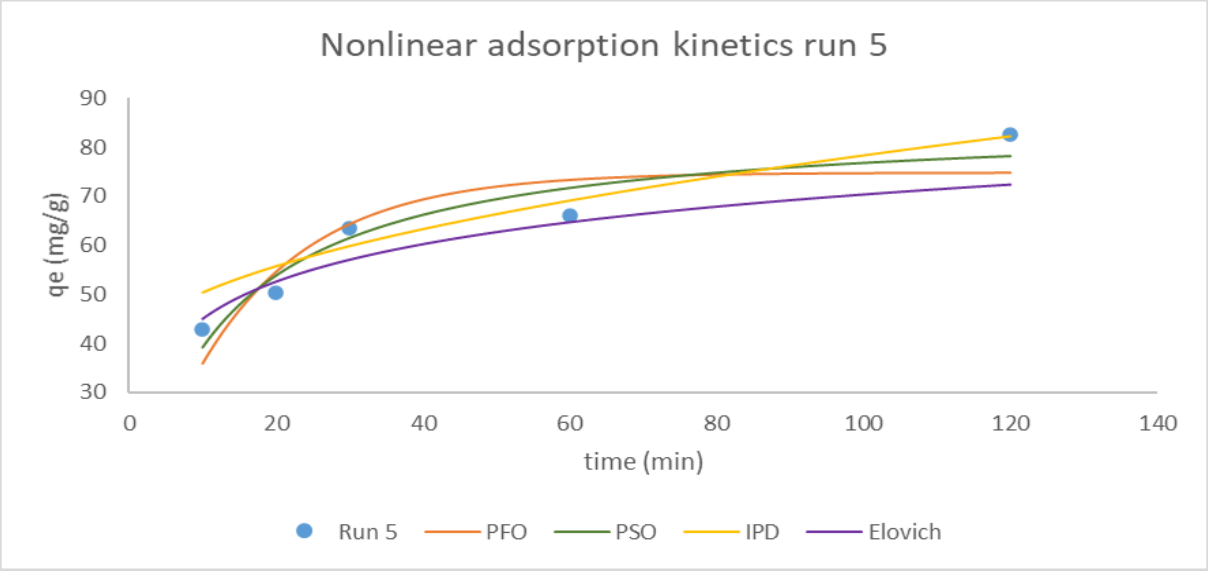

Figure 4-35: Nonlinear adsorption kinetics run 5

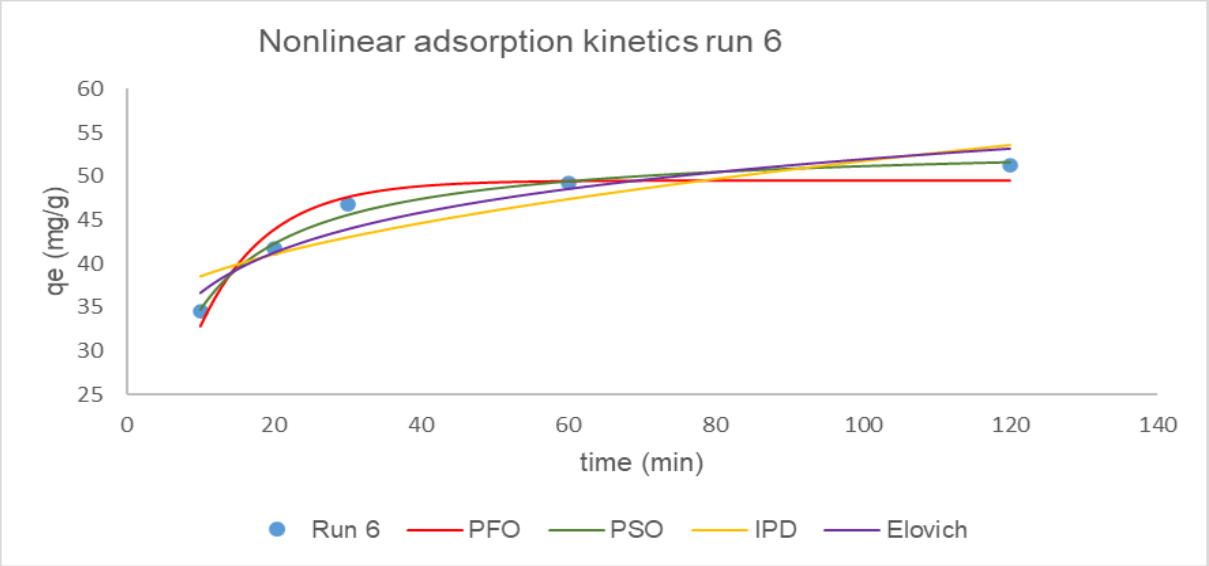

Figure 4-36: Nonlinear adsorption kinetics run 6

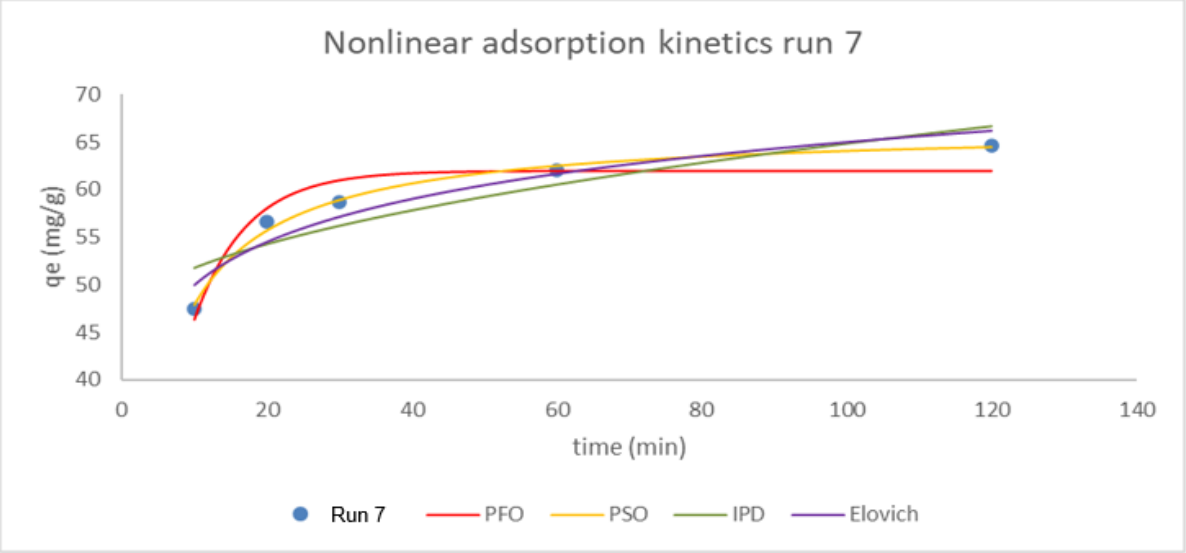

Figure 4-37: Nonlinear adsorption kinetics run 7

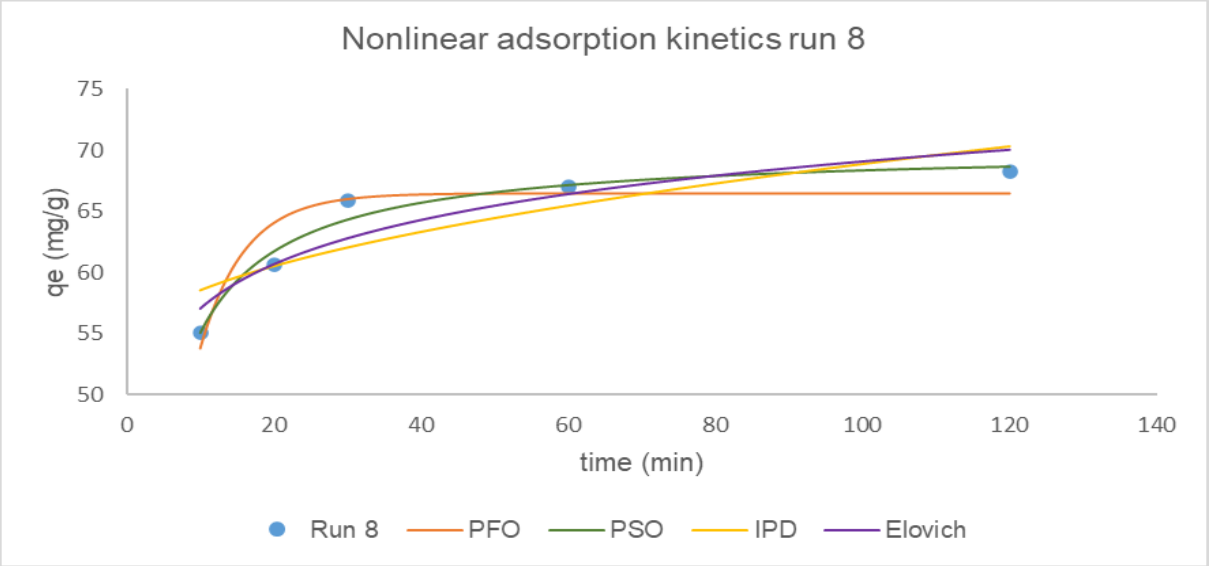

Figure 4-38: Nonlinear adsorption kinetics run 8

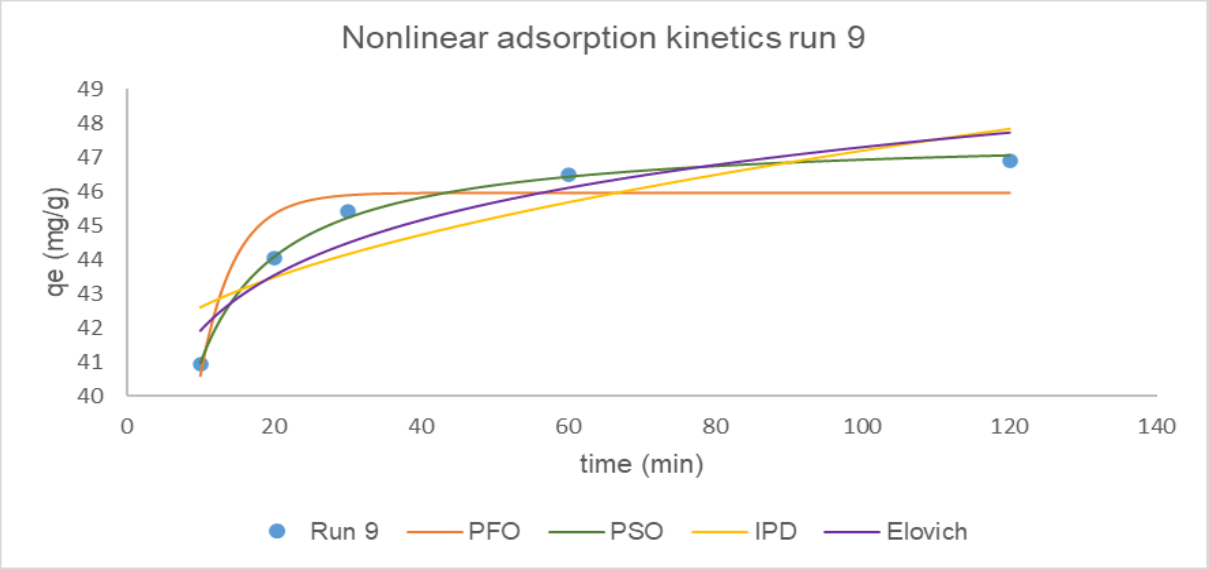

Figure 4-39: Nonlinear adsorption kinetics run 9

4.10 Nonlinear adsorption kinetics constants

Table 4-11: Nonlinear adsorption kinetics constants

Equation	Parameter	1	2	3	4	5	6	7	8	9
PFO	qe exp (mg/g)	40,5	58,9	58,87	48,83	82,65	51,25	64,675	68,25	46,892
	qe cal (mg/g)	38,59	57,48	56,39	47,62	74,8	49,5	61,96	66,45	47,7
	kf (min-1)	0,16	0,067	0,139	0,32	0,065	0,108	0,137	0,155	0,214
	R^2	0,86	0,91	0,8	0,49	0,8	0,93	0,906	0,859	0,86
PSO										
	qe exp (mg/g)	40,5	58,9	58,87	48,83	82,65	51,25	64,675	68,25	46,892
	qe cal (mg/g)	39,9	59,4	58,67	48,2	78,2	51,6	66,55	68,65	47,05
	ks (g/mg min)	0,00819	0,0016	0,0043	0,03319	0,00097	0,0034	0,00385	0,00516	0,01274
	R^2	0,97	0,95	0,967	0,84	0,91	0,98	0,99	0,96	0,99
IPD										
	Kid(mg/g.$min^{0.5}$)	0,98	3,4	1,36	0,21	4,08	1,98	1,91	1,51	0,67
	C (mg/g)	30,42	25,35	45,27	46,1	37,47	32,43	45,72	53,76	40,47
	R^2	0,81	0,78	0,83	0,77	0,90	0,77	0,79	0,71	0,72
Elovich										
	α (mg/g.min)	5873,19	19,039	1054,44	2,4E+16	63,32	163,09	1386,3	28833,64	14200000
	β (g/mg)	0,299	0,085	0,164	0,86	0,092	0,15	0,153	0,19	0,42
	R^2	0,91	0,87	0,95	0,97	0,87	0,9	0,91	0,85	0,87

4.11 Error Analysis

In order to evaluate the suitability of model equations to experimental results, an error function assessment is used. Error functions are statistical tools used to measure deviation of theoretically predicted data from the values of experimental data (Moussout et al., 2018). The adsorption models and kinetic models were validated using three different statistical error functions namely, coefficient of determination (R^2), sum of square error (SSE) and sum of absolute error (SAE). The best fit model will be the model with lowest values of r^2, SSE and SAE. The equations used for SAE and SSE are as follows:

$$SAE = \sum_{i=1}^{N} |q_{exp} - q_{cal}|$$

$$SSE = \sum_{i=1}^{N} (q_{exp} - q_{cal})^2$$

Where q_{exp} is the experimental adsorption capacity at equilibrium, q_{cal} is the theoretical adsorption capacity at equilibrium and N is the is the experimental sample number.

4.11.1 Sum of absolute Error adsorption isotherms

Table 4-12: Sum of absolute error analysis on isotherm data

SAE				
Temperature	Langmuir	Freundlich	Temkin	D- R
25	1,51	1,06	1,25	1,68
37,5	5,32	0,44	0,87	6,77
50	14,44	3,31	7,77	11,92

4.11.2 Sum of square error adsorption isotherms

Table 4-13: Sum of square error on isotherm data

SSE				
Temperature	Langmuir	Freundlich	Temkin	D- R
25	1,1305	0,6058	0,9025	0,9558
37,5	11,303	0,1398	0,2673	18,3329
50	83,026	4,057	21,76	55,8834

4.11.3 Experimental vs theoretical q_e values for adsorption Isotherms

Table 4-14: Experimental and calculated q_e values for adsorption isotherms

q_{exp}	Langmuir	Freundlich	Temkin	DR
58,9	58,63	59,8	59,17	58,44
51,25	50,25	50,56	51,2	51,86
40,5	40,26	40,86	40,2	39,89
68,25	66,27	68,27	67,86	66,47
58,87	61,49	58,82	59,11	60,2
47,15	46,43	47,52	46,58	43,49
82,65	77,25	81,85	80,98	78,43
64,68	71,75	66,3	66,94	70,58
48,83	46,86	47,94	45,35	47,023

4.12 Error Analysis Adsorption Kinetics

4.12.1 Experimental and theoretical q_e values adsorption kinnetics

Table 4-15: Experimental and calculated q_e values for adsorption kinetics

	q_{exp}	PFO	PSO	IPD
1	40.5	38.59	39.9	41.24
2	58.9	57.4	59.4	62.67
5	58.87	56.39	58.67	60.28
9	48.83	47.62	48.2	48.48
10	82.650	74.83	78.2	82.26
14	51.250	49.5	51.6	61.79
15	64.675	61.96	66.55	66.65
16	68.250	66.46	68.65	70.317
17	46.892	45.95	47.05	47.8

4.12.2 Sum of absolute error adsorption kinetics

Table 4-16: Sum of absolute error analysis adsorption kinetics

Run	PFO	PSO	IPD
1	1.91	0.6	0.74
2	1.5	0.5	3.77
5	2.48	0.2	1.44
9	1.21	0.63	0.35
10	7.82	4.45	0.39
14	1.75	0.35	10.54
15	2.715	1.875	1.975
16	1.79	0.4	2.067
17	0.942	0.158	0.908

4.12.3 Sum of Square Error adsorption kinetics

Table 4-17: Sum of square error analysis adsorption kinetics

Run	PFO	PSO	IPD
1	3.6481	0.36	0.5476
2	2.25	0.25	14.2129
5	6.1504	0.04	1.9881
9	1.4641	0.3969	0.1225
10	61.1524	19.8025	0.1521
14	3.0625	0.1225	111.0916
15	7.371225	3.515625	3.900625
16	3.2041	0.16	4.272489
17	0.887364	0.024964	0.824464

4.13 Linear and nonlinear kinetics comparison

The use of linearized kinetics equations is commonly used as an indicator for model fit tightness. However the transforms of nonlinear to linear inherently alter the error functions of these equations and may also violate the error variance and normality assumptions of standard least squares (Ngakou et al., 2019). Ngakou et al. (2019) found that transformations of nonlinear isotherm equations to linear forms alters the error structure and violates the error structures and normality assumptions. The evaluation of the PFO data between the linear and nonlinear shows that although the R^2 values are comparable but the calculated qe values are quite different. The q_e calculated values for the nonlinear regression are much closer to that of the experimental values whereas in the linear regression the values are not in agreement. The K_f values between the two methods are also different from each other showing the nonlinear regression to have lower rate constants than linear regression rate constant. The PSO values for q_e calculated and q_e experimental agree with each other in both linear and nonlinear cases. The Ks values are also quite close to each other showing very little variance between the linear and nonlinear regression for PSO. The C values and Kid values for intraparticle diffusion were within reasonable agreement with each other for linear and nonlinear regression. The R^2 values were also quite similar to one another. These findings illustrate that the use of linear regression can be useful and can be a good indicator for the kinetics of the system however the results of linear regression can be misleading as shown in the case of PFO linear regression. In a study performed by (López-Luna et al., 2019), where both linear and nonlinear regression was used in the adsorption of arsenic onto manganese ferrite nanoparticles, made similar findings where only the PFO nonlinear model fitted the data and the linear PFO data didn't and both linear and nonlinear PSO models described the data well. In a similar study performed by Moussout et al. (2018) where critical analysis of linear and nonlinear PFO and PSO kinetic models were evaluated. The study found that the decision between linear and nonlinear models are difficult and vary from system to system. This is due to kinetic parameters from the models being the same and the error computations are reasonable in both cases. However nonlinear models appear to be more suitable than their linear counterparts for the modelling of kinetics of adsorption in liquid phase. These findings are in line with the findings of this study. Moussout et al. (2018) also goes onto state the q_e values are the main determining factor into which kinetic model the data follows, thus for this study the data is best described by PSO kinetic model. The study performed by Sharma et al. (2020) showed similar findings to this study stating it is not appropriate to use the coefficient of determinations of linear regression as a method for comparing the best fitting model. The author goes on to state different outcomes obtained by linear regression for the same kinetic

model shows the real problems and complexities in estimating kinetic parameters by linearisation technique.

CHAPTER 5

Optimisation using Response Surface Methodology (RSM)

5 Optimisation using Response Surface Methodology

5.1 Introduction

Response surface methodology (RSM) is a collection of mathematical and statistical techniques based on a polynomial equation's fit to the experimental equation to statistically predict and understand system behaviour (Mukwevho et al., 2020). RSM was developed to reduce and simplify multivariable experimental design, enabling users to identify the process's ideal variables. RSM allows for the reduction in experimental runs and reduces costs (Najib et al., 2017). The most used second order RSM designs are 3^k factorial, central composite and Box-Behnken designs with the most popular being central composite due to their simplicity and good efficiency. The aim was to predict the response of COD & Anionic Surfactant removal and optimize the process to achieve the desired outcomes.

5.2 Adsorption performance predicted using RSM BBD with COD removal

Design expert 10 software was used to analyse the measured responses of COD removal and anionic surfactant removal. The Box-Behnken model with one centre point was used for the design. A total of 26 experiments were conducted. The effects of three factors were evaluated-namely, pH ranging from 2 to 10, temperature ranging from 25^0C to 50^0C and adsorbent concentration ranging from 100mg/l to 300mg/l. The RSM was used to understand the interactions between the independent variables. This was achieved by fitting the experimental data to a polynomial quadratic equation to obtain regression coefficients. Analysis of variance (ANOVA) was used to evaluate the validity and significance of the fitted model. The Coefficient of determination R^2 predicted R^2, adjusted R^2, lack of fit, adequate precision, F-value and p-value were used to evaluate the model's quality and accuracy. The significance level was set to 0.05.

5.3 Chemical Oxygen Demand

The design matrix indicating experimental run order and output data for the BBD can be seen in Table 5-1. The data obtained from the 26 experimental runs that were conducted were fitted into a polynomial quadratic equation as shown in Equation 5-1 in terms of coded factors

Table 5-1: COD Design Matrix

	FACTORS			COD Removal %	
Run	A: pH	B: Temp(^{0}C)	C: Dosage (mg/l)	Experimental Values	Prediction Values
1	2	37.5	100	50.371	50.9103
2	10	37.5	300	84	86.1375
3	6	25	300	68	68.475
4	10	50	200	80	78.6125
5	10	37.5	100	50	40.86
6	6	25	100	28	34.75
7	2	25	200	76	66.3875
8	10	25	200	48	56.3875
9	6	37.5	200	48	44
10	6	50	300	92	89.25
11	6	50	100	44	45.425
12	2	37.5	300	68	83.175
13	2	50	200	76	75.6125
14	2	37.5	100	48	50.8625
15	10	37.5	300	92	86.1375
16	6	25	300	64	68.475
17	10	50	200	64	78.6125
18	10	37.5	100	40.705	40.501
19	6	25	100	32	34.75
20	2	25	200	70	66.3875
21	10	25	200	66	56.3875
22	6	37.5	200	40	44
23	6	50	300	96	89.25
24	6	50	100	51.8	45.425
25	2	37.5	300	90	83.1375
26	2	50	200	74	75.6125

The experimental and predicted of COD removal values for the 26 experiments presented in Table 5-1, where the results indicated that a maximum COD removal of 96% was achieved with experiment 22, at pH, temperature and dosage of 6, 50^{O}C and 300mg/l, respectively. A close correlation between experimental and predicted values was found when a fair agreement was reached between the R^2 predicted.

Table 5-2: ANOVA COD Analysis

Analysis of Variance Table [Partial sum of squares – Type III]					
Source	**Sum of Squares**	**Degree of Freedom**	**Mean Square**	**F Value**	**p-value Prob > F**
Model	8446.39	9	938.49	13.70	< 0.0001[1]
A-pH	49.00	1	49.00	0.72	0.4101[2]
B-Temperature	989.10	1	989.10	14.44	0.0016[1]
C-Dosage	6014.00	1	6014.00	87.80	< 0.0001[1]
AB	84.50	1	84.50	1.23	0.2831[2]
AC	84.50	1	84.50	1.23	0.2831[2]
BC	51.01	1	51.01	0.74	0.4009[2]
A^2	1100.06	1	1100.06	16.06	0.0010[1]
B^2	433.46	1	433.46	6.33	0.0229[1]
C^2	150.49	1	150.49	2.20	0.1577[2]
Residual	1095.93	16	68.50	-	-
Lack of Fit	373.51	3	124.50	2.24	0.1321[2]
Pure Error	722.42	13	55.57	-	-
Cor Total	9542.32	25	-	-	-
Standard deviation	8.28	-	-	R^2	0.8852
mean	63.07	-	-	Adjusted R^2	0.8205
Coefficient of variance %	13.2	-	-	Predicted R^2	0.7012

The reliability, quality and accuracy of the fitted quadratic model were evaluated using analysis of variance (ANOVA), as shown in Table 5.2

$$\text{COD Removal \%} = 44 + -1.75A + 7.8625B + 19.3875C + 3.25AB + 3.25AC + 2.525BC + 15.5125A^2 + 9.7375B^2 + 5.7375C^2$$

Equation 5-1: COD Removal %

The model F-value of 13.70 implies the model is significant and that there is a 0.01% chance that an F value this large could occur due to noise. The model coefficient (R^2) was 0.8852 and it can be said 88.5% of the model predicted values matched the experimental values showing the quadratic model is a good fit. The predicted R^2, 0.701 is in reasonable agreement with the adjusted R^2 of 0.8205, i.e., the difference is less than 0.2. Adequate precision measures the signal to noise ratio with a ratio of greater than four desirable. The ratio of 10.618 shows adequate precision. This model can be used to navigate the design space. The Lack of Fit F-value of 2.24 implies the Lack of Fit is not significant relative to the pure error. There is a 13.21% chance that a Lack of Fit F-value this large could occur due to noise. Non-significant lack of fit is good.

5.4 COD Model Validation

After the regression model was developed, the fitted model was tested to approximate the actual system accurately. Three types of model diagnostics were used for verification, namely: the normal, residual and predicted vs experimental plot

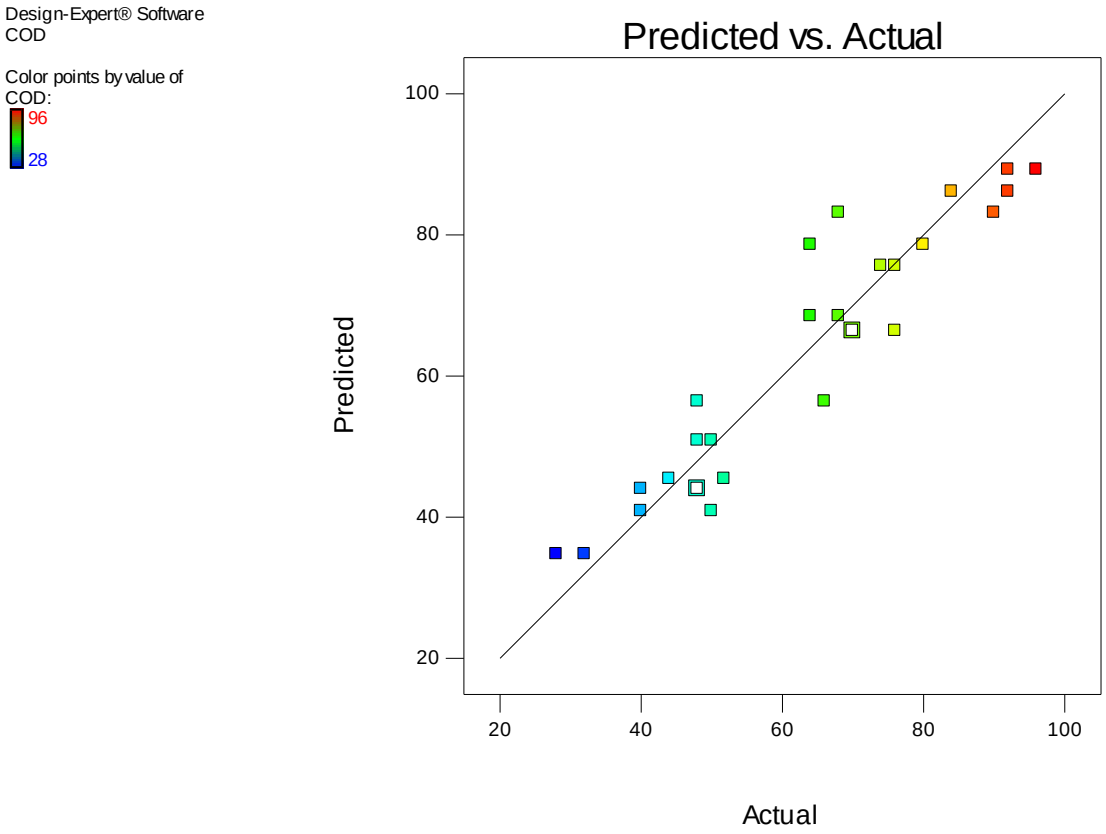

Figure 5-1: Actual vs Predicted Values for COD

The validation of the COD removal model was evaluated through the relationship between the actual and predicted values as presented in Figure 5.1. The predicted values are relatively close to the observed experimental COD values showing that the model was adequate for the prediction of COD removal (Najib et al., 2017)

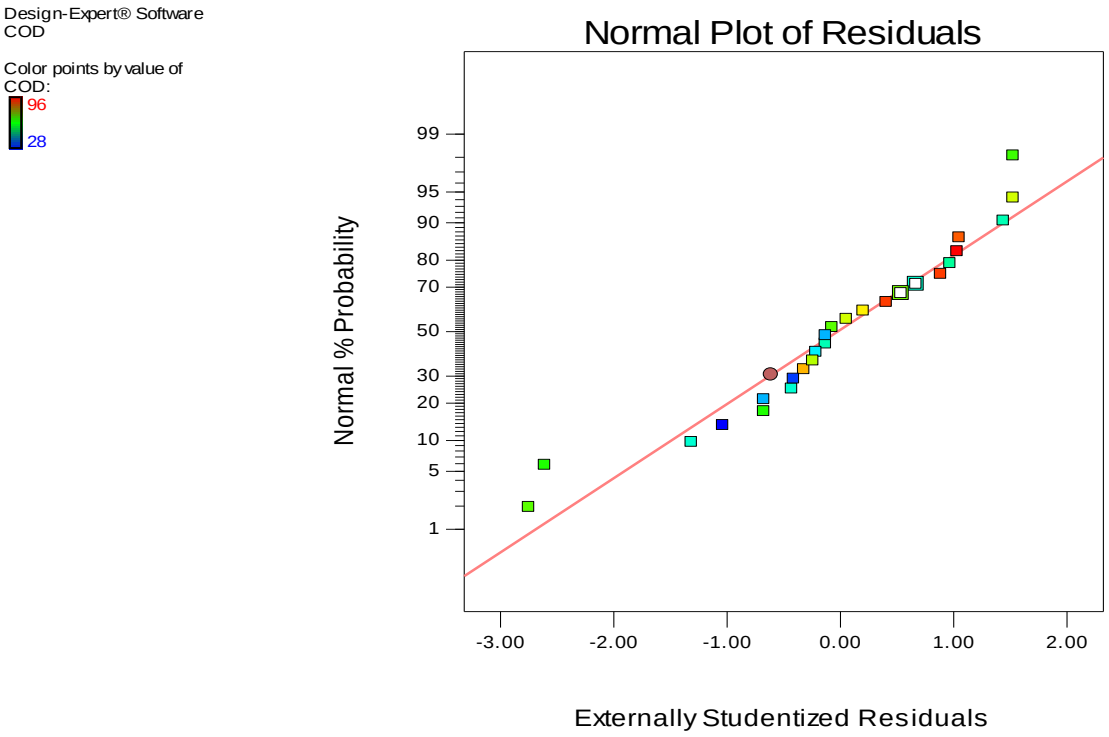

Figure 5-2: Normal plot of residuals COD

The normality of the data can be assessed by plotting the normal probability plot (NPP) of the residuals as seen in Figure 5.2. The NPP is a graphical technique is to check whether a data set is approximately normally distributed. The residual is the difference between the observed and predicted values from the regression. If the plot points are reasonably close to the straight line it can be surmised that the data is normally distributed. Figure 5.2 shows the shows the normal probability plot and shows that the points are closely aligned, suggesting normal distribution. The linear fit of the data shows there was no specious problem with the normality of the data. Figure 5.3 shows the plot of the residuals versus the predicted response. The residuals are scattered randomly about zero i.e. the errors have a constant variance (Hasan et al., 2009).

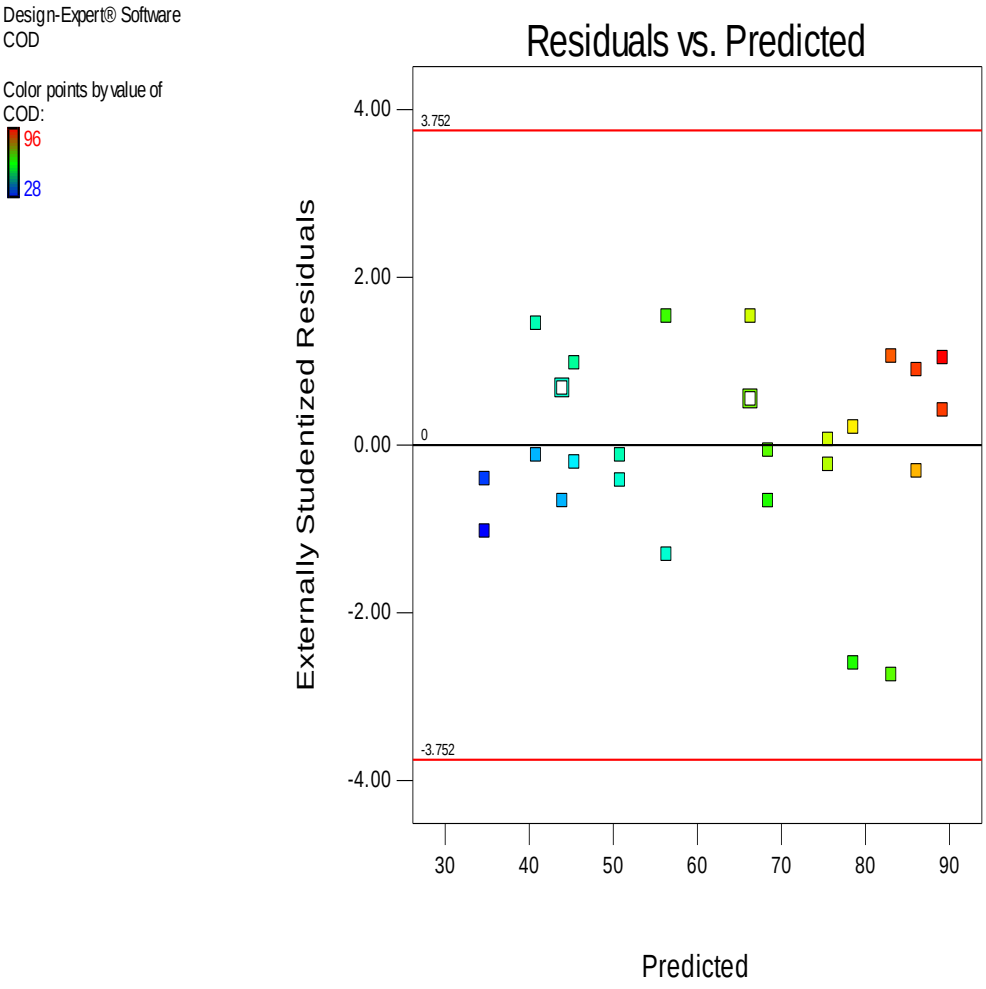

Figure 5-3: Residual vs Predicted COD

5.5 Effect of process parameters on COD removal

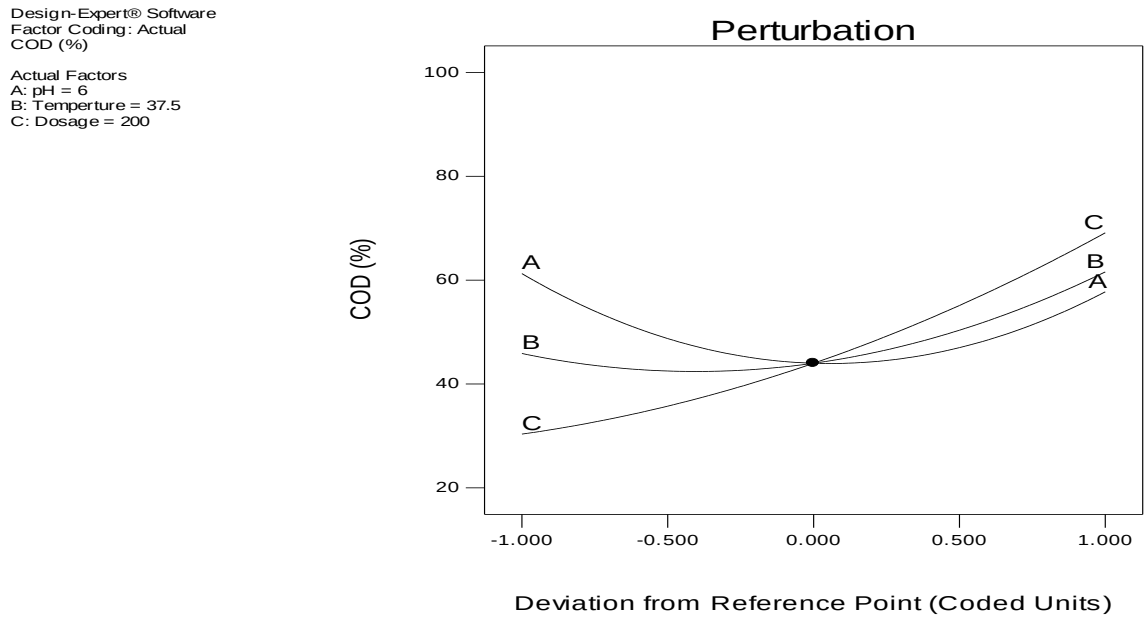

Figure 5-4: Perturbation plot COD

The removal of COD during adsorption of real carwash wastewater was related to the process parameters investigated. The prediction of COD removal was required in order to develop a model which will aid in process optimisation of process parameters. The perturbation plot is an important diagrammatic plot, which illustrates the effect of all factors at a particular point within the design space. The benefit of this plot helps with selecting axes and constants in the contour and 3D response. The perturbation plot also illustrates how sensitive process parameters are to change. Figure 5.4 illustrates the perturbation plot highlighting the effect of pH, Adsorbent concentration and temperature on COD removal. It can be seen from figure 5.4 that adsorbent concentration is highly sensitive to change. When the concentration is increased by 1 coded unit the COD removal increases by over 20%. When looking at pH and temperature it can be seen it's not as sensitive as adsorbent concentration. When increasing both parameters by 1 coded unit an increase of approximately 10% COD removal can be observed. Comparisons of the effect of factors can be made at certain plots in the design space using a perturbation plot however it does not show the effects of the interaction between process parameters (Ince & Ince, 2017). Interaction plots between the process parameters and its effect on COD removal

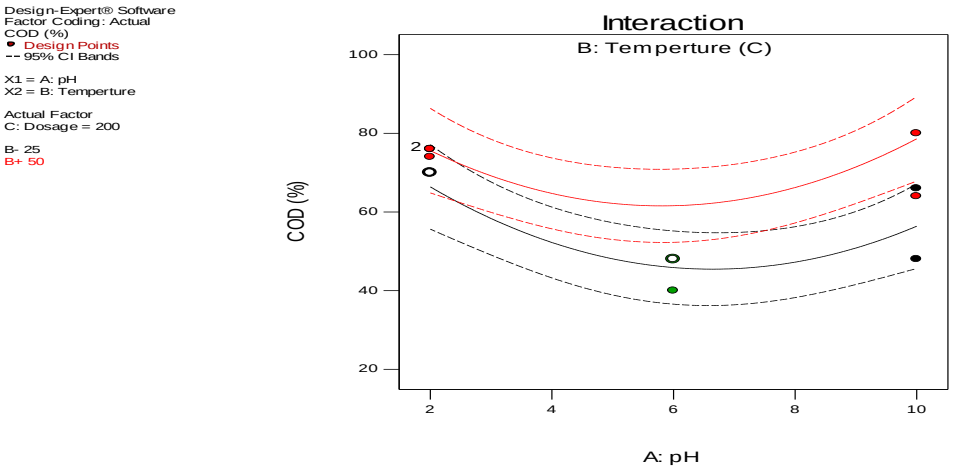

Figure 5-5: Interaction plot COD: Temperature and pH

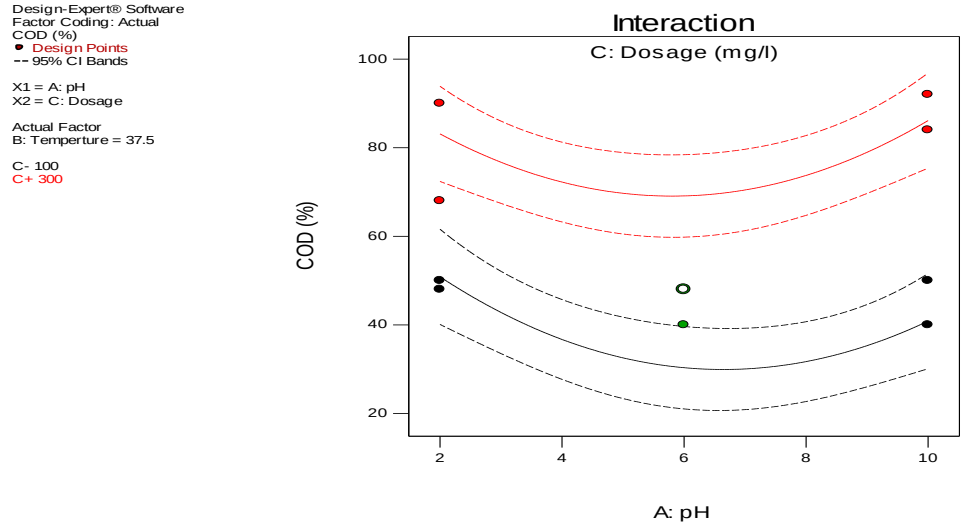

Figure 5-6: Interaction plot COD: Dosage and pH

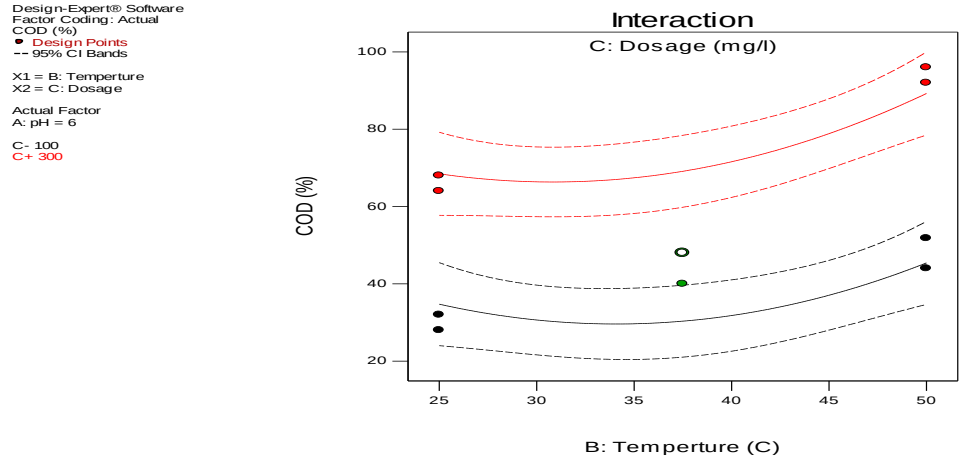

Figure 5-7: Interaction plot COD: Dosage and Temperature

5.6 2D contour plots and 3D response surface graphs

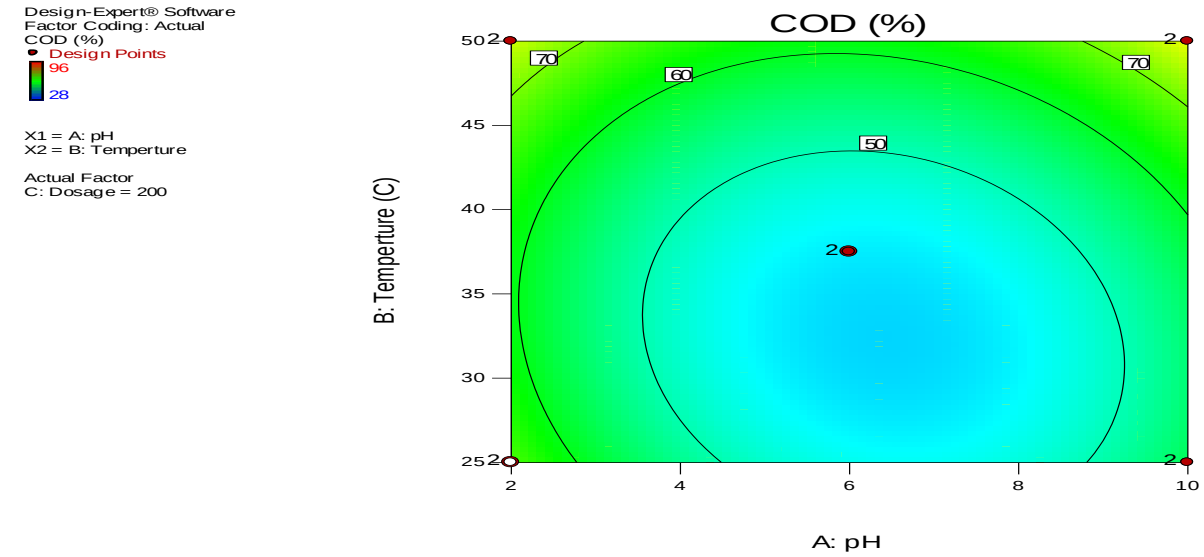

Figure 5-8: 2-D Contour plot COD: Temperature vs pH

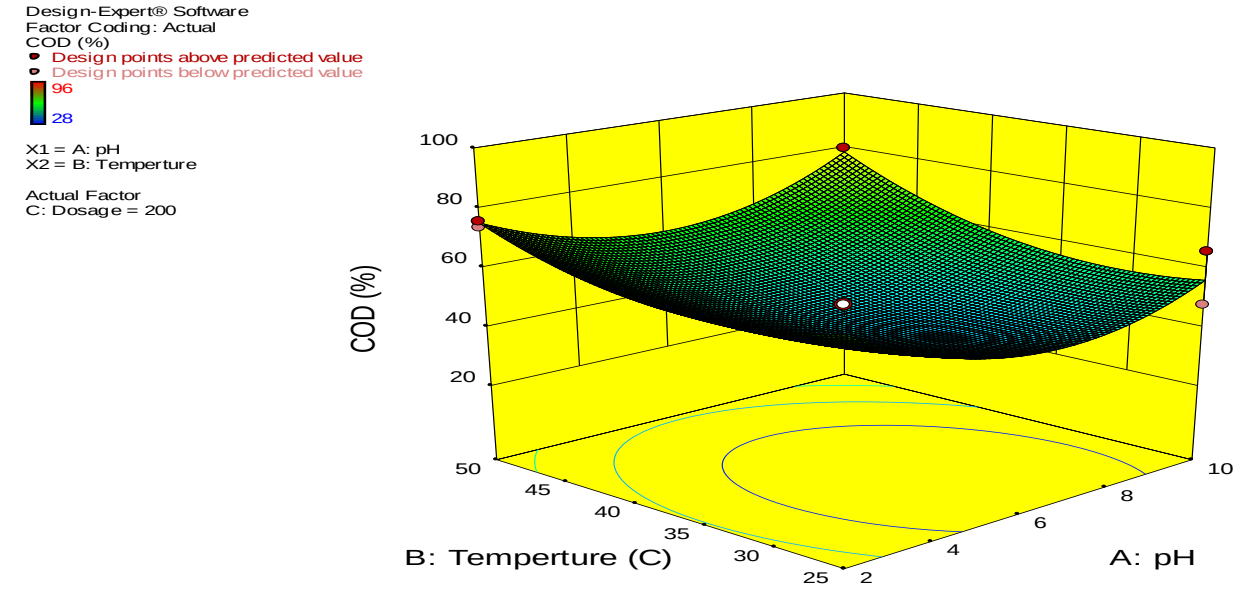

Figure 5-9:3-D Contour plot COD: Temperature vs pH

Two dimensional contour plots and three dimensional response surface grphs are useful in determining mximum, minimum and middle response points. Figures 5.8 and 5.9 shows the effect of pH and temperature on COD removal. It can be seen that COD removal increases with an increase in temperatrue and in a pH region of 2-3.

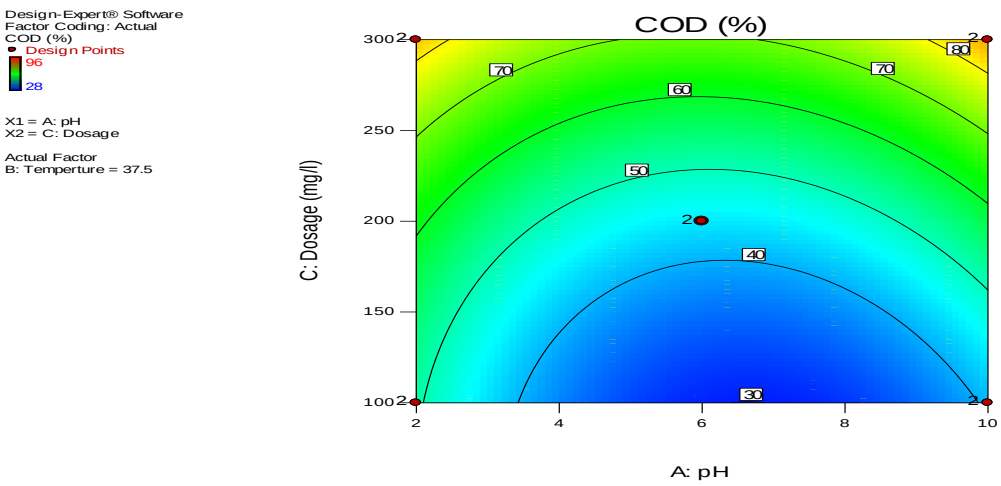

Figure 5-10: 2-D Contour plot COD: Dosage vs pH

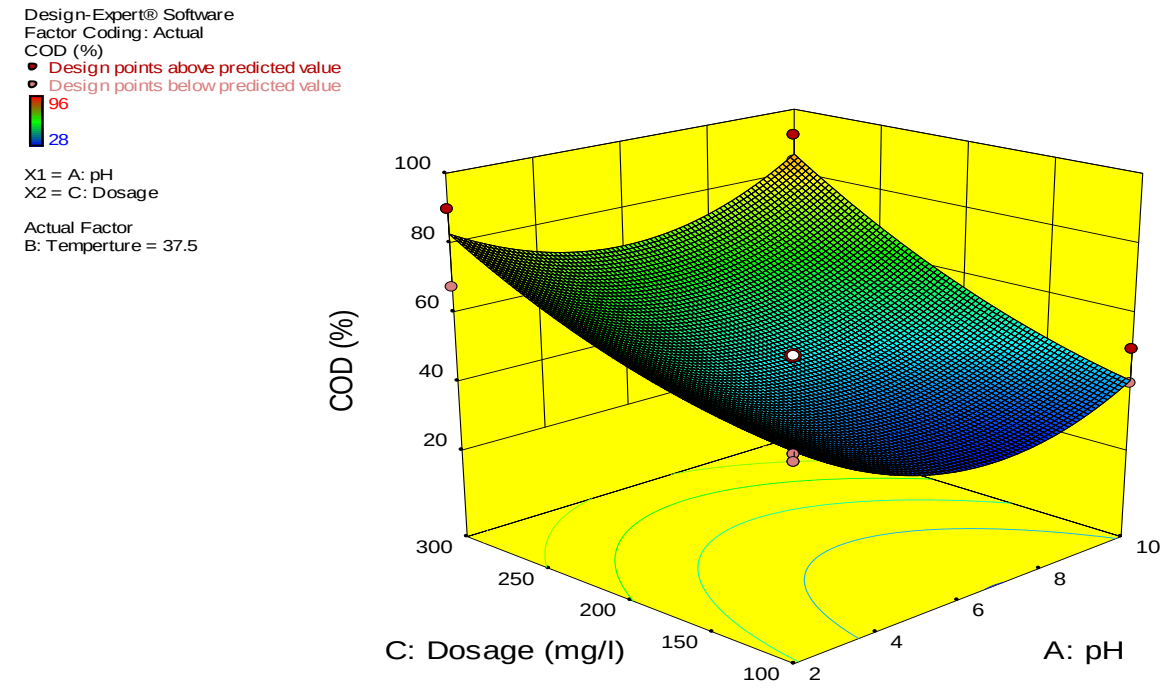

Figure 5-11: 3-D Contour plot COD: Dosage vs pH

Figures 5.10 and 5.11 represent the effect adsorbent concentration and pH has on COD removal. It can be seen that adsorbent concentration has a more profound effect on COD removal than pH. It is observed that with an increase in adsorbent concentration the COD removal profoundly increased. pH had a small effect on the COD removal however the best COD removal can be obtained in very high and very low pH.

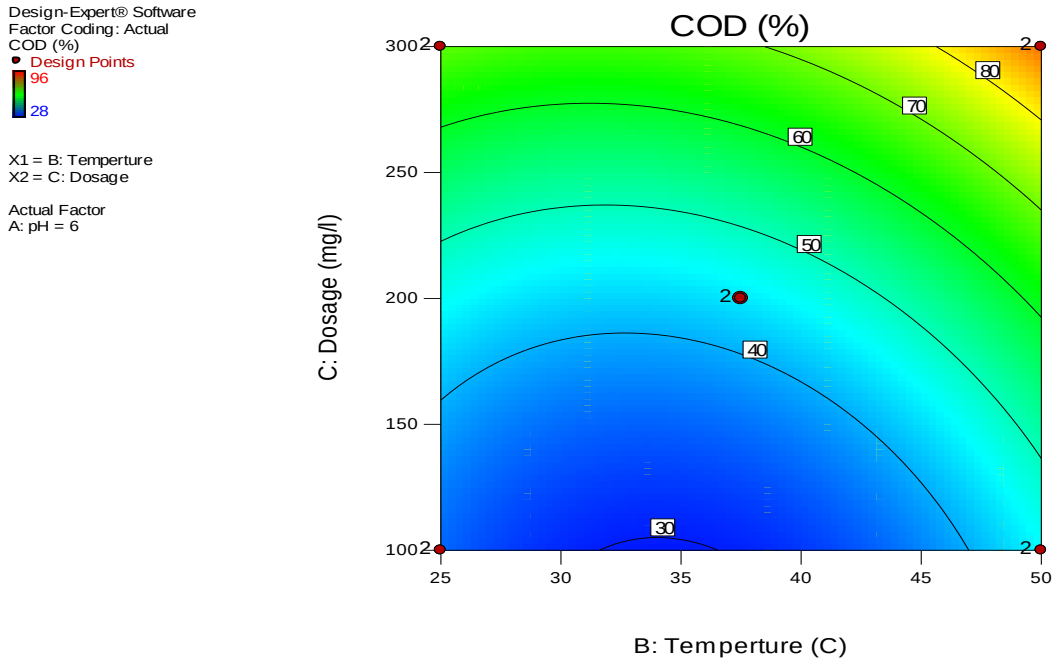

Figure 5-12: 2-D Contour plot COD: Temperature vs Dosage

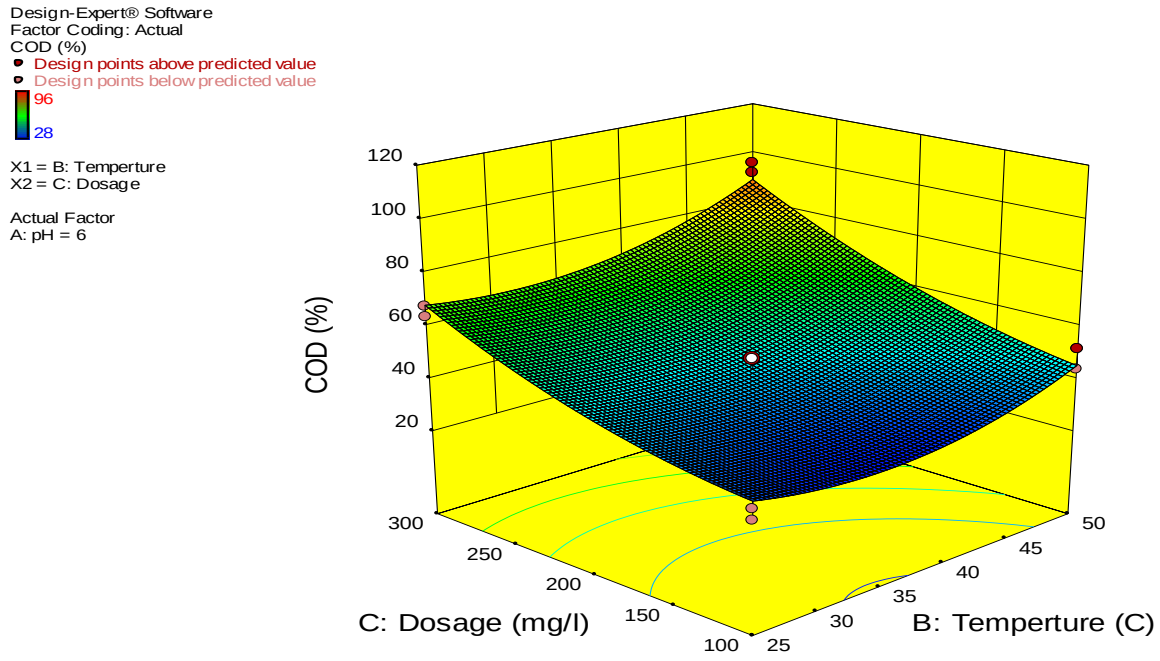

Figure 5-13: 3-D Contour plot COD: Temperature vs Dosage

Figures 5.12 and 5.13 represent the effects of Temperature and adsorbent concentration on COD removal. It can be observed that both parameters effect the COD removal, however adsorbent concentration has a greater effect. From the plots it can be seen an increase in both temperature and adsorbent concentration increase COD. These plots indicates that adsorbent dosage and temperature has a much greater effect on COD removal than pH.

5.7 COD cube model

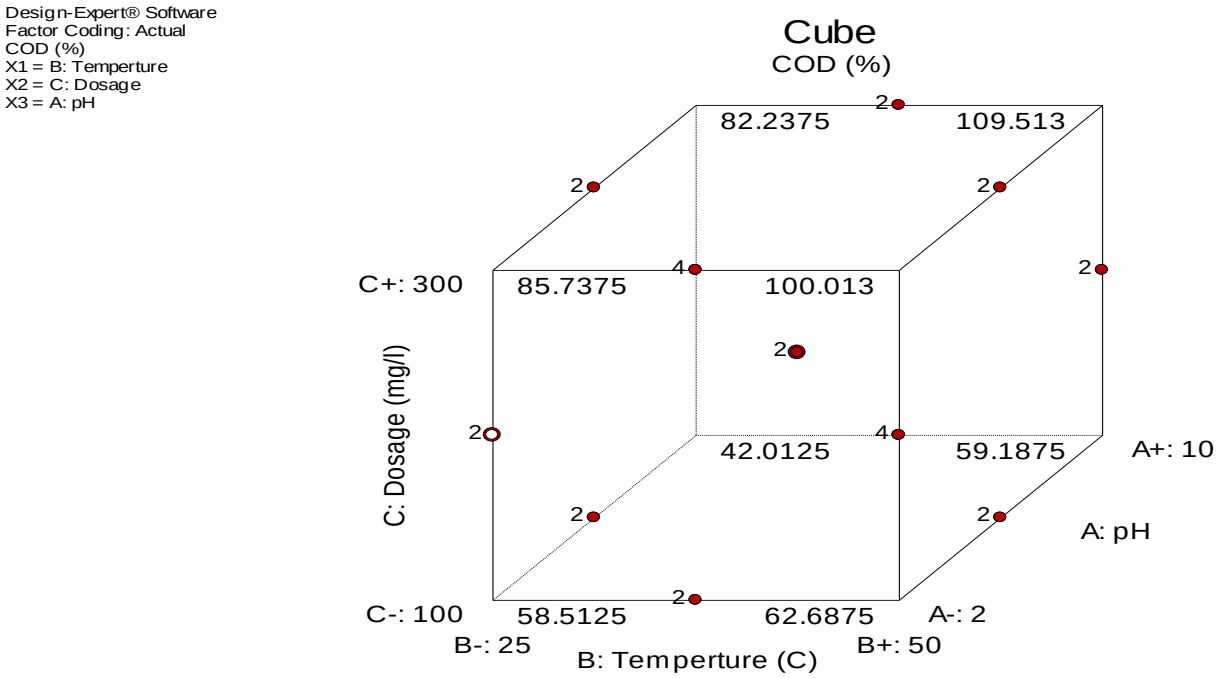

Figure 5-14: COD cube model

5.8 Anionic Surfactants RSM

Table 5-3: AS design matrix

	FACTORS			Anionic Surfactant Removal %	
Run	pH	Temperature (^{0}C)	Dosage (mg/l)	Experimental	Prediction
1	2	37.5	100	59.67	58.43
2	10	37.5	300	86.00	89.60
3	6	25	300	81.30	81.15
4	10	50	200	83.30	84.78
5	10	37.5	100	57.83	52.78
6	6	25	100	40.00	41.91
7	2	25	200	81.80	79.80
8	10	25	200	68.88	69.10
9	6	37.5	200	78.16	78.50
10	6	50	300	98.13	95.10
11	6	50	100	45.16	54.91
12	2	37.5	300	99.90	100.00
13	2	50	200	90.30	91.05
14	2	37.5	100	57.83	58.43
15	10	37.5	300	92.67	89.65
16	6	25	300	80.67	81.15
17	10	50	200	81.60	84.79
18	10	37.5	100	52.07	52.78
19	6	25	100	38.50	41.91
20	2	25	200	82.47	79.79
21	10	25	200	70.30	69.10
22	6	37.5	200	78.83	78.50
23	6	50	300	97.40	95.10
24	6	50	100	65.00	54.91
25	2	37.5	300	97.60	100.00
26	2	50	200	90.83	91.05

The design expert software was used for the determination of optimum conditions for the adsorption of anionic surfactants onto powdered activated carbon. The design approach used was response surface methodology with a Box Behnken design. Table 5.3 describes the experimental approach showing the conditions for each run as well as the experimental and predicted values for the removal of Anionic surfactants.

Table 5-4: AS Anova analysis

Analysis of variance table [Partial sum of squares - Type III]					
Source	Sum of Squares	Degree of Freedom	Mean Square	F Value	p-value Prob > F
Model	8041.65	9	893.52	45.31	< 0.0001
A-pH	287.67	1	287.67	14.59	0.0015
B-Temperature	726.30	1	726.30	36.83	< 0.0001
C-Dosage	6308.45	1	6308.45	319.91	< 0.0001
AB	9.81	1	9.81	0.50	0.4907
AC	16.01	1	16.01	0.81	0.3809
BC	0.45	1	0.45	0.023	0.8817
A^2	111.49	1	111.49	5.65	0.0302
B^2	23.11	1	23.11	1.17	0.2950
C^2	290.85	1	290.85	14.75	0.0014
Residual	315.51	16	19.72		
Lack of Fit	70.66	3	23.55	1.25	0.3318
Pure Error	244.84	13	18.83		
Cor Total	8357.16	25			
Standard Deviation	4.44			R-squared	0.9622
mean	75.24			Adjusted R-squared	0.9410.
Coefficient of variance	5.90			Predicted R-squared	0.90333

The reliability, quality and accuracy of the fitted quadratic model were evaluated using analysis of variance (ANOVA), as shown in Table 5.4

Anionic surfactant Removal % = 78.495 + -4.24019 * A + 6.7375 * B + 19.8564 * C + 1.1075 * AB + -1.41462 * AC + 0.2375 * BC + 4.93856 * A^2 + -2.24856 * B^2 + -7.97644 * C^2

Equation 5-2

The model F-value of 45.31 implies the model is significant and that there is a 0.01% chance that an F value this large could occur due to noise. The model coefficient (R^2) was 0.9622 and it can be said 96.22% of the model predicted values matched the experimental values showing the quadratic model is a good fit. The predicted R^2, 0.903 is in reasonable agreement with the adjusted R^2 of 0.9410, i.e., the difference is less than 0.2. Adequate precision measures the signal to noise ratio with a ratio of greater than four desirable. The ratio of 21.44 shows adequate precision. This model can be used to navigate the design space. The Lack of Fit F-value of 1.25 implies the Lack of Fit is not significant relative to the pure error. There is a 33.18% chance that a Lack of Fit F-value this large could occur due to noise. Non-significant lack of fit is good. The final model in terms of coded factors is represented by equation 5.2

2

5.9 Anionic surfactant model validation

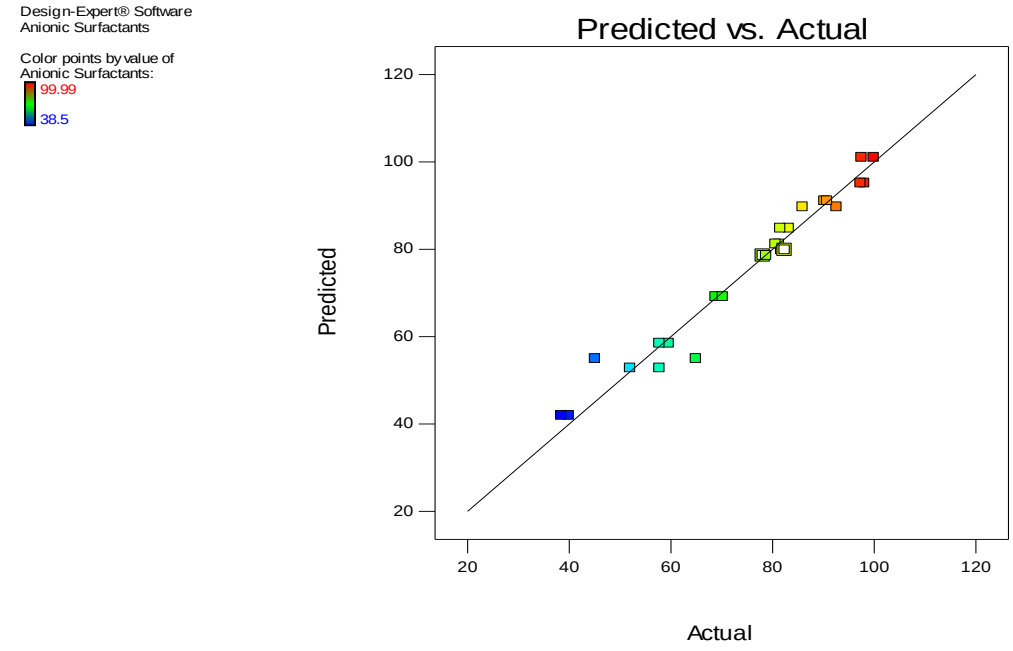

Figure 5-15: Predicted vs actual AS

The validation of the anionic surfactant removal model was evaluated through the relationship between the actual and predicted values as presented in figure 5.15. The predicted values are relatively close to the observed experimental COD values showing that the model was adequate for the prediction of anionic surfactant removal.

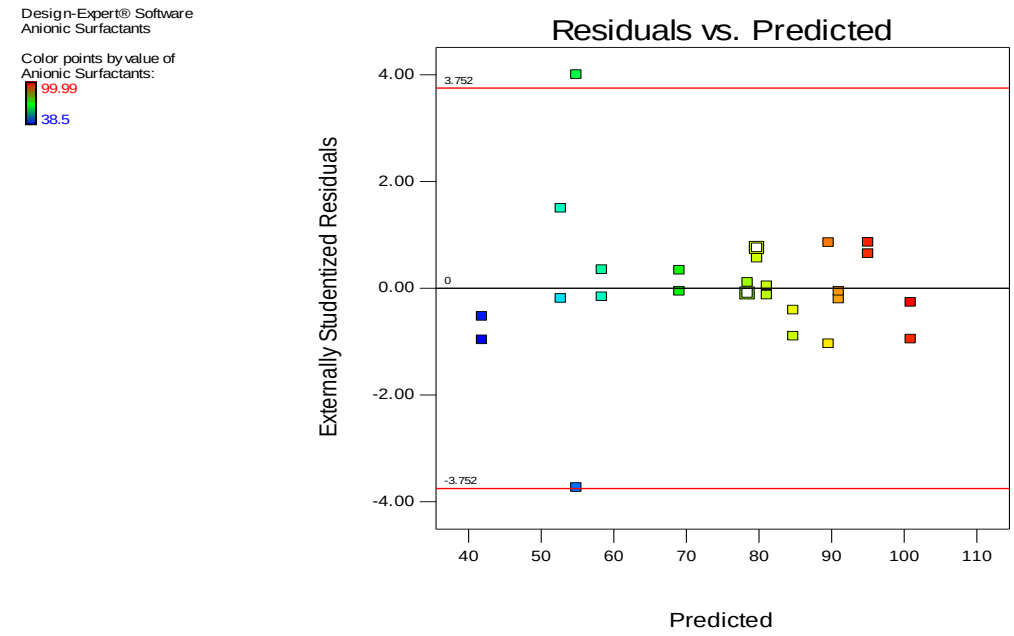

Figure 5-16: Residuals vs predicted AS

The normality of the data can be assessed by plotting the normal probability plot (NPP) of the residuals as seen in figure 5.16. If the points on the plot are close to the straight line it can be surmised that the data is normally distributed. Figure 5.16 shows the normal probability plot and the points are closely aligned thus suggesting normal distribution. The linear fit of the data shows there was no specious problem with the normality of the data. Figure 5.17 shows the plot of the residuals versus the predicted response. The residuals are scattered randomly about zero i.e., the errors have a constant variance

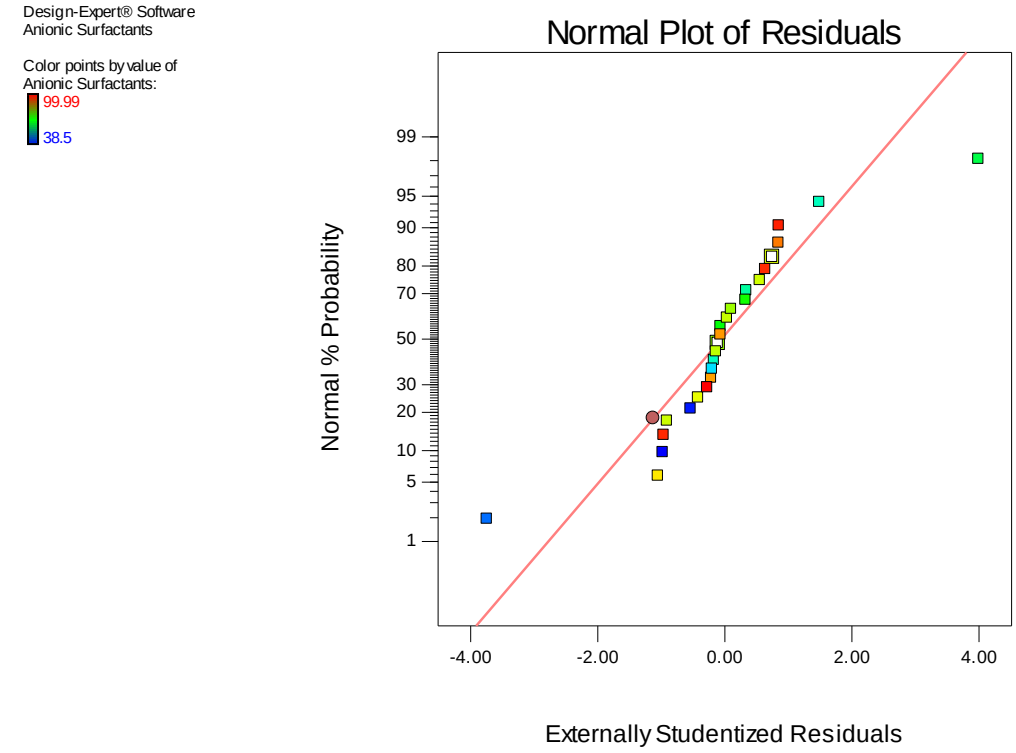

Figure 5-17: Normal plot of residuals AS

5.10 Effect of process parameters

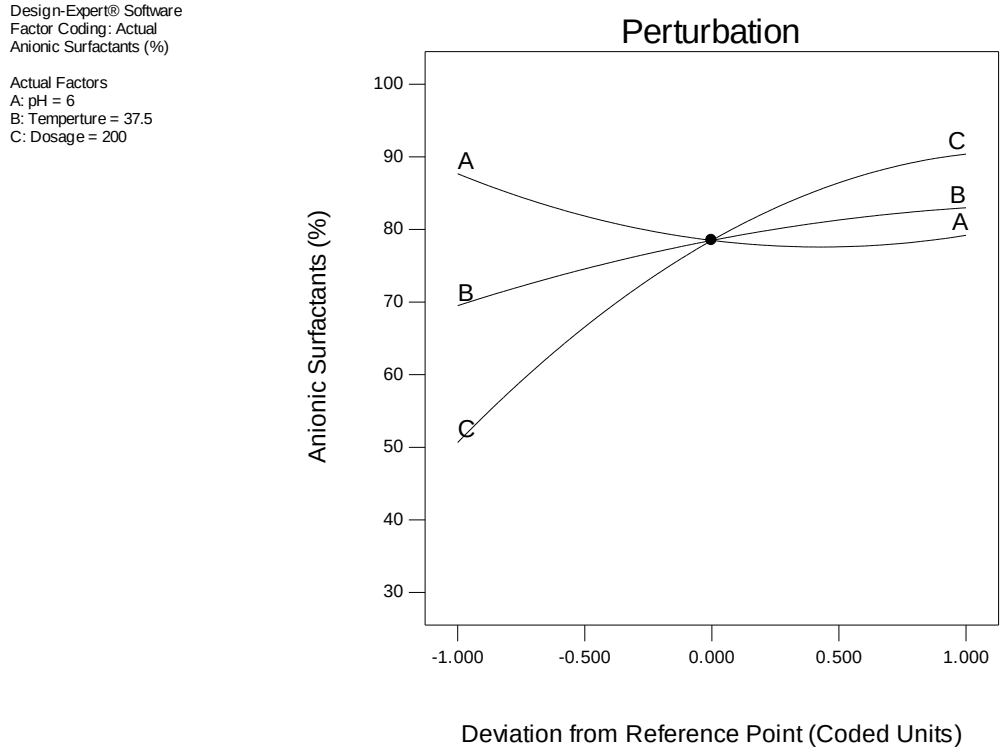

Figure 5-18: AS pertubation plot

The removal of anionic surfactants during adsorption of real carwash wastewater was related to the process parameters investigated. The prediction of anionic surfactant removal was required in order to develop a model which will aid in process optimisation of process parameters. Figure 5.18 illustrates the perturbation plot highlighting the effect of pH, Adsorbent concentration and temperature on anionic surfactants removal. When the adsorbent concentration is increased by 2 coded units the COD removal increases by approximately 40%. When looking at pH and temperature it can be seen it's not as sensitive as adsorbent concentration. When increasing pH parameters by 2 coded units a decrease of approximately 10% COD removal can be observed. For temperature, an increase in 2 coded units resulted in an increase of 10% COD removal. Comparisons of the effect of factors can be made at certain plots in the design space using a perturbation plot however it does not show the effects of the interaction between process parameters

5.11 Interaction plots between the process parameters and its effect on Anionic surfactant removal

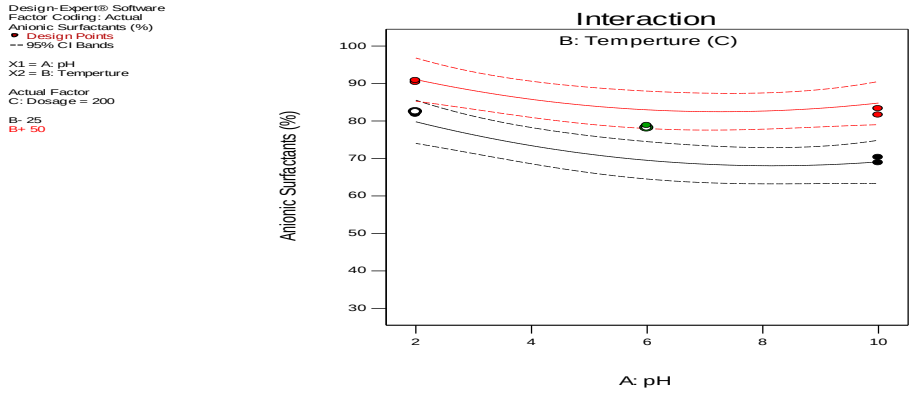

Figure 5-19: Interaction plot AS: Temperature and pH

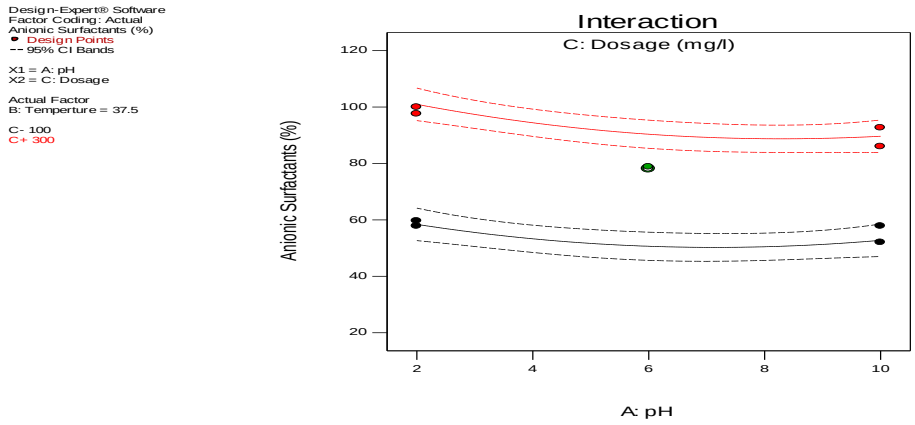

Figure 5-20: Interaction plot AS: Dosage and pH

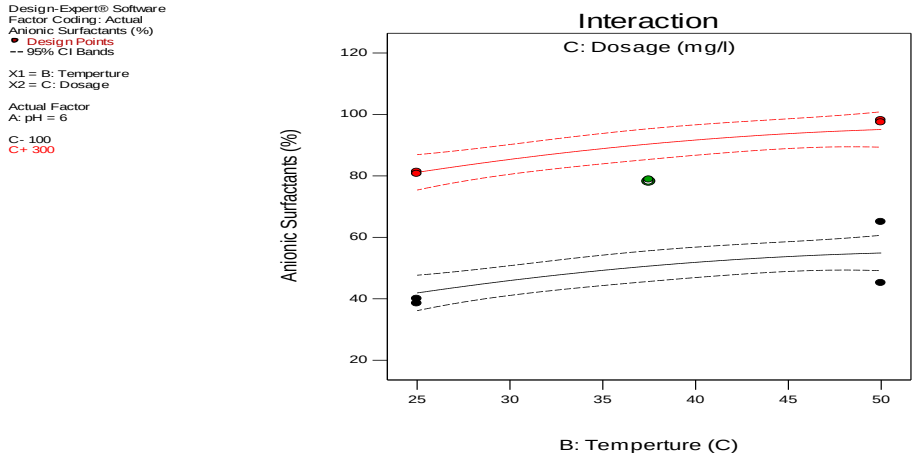

Figure 5-21: Interaction plot AS: Temperature and Dosage

5.12 2D and 3D plots contour plots for AS

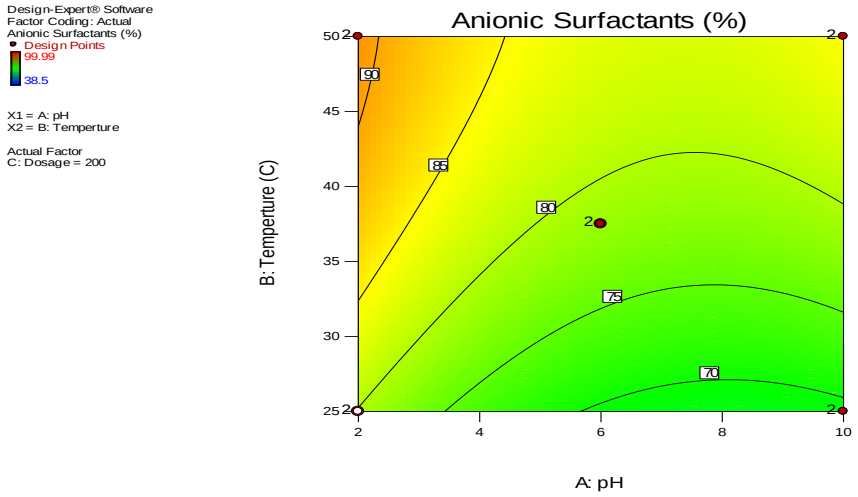

Figure 5-22: 2-D Contour plot AS: pH vs Temperature

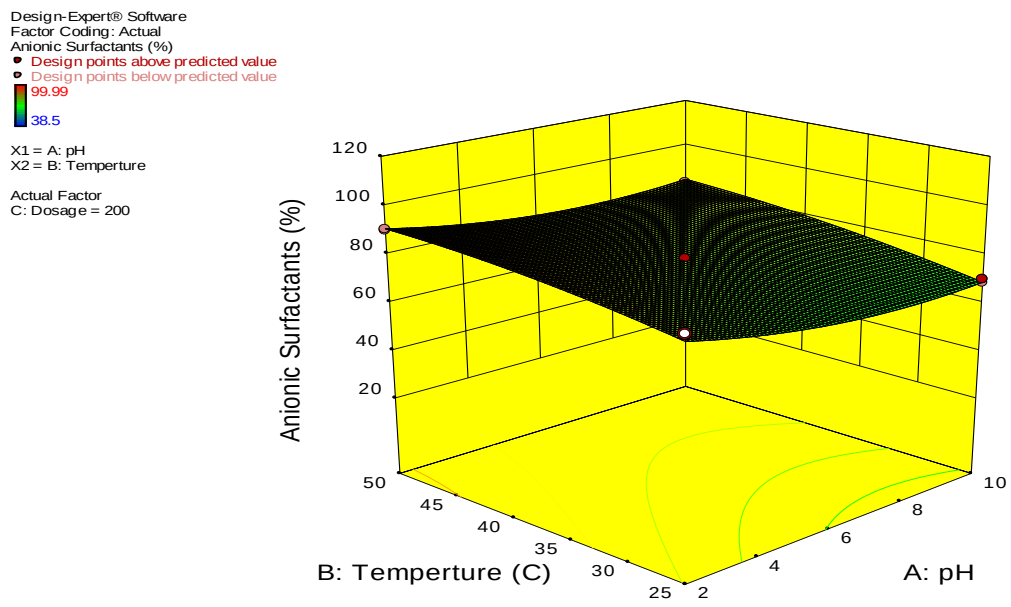

Figure 5-23: 3-D Contour plot AS: pH vs Temperature

Two dimensional contour plots and three dimensional response surface graphs are useful in determining mximum, minimum and middle response points. Figures 5.22 and 5.23 shows the effect of pH and temperature on anionic surfactant removal. It can be seen that surfactant removal increases with an increase in temperatrue and in a pH region of 2-3. Thus temperature has a larger effect on surfactant removal than pH.

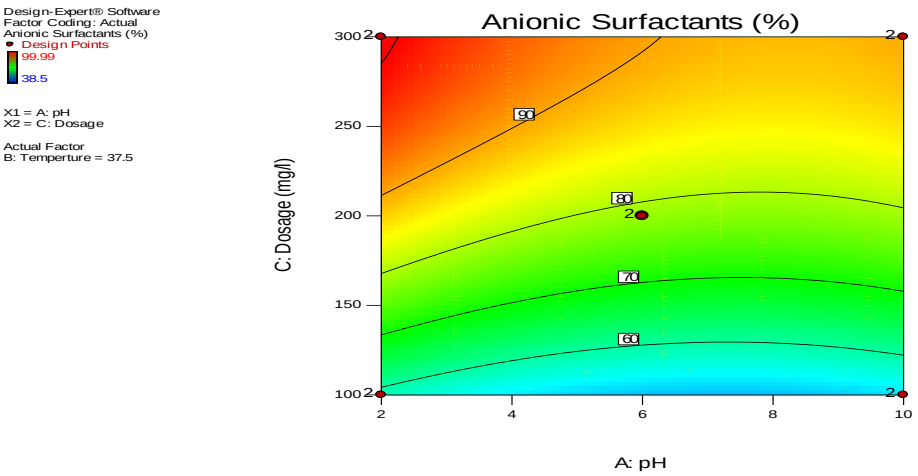

Figure 5-24: 2-D Contour plot AS: pH vs Dosage

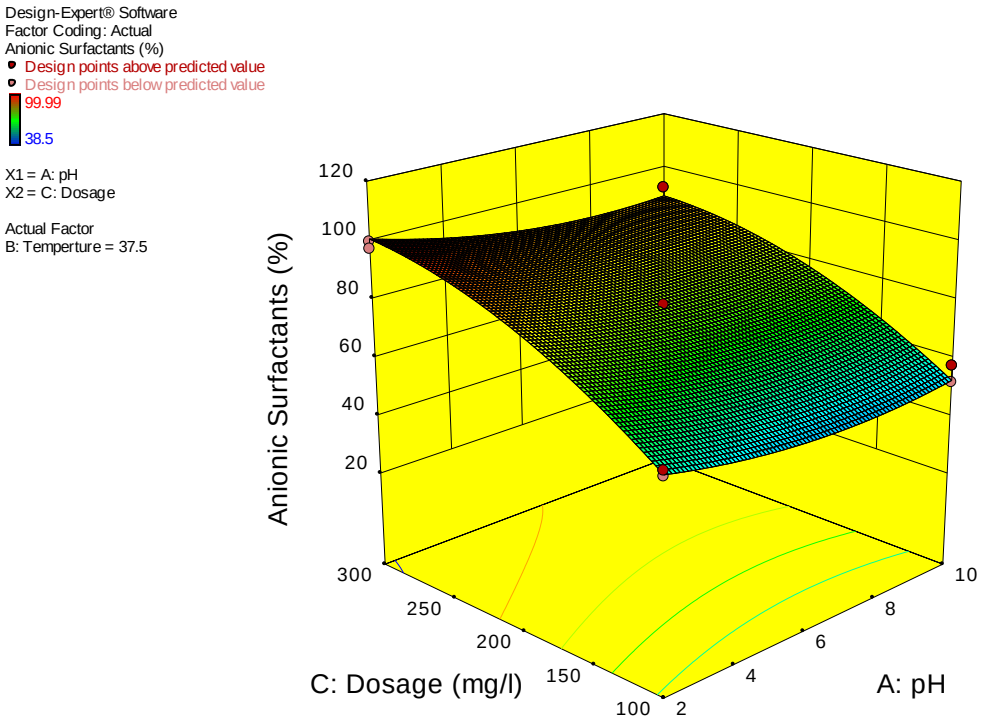

Figure 5-25: 3-D Contour plot AS: pH vs Dosage

Figures 5.24 and 5.25 represent the effect adsorbent concentration and pH has on surfactant removal. It can be seen that adsorbent concentration has a more profound effect on surfactant removal than pH. It is observed that with an increase in adsorbent concentration the COD removal

profoundly increased. pH had a small effect on the surfactant removal however the best COD removal can be obtained in very low pH levels.

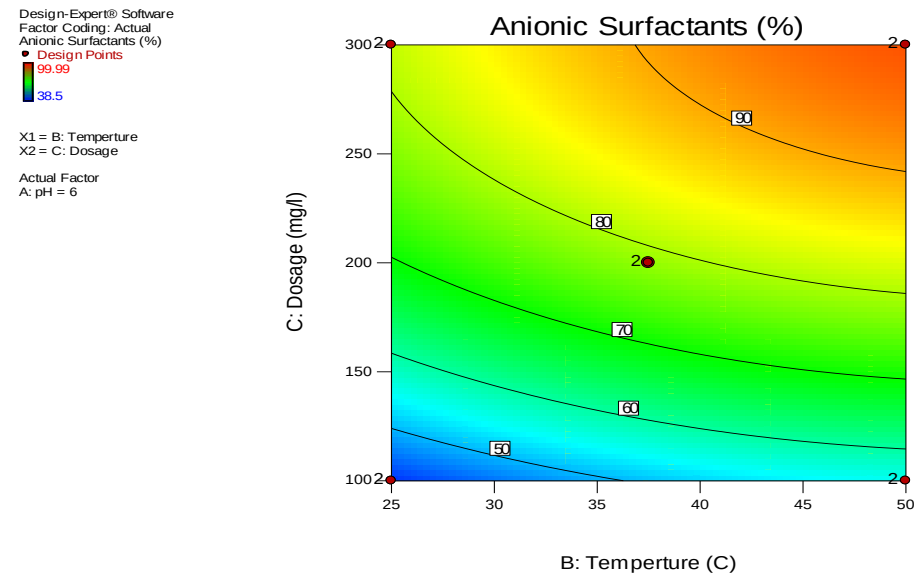

Figure 5-26: 2-D Contour plot AS: Temperature vs Dosage

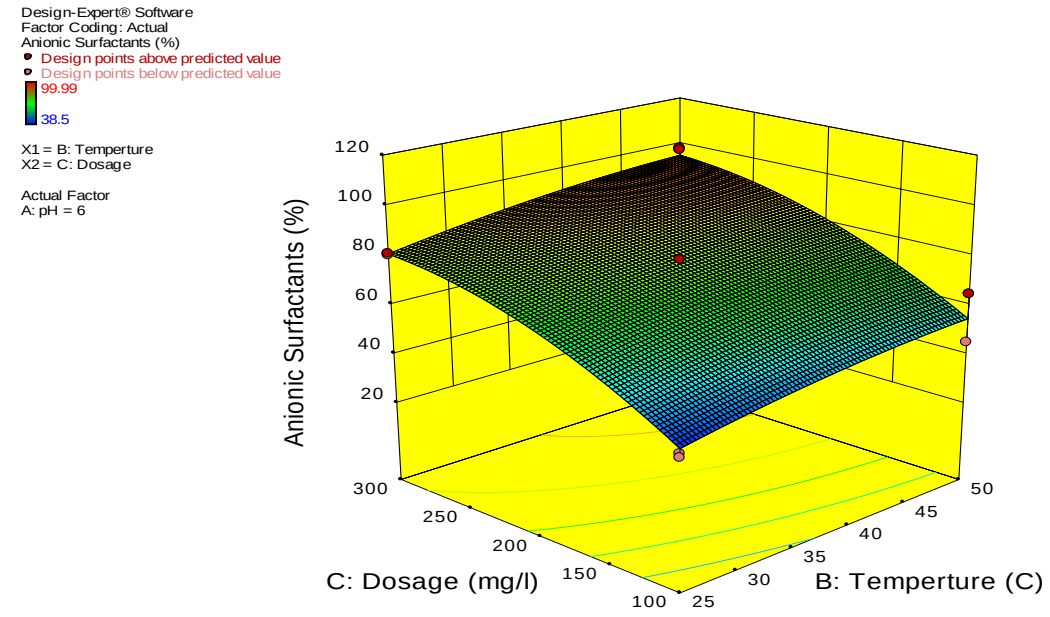

Figure 5-27: 2-D Contour plot AS: Temperature vs Dosage

Figures 5.26 and 5.27 represent the effects of Temperature and adsorbent concentration on surfactant removal. It can be observed that both parameters effect the surfactant removal, however adsorbent concentration has a greater effect. From the plots it can be seen an increase in both temperature and adsorbent concentration increase surfactant. These plots indicates that adsorbent dosage and temperature has a much greater effect on surfactant removal than pH.

5.13 Anionic Surfactant cube model

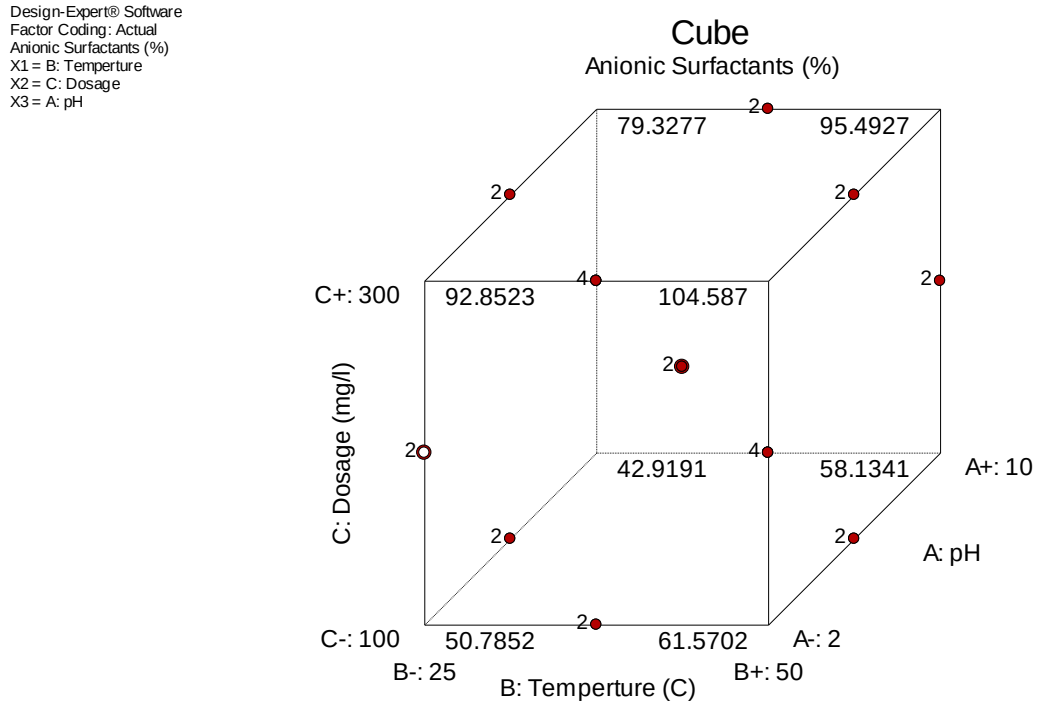

Figure 5-28: AS cube model

CHAPTER 6

Conclusion and Recommendations

6 Conclusion and Recommendations

6.1 Conclusion

The integrated treatment process used in this study consisted of two steps, chemical coagulation and adsorption. The treatment processes were investigated to obtain the most favourable conditions for the removal of COD, FOG and anionic surfactants (AS) in carwash wastewater.

The process of chemical coagulation investigated the effect of coagulant dosage on FOG, COD and AS removal. The process of adsorption investigated the effects of temperature, pH and dosage on the removal of AS, COD and FOG. The adsorption data was then fitted to adsorption isotherm and kinetic models to describe the process.

The first step, chemical coagulation using a dosage of 120mg/l showed excellent removal efficiencies. At these conditions, the COD was reduced by 79.8%, the AS by 44.82%, the FOG by 96% and turbidity by 99.5%.

The functional groups and morphological structures of the commercial activated carbon were determined using SEM and FTIR. This showed the activated carbon to have a porous structure and contain bonds favourable for the adsorption of AS.

The second step, adsorption using commercial PAC showed excellent results at conditions of pH:6, dosage: 300mg/l and temperature of 50^0C. the results at these conditions showed a COD removal of 94%, AS removal of 97% and FOG removal of 100%. Of the three operating parameters tested it is noted that PAC dosage had the largest effect increasing removal percentage by over 50% when moving from 100mg/l to 300mg/l. the other two variables showed marginal improvement in COD and AS removal. From this evidence it can be said the adsorption of AS and COD onto PAC occurs best at low pH values and high temperatures. The process of adsorption of AS and COD onto PAC is endothermic in nature, occurs spontaneously and exhibits increased randomness as temperature increases. The adsorption is governed by pseudo second order reaction kinetics and follows the Freundlich and Temkin isotherms closely. The adsorption mechanism was revealed to be predominantly chemisorption with subordinate physical adsorption.

The use of linear isotherm and kinetic models were shown to be a good indicator for the system however were proven to be inadequate when compared to nonlinear regression providing better clarity as to which models fit the system best. The comparison between the two methods showed the transformation of isotherm and kinetic models from nonlinear to linear implicitly alters the error structure. Therefore, the use of nonlinear regression analysis should be the main consideration when characterizing an adsorption system.

Design Expert 10 successfully predicted the optimum conditions for the adsorption of AS and COD from carwash wastewater onto commercial PAC. Anionic surfactant, COD and FOG removal using an integrated treatment process of chemical coagulation and adsorption was successful for municipal discharge and reuse applications

6.2 Recommendations

Future studies should investigate activated carbon and its functional groups' characterisation to target the removal of anionic surfactants from carwash wastewater specifically. The use of natural coagulants that are environmentally friendly and target anionic surfactant removal should be looked at. Lastly, activated carbon regeneration and reuse should be investigated to minimize the waste produced.

CHAPTER 7

References

7 References

Aboulhassan, M.A., Souabi, S., Yaacoubi, A. & Baudu, M. 2006. Removal of surfactant from industrial wastewaters by coagulation flocculation process. *International Journal of Environmental Science and Technology*, 3(4): 327–332.

Adamson, A.W. & Gast, A.P. 1967. *Physical chemistry of surfaces*. Interscience New York.

Aguayo-Villarreal, I.A., Bonilla-Petriciolet, A., Hernández-Montoya, V., Montes-Morán, M.A. & Reynel-Avila, H.E. 2011. Batch and column studies of Zn2+ removal from aqueous solution using chicken feathers as sorbents. *Chemical Engineering Journal*, 167(1): 67–76.

Akhmouch, A., Clavreul, D. & Glas, P. 2018. Introducing the OECD Principles on Water Governance. *Water International*, 43(1): 5–12. https://doi.org/10.1080/02508060.2017.1407561.

Aksoyoglu, S. 1989. Sorption of U(VI) on granite. *Journal of Radioanalytical and Nuclear Chemistry Articles*, 134(2): 393–403.

Al-Gheethi, A.A., Mohamed, R.M.S.R., Rahman, M.A.A., Johari, M.R. & Kassim, A.H.M. 2016. Treatment of Wastewater from Car Washes Using Natural Coagulation and Filtration System. *IOP Conference Series: Materials Science and Engineering*, 136(1).

Al-Ghouti, M.A. & Da'ana, D.A. 2020. Guidelines for the use and interpretation of adsorption isotherm models: A review. *Journal of Hazardous Materials*, 393(February): 122383. https://doi.org/10.1016/j.jhazmat.2020.122383.

Alasad, A.M. 2019. Adsorption of Cu(II), Ni(II) and Zn(II) ions by nano kaolinite: Thermodynamics and kinetics studies. : 258–268.

Allen, S.J., Mckay, G. & Porter, J.F. 2004. Adsorption isotherm models for basic dye adsorption by peat in single and binary component systems. *Journal of colloid and interface science*, 280(2): 322–333.

Asha, M.N., Chandan, K.S., Harish, H.P., NikhileswarReddy, S., Sharath, K.S. & Liza, G.M. 2016. Recycling of Waste Water Collected from Automobile Service Station. *Procedia Environmental Sciences*, 35: 289–297. http://dx.doi.org/10.1016/j.proenv.2016.07.009.

Ayawei, N., Ebelegi, A.N. & Wankasi, D. 2017. Modelling and Interpretation of Adsorption Isotherms. *Journal of Chemistry*, 2017.

Aygun, a & Yilmaz, T. 2010. Improvement of Coagulation-Flocculation Process for Treatment of Detergent Wastewaters Using Coagulant Aids. *International Journal of Chemical and Environmental Engineering*, 1(2): 97–101.

Ayranci, E. & Duman, O. 2007. Removal of anionic surfactants from aqueous solutions by

adsorption onto high area activated carbon cloth studied by in situ UV spectroscopy. *Journal of Hazardous Materials*, 148(1–2): 75–82.

Azizian, S. 2004. Kinetic models of sorption: a theoretical analysis. *Journal of colloid and Interface Science*, 276(1): 47–52.

Baddor, I.M., Farhoud, N., Mohammed, I., Abdel-Magid, D., Alshami, S., Hassan Ahmad, F. & Asaad, E. 2014. Study of car wash wastewater treatment by adsorption. In *International Conference of Engineering, Information Technology, and Science*. 2–22.

Balarak, D., Mostafapour, F., Azarpira, H. & Joghataei, A. 2017. Langmuir, Freundlich, Temkin and Dubinin–radushkevich Isotherms Studies of Equilibrium Sorption of Ampicilin unto Montmorillonite Nanoparticles. *Journal of Pharmaceutical Research International*, 20(2): 1–9.

Bansal, R.C. & Goyal, M. 2005. *Activated Adsorption Carbon*.

Bashiri, M. & Farshbaf Geranmayeh, A. 2011. Tuning the parameters of an artificial neural network using central composite design and genetic algorithm. *Scientia Iranica*, 18(6): 1600–1608. http://dx.doi.org/10.1016/j.scient.2011.08.031.

Bautista-Toledo, M.I., Méndez-Díaz, J.D., Sánchez-Polo, M., Rivera-Utrilla, J. & Ferro-García, M.A. 2008. Adsorption of sodium dodecylbenzenesulfonate on activated carbons: Effects of solution chemistry and presence of bacteria. *Journal of Colloid and Interface Science*, 317(1): 11–17.

Bazrafshan, E., Mostafapoor, F., Soori, M.M. & Mahvi, A.H. 2012. Carwash Wastewater Treatment by Combined Chemical Coagulation and Electrocoagulation Process. *Fresenius Environmental Bulletin*, 21(9 A): 2694–2701.

Bedin, K.C., Martins, A.C., Cazetta, A.L., Pezoti, O. & Almeida, V.C. 2016. KOH-activated carbon prepared from sucrose spherical carbon: Adsorption equilibrium, kinetic and thermodynamic studies for Methylene Blue removal. *Chemical Engineering Journal*, 286: 476–484.

Belaid, K.D., Kacha, S., Kameche, M. & Derriche, Z. 2013. Adsorption kinetics of some textile dyes onto granular activated carbon. *Journal of Environmental Chemical Engineering*, 1(3): 496–503.

Bertule, M., Glennie, P., Bjørnsen, P.K., Lloyd, G.J., Kjellen, M., Dalton, J., Rieu-Clarke, A., Romano, O., Tropp, H., Newton, J. & Harlin, J. 2018. Monitoring water resources governance progress globally: Experiences from monitoring SDG indicator 6.5.1 on integrated water resources management implementation. *Water (Switzerland)*, 10(12).

Boubaker, F. & Ridha, B.C. 2020. Esparto paper industry wastewater treatment by adsorption onto powdered activated carbon onto powdered activated carbon. *International Journal of*

Environmental Analytical Chemistry, 00(00): 1–18. https://doi.org/10.1080/03067319.2020.1711897.

Bourblanc, M. & Blanchon, D. 2014. The challenges of rescaling south african water resources management: Catchment management agencies and interbasin transfers. *Journal of Hydrology*, 519(PC): 2381–2391. http://dx.doi.org/10.1016/j.jhydrol.2013.08.001.

Boussu, K., Kindts, C., Vandecasteele, C. & Van der Bruggen, B. 2007. Applicability of nanofiltration in the carwash industry. *Separation and Purification Technology*, 54(2): 139–146.

Boyd, G.E., Adamson, A.W. & Myers Jr, L.S. 1947. The exchange adsorption of ions from aqueous solutions by organic zeolites. II. Kinetics1. *Journal of the American Chemical Society*, 69(11): 2836–2848.

Cazetta, A.L., Vargas, A.M.M., Nogami, E.M., Kunita, M.H., Guilherme, M.R., Martins, A.C., Silva, T.L., Moraes, J.C.G. & Almeida, V.C. 2011. NaOH-activated carbon of high surface area produced from coconut shell: Kinetics and equilibrium studies from the methylene blue adsorption. *Chemical Engineering Journal*, 174(1): 117–125.

Cheng, S.J., Miao, J.M. & Wu, S.J. 2012. Investigating the effects of operational factors on PEMFC performance based on CFD simulations using a three-level full-factorial design. *Renewable Energy*, 39(1): 250–260. http://dx.doi.org/10.1016/j.renene.2011.08.009.

Cheung, C.W., Porter, J.F. & McKay, G. 2000. Elovich equation and modified second-order equation for sorption of cadmium ions onto bone char. *Journal of Chemical Technology & Biotechnology*, 75(11): 963–970.

Chiou, M.S. & Li, H.Y. 2002. Equilibrium and kinetic modeling of adsorption of reactive dye on cross-linked chitosan beads. *Journal of Hazardous Materials*, 93(2): 233–248.

Chowdhury, S., Mishra, R., Saha, P. & Kushwaha, P. 2011. Adsorption thermodynamics, kinetics and isosteric heat of adsorption of malachite green onto chemically modified rice husk. *Desalination*, 265(1–3): 159–168. http://dx.doi.org/10.1016/j.desal.2010.07.047.

Colvin, C., Muruven, D., Lindley, D., Gordon, H. & Schachtschneider, K. 2016. Water Facts and Futures: Rethinking South Africa's Water Future. *WWF-SA 2016 Water Facts and Futures*: 2–96.

Cooney, D.O. 1998. *Adsorption design for wastewater treatment*. CRC press.

Czitrom, V. 1999. One-factor-at-a-time versus designed experiments. *American Statistician*, 53(2): 126–131.

Dao, M.T., Nguyen, T.T.T., Nguyen, X. Du, La, D.D., Nguyen, D.D., Chang, S.W., Chung, W.J. & Nguyen, V.K. 2020. Toxic metal adsorption from aqueous solution by activated biochars

produced from Macadamia nutshell waste. *Sustainability (Switzerland)*, 12(19).

Darwish, A.A.A., Rashad, M. & AL-Aoh, H.A. 2019. Methyl orange adsorption comparison on nanoparticles: isotherm, kinetics, and thermodynamic studies. *Dyes and Pigments*, 160: 563–571.

Dejang, N., Somprasit, O. & Chindaruksa, S. 2015. *A Preparation of Activated Carbon from Macadamia Shell by Microwave Irradiation Activation*. Elsevier B.V. http://dx.doi.org/10.1016/j.egypro.2015.11.556.

Department of Water Affairs and Forsetry. 2013. National Water Resource Strategy - 2nd edition 2013. *Water Resources*: 201. http://www.dwa.gov.za/documents/Other/Strategic Plan/NWRS2-Final-email-version.pdf.

Dubinin, Mm. 1960. The potential theory of adsorption of gases and vapors for adsorbents with energetically nonuniform surfaces. *Chemical Reviews*, 60(2): 235–241.

Eletta, O.A.A., Mustapha, S.I., Ajayi, O.A. & Ahmed, A.T. 2018. Optimization of dye removal from textile wastewater using activated carbon from sawdust. *Nigerian Journal of Technological Development*, 15(1): 26.

Enoh, B.S. & Christopher, W. 2015. Adsorption of metal ions from carwash wastewater by phosphoric acid modified clay: Kinetics and thermodynamic studies. *Adsorption*, 7(4).

Fagundes-klen, R. & Dotto, J. 2019. Performance of different coagulants in the coagulation / fl occulation process of textile wastewater. , 208: 656–665.

Foo, K.Y. & Hameed, B.H. 2010. Insights into the modeling of adsorption isotherm systems. *Chemical Engineering Journal*, 156(1): 2–10.

Foroughi, M., Chavoshi, S., Bagheri, M., Yetilmezsoy, K. & Samadi, M.T. 2018. Alum-based sludge (AbS) recycling for turbidity removal in drinking water treatment: an insight into statistical, technical, and health-related standpoints. *Journal of Material Cycles and Waste Management*, 20(4): 1999–2017.

Geankoplis, C.J. 2003. *Transport processes and separation process principles:(includes unit operations)*. Prentice Hall Professional Technical Reference.

Ghiaci, M., Abbaspur, A., Kia, R. & Seyedeyn-Azad, F. 2004. Equilibrium isotherm studies for the sorption of benzene, toluene, and phenol onto organo-zeolites and as-synthesized MCM-41. *Separation and purification technology*, 40(3): 217–229.

De Gisi, S., Lofrano, G., Grassi, M. & Notarnicola, M. 2016. Characteristics and adsorption capacities of low-cost sorbents for wastewater treatment: A review. *Sustainable Materials and Technologies*, 9: 10–40. http://dx.doi.org/10.1016/j.susmat.2016.06.002.

Gong, R., Sun, Y., Chen, J., Liu, H. & Yang, C. 2005. Effect of chemical modification on dye

adsorption capacity of peanut hull. *Dyes and Pigments*, 67(3): 175–181.

Gupta, S., Pal, A., Kumar Ghosh, P. & Bandyopadhyay, M. 2003. Performance of waste activated carbon as a low-cost adsorbent for the removal of anionic surfactant from aquatic environment. *Journal of Environmental Science and Health - Part A Toxic/Hazardous Substances and Environmental Engineering*, 38(2): 381–397.

Harding, G., Courtney, C. & Russo, V. 2017. When geography matters . A location-adjusted blue water footprint of commercial beef in South Africa. *Journal of Cleaner Production*, 151: 494–508. http://dx.doi.org/10.1016/j.jclepro.2017.03.076.

Hasan, S.H., Srivastava, P. & Talat, M. 2009. Biosorption of Pb(II) from water using biomass of Aeromonas hydrophila: Central composite design for optimization of process variables. *Journal of Hazardous Materials*, 168(2–3): 1155–1162.

Hashim, N.H. & Zayadi, N. 2016. Pollutants characterization of car wash wastewater. *MATEC Web of Conferences*, 47: 4–9.

El Hassani, K., Beakou, B.H. & Anouar, A. 2018. Analysis of adsorption of azo dye onto NiAl-CO3 using Box-Behnken design approach and desirability function. *Journal of Materials and Environmental Science*, 9(2): 520–527. https://www.scopus.com/inward/record.uri?eid=2-s2.0-85040075158&doi=10.26872%2Fjmes.2018.9.2.56&partnerID=40&md5=d364e61fe8f03d6737d1535ad2187140.

Hill, T.L. 1952. Theory of physical adsorption. In *Advances in catalysis*. Elsevier: 211–258.

Ince, M. & Ince, O.K. 2017. Box-Behnken design approach for optimizing removal of copper from wastewater using a novel and green adsorbent. *Atomic Spectroscopy*, 38(6): 200–207.

Isam, M., Baloo, L., Kutty, S.R.M. & Yavari, S. 2019. Optimisation and modelling of Pb(II) and Cu(II) biosorption onto red algae (Gracilaria changii) by using response surface methodology. *Water (Switzerland)*, 11(11).

Jasper, E.E., Ajibola, V.O. & Onwuka, J.C. 2020. Nonlinear regression analysis of the sorption of crystal violet and methylene blue from aqueous solutions onto an agro-waste derived activated carbon. *Applied Water Science*, 10(6): 1–11. https://doi.org/10.1007/s13201-020-01218-y.

Jiang, J.Q. & Graham, N.J.D. 1998a. Pre-polymerised inorganic coagulants and phosphorus removal by coagulation - A review. *Water SA*, 24(3): 237–244.

Jiang, J.Q. & Graham, N.J.D. 1998b. Preparation and characterisation of an optimal polyferric sulphate (PFS) as a coagulant for water treatment. *Journal of Chemical Technology and Biotechnology*, 73(4): 351–358.

Jiang, S., Li, Y. & Ladewig, B.P. 2017. A review of reverse osmosis membrane fouling and control strategies. *Science of the Total Environment*, 595: 567–583. http://dx.doi.org/10.1016/j.scitotenv.2017.03.235.

Kajjumba, G.W., Emik, S., Öngen, A., Ozcan, K. & Aydin, S. 2018. Modelling of adsorption kinetic processes—errors, theory and application. In *Advanced sorption process applications*. IntechOpen.

Karim, M.M., Das, A.K. & Lee, S.H. 2006. Treatment of colored effluent of the textile industry in Bangladesh using zinc chloride treated indigenous activated carbons. *Analytica Chimica Acta*, 576(1): 37–42.

kaur, K., Rani, S., and Mahajan, K. 2012. Adsorption kinetics for the removal of hazardous dye Congo Red Biowaste Materials as Adsorbents. *Journal of Chemistry*, 2013: 12.

Kuang, Y., Zhang, X. & Zhou, S. 2020. Adsorption of methylene blue in water onto activated carbon by surfactant modification. *Water (Switzerland)*, 12(2): 1–19.

Langmuir, I. 1916. The constitution and fundamental properties of solids and liquids. Part I. Solids. *Journal of the American chemical society*, 38(11): 2221–2295.

Lau, W.J., Ismail, A.F. & Firdaus, S. 2013. Car wash industry in Malaysia: Treatment of car wash effluent using ultrafiltration and nanofiltration membranes. *Separation and Purification Technology*, 104: 26–31. http://dx.doi.org/10.1016/j.seppur.2012.11.012.

Laus, R., Costa, T.G., Szpoganicz, B. & Fávere, V.T. 2010. Adsorption and desorption of Cu(II), Cd(II) and Pb(II) ions using chitosan crosslinked with epichlorohydrin-triphosphate as the adsorbent. *Journal of Hazardous Materials*, 183(1–3): 233–241.

Leiknes, T. & Ødegaard, H. 2007. The development of a biofilm membrane bioreactor. *Desalination*, 202(1–3): 135–143.

Limousin, G., Gaudet, J.P., Charlet, L., Szenknect, S., Barthès, V. & Krimissa, M. 2007. Sorption isotherms: A review on physical bases, modeling and measurement. *Applied Geochemistry*, 22(2): 249–275.

Lofrano, G. 2012. *Emerging compounds removal from wastewater: natural and solar based treatments*. Springer Science & Business Media.

López-Luna, J., Ramírez-Montes, L.E., Martinez-Vargas, S., Martínez, A.I., Mijangos-Ricardez, O.F., González-Chávez, M. del C.A., Carrillo-González, R., Solís-Domínguez, F.A., Cuevas-Díaz, M. del C. & Vázquez-Hipólito, V. 2019. Linear and nonlinear kinetic and isotherm adsorption models for arsenic removal by manganese ferrite nanoparticles. *SN Applied Sciences*, 1(8): 1–19. https://doi.org/10.1007/s42452-019-0977-3.

Malik, Q.H. 2018. Performance of alum and assorted coagulants in turbidity removal of muddy

water. *Applied Water Science*, 8(1): 1–4.

Martins, A.C., Pezoti, O., Cazetta, A.L., Bedin, K.C., Yamazaki, D.A.S., Bandoch, G.F.G., Asefa, T., Visentainer, J. V. & Almeida, V.C. 2015. Removal of tetracycline by NaOH-activated carbon produced from macadamia nut shells: Kinetic and equilibrium studies. *Chemical Engineering Journal*, 260: 291–299. http://dx.doi.org/10.1016/j.cej.2014.09.017.

Maya Saphira Radin Mohamed, R., Mariam Ibrahim Kutty, N.A. & Hashim Mohd Kassim, A. 2014. Efficiency of Using Commercial and Natural Coagulants in Treating Car Wash Wastewater Treatment. *Australian Journal of Basic and Applied Sciences Aust. J. Basic & Appl. Sci*, 8(816): 227–234. www.ajbasweb.com.

Mazumber, D. & Mukherjee, S. 2011. Treatment of Automobile Service Station Wastewater by Coagulation and Activated Sludge Process. *International Journal of Environmental Science and Development*, 2(1): 64–69. http://www.ijesd.org/show-29-346-1.html.

McCabe, W.L., Smith, J.C. & Harriott, P. 1993. *Unit operations of chemical engineering*. McGraw-hill New York.

McKenzie, R., Siqalaba, Z. & Wegelin, W. 2012. *The State of Non-Revenue Water in South Africa (2012) - WRC Report No. TT 522/12*.

Moazzem, S., Wills, J., Fan, L., Roddick, F. & Jegatheesan, V. 2018. Performance of ceramic ultrafiltration and reverse osmosis membranes in treating car wash wastewater for reuse. *Environmental Science and Pollution Research*, 25(9): 8654–8668.

Möbius, D., Miller, R. & Fainerman, V.B. 2001. *Surfactants: chemistry, interfacial properties, applications*. Elsevier.

Moussout, H., Ahlafi, H., Aazza, M. & Maghat, H. 2018. Critical of linear and nonlinear equations of pseudo-first order and pseudo-second order kinetic models. *Karbala International Journal of Modern Science*, 4(2): 244–254. https://doi.org/10.1016/j.kijoms.2018.04.001.

Mukerjee, R. & Wu, C.F.J. 2007. *A modern theory of factorial design*. Springer Science & Business Media.

Mukwevho, M.J., Maharajh, D. & Chirwa, E.M.N. 2020. Evaluating the effect of ph, temperature, and hydraulic retention time on biological sulphate reduction using response surface methodology. *Water (Switzerland)*, 12(10): 1–17.

Mutegoa, E., Onoka, I. & Hilonga, A. 2014. PREPARATION OF ACTIVATED CARBON WITH DESIRED PROPERTIES THROUGH Rjeas. , (November).

Myers, A.L. & Prausnitz, J.M. 1965. Thermodynamics of mixed-gas adsorption. *AIChE Journal*, 11(1): 121–127.

N'diaye, A.D. & Kankou, M.S.A. 2020. Modeling of adsorption isotherms of pharmaceutical

products onto various adsorbents : A Short Review. *Journal of Material and Environmental Science*, 11(8): 1264–1276.

Najib, T., Solgi, M., Farazmand, A., Heydarian, S.M. & Nasernejad, B. 2017. Optimization of sulfate removal by sulfate reducing bacteria using response surface methodology and heavy metal removal in a sulfidogenic UASB reactor. *Journal of Environmental Chemical Engineering*, 5(4): 3256–3265.

Ncibi, M.C. 2008. Applicability of some statistical tools to predict optimum adsorption isotherm after linear and non-linear regression analysis. *Journal of Hazardous Materials*, 153(1–2): 207–212.

Ngakou, C.S., Anagho, G.S. & Ngomo, H.M. 2019. Non-linear Regression Analysis for the Adsorption Kinetics and Equilibrium Isotherm of Phenacetin onto Activated Carbons. *Current Journal of Applied Science and Technology*, (July): 1–18.

NIST/SEMATECH. 2012. e-Handbook of Statistical Methods. http://www.itl.nist.gov/div898/handbook/ 1 April 2021.

Obayomi, K.S., Bello, J.O., Yahya, M.D., Chukwunedum, E. & Adeoye, J.B. 2020. Statistical analyses on effective removal of cadmium and hexavalent chromium ions by multiwall carbon nanotubes (MWCNTs). *Heliyon*, 6(6).

Oh, K.S., Leong, J.Y.C., Poh, P.E., Chong, M.N. & Lau, E. Von. 2018. A review of greywater recycling related issues: Challenges and future prospects in Malaysia. *Journal of Cleaner Production*, 171: 17–29. https://doi.org/10.1016/j.jclepro.2017.09.267.

Pal, A., Pan, S. & Saha, S. 2013. Synergistically improved adsorption of anionic surfactant and crystal violet on chitosan hydrogel beads. *Chemical Engineering Journal*, 217: 426–434. http://dx.doi.org/10.1016/j.cej.2012.11.120.

Panizza, M. & Cerisola, G. 2010. Applicability of electrochemical methods to carwash wastewaters for reuse. Part 1: Anodic oxidation with diamond and lead dioxide anodes. *Journal of Electroanalytical Chemistry*, 638(1): 28–32. http://dx.doi.org/10.1016/j.jelechem.2009.10.025.

Papegowda, P.K. & Syed, A.A. 2017. Isotherm, Kinetic and Thermodynamic Studies on the Removal of Methylene Blue Dye from Aqueous Solution Using Saw Palmetto Spent. *International Journal of Environmental Research*, 11(1): 91–98.

Pezoti, O., Cazetta, A.L., Souza, I.P.A.F., Bedin, K.C., Martins, A.C., Silva, T.L. & Almeida, V.C. 2014. Adsorption studies of methylene blue onto ZnCl2-activated carbon produced from buriti shells (Mauritia flexuosa L.). *Journal of Industrial and Engineering Chemistry*, 20(6): 4401–4407.

Qiu, H., Lv, L., Pan, B.C., Zhang, Q.J., Zhang, W.M. & Zhang, Q.X. 2009. Critical review in adsorption kinetic models. *Journal of Zhejiang University: Science A*, 10(5): 716–724.

Ragheb, S.M. 2013. Phosphate removal from aqueous solution using slag and fly ash. *HBRC Journal*, 9(3): 270–275.

Rajamohan, N., Rajasimman, M., Rajeshkannan, R. & Saravanan, V. 2014. Equilibrium, kinetic and thermodynamic studies on the removal of Aluminum by modified Eucalyptus camaldulensis barks. *Alexandria Engineering Journal*, 53(2): 409–415. http://dx.doi.org/10.1016/j.aej.2014.01.007.

Rodriguez Boluarte, I.A., Andersen, M., Pramanik, B.K., Chang, C.Y., Bagshaw, S., Farago, L., Jegatheesan, V. & Shu, L. 2016. Reuse of car wash wastewater by chemical coagulation and membrane bioreactor treatment processes. *International Biodeterioration and Biodegradation*, 113: 44–48. http://dx.doi.org/10.1016/j.ibiod.2016.01.017.

RotoCarb. ProCarb Technical Data Sheet. *2019*. http://www.rotocarb.co.za/wp-content/uploads/2019/04/TDS-ProCarb-PAC.pdf 11 April 2021.

RSA. 1998. National Water Act (Act No. 36 of 1998). *Government Gazette*, 19182.

Rubí-Juárez, H., Barrera-Díaz, C., Linares-Hernández, I., Fall, C. & Bilyeu, B. 2015. A combined electrocoagulation-electrooxidation process for carwash wastewater reclamation. *International Journal of Electrochemical Science*, 10(8): 6754–6767.

Rudzinski, W. & Panczyk, T. 2000. Kinetics of isothermal adsorption on energetically heterogeneous solid surfaces: a new theoretical description based on the statistical rate theory of interfacial transport. *The Journal of Physical Chemistry B*, 104(39): 9149–9162.

Saha, P. & Chowdhury, S. 2011. Insight Into Adsorption Thermodynamics. *Thermodynamics*.

Sanda, O., Amoo, K.I. & Taiwo, E.A. 2017. Studies on the Adsorption of Indigo Dye From Aqueous Media Onto Carbonised Sugarcane Bagasse. , 25(1): 40–47.

Sarmadi, M., Foroughi, M., Najafi Saleh, H., Sanaei, D., Zarei, A.A., Ghahrchi, M. & Bazrafshan, E. 2020. Efficient technologies for carwash wastewater treatment: a systematic review. *Environmental Science and Pollution Research*, 27(28): 34823–34839.

Sasi Kumar, N. & Chauhan, M.S. 2018. Treatment of Car Washing Unit Wastewater—A Review. *Water science and Technology Library*: 247–255.

Sharma, P., Jain, R., Premi, A., Kumar, N. & Parashar, A. 2020. Linear and non-linear regression analysis for the sorption kinetics of Tropaeoline 000 onto Nano Talc. *International Journal of Environmental Analytical Chemistry*, 00(00): 1–16. https://doi.org/10.1080/03067319.2020.1751143.

Simsek, E.B. & Beker, U. 2014. Equilibrium arsenic adsorption onto metallic oxides : Isotherm

models, error analysis and removal mechanism. *Korean Journal of Chemical Engineering*, 31(11): 2057–2069.

Siyal, A.A., Shamsuddin, M.R., Low, A. & Rabat, N.E. 2020. A review on recent developments in the adsorption of surfactants from wastewater. *Journal of Environmental Management*, 254: 109797. http://www.sciencedirect.com/science/article/pii/S0301479719315154.

Steber, J. 2007. *The Ecotoxicity of Cleaning Product Ingredients*. Elsevier B.V. http://dx.doi.org/10.1016/B978-0-444-51664-0.50022-X.

Sun, X. & Zhang, Z. 2004. Optimizing the novel formulation of liposome-polycation-DNA complexes (LPD) by central composite design. *Archives of Pharmacal Research*, 27(7): 797–805.

Talens-Alesson, F.I., Anthony, S. & Bryce, M. 2006. Removal of phenol by adsorptive micellar flocculation: Multi-stage separation and integration of wastes for pollution minimisation. *Colloids and Surfaces A: Physicochemical and Engineering Aspects*, 276(1–3): 8–14.

Tan, K.L. & Hameed, B.H. 2017. Insight into the adsorption kinetics models for the removal of contaminants from aqueous solutions. *Journal of the Taiwan Institute of Chemical Engineers*, 74: 25–48.

Tchobanoglus, G., Burton, F. & Stensel, H.D. 2003. Wastewater engineering: Treatment and reuse. *American Water Works Association. Journal*, 95(5): 201.

Tony, M.A. & Bedri, Z. 2014. Experimental design of photo-Fenton reactions for the treatment of car wash wastewater effluents by response surface methodological analysis. *Advances in Environmental Chemistry*, 2014.

Tran, H.N., You, S.-J., Hosseini-Bandegharaei, A. & Chao, H.-P. 2017. Mistakes and inconsistencies regarding adsorption of contaminants from aqueous solutions: a critical review. *Water research*, 120: 88–116.

Veit, M.T., Novais, Í.G.V., Juchen, P.T., Palácio, S.M., da Cunha Gonçalves, G. & Zanette, J.C. 2020. Automotive Wash Effluent Treatment Using Combined Process of Coagulation/Flocculation/Sedimentation–Adsorption. *Water, Air, and Soil Pollution*, 231(10). http://dx.doi.org/10.1007/s11270-020-04862-x.

Vijayaraghavan, G.; Sivakumar, T.. V.K. 2011. Application of Plant Based Coagulants for Waste Water Treatment. *International Journal of Advanced Engineering Research and Studies*, 1(1): 88–92.

Vijayaraghavan, K., Padmesh, T.V.N., Palanivelu, K. & Velan, M. 2006. Biosorption of nickel (II) ions onto Sargassum wightii: application of two-parameter and three-parameter isotherm models. *Journal of hazardous materials*, 133(1–3): 304–308.

Weber, W.J. & Morris, J.C. 1963. Kinetics of adsorption on carbon from solution. *Journal of the Sanitary Engineering Division*, 89(2): 31–60.

Zaneti, R.N., Etchepare, R. & Rubio, J. 2013. Car wash wastewater treatment and water reuse - A case study. *Water Science and Technology*, 67(1): 82–88.

Zhai, J., Huang, Z., Rahaman, M.H., Li, Y., Mei, L., Ma, H., Hu, X., Xiao, H., Luo, Z. & Wang, K. 2017. Comparison of coagulation pretreatment of produced water from natural gas well by polyaluminium chloride and polyferric sulphate coagulants. *Environmental Technology (United Kingdom)*, 38(10): 1200–1210.

Zhang, R. & Somasundaran, P. 2006. Advances in adsorption of surfactants and their mixtures at solid/solution interfaces. *Advances in Colloid and Interface Science*, 123–126(SPEC. ISS.): 213–229.

Zhou, X. 2020. Correction to the calculation of Polanyi potential from Dubinnin-Rudushkevich equation. *Journal of Hazardous Materials*, 384(xxxx): 121101. https://doi.org/10.1016/j.jhazmat.2019.121101.

Zor, S. 2004. Investigation of the adsorption of anionic surfactants at different pH values by means of active carbon and the kinetics of adsorption. *Journal of the Serbian Chemical Society*, 69(1): 25–32.

Zouboulis, A.I., Moussas, P.A. & Vasilakou, F. 2008. Polyferric sulphate: Preparation, characterisation and application in coagulation experiments. *Journal of Hazardous Materials*, 155(3): 459–468.

Appendices

Appendices

Appendix A: South African wastewater discharge standards

Table A- 1: South African wastewater discharge standards

SUBSTANCE/PARAMETER	GENERAL LIMIT
Fecal Coliforms (per 100 ml)	1000
Chemical Oxygen Demand (mg/l)	75 (i)
pH	5,5-9,5
Ammonia as Nitrogen (mg/l)	6
Nitrate/Nitrite as Nitrogen (mg/l)	15
Chlorine as Free Chlorine (mg/l)	0,25
Suspended Solids (mg/l)	25
Electrical Conductivity (mS/m)	150 mS/m
Ortho-Phosphate as phosphorous (mg/l)	10
Fluoride (mg/l)	1
Soap, oil or grease (mg/l)	2,5
Dissolved Arsenic (mg/l)	0,02
Dissolved Cadmium (mg/l)	0,005
Dissolved Chromium (VI) (mg/l)	0,05
Dissolved Copper (mg/l)	0,01
Dissolved Cyanide (mg/l)	0,02
Dissolved Iron (mg/l)	0,3
Dissolved Lead (mg/l)	0,01
Dissolved Manganese (mg/l)	0,1
Mercury and its compounds (mg/l)	0,005
Dissolved Selenium (mg/l)	0,02
Dissolved Zinc (mg/l)	0,1
Boron (mg/l)	1

Appendix B: Surfactant Kinetic data from batch adsorption experiments

Table B-1. 1: Experiment Conditions Run 1

Dosage (g/l)	0.15
pH	6
Temp ©	25
Volume (l)	0.5
IC (mg/l)	15

Table B-1. 2: Kinetic data run 1

Time (min)	0	10	20	30	60	120
Concentration run 1.1(mg/l)	15	5.28	4.3	4	3.8	2.8
Adsorption capacity run 1.1 (mg/g)	0	32.333	35.66	36.6	37.333	40.66
Concentration run 1.2 (mg/l)	15	5.82	4.063	3.663	3.2	2.9
Adsorption capacity run 1.2 (mg/g)	0	30.57	36.4	37.79	39.33	40.33
Average Concentration (mg/l)	0	31.47	36.06	37.22	38.33	40.5
Average Adsorption Capacity (mg/g)	15	5.57	4.18	3.81	3.5	2.85

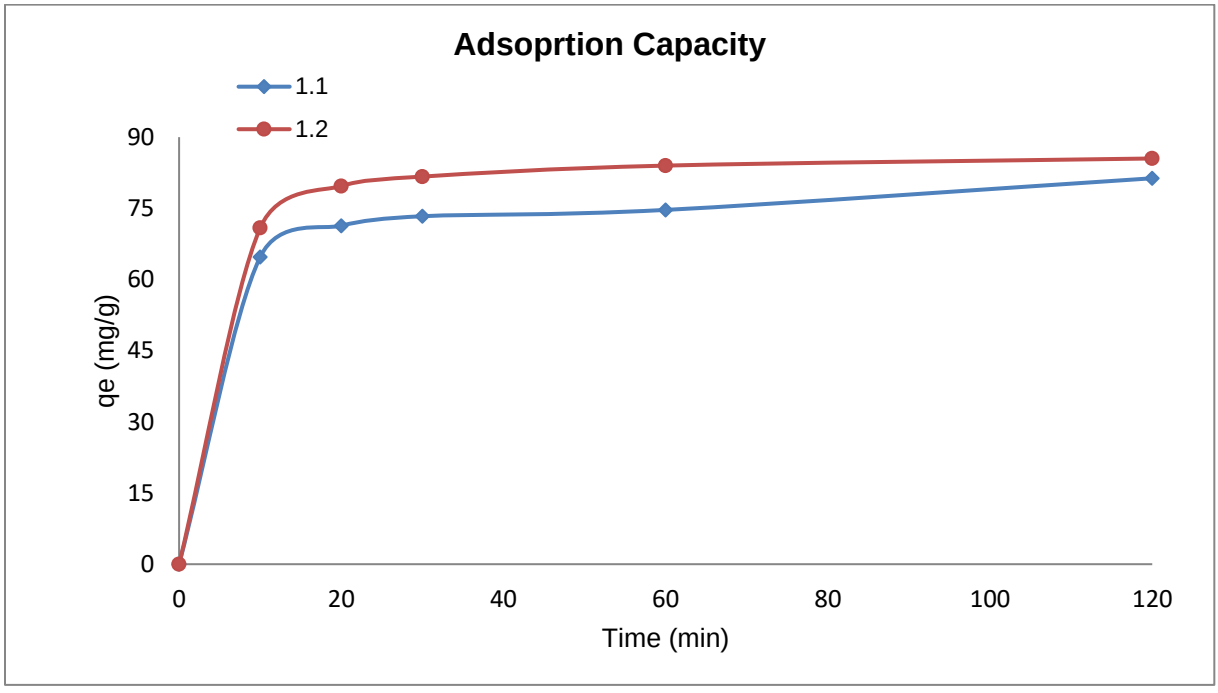

Figure B-1. 1: Adsorption capacity Experiment 1

Data analysis report on the two ranges of kinetic data

Data analysis using Microsoft Excel was performed to assess the significance of data of an experimental run and the 'duplicate run' has a significant difference or not.

F-test two-sample for variances

	Variable 1	Variable 2
Mean	3,9856	3,9331
Variance	0,6565	1,3216
Observations	5	5
df	4	4
F	0,4968	
P(F<=f) one-tail	0,2573	
F Critical one-tail	0,15653	

t-Test: Two-Sample Assuming Unequal Variances

	Variable 1	Variable 2
Mean	3,98566	3,9331
Variance	0,6565	1,3216
Observations	5	5
Hypothesized Mean Difference	0	
df	7	
t Stat	0,08356	
P(T<=t) one-tail	0,46787	
t Critical one-tail	1,89457	
P(T<=t) two-tail	0,9357	
t Critical two-tail	2,3646	

Table B-1. 3: Experiment Conditions Run 2

Dosage (g)	0.05
pH	6
Temp ©	25
Volume (l)	0.5
IC (mg/l)	15

Table B-1. 4: Kinetic data Run 2

Time (min)	0	10	20	30	60	120
Concentration run 2.1(mg/l)	15	10.2	9.45	9.2	9.2	9
Adsorption capacity run 2.1 (mg/g)	0	48	55.5	58	58	60
Concentration run 2.2 (mg/l)	15	13.5	13.05	10.3	9.85	9.22
Adsorption capacity run 2.2 (mg/g)	0	15	19.5	47	51.5	57.8
Average Concentration (mg/l)	0	48	55.5	58	58	60
Average Adsorption Capacity (mg/g)	15	11.85	11.25	9.75	9.525	9.11

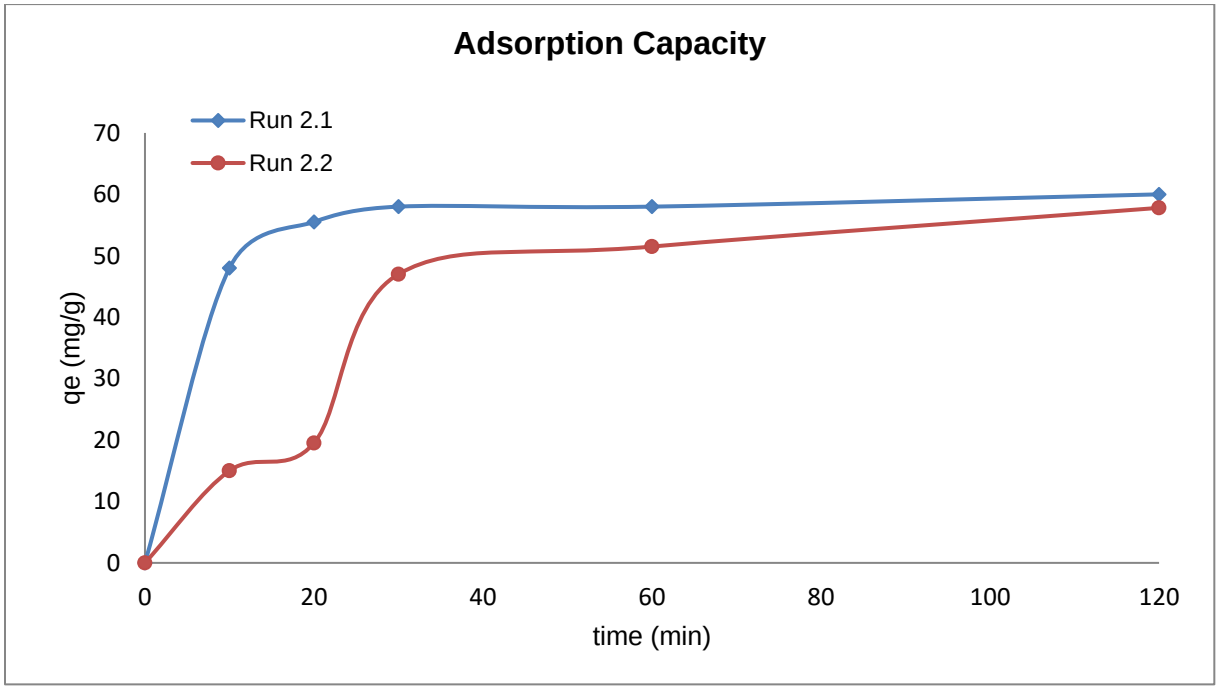

Figure B-1. 2: Adsorption capacity run 2

Data analysis report on the two ranges of kinetic data

Data analysis using Microsoft Excel was performed to assess the significance of data of an experimental run and the 'duplicate run' has a significant difference or not.

F-test two sample variance

	variable 1	Variable 2
Mean	3,98566	3,9331
Variance	0,6565	1,3216
Observations	5	5
df	4	4
F	0,4968	
P(F<=f) one-tail	0,2573	
F Critical one-tail	0,1565	

t-test two sample assuming unequal variance

	variable 1	variable 2
Mean	9,41	11,184
Variance	0,220	3,816
Observations	5	5
Hypothesized Mean Difference	0	
df	4	
t Stat	-1,974	
P(T<=t) one-tail	0,059	
t Critical one-tail	2,131	
P(T<=t) two-tail	0,119	
t Critical two-tail	2,776	

Table B-1. 5: Experiment conditions run 3

Dosage (g)	0.1
pH	2
Temp ©	25
Volume (l)	0.5
IC (mg/l)	15

Table B-1. 6: Kinetic data run 3

Time (min)	0	10	20	30	60	120
Concentration run 3.1(mg/l)	15	6.6	6.15	5.94	4.29	2.73
Adsorption capacity run 3.1 (mg/g)	0	42	44.25	45.3	53.55	61.35
Concentration run 3.2 (mg/l)	15	6.171	5.094	4.995	4.3623	2.63
Adsorption capacity run 3.2 (mg/g)	0	44.14	49.53	50.025	53.18	61.85
Average Concentration (mg/l)	15	6.38	5.622	5.4675	4.32	2.68
Average Adsorption Capacity (mg/g)	0	43.07	46.89	47.66	53.36	61.6

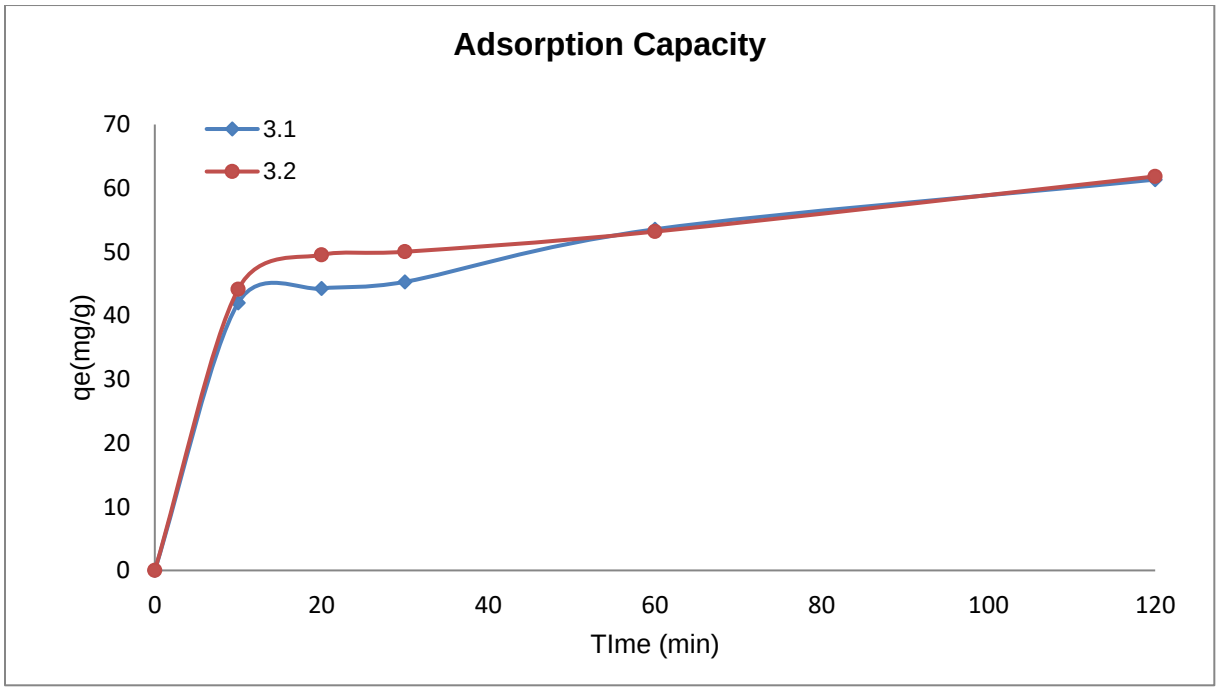

Figure B-1. 3: Adsorption capacity run 3

Data analysis report on the two ranges of kinetic data

Data analysis using Microsoft Excel was performed to assess the significance of data of an experimental run and the 'duplicate run' has a significant difference or not.

F-test two sample for variances

	variable 1	variable 2
Mean	5,142	4,650
Variance	2,580	1,698
Observations	5	5
df	4	4
F	1,519	
P(F<=f) one-tail	0,347	
F Critical one-tail	6,388	

t-test two sample assuming unequal variance

	variable 1	variable 2
Mean	5,142	4,650
Variance	2,580	1,698
Observations	5	5
Hypothesized Mean Difference	0	
df	8	
t Stat	0,531	
P(T<=t) one-tail	0,304	
t Critical one-tail	1,859	
P(T<=t) two-tail	0,609	
t Critical two-tail	2,306	

Table B-1. 7: Experimental conditions run 4

Dosage (g)	0.1
pH	6
Temp ©	25
Volume (l)	0.5
IC (mg/l)	15

Table B-1. 8: Kinetic data run 4

Time (min)	0	10	20	30	60	120
Concentration run 4.1(mg/l)	15	8.69	7.33	6.22	4.62	4.7
Adsorption capacity run 4.1 (mg/g)	0	31.54	38.30	43.86	51.85	51.5
Concentration run 4.2 (mg/l)	15	8.391	6.56	6.06	4.76	4.45
Adsorption capacity run 4.2 (mg/g)	0	33.04	42.2	44.7	51.2	52.75
Average Concentration (mg/l)	15	8.54	6.94	6.14	4.69	4.57
Average Adsorption Capacity (mg/g)	0	32.29	40.25	44.28	51.52	52.12

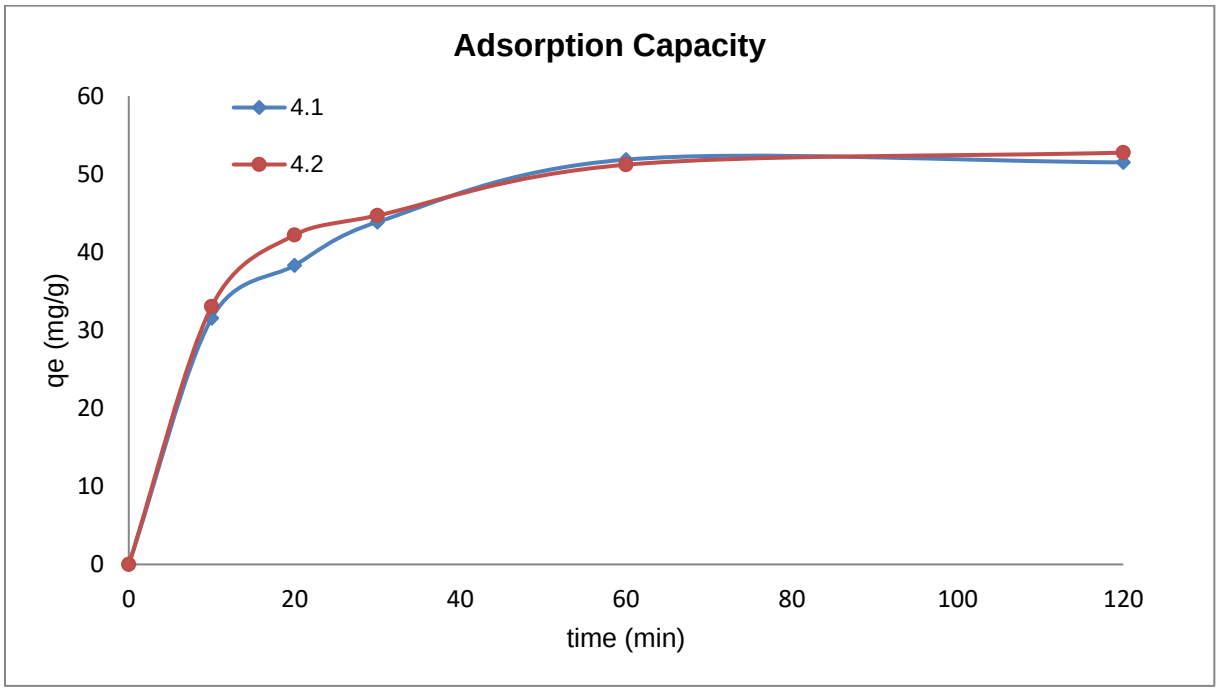

Figure B-1. 4: Adsorption capacity run 4

Data analysis report on the two ranges of kinetic data

Data analysis using Microsoft Excel was performed to assess the significance of data of an experimental run and the ‘duplicate run’ has a significant difference or not.

F-test two-sample for variances

	variable 1	variable 2
Mean	6,317	6,044
Variance	3,038	2,491
Observations	5	5
df	4	4
F	1,219	
P(F<=f) one-tail	0,426	
F Critical one-tail	6,388	

t-test two sample assuming unequal variance

	variable 1	variable 2
Mean	6,317	6,044
Variance	3,038	2,491
Observations	5	5
Hypothesized Mean Difference	0	
df	8	
t Stat	0,259	
P(T<=t) one-tail	0,400	
t Critical one-tail	1,859	
P(T<=t) two-tail	0,801	
t Critical two-tail	2,306	

Table B-1. 9: Experimental conditions run 5

Dosage (g)	0.1
pH	6
Temp ©	37.5
Volume (l)	0.5
IC (mg/l)	15

Table B-1. 10: Kinetic data run 5

Time (min)	0	10	20	30	60	120
Concentration run 5.1(mg/l)	15	5.328	4.995	3.95	3.596	3.275
Adsorption capacity run 5.1 (mg/g)	0	48.36	50.02	55.25	57.02	58.62
Concentration run 5.2 (mg/l)	15	7.059	5.396	4.229	3.6297	3.175
Adsorption capacity run 5.2 (mg/g)	0	39.70	48.02	53.85	56.85	59.12
Average Concentration (mg/l)	15	6.193	5.195	4.089	3.612	3.225
Average Adsorption Capacity (mg/g)	0	44.03	49.02	54.55	56.93	58.87

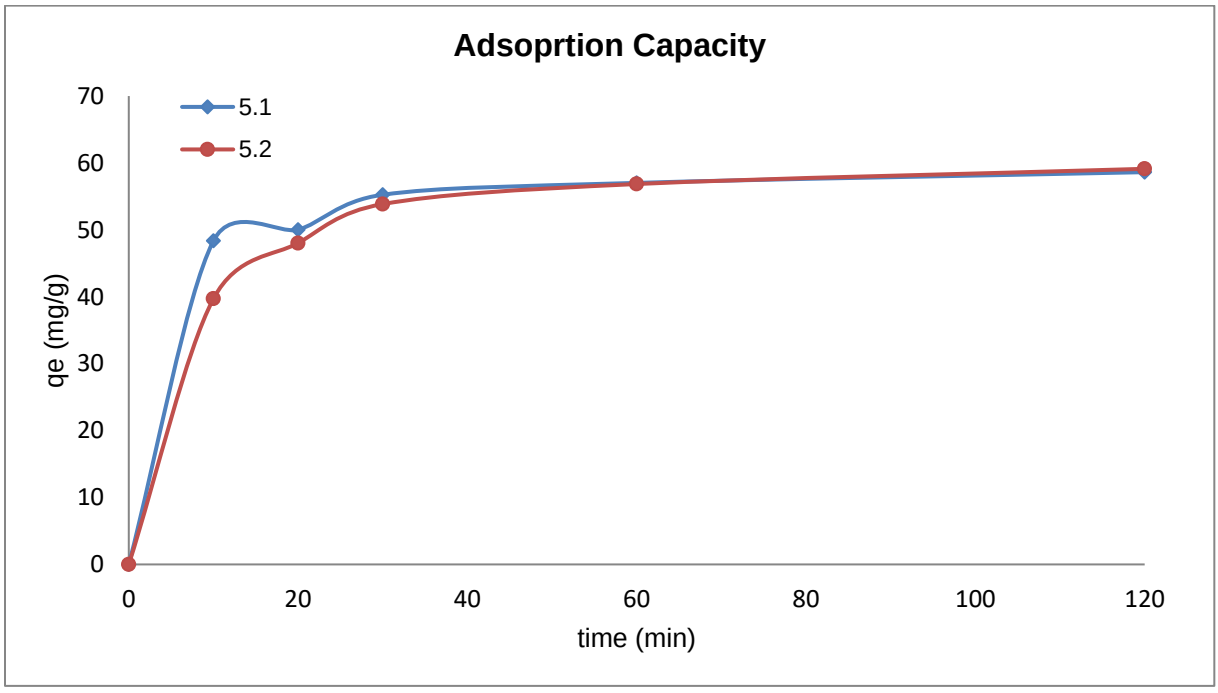

Figure B-1. 5: Adsorption capacity run 5

Data analysis report on the two ranges of kinetic data

Data analysis using Microsoft Excel was performed to assess the significance of data of an experimental run and the 'duplicate run' has a significant difference or not.

F-test two sample variance

	Variable 1	Variable 2
Mean	4.228	4.697
Variance	0.795801	2.435
Observations	5	5
df	4	4
F	0.326	
P(F<=f) one-tail	0.152	
F Critical one-tail	0.156	

t-test two sample assuming unequal variance

	Variable 1	Variable 2
Mean	4.228	4.697
Variance	0.795	2.435
Observations	5	5
Hypothesized Mean Difference	0	
df	6	
t Stat	-0.583	
P(T<=t) one-tail	0.290	
t Critical one-tail	1.943	
P(T<=t) two-tail	0.580	
t Critical two-tail	2.446	

Experiment 6

Table B-1. 11: Experimental conditions run 6

Dosage (g)	0.05
pH	2
Temp ©	37.5
Volume (l)	0.5
IC (mg/l)	15

Table B-1. 12: Kinetic data run 6

Time (min)	0	10	20	30	60	120
Concentration run 6.1(mg/l)	15	8.524	8.15	7.25	6.5	6.049
Adsorption capacity run 6.1 (mg/g)	0	64.75	68.5	77.5	85	89.51
Concentration run 6.2 (mg/l)	15	9.024	7.026	7.25	6.46	6.025
Adsorption capacity run 6.2 (mg/g)	0	59.76	79.74	77.5	85.4	89.75
Average Concentration (mg/l)	15	8.774	7.588	7.25	6.48	6.037
Average Adsorption Capacity (mg/g)	0	62.25	74.12	77.5	85.2	89.63

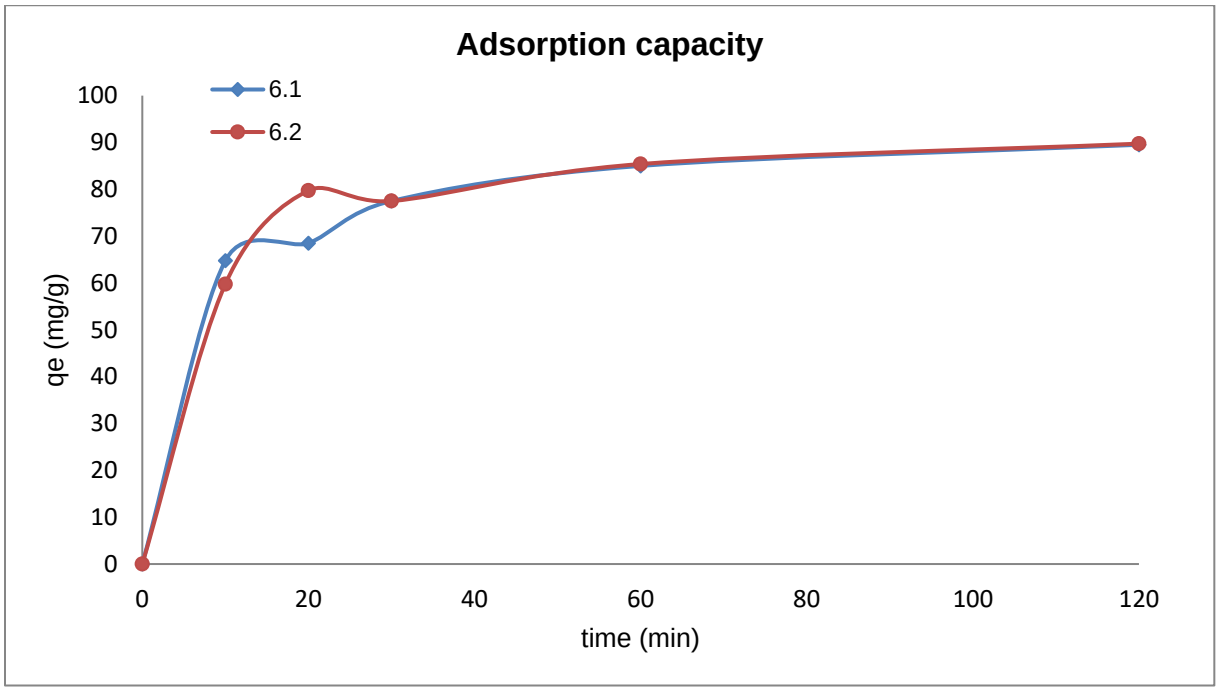

Figure B-1. 6: Adsorption capacity run 6

Data analysis report on the two ranges of kinetic data

Data analysis using Microsoft Excel was performed to assess the significance of data of an experimental run and the 'duplicate run' has a significant difference or not.

F-test two-sample for variances

	Variable 1	Variable 2
Mean	7.294	7.157
Variance	1.107	1.319
Observations	5	5
df	4	4
F	0.839	
P(F<=f) one-tail	0.434	
F Critical one-tail	0.156	

t-test two sample assuming unequal variance

	Variable 1	Variable 2
Mean	7.294	7.157
Variance	1.107	1.319
Observations	5	5
Hypothesized Mean Difference	0	
df	8	
t Stat	0.197	
P(T<=t) one-tail	0.424	
t Critical one-tail	1.859	
P(T<=t) two-tail	0.848	
t Critical two-tail	2.306	

Experiment 7

Table B-1. 13: Experimental conditions run 7

Dosage (g)	0.15
pH	10
Temp ©	37.5
Volume (l)	0.5
IC (mg/l)	15

Table B-1. 14: Kinetic data run 7

Time (min)	0	10	20	30	60	120
Concentration run 7.1(mg/l)	15	3.4	3.28	3.16	2.26	2.1
Adsorption capacity run 7.1 (mg/g)	0	38.66	39.06	39.46	42.46	43
Concentration run 7.2 (mg/l)	15	2.84	2.6	2.36	1.24	1.1
Adsorption capacity run 7.2 (mg/g)	0	40.53	41.33	42.13	45.86	46.33
Average Concentration (mg/l)	15	3.12	2.94	2.76	1.75	1.6
Average Adsorption Capacity (mg/g)	0	39.6	40.2	40.8	44.17	44.67

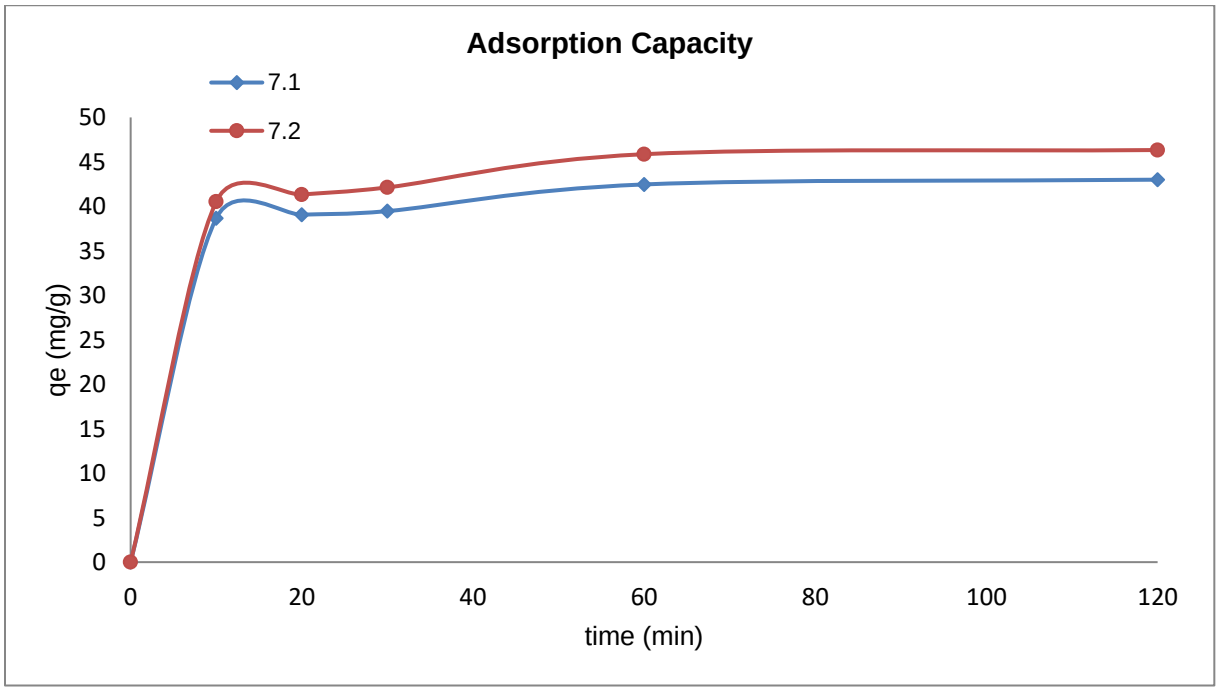

Figure B-1. 7: Adsorption capacity run 7

Data analysis report on the two ranges of kinetic data

Data analysis using Microsoft Excel was performed to assess the significance of data of an experimental run and the 'duplicate run' has a significant difference or not.

F-test two-sample for variances

	Variable 1	Variable 2
Mean	2.84	2.028
Variance	0.373	0.644
Observations	5	5
df	4	4
F	0.579	
P(F<=f) one-tail	0.304	
F Critical one-tail	0.156	

t-test two sample assuming unequal variance

	Variable 1	Variable 2
Mean	2.84	2.028
Variance	0.373	0.644
Observations	5	5
Hypothesized Mean Difference	0	
df	7	
t Stat	1.799	
P(T<=t) one-tail	0.057	
t Critical one-tail	1.894	
P(T<=t) two-tail	0.114	
t Critical two-tail	2.364	

Experiment 8

Table B-1. 15: Experimental conditions run 8

Dosage (g)	0.1
pH	10
Temp ©	50
Volume (l)	0.5
IC (mg/l)	15

Table B-1. 16: Kinetic data run 8

Time (min)	0	10	20	30	60	120
Concentration run 8.1(mg/l)	15	5.46	4.4	3.18	3.12	2.5
Adsorption capacity run 8.1 (mg/g)	0	47.7	53	59.1	59.4	62.5
Concentration run 8.2 (mg/l)		5.06	4.14	3.74	2.84	2.72
Adsorption capacity run 8.2 (mg/g)		49.7	54.3	56.3	60.8	61.4
Average Concentration (mg/l)		5.26	4.27	3.46	2.98	2.61
Average Adsorption Capacity (mg/g)	0	48.7	53.65	57.7	60.1	61.95

‘

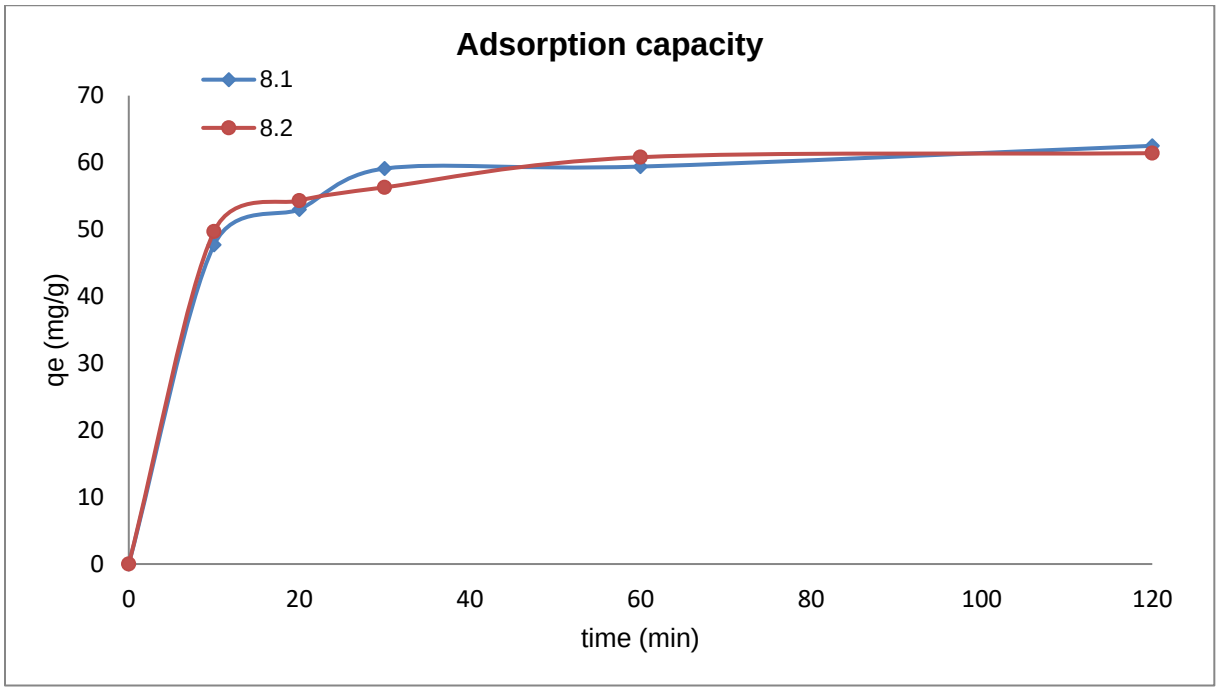

Figure B-1. 8: Adsorption capacity run 8

Data analysis report on the two ranges of kinetic data

Data analysis using Microsoft Excel was performed to assess the significance of data of an experimental run and the 'duplicate run' has a significant difference or not.

F-test two-sample for variances

	Variable 1	Variable 2
Mean	3.732	3.7
Variance	1.407	0.936
Observations	5	5
df	4	4
F	1.503	
P(F<=f) one-tail	0.351	
F Critical one-tail	6.388	

t-test two sample assuming unequal variance

	Variable 1	Variable 2
Mean	3.732	3.7
Variance	1.407	0.936
Observations	5	5
Hypothesized Mean Difference	0	
df	8	
t Stat	0.046	
P(T<=t) one-tail	0.481	
t Critical one-tail	1.859	
P(T<=t) two-tail	0.963	
t Critical two-tail	2.306	

Experiment 9

Table B-1. 17: Experimental conditions run 9

Dosage (g)	0.15
pH	6
Temp ©	50
Volume (l)	0.5
IC (mg/l)	15

Table B-1. 18: Kinetic data run 9

Time (min)	0	10	20	30	60	120
Concentration run 9.1(mg/l)	15	1.183	0.787	0.733	0.69	0.28
Adsorption capacity run 9.1 (mg/g)	0	46.05	47.37	47.567	47.7	49.06
Concentration run 9.2 (mg/l)	15	1.278	1.24	0.89	0.73	0.39
Adsorption capacity run 9.2 (mg/g)	0	45.74	45.86	47.03	47.56	48.7
Average Concentration (mg/l)		1.231	1.014	0.812	0.71	0.335
Average Adsorption Capacity (mg/g)	0	45.89	46.62	47.29	47.63	48.88

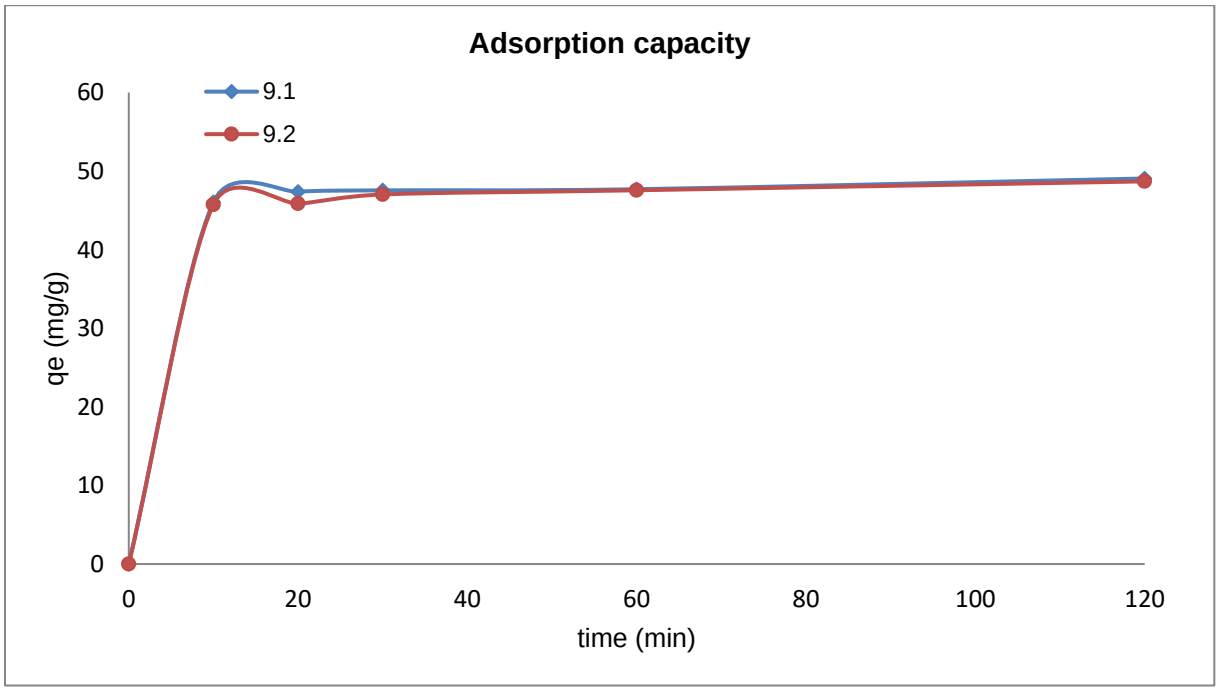

Figure B-1. 9: Adsorption capacity run 9

Data analysis report on the two ranges of kinetic data

Data analysis using Microsoft Excel was performed to assess the significance of data of an experimental run and the 'duplicate run' has a significant difference or not.

F-test two-sample for variances

	Variable 1	Variable 2
Mean	0.734	0.905
Variance	0.103	0.136
Observations	5	5
df	4	4
F	0.754	
P(F<=f) one-tail	0.395	
F Critical one-tail	0.156	

t-test two sample assuming unequal variance

	Variable 1	Variable 2
Mean	0.734	0.905
Variance	0.103	0.136
Observations	5	5
Hypothesized Mean Difference	0	
df	8	
t Stat	-0.779	
P(T<=t) one-tail	0.229	
t Critical one-tail	1.859	
P(T<=t) two-tail	0.458	
t Critical two-tail	2.306	

Experiment 10

Table B-1. 19: Experimental conditions run 10

Dosage (g)	0.05
pH	6
Temp ©	50
Volume (l)	0.5
IC (mg/l)	15

Table B-1. 20: Kinetic data run 10

Time (min)	0	10	20	30	60	120
Concentration run 10.1(mg/l)	15	10.85	10.1	8.8	8.5	8.23
Adsorption capacity run 10.1 (mg/g)	0	41.5	49	62	65	67.75
Concentration run 10.2 (mg/l)	15	10.6	9.85	8.5	8.3	5.25
Adsorption capacity run 10.2 (mg/g)	0	44	51.5	65	67	97.5
Average Concentration (mg/l)	15	10.73	9.975	8.65	8.4	6.737
Average Adsorption Capacity (mg/g)	0	42.75	50.25	63.5	66	82.63

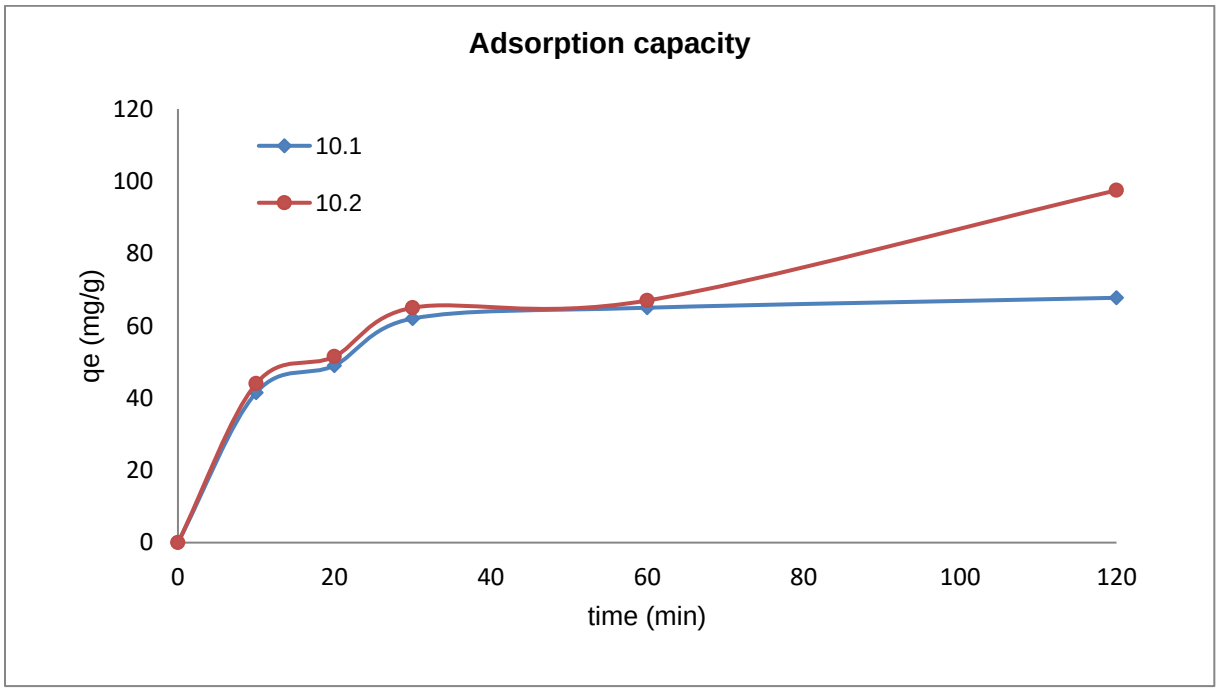

Figure B-1. 10: Adsorption capacity run 10

Data analysis report on the two ranges of kinetic data

Data analysis using Microsoft Excel was performed to assess the significance of data of an experimental run and the 'duplicate run' has a significant difference or not.

F-test two-sample for variances

	Variable 1	Variable 2
Mean	9.295	8.5
Variance	1.272	4.208
Observations	5	5
df	4	4
F	0.302	
P(F<=f) one-tail	0.136	
F Critical one-tail	0.156	

t-test two sample assuming unequal variance

	Variable 1	Variable 2
Mean	9.295	8.5
Variance	1.272	4.208
Observations	5	5
Hypothesized Mean Difference	0	
df	6	
t Stat	0.759	
P(T<=t) one-tail	0.238	
t Critical one-tail	1.943	
P(T<=t) two-tail	0.476	
t Critical two-tail	2.446	

Experiment 11

Table B-1. 21: Experimental conditions run 11

Dosage (g)	0.15
pH	2
Temp ©	37.5
Volume (l)	0.5
IC (mg/l)	15

Table B-1. 22: Kinetic data run 11

Time (min)	0	10	20	30	60	120
Concentration run 11.1(mg/l)	15	3.5	2.6	1.46	0.76	0.01
Adsorption capacity run 11.1 (mg/g)	0	38.33	41.33	45.13	47.466	49.967
Concentration run 11.2 (mg/l)	15	3.5	2.8	1.82	0.98	0.36
Adsorption capacity run 11.2 (mg/g)	0	38.33	40.67	43.93	46.73	48.8
Average Concentration (mg/l)	15	3.5	2.7	1.64	0.87	0.185
Average Adsorption Capacity (mg/g)	0	38.33	41	44.53	47.1	49.38

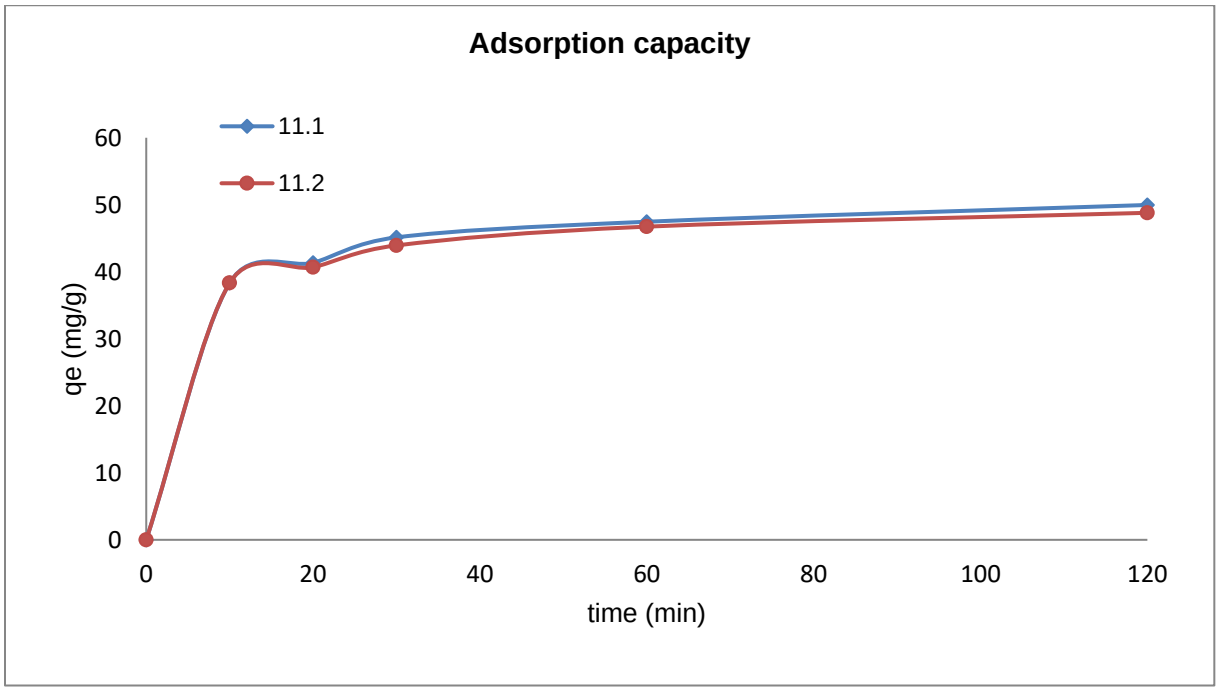

Figure B-1. 11: Adsorption capacity run 11

Data analysis report on the two ranges of kinetic data

Data analysis using Microsoft Excel was performed to assess the significance of data of an experimental run and the 'duplicate run' has a significant difference or not.

F-test two-sample for variances

	Variable 1	Variable 2
Mean	1.666	1.892
Variance	1.960	1.648
Observations	5	5
df	4	4
F	1.189	
P(F<=f) one-tail	0.435	
F Critical one-tail	6.388	

t-test two sample assuming unequal variance

	Variable 1	Variable 2
Mean	1.666	1.892
Variance	1.960	1.648
Observations	5	5
Hypothesized Mean Difference	0	
df	8	
t Stat	-0.266	
P(T<=t) one-tail	0.398	
t Critical one-tail	1.859	
P(T<=t) two-tail	0.796	
t Critical two-tail	2.306	

Experiment 12

Table B-1. 23: Experimental conditions run 12

Dosage (g)	0.1
pH	2
Temp ©	50
Volume (l)	0.5
IC (mg/l)	15

Table B-1. 24: Kinetic data run 12

Time (min)	0	10	20	30	60	120
Concentration run 12.1(mg/l)	15	1.96	1.66	1.62	1.45	1.45
Adsorption capacity run 12.1 (mg/g)	0	65.2	66.7	66.9	67.75	67.75
Concentration run 12.2 (mg/l)	15	2.44	1.74	1.45	1.42	1.375
Adsorption capacity run 12.2 (mg/g)	0	62.8	66.3	67.75	67.9	68.12
Average Concentration (mg/l)	15	2.2	1.7	1.535	1.435	1.41
Average Adsorption Capacity (mg/g)	0	64	66.5	67.32	67.82	67.93

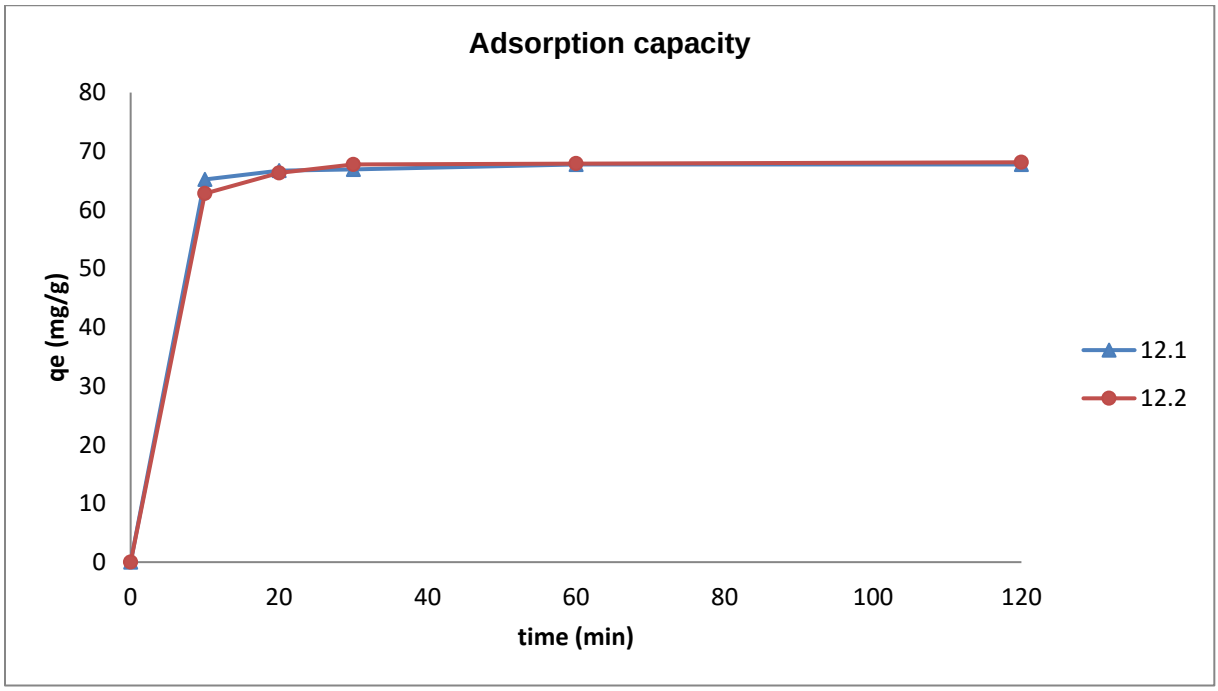

Figure B-1. 12: Adsorption capacity run 12

Data analysis report on the two ranges of kinetic data

Data analysis using Microsoft Excel was performed to assess the significance of data of an experimental run and the 'duplicate run' has a significant difference or not.

F-test two-sample for variances

	Variable 1	Variable 2
Mean	1.628	1.685
Variance	0.043	0.198
Observations	5	5
df	4	4
F	0.219	
P(F<=f) one-tail	0.085	
F Critical one-tail	0.156	

t-test two sample assuming unequal variance

	Variable 1	Variable 2
Mean	1.628	1.685
Variance	0.043	0.198
Observations	5	5
Hypothesized Mean Difference	0	
df	6	
t Stat	-0.258	
P(T<=t) one-tail	0.402	
t Critical one-tail	1.943	
P(T<=t) two-tail	0.804	
t Critical two-tail	2.446	

Experiment 13

Table B-1. 25: Experimental conditions run 13

Dosage (g)	0.05
pH	10
Temp ©	37.5
Volume (l)	0.5
IC (mg/l)	15

Table B-1. 26: Kinetic data run 13

Time (min)	0	10	20	30	60	120
Concentration run 12.1(mg/l)	15	8.175	7.525	7.425	6.525	6.325
Adsorption capacity run 12.1 (mg/g)	0	68.25	74.75	75.75	84.75	86.75
Concentration run 12.2 (mg/l)	15	8.625	8.525	8	7.765	7.19
Adsorption capacity run 12.2 (mg/g)	0	63.75	64.75	70	72.35	78.1
Average Concentration (mg/l)	15	8.4	8.025	7.712	7.145	6.75
Average Adsorption Capacity (mg/g)	0	66	69.75	72.87	78.55	82.42

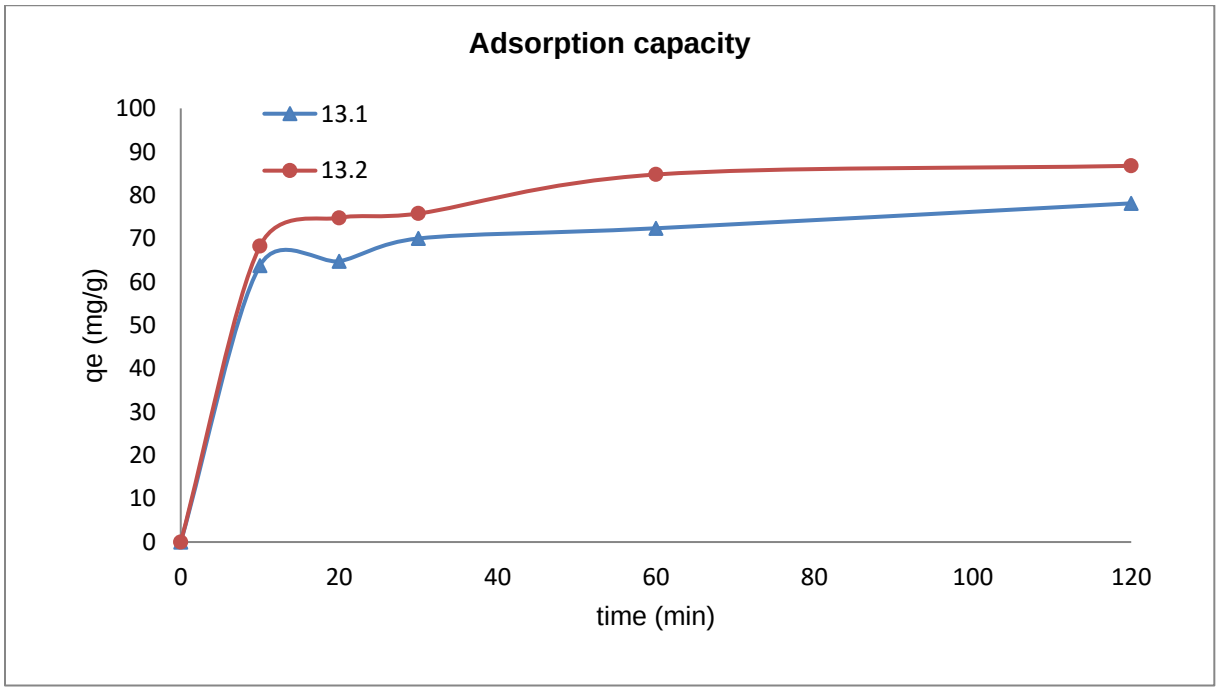

Figure B-1. 13: Adsorption capacity run 13

Data analysis report on the two ranges of kinetic data

Data analysis using Microsoft Excel was performed to assess the significance of data of an experimental run and the 'duplicate run' has a significant difference or not.

F-test two-sample for variances

	Variable1	Variable2
Mean	7.195	8.021
Variance	0.582	0.343
Observations	5	5
df	4	4
F	1.692	
P(F<=f) one-tail	0.311	
F Critical one-tail	6.388	

t-test two sample assuming unequal variance

	Variable 1	Variable 2
Mean	7.195	8.021
Variance	0.582	0.343
Observations	5	5
Hypothesized Mean Difference	0	
df	8	
t Stat	-1.919	
P(T<=t) one-tail	0.045	
t Critical one-tail	1.859	
P(T<=t) two-tail	0.091	
t Critical two-tail	2.306	

Experiment 27

Table B-1. 27: Experimental conditions run 27

Dosage (g)	0.1
pH	6
Temp ©	25
Volume (l)	0.5
IC (mg/l)	15

Table B-1. 28: Kinetic data run 27

Time (min)	0	10	20	30	60	120
Concentration run 27.1(mg/l)	15	8.385	7.125	6.435	5.81	5.25
Adsorption capacity run 27.1 (mg/g)	0	33.07	39.375	42.83	45.95	48.75
Concentration run 27.2 (mg/l)	15	7.85	6.15	4.83	4.51	4.25
Adsorption capacity run 27.2 (mg/g)	0	35.75	44.25	50.85	52.45	53.75
Average Concentration (mg/l)	15	8.12	6.63	5.63	5.16	4.75
Average Adsorption Capacity (mg/g)	0	34.41	41.81	46.83	49.2	51.25

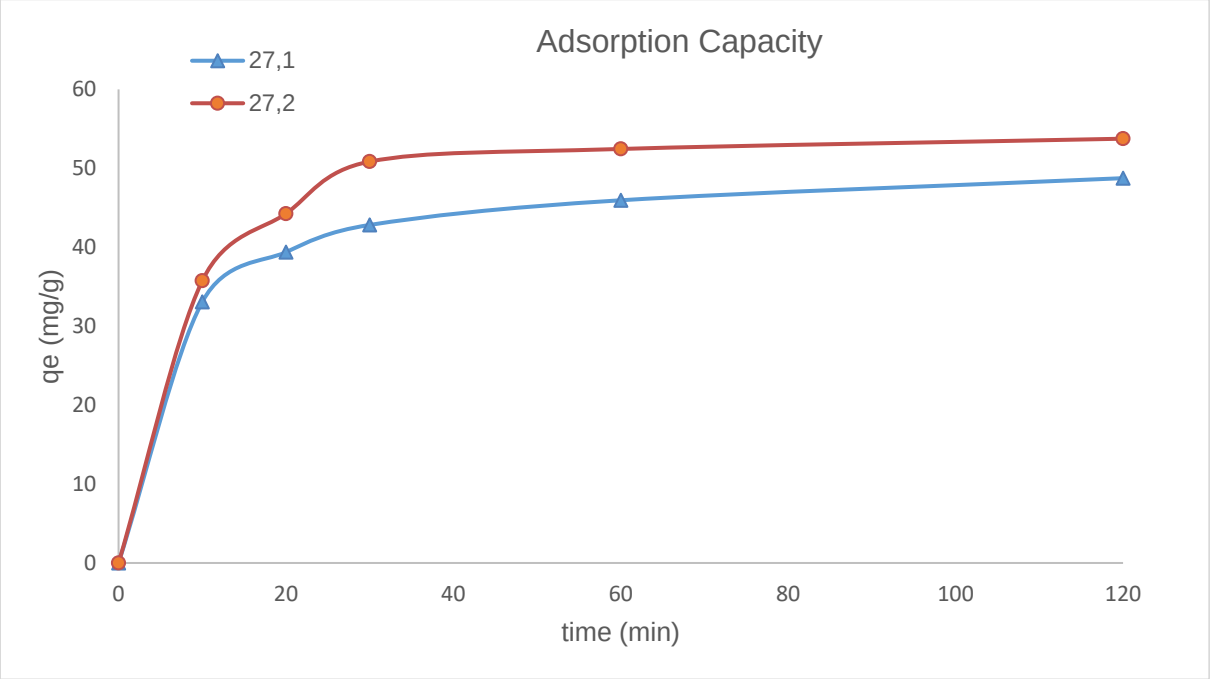

Figure B-1. 14: Adsorption capacity run 27

Data analysis report on the two ranges of kinetic data

Data analysis using Microsoft Excel was performed to assess the significance of data of an experimental run and the 'duplicate run' has a significant difference or not.

F-test two-sample for variances

	Variable 1	Variable 2
Mean	6.601	5.518
Variance	1.483	2.233
Observations	5	5
df	4	4
F	0.664	
P(F<=f) one-tail	0.350	
F Critical one-tail	0.156	

t-test two sample assuming unequal variance

	Variable 1	Variable 2
Mean	6.601	5.518
Variance	1.483	2.233
Observations	5	5
Hypothesized Mean Difference	0	
df	8	
t Stat	1.255	
P(T<=t) one-tail	0.122	
t Critical one-tail	1.859	
P(T<=t) two-tail	0.244	
t Critical two-tail	2.306	

Experiment 28

Table B-1. 29: Experimental conditions run 28

Dosage (g)	0.1
pH	6
Temp ©	50
Volume (l)	0.5
IC (mg/l)	15

Table B-1. 30: Kinetic data run 28

Time (min)	0	10	20	30	60	120
Concentration run 28.1(mg/l)	15	5.68	3.218	2.95	2.7	2.65
Adsorption capacity run 28.1 (mg/g)	0	46.57	58.91	60.25	61.5	61.75
Concentration run 28.2 (mg/l)	15	5.315	4.128	3.6	2.5	1.48
Adsorption capacity run 28.2 (mg/g)	0	48.42	54.36	57	62.5	67.6
Average Concentration (mg/l)	15	5.5	3.673	3.275	2.6	2.065
Average Adsorption Capacity (mg/g)	0	47.5	56.63	58.62	62	64.67

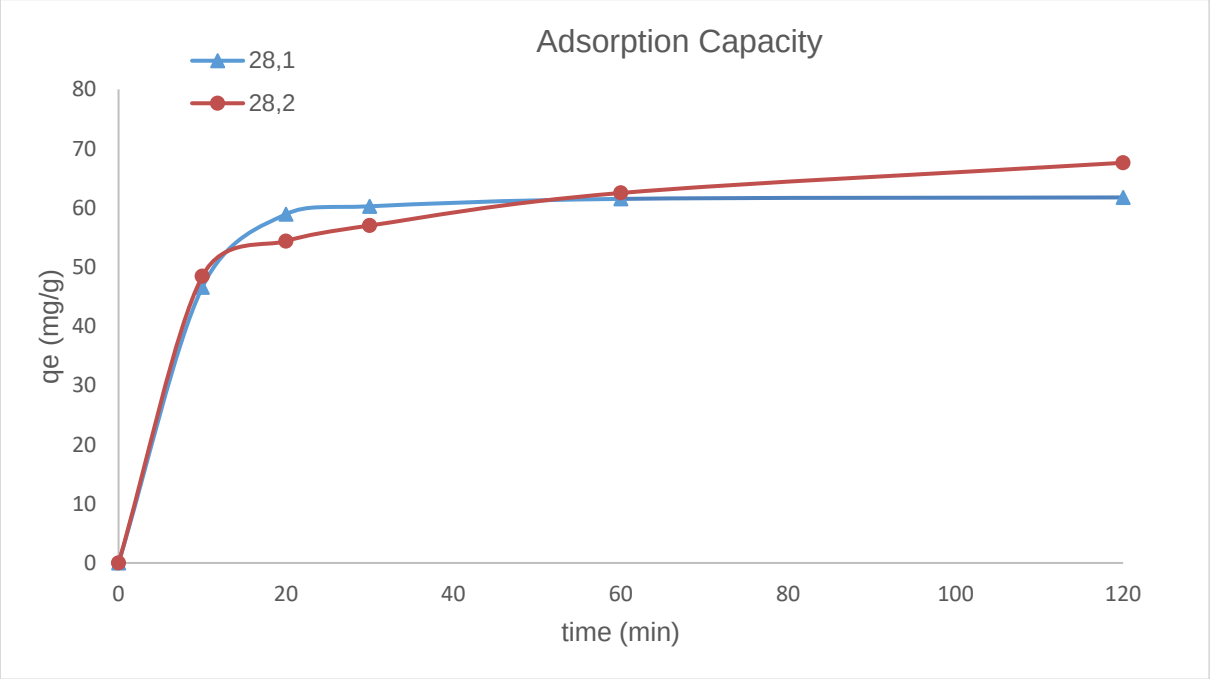

Figure B-1. 15: Adsorption capacity run 28

Data analysis report on the two ranges of kinetic data

Data analysis using Microsoft Excel was performed to assess the significance of data of an experimental run and the 'duplicate run' has a significant difference or not.

F-test two-sample for variances

	Variable 1	Variable 2
Mean	3.440	3.404
Variance	1.625	2.183
Observations	5	5
df	4	4
F	0.744	
P(F<=f) one-tail	0.390	
F Critical one-tail	0.156	

t-test two sample assuming unequal variance

	Variable 1	Variable 2
Mean	3.440	3.404
Variance	1.625	2.183
Observations	5	5
Hypothesized Mean Difference	0	
df	8	
t Stat	0.041	
P(T<=t) one-tail	0.484	
t Critical one-tail	1.859	
P(T<=t) two-tail	0.968	
t Critical two-tail	2.306	

Experiment 29

Table B-1. 31: Experimental conditions run 29

Dosage (g)	0.1
pH	6
Temp ©	25
Volume (l)	0.5
IC (mg/l)	15

Table B-1. 32: Kinetic data run 29

Time (min)	0	10	20	30	60	120
Concentration run 29.1(mg/l)	15	9.915	9.12	8.7	8.65	8.5
Adsorption capacity run 29.1 (mg/g)	0	50.85	58.8	63	63.5	65
Concentration run 29.2 (mg/l)	15	9.05	8.75	8.12	7.95	7.85
Adsorption capacity run 29.2 (mg/g)	0	59.5	62.5	68.8	70.5	71.5
Average Concentration (mg/l)	15	9.482	8.935	8.41	8.3	8.175
Average Adsorption Capacity (mg/g)	0	55.17	60.65	65.9	67	68.25

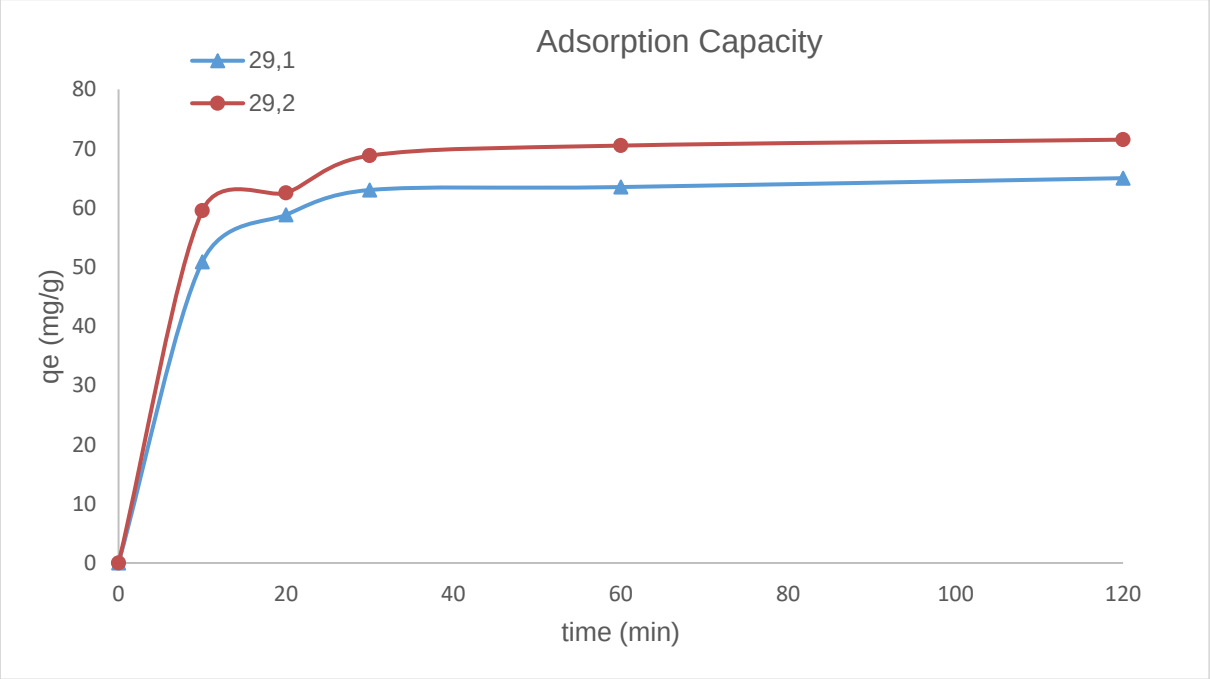

Figure B-1. 16: Adsorption capacity run 29

Data analysis report on the two ranges of kinetic data

Data analysis using Microsoft Excel was performed to assess the significance of data of an experimental run and the 'duplicate run' has a significant difference or not.

F-test two-sample for variances

	Variable 1	Variable 2
Mean	8.977	8.344
Variance	0.327	0.278
Observations	5	5
df	4	4
F	1.178	
P(F<=f) one-tail	0.438	
F Critical one-tail	6.388	

t-test two sample assuming unequal variance

	Variable 1	Variable 2
Mean	8.977	8.344
Variance	0.327	0.278
Observations	5	5
Hypothesized Mean Difference	0	
df	8	
t Stat	1.818	
P(T<=t) one-tail	0.053	
t Critical one-tail	1.859	
P(T<=t) two-tail	0.106	
t Critical two-tail	2.306	

Experiment 30

Table B-1. 33: Experimental conditions run 30

Dosage (g)	0.1
pH	6
Temp ©	25
Volume (l)	0.5
IC (mg/l)	15

Table B-1. 34: Kinetic data run 30

Time (min)	0	10	20	30	60	120
Concentration run 30.1(mg/l)	15	2.856	1.86	1.41	1.12	1.01
Adsorption capacity run 30.1 (mg/g)	0	40.48	43.8	45.3	46.26	46.63
Concentration run 30.2 (mg/l)	15	2.593	1.71	1.35	0.98	0.855
Adsorption capacity run 30.2 (mg/g)	0	41.35	44.3	45.5	46.73	47.15
Average Concentration (mg/l)	15	2.7245	1.785	1.38	1.05	0.93
Average Adsorption Capacity (mg/g)	0	40.91	44.05	45.4	46.5	46.89

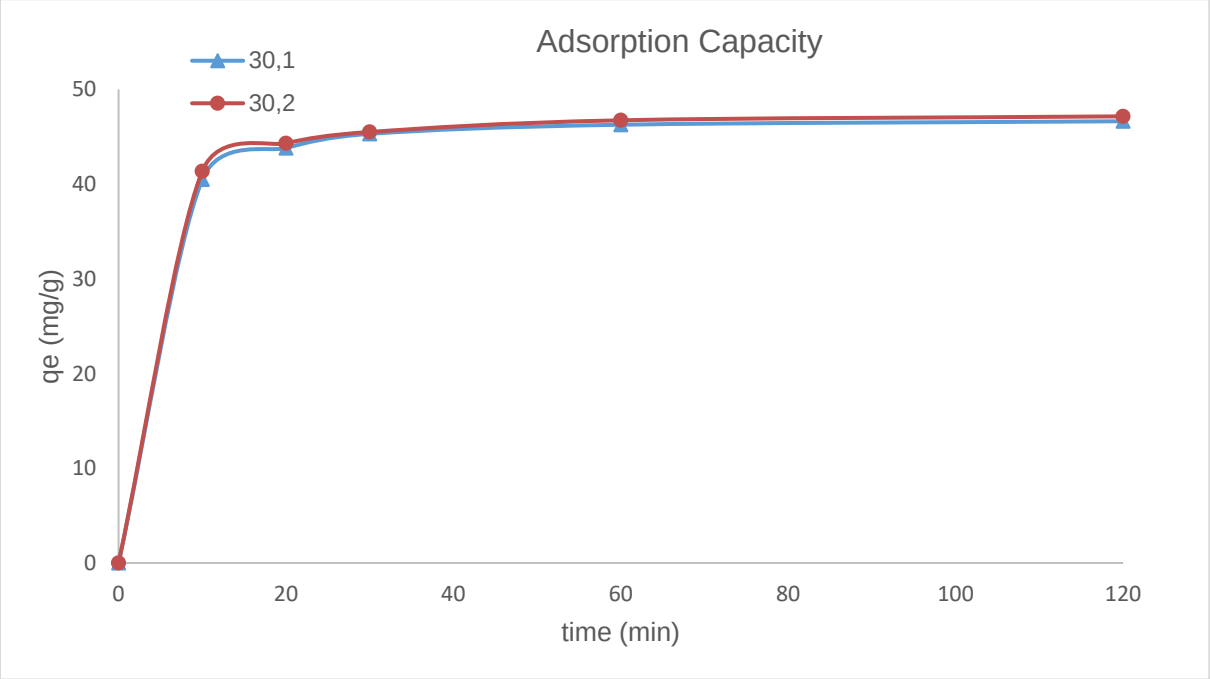

Figure B-1. 17: Adsorption capacity run 30

Data analysis report on the two ranges of kinetic data

Data analysis using Microsoft Excel was performed to assess the significance of data of an experimental run and the 'duplicate run' has a significant difference or not.

F-test two-sample for variances

	Variable 1	Variable 2
Mean	1.651	1.497
Variance	0.561	0.486
Observations	5	5
df	4	4
F	1.153	
P(F<=f) one-tail	0.446	
F Critical one-tail	6.388	

t-test two sample assuming unequal variance

	Variable 1	Variable 2
Mean	1.651	1.497
Variance	0.561	0.486
Observations	5	5
Hypothesized Mean Difference	0	
df	8	
t Stat	0.335	
P(T<=t) one-tail	0.372	
t Critical one-tail	1.859	
P(T<=t) two-tail	0.745	
t Critical two-tail	2.306	

Appendix: C Adsorption COD and Turbidity data

COD Data

Table C- 1: COD adsorption data

Run	pH	dosage (mg/l)	Temperature (^{0}C)	Run	%Removal	Duplicate	%Removal
1	6	300	25	80	90	85	66
2	6	100	25	180	170	175	30
3	2	200	25	60	75	67.5	73
4	10	200	25	135	85	110	56
5	6	200	37.5	130	150	140	44
6	2	100	37.5	125	130	127.5	49
7	10	300	37.5	40	20	30	88
8	10	200	50	50	90	70	72
9	6	300	50	20	10	15	94
10	6	100	50	140	120	130	48
11	2	300	37.5	80	25	52.5	79
12	2	200	50	60	65	62.5	75
13	10	100	37.5	125	120	122.5	51

Average COD Removal

Table C- 2: Average COD removal

Average COD Removal (mg/l)	% Removal
85	66
175	30
67.5	73
110	56
140	44
127.5	49
30	88
70	72
15	94
130	48
52.5	79
62.5	75
122.5	51

Turbidity Data

Table C- 3: Turbidity data

	Run	Duplicate
1	2.37	2.03
2	1.94	1.46
3	0.75	1.24
4	1.6	2.52
5	1.9	2.84
6	1.27	0.87
7	1.14	1.5
8	2.56	1.53
9	1.44	0.61
10	2.64	0.67
11	0.42	1.31
12	0.58	0.99
13	1.60	1.76

Appendix D: Chemical coagulation COD, turbidity, FOG and surfactant data

Chemical coagulation data

Chemical coagulation data for the removal of COD, FOG, anionic surfactant and turbidity at 40, 80 and 120 mg/l PFS dosage, initial wastewater pH of 6 and stirring speed of 300 rpm for 1 minute and 100 rpm for 25 minutes.

Table D- 1: Chemical coagulation data at 40mg/l PFS dosage

40 mg/l				
Pollutant	cod	AS	fog	NTU
Run 1.1	290	29.25	0.5	14.6
Run 1.2	300	30.5	0.5	10.94
Average	295	29.88	0.5	12.77
% Removal	70.5	14.64	98.33	87.23

Table D- 2: Chemical coagulation data at 40mg/l PFS dosage

80mg/l				
Pollutant	cod	AS	fog	NTU
Run 1.1	250	29.5	0.5	5.3
Run 1.2	230	25.875	0.5	6.8
Average	240	27.6875	0.5	6.05
% Removal	76	20.89	98.33	93.95

Table D- 3: Chemical coagulation data at 40mg/l PFS dosage

120 mg/l				
Pollutant	cod	AS	fog	NTU
Run 1.1	190	18.13	1.25	0.61
Run 1.2	220	20.5	1	0.42
Average	205	19.32	1.125	0.515
% Removal	79.5	44.82	96.25	99.48

Appendix E: Sample Calculations

Pollutant removal percentage

% Surfactant removal was calculated

$$\%Surfactant\ removal = \frac{Inital - final}{inital} \times 100$$

$$\%Surfactant\ removal = \frac{15 - 2.8l}{15} \times 100$$

$$\%Surfactant\ removal = 81.33$$

Adsorption Capacity

The equilibrium adsorption capacity and the adsorption capacity at any time was calculated using equation:

$Qe = \frac{C_o - C_e}{m} \times v$

$Qe = \frac{15-2.9}{0.15} \times 0.5$

$Qe = 40.5\ mg/g$

Langmuir Isotherm

$$q_e = \frac{q_m K_L C_e}{1 + K_L C_e}$$

K_L and q_m were determined from the linearized form of equation 2.2 as shown below

$$\frac{C_e}{q_e} = \frac{1}{q_m} C_e + \frac{1}{K_L q_m}$$

Where the slope of the equation is $\frac{1}{q_m}$ and the intercept is $\frac{1}{q_m K_L}$

The equation of the linearized plot of the Langmuir isotherm was then used to calculate the variables

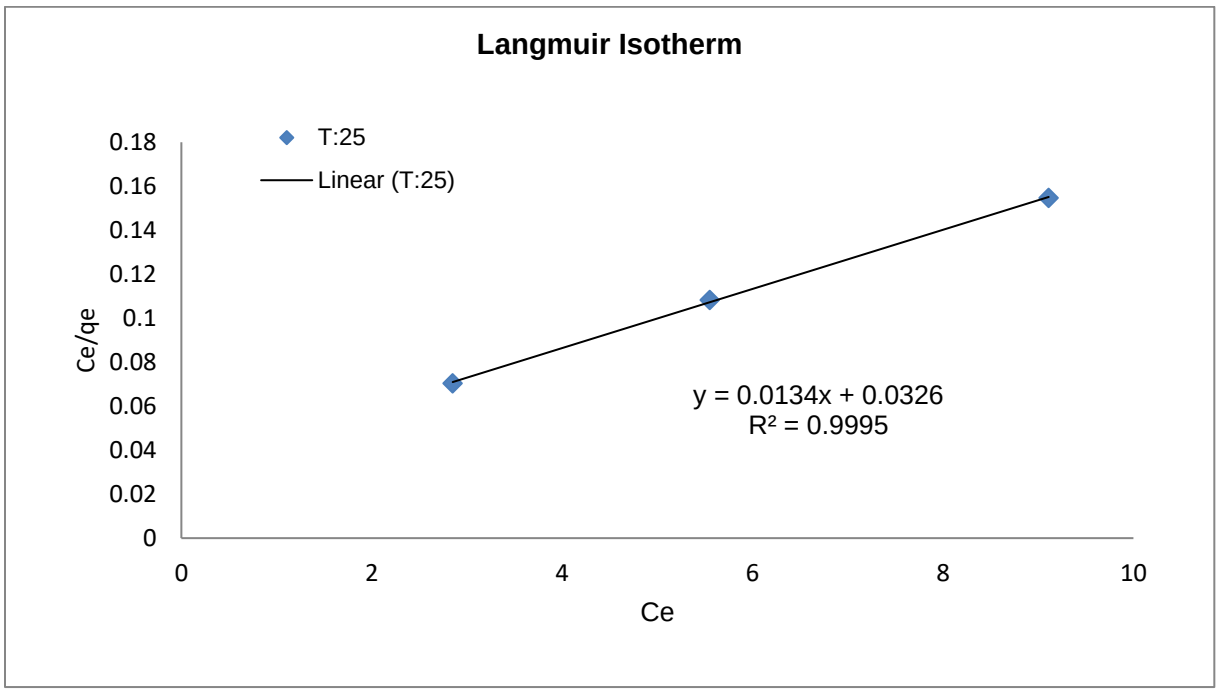

Y = 0.0134x + 0.0326

$$0.0134 = \frac{1}{q_m}$$

q_m = 74.63 mg/g

$$0.0326 = \frac{1}{q_m K_L}$$

K_L = 0.41 L/g

R_L was calculated using equation 2.4.

$$R_L = \frac{1}{1 + K_L C_o}$$

$$R_L = \frac{1}{1 + (0.41 \times 15)}$$

R_L = 0.1395

Freundlich Isotherm

Equation 2.2.9

$$q_e = K_f C^{\frac{1}{n}}$$

The linear form of the Freundlich isotherm, Equation 2.6, was used to plot log q_e versus C_e. This allowed for the determination of the constant K_f and exponent 1/n.

$$logq_e = logK_F + \frac{1}{n} logC_e$$

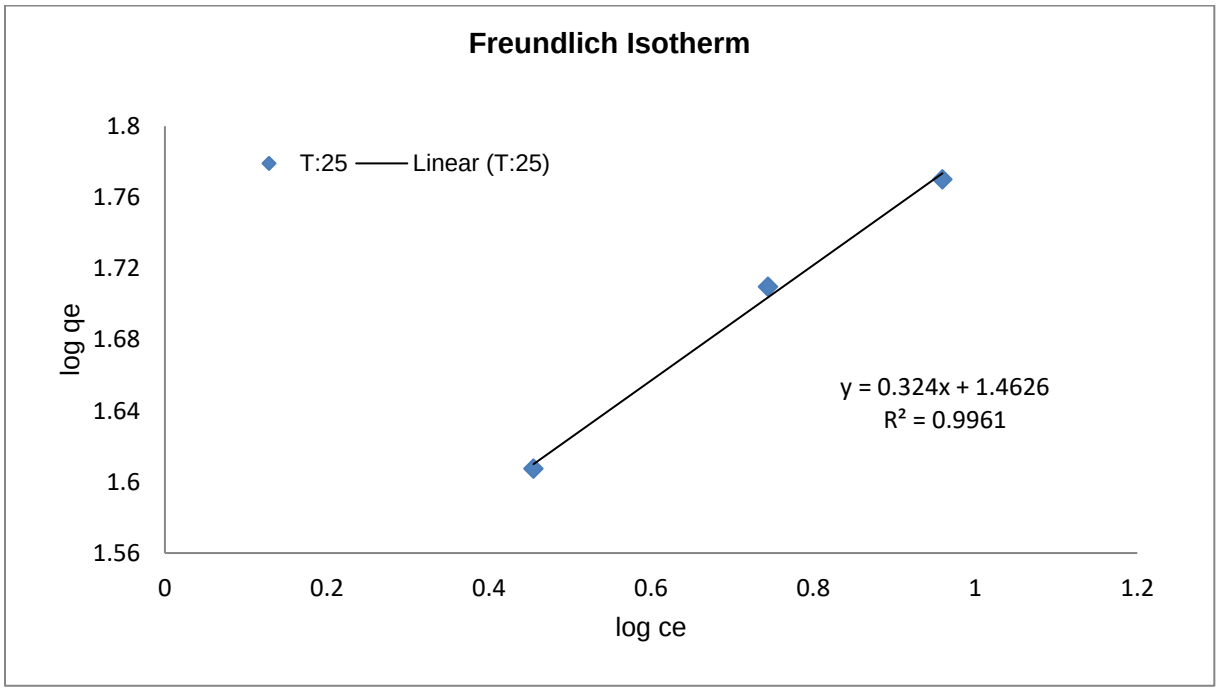

Y = 0.324x + 1.426

0.7562 = 1/n

n = 3.084

1.4626 = ln(K)

K = 4.16

Dubinin-Raduschkevich isotherm

Equation 2.7 was used to fit data to the Dubinin-Raduschkevich isotherm.

$$q_e = q_m exp k^2$$

The Polanyi potential (Ɛ) (J/mol) was calculated with Equation 2.8.

$$\varepsilon = RTln\left(1 + \frac{1}{C_e}\right)$$

The linear form of Equation 2.8 allows for the values of q_m and K to be deduced by plotting Ln(qe) versus Ɛ²

ln (q_e) = ln ($q_m K^2$)

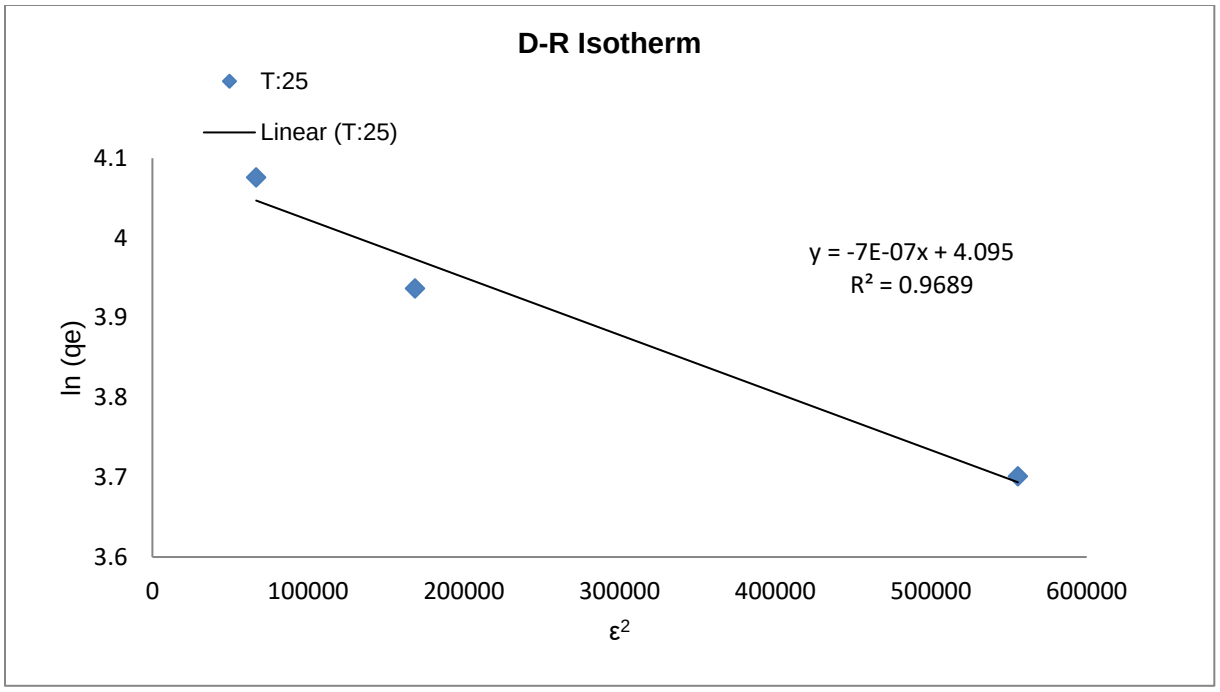

Y = $7x10^{-7}$ + 4.095

ln (q_m) = 4.095

q_m = 60.5

$7x10^{-7}$ = k

The mean energy of adsorption (E) can be calculated from Equation 2.10

$E = -2K^{-1/2}$

$$E = \frac{1}{\sqrt{7 \times 10^{-7}}}$$

E = 845.15 j/mol

Temkin Isotherm

Equation 2.7 was used to fit data to the Temkin isotherm.

$$q_e = \frac{Rt}{b} lnK_T + \frac{RT}{b} lnC_e$$

The linear form of Equation 2.8 allows for the values of k and b to be deduced by plotting ln(c_e) versus q_e

K = exp (15.851/23.955)

K = 4.53

b = 15.851

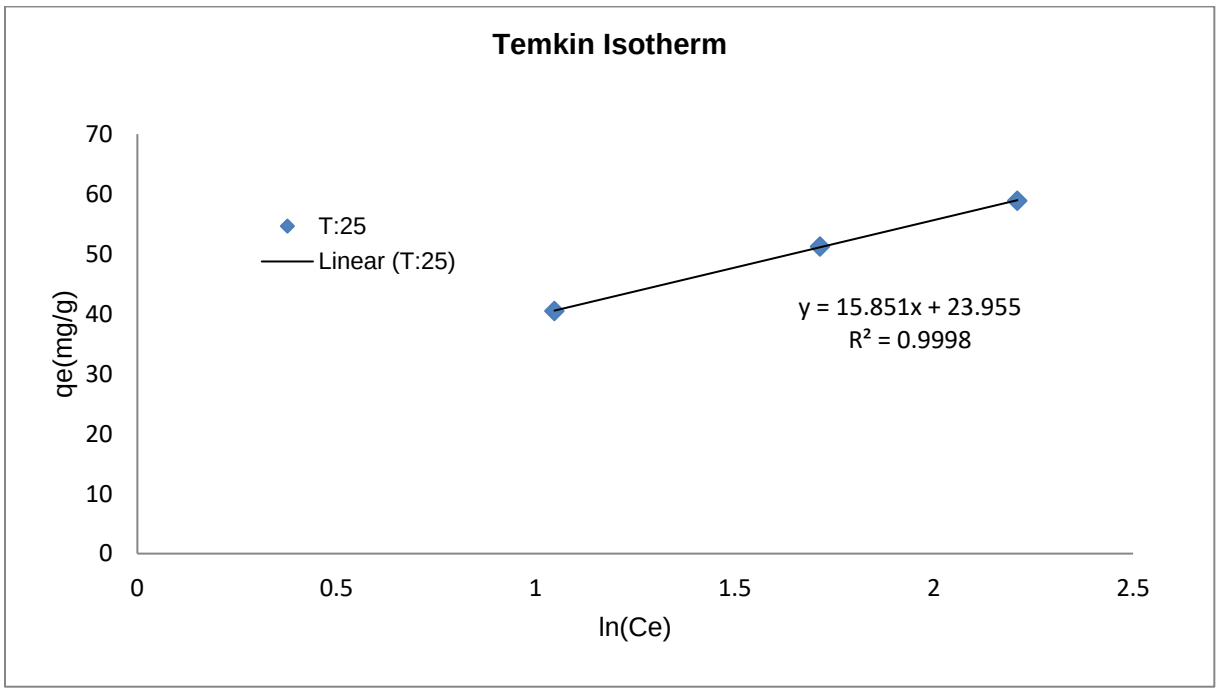

Pseudo-first order kinetics

The data was fitted to first order kinetics model using the following equation

$$log(q_e - q_t) = logq_e - k_1 t$$

The following equation was used to plot log(qe-qt) versus time. From slope and intercept, k_f and qe calculated was found

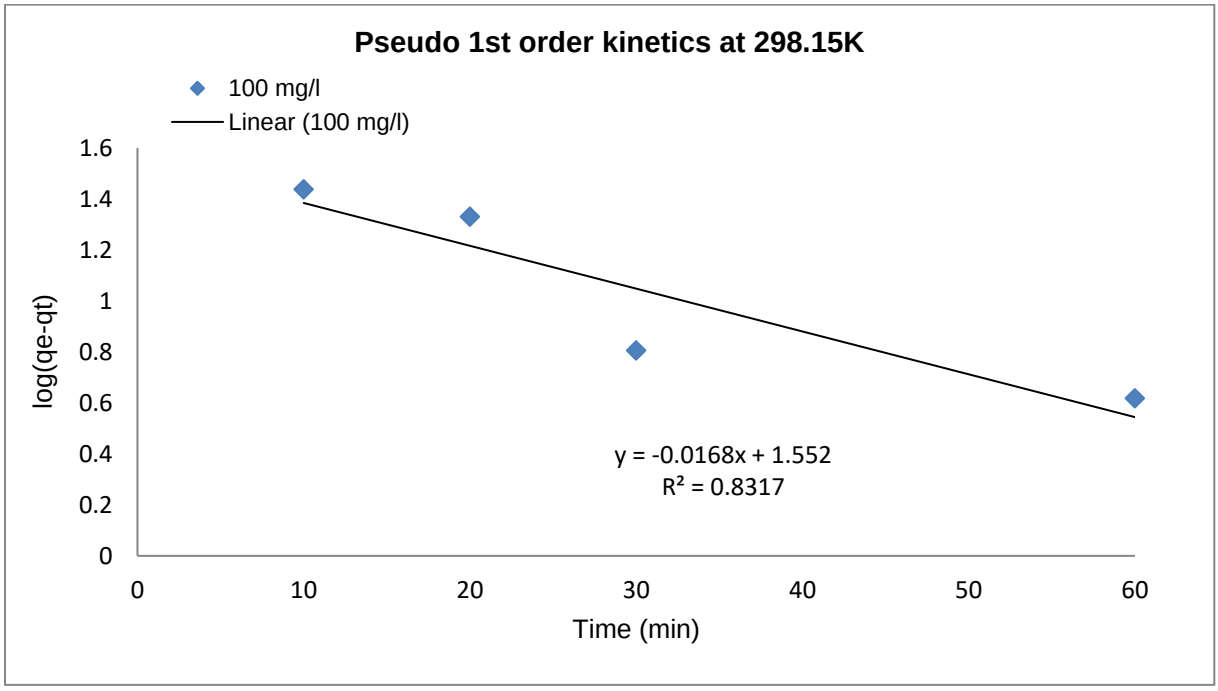

$q_e = 10^{1.552}$

q_e = 35.64 mg/g

K_f = 2.303 x 0.0168

K_f = 0.0386 min^{-1}

Pseudo-second order kinetics

The following equation was used to fit the data to second order kinetics:

$$\frac{t}{qt} = \frac{1}{K_2 q_e^2} + \frac{1}{q_e}$$

The following equation was used to plot t/qt versus time. From slope and intercept, k2 and qe calculated was found

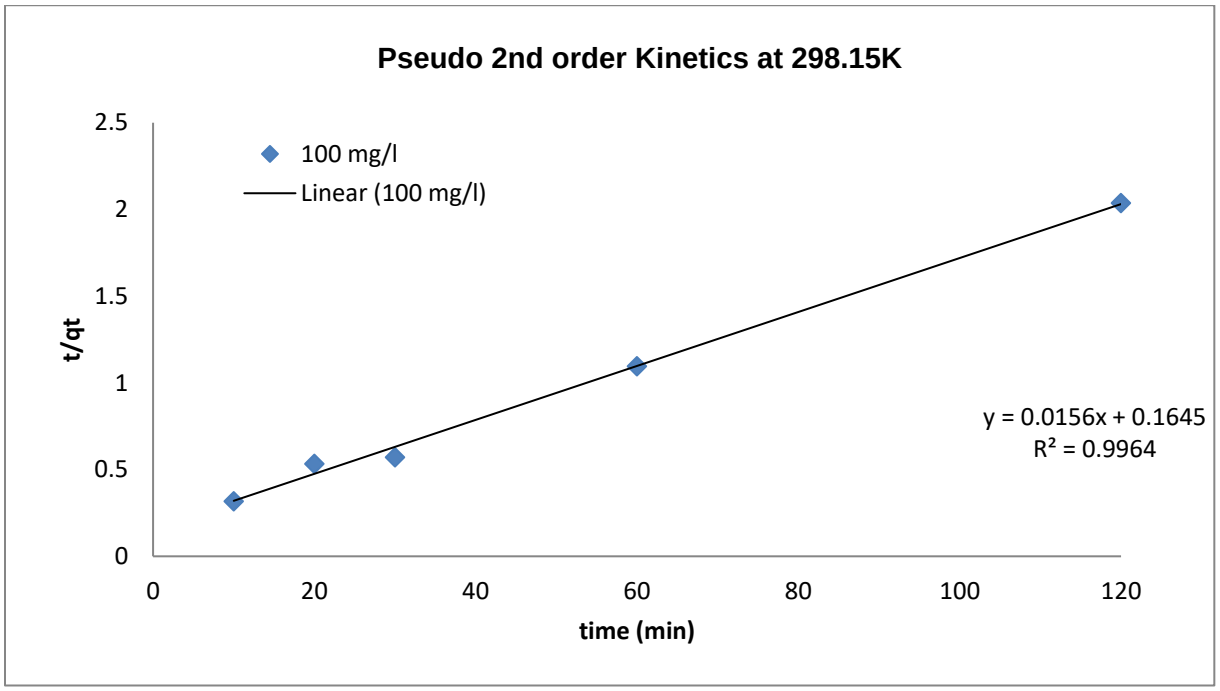

$$qe = \frac{1}{slope}$$

q_e = 1/0.0156

q_e = 66.25 mg/g

$$K_2 = \frac{1}{slope\ q_e^2}$$

$$K_s = \frac{1}{0.1645 \times 58.89^2}$$

$K_s = 0.00175$

Intraparticle diffusion

The following equation was used to fit the data to second order kinetics:

$$q_t = K_d t^{1/2} + C$$

A plot of qt versus $t^{0.5}$ was plotted and used to determine the values of K_{id} and C

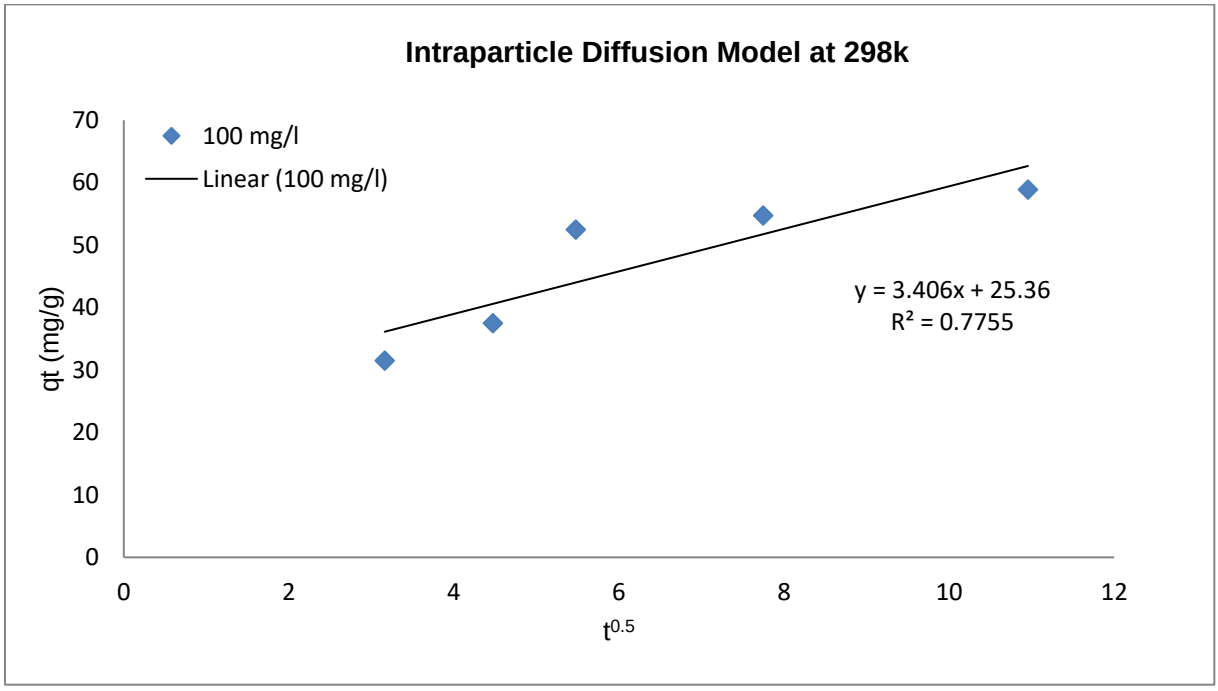

K_{id} = 3.406

C = 25.36 mg/g

Adsorption thermodynamics

The following equation was used to calculate Gibbs free energy.

$\Delta G° = \Delta H° - T\Delta S°$l

A plot of log(q_e/C_e) versus 1/T was used to find enthalpy and entropy using the following equation.

$$ln\frac{q_e}{c_e} = \frac{\Delta S}{R} - \frac{\Delta H}{RT}$$

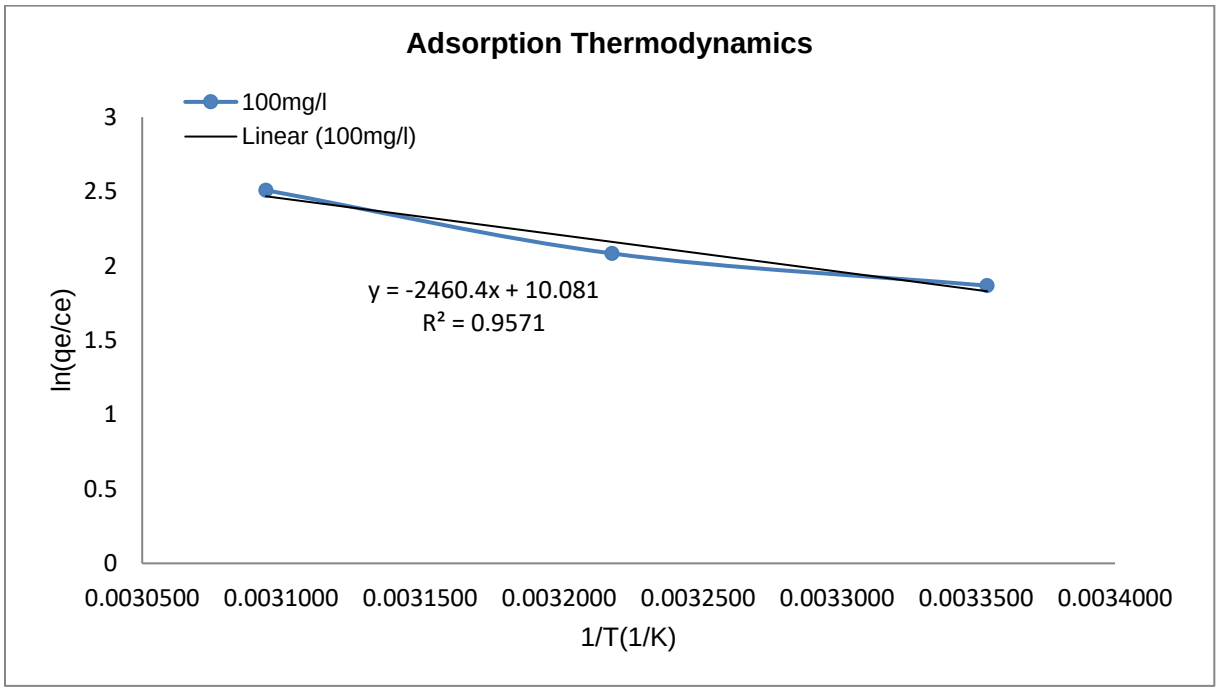

Y = -2460.4X + 10.081

$slope = \frac{\Delta H}{R}$

$\Delta H = -2460.4 \times -8.314$

$\Delta H = 20456\frac{j}{mol}$

ΔH = 20.465 Kj/mol

$intercept = \frac{\Delta S}{R}$

$\Delta S = 10.081 \times 8.314$

ΔS = 0.084 Kj/mol

ΔG = 20.465 – 298.15X0.084

ΔG = -4.533 Kj/mol

Appendix F: Sample preparation and analytical procedures

COD determination procedure

The COD of all samples tested were done using HANNA COD high range reagents. The procedure followed was that given in the instruction guide provided by HANNA. Certain samples tested for COD were also sent away to an independent laboratory for validation of results

Surfactant Procedure'

The Surfactant concentration of all samples tested were done using HANNA MBAS test kits. The procedure followed was that given in the instruction guide provided by HANNA.

Electrical Conductivity (EC)

The EC was read off the EC meters when the probe of the EC meter was placed inside the feed or the treated samples.

Total Dissolved Solids (TDS)

TDS was read off the EC meters